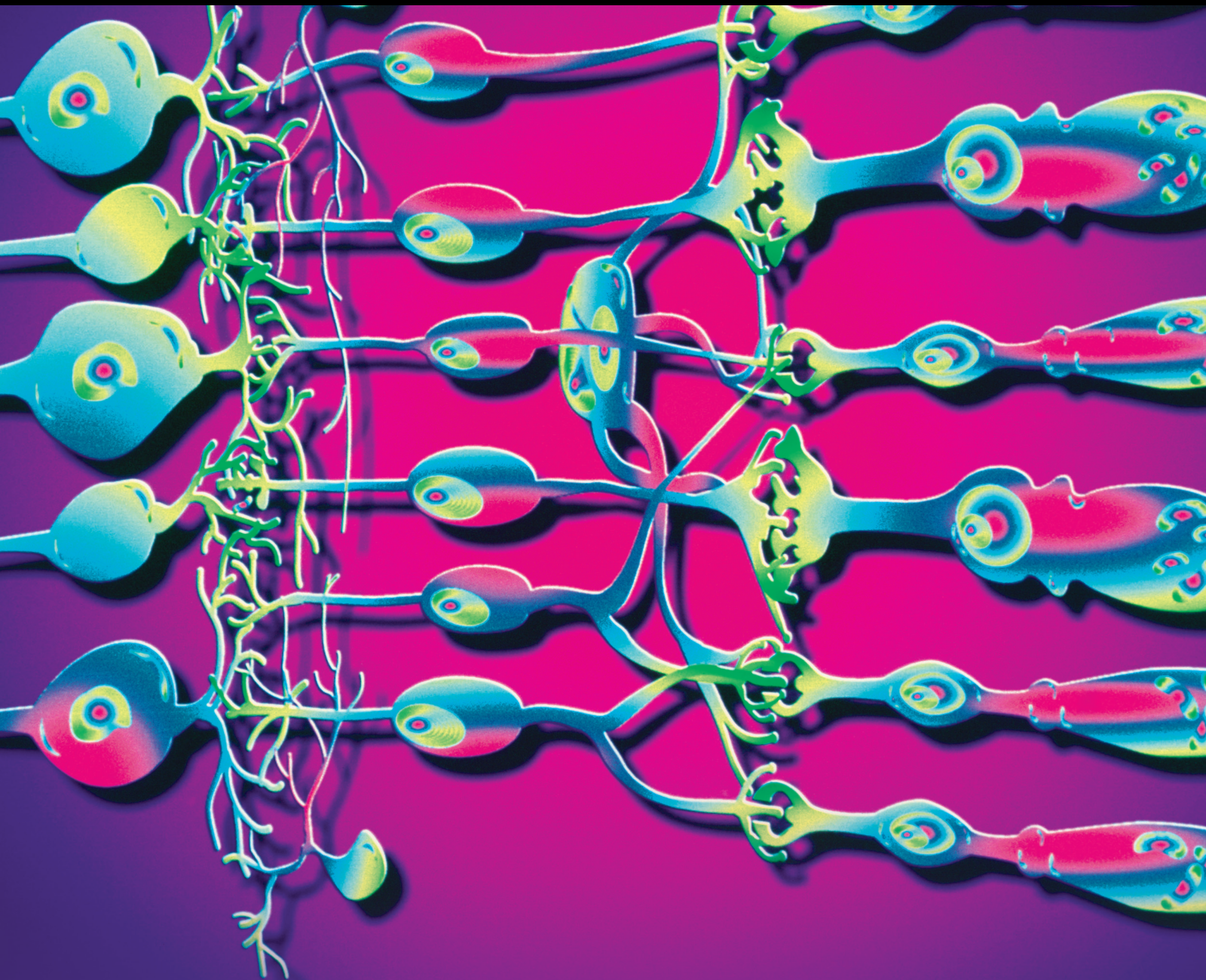


Retinal Biomarkers and Predictors in the Era of Multimodal Imaging

Lead Guest Editor: Serena Fragiotta

Guest Editors: Rosa Dolz-Marco, Yoichi Sakurada, Orly Gal-Or, and Gianluca Scuderi





Retinal Biomarkers and Predictors in the Era of Multimodal Imaging

Journal of Ophthalmology

**Retinal Biomarkers and Predictors in
the Era of Multimodal Imaging**

Lead Guest Editor: Serena Fragiotta


Guest Editors: Rosa Dolz-Marco, Yoichi Sakurada,
Orly Gal-Or, and Gianluca Scuderi







Copyright © 2021 Hindawi Limited. All rights reserved.

This is a special issue published in "Journal of Ophthalmology." All articles are open access articles distributed under the Creative Commons Attribution License, which permits unrestricted use, distribution, and reproduction in any medium, provided the original work is properly cited.

Chief Editor

Steven F. Abcouwer , USA













Associate Editors

Sentaro Kusuhara , Japan
Tamer A. Macky , Egypt
Lawrence S. Morse, USA
Jena J. Steinle , USA
Tomasz Zarnowski , Poland

Academic Editors


Steven F. Abcouwer, USA
Monica L. Acosta , New Zealand
Hamid Ahmadieh , Iran
Hee B. Ahn, Republic of Korea
Siamak Ansari-Shahrezaei , Austria
Taras Ardan , Czech Republic
Francisco Arnalich-Montiel , Spain
Kofi Asiedu , Ghana
Takayuki Baba , Japan
Stefano Baiocchi, Italy
Angelo Balestrazzi , Italy
Antonio Benito , Spain
Maja Bohac, Croatia
Mehmet Borazan, Turkey
Carlo Cagini , Italy
Gonzalo Carracedo , Spain
Arturo Carta , Italy
Alejandro Cerviño , Spain
Colin Clement , Australia
Inés Contreras , Spain
Ciro Costagliola, United Kingdom
Luca D'Andrea, Italy
Roberto Dell'Omo, Italy
Simone Donati, Italy
Manuel S. Falcão , Portugal
Bao Jian Fan , USA
Paulo Fernandes , Portugal
Michele Figus , Italy
Paolo Fogagnolo , Italy
Maria-Andreea Gamulescu, Germany
Diego García-Ayuso , Spain
Jose M. González-Meijome , Portugal
Vlassis Grigoropoulos , Greece
Carl Peter Herbort, Switzerland
Shigeru Honda , Japan
Pierluigi Iacono , Italy

Claudio Iovino , Italy
Takashi Kojima , Japan
George Kymionis, Greece
Hong LIANG , France
Achim Langenbacher , Germany
Van C. Lansingh , Mexico
Paolo Lanzetta , Italy
Theodore Leng , USA
Shengjie Li , China
Su-Ho Lim , Republic of Korea
Antonio Longo , Italy
Norberto López-Gil , Spain
Andrea Lucisano , Italy
Angel Luis Ortega , Spain
Marco Lupidi , Italy
Edward Manche, USA
Marco Marengo , Italy
Colm McAlinden , United Kingdom
Enrique Mencía-Gutiérrez , Spain
Paolo Milani , Italy
Elad Moisseiev , Israel
Mário Monteiro, Brazil
Paolo Mora , Italy
Majid M. Moshirfar , USA
Jean-Claude Mwanza , USA
Carlo Nucci , Italy
Akio Oishi , Japan
Giovanni William Oliverio , Italy
Neville Osborne, United Kingdom
Ji-jing Pang , USA
Georgios Panos, United Kingdom
Mohit Parekh , United Kingdom
Sudhir Patel , Scotland
Enrico Peiretti , Italy
David P. Piñero , Spain
Eli Pradhan, Nepal
Antonio Queiros , Portugal
Anthony G. Robson, United Kingdom
Mario R. Romano , Italy
Wataru Saito , Japan
Juan A. Sanchis-Gimeno , Spain
Dirk Sandner , Germany
Ana Raquel Santiago , Portugal
Rehman Siddiqui , Pakistan
Bartosz Sikorski , Poland

Shivalingappa K. Swamynathan , USA
Nóra Szentmáry, Hungary
Masaru Takeuchi , Japan
Suphi Taneri , Germany
Miguel Teus , Spain
Biju B. Thomas , USA
Oren Tomkins-Netzer , United Kingdom
Lisa Toto , Italy
Maurizio Uva , Italy
Manuel Vidal-Sanz, Spain
Paolo Vinciguerra , Italy
Nilufer Yesilirmak , Turkey
Vicente Zanon-Moreno , Spain
Yedi Zhou , China



Contents

Significance of Hyperreflective Foci as an Optical Coherence Tomography Biomarker in Retinal Diseases: Characterization and Clinical Implications

Serena Fragiotta , Solmaz Abdolrahimzadeh , Rosa Dolz-Marco , Yoichi Sakurada , Orly Gal-Or , and Gianluca Scuderi 

Review Article (10 pages), Article ID 6096017, Volume 2021 (2021)

Optic Nerve Head Hemoglobin Levels in Glaucoma: A Structural and Functional Correlation Study

Janaina A. G. Rocha, Diego T. Dias, Maria Betânia C. Lemos, Fábio N. Kanadani, Augusto Paranhos Jr., Carolina P. B. Gracitelli , and Tiago S. Prata 

Research Article (8 pages), Article ID 9916102, Volume 2021 (2021)

Near-Infrared Reflectance Imaging in Retinal Diseases Affecting Young Patients

Solmaz Abdolrahimzadeh , Chiara Ciancimino , Flaminia Grassi , Edoardo Sordi , Serena Fragiotta , and Gianluca Scuderi 





Review Article (11 pages), Article ID 5581851, Volume 2021 (2021)

OCT Biomarkers in Neovascular Age-Related Macular Degeneration: A Narrative Review

Cristian Metrangolo , Simone Donati , Marco Mazzola , Liviana Fontanel , Walter Messina , Giulia D'alterio , Marisa Rubino , Paolo Radice , Elias Premi , and Claudio Azzolini 



Review Article (16 pages), Article ID 9994098, Volume 2021 (2021)

Characterizing Flow and Structure of Diabetic Retinal Neovascularization after Intravitreal Anti-VEGF Using Optical Coherence Tomography Angiography: A Pilot Study

Christof Haensli , Katrin Fasler , Daniel Barthelmes , and Sandrine A. Zweifel 





Research Article (16 pages), Article ID 2942197, Volume 2021 (2021)

Clinical Characteristics of Paracentral Acute Middle Maculopathy in Eyes with Retinal Vascular Occlusion Diseases in Chinese Patients

Zhengwei Zhang , Yunjia Jiang , Xiaoli Huang , Zhifeng Wu , and Bilian Ke 

Research Article (8 pages), Article ID 8867570, Volume 2021 (2021)

Clinical Features, Prognosis, and Long-Term Response to Ranibizumab of Macular CNVs in Pattern Dystrophies Spectrum: A Pilot Study

Lorenzo Casillo , Stefano Tricarico , Laura Contento , and Enzo M. Vingolo 



Research Article (6 pages), Article ID 6698522, Volume 2021 (2021)

Optical Coherence Tomography Predictors of Favorable Functional Response in Naïve Diabetic Macular Edema Eyes Treated with Dexamethasone Implants as a First-Line Agent

Alessandro Meduri , Giovanni William Oliverio , Luigi Trombetta , Marta Giordano , Leandro Inferrera , and Costantino John Trombetta 

Research Article (5 pages), Article ID 6639418, Volume 2021 (2021)

Retinal Structural and Microvascular Alterations in Different Acute Ischemic Stroke Subtypes

Ying Zhang, Ce Shi, Yihong Chen, Weicheng Wang, Shenghai Huang, Zhao Han, Xianda Lin, Fan Lu , and Meixiao Shen 

Research Article (10 pages), Article ID 8850309, Volume 2020 (2020)

Review Article

Significance of Hyperreflective Foci as an Optical Coherence Tomography Biomarker in Retinal Diseases: Characterization and Clinical Implications

Serena Fragiotta ¹, Solmaz Abdolrahimzadeh ¹, Rosa Dolz-Marco ²,
Yoichi Sakurada ³, Orly Gal-Or ⁴, and Gianluca Scuderi ¹

¹Ophthalmology Unit, Department NESMOS, S. Andrea Hospital, University of Rome “La Sapienza”, Rome, Italy

²Unit of Macula, Ophthalmologist Clinic, Valencia, Spain

³University of Yamanashi, Yamanashi, Japan

⁴Department of Ophthalmology, Rabin Medical Center, Petah Tikva, Israel

Correspondence should be addressed to Serena Fragiotta; serena.fragiotta@uniroma1.it

Received 19 May 2021; Accepted 30 November 2021; Published 17 December 2021

Academic Editor: Paolo Milani

Copyright © 2021 Serena Fragiotta et al. This is an open access article distributed under the Creative Commons Attribution License, which permits unrestricted use, distribution, and reproduction in any medium, provided the original work is properly cited.

Hyperreflective foci (HRF) is a term coined to depict hyperreflective dots or roundish lesions within retinal layers visualized through optical coherence tomography (OCT). Histopathological correlates of HRF are not univocal, spacing from migrating retinal pigment epithelium cells, lipid-laden macrophages, microglial cells, and extravasated proteinaceous or lipid material. Despite this, HRF can be considered OCT biomarkers for disease progression, treatment response, and prognosis in several retinal diseases, including diabetic macular edema, age-related macular degeneration (AMD), retinal vascular occlusions, and inherited retinal dystrophies. The structural features and topographic location of HRF guide the interpretation of their significance in different pathological conditions. The presence of HRF less than 30 μm with reflectivity comparable to the retinal nerve fiber layer in the absence of posterior shadowing in diabetic macular edema indicates an inflammatory phenotype with a better response to steroidal treatment. In AMD, HRF overlying drusen are associated with the development of macular neovascularization, while parafoveal drusen and HRF predispose to macular atrophy. Thus, HRF can be considered a key biomarker in several common retinal diseases. Their recognition and critical interpretation via multimodal imaging are vital to support clinical strategies and management.

1. Introduction

The advent of optical coherence tomography (OCT) has dramatically changed the comprehension of pathophysiological mechanisms underlying retinal disease by detecting novel structural alterations *in vivo* [1]. The term “hyperreflective foci (HRF)” was coined to describe any hyperreflective lesion, focal or dotted in appearance, visualized on OCT at any retinal layer [2]. However, the clinicopathological correlate of HRF remains uncertain, ranging from lipid extravasation in diabetic macular edema (DME) [2], migrating retinal pigment epithelium (RPE) cells,

macrophages/microglia in AMD [3–5], and degenerated photoreceptor cells [6].

The presence of HRF has revealed prognostic and clinical implications in several retinal diseases [7–12] and has influenced the evaluation of treatment response in DME [13,14]. In particular, HRF have been hypothesized to represent microglial cells when responding to specific morphometric criteria visible on OCT B-scans. Their characterization has improved the recognition of a preponderant inflammatory component that drives the management and treatment response of DME [15–18]. Beyond the established role of HRF as biomarkers in DME, their

recognition and evaluation in various other retinal disorders might lead to a change in management, treatment, and prognosis.

The present study aims to provide an overview of the existing literature on HRF as OCT biomarkers associated with disease progression, treatment response, and prognosis of several retinal disorders, including DME, AMD retinal vein occlusion, retinal dystrophies, and uveitis.

2. Methods

A literature search of the Medline database was performed using the term “hyperreflective foci” for articles published in English, last accessed on 9th December 2020. The articles selected described the clinical and prognostic implications of intraretinal and choroidal HRF detected in retinal diseases. Of 212 publications, 119 manuscripts published between 2005 and 2020 are reported in this narrative literature review. Reference lists of the selected manuscripts were also analyzed to retrieve other relevant studies.

3. Diabetic Retinopathy

3.1. Origin and Morphometry of Hyperreflective Foci. The presence of HRF in treatment-naïve DME was first described by Bolz et al. [2] as hyperreflective dots distributed throughout all the retinal layers, often within the septae between cystoid spaces, or confluent lesions located in the outer retinal layers, or focal deposits within the vascular wall of microaneurysms. These hyperreflective lesions were believed to represent extravasated protein and/or lipid deposits, precursors of hard exudates, that tended to resorb along with intraretinal fluid after laser treatment [2,19,20].

Another theory hypothesized that HRF were lipid-laden macrophages migrating into cystoid spaces as a consequence of blood-retinal barrier (BRB) breakdown [21,22]. However, with the introduction of OCT angiography (OCTA), it was noticed that some HRF presented decorrelation signals, possibly an expression of morphological changes in microglia/macrophages or intracellular organelles containing highly reflective material [23]. Glial cell proliferation represents one of the main alterations in diabetic retinopathy, and the role of microglia is essential to maintain retinal homeostasis and the inflammatory response [24].

Suspended scattering particles in motion (SSPiM) is a novel OCTA feature characterized by a flow artifact produced by moving material within cystic spaces possibly due to large molecules such as serum proteins and albumin permeated through the retinal interstitium [25]. SSPiM is closely related to the number of HRF and is considered the product of severe inner BRB breakdown. Accordingly, hyperreflective cystoid spaces, detected either on OCT B-scans or OCTA, often co-localize with HRF [25,26].

Combined multimodal analysis showed that HRF mainly occupy the outer nuclear layer (ONL) and outer plexiform layer (OPL) with distribution of the smallest foci in the inner nuclear layer (INL) and inner plexiform layer (IPL) and posterior shadowing caused by larger foci [27]. The identification of HRF on OCT B-scans demonstrated high

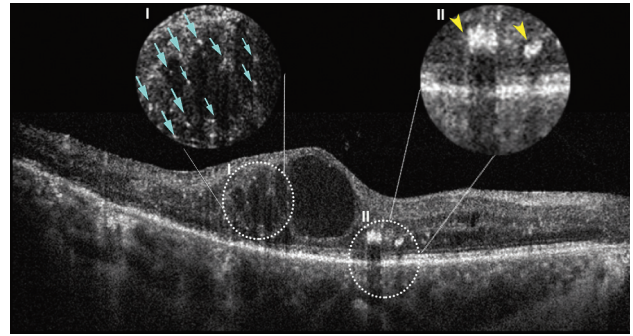


FIGURE 1: Spectral-domain optical coherence tomography B-scan showing the morphological differences between the inflammatory hyperreflective foci (Inset I is characterized by small size ($\leq 30 \mu\text{m}$), the absence of posterior shadowing, inner and outer retinal location, and the reflectivity similar to the retinal nerve fiber layer (light blue arrows), and other subtypes of hyperreflective material (Inset II) such as retinal exudates are characterized by preferential location in the outer retinal layers, size $> 30 \mu\text{m}$, the presence of posterior shadowing, and reflectivity similar to the retinal pigment epithelium (yellow arrowheads)).

interobserver reproducibility, comparable to other retinal OCT features detected in DME such as intraretinal fluid, diffuse retinal edema, subretinal fluid, and vitreomacular traction [28].

HRF cannot be identified with clinical examination because of their small size and axial thickness, and appropriate imaging resolution is necessary for their recognition. It was hypothesized that the foci gradually tend to grow and coalesce into visible lesions as hard exudates [27]. On near-infrared autofluorescence (NIR-AF), a patchy hyperhypoautofluorescent signal described as a mosaic pattern was associated with the presence of HRF in the outer retinal layers and external limiting membrane (ELM) disruption and was considered a biomarker of photoreceptor damage [29]. Likewise, a granular appearance on both short-wavelength fundus autofluorescence (FAF) and NIR-AF was associated with the presence of HRF and visual impairment [29].

Interestingly, Lee et al. [30] demonstrated that the CD14 proinflammatory cytokine expressed by microglia, monocytes, and macrophages correlated with HRF, located in the inner retina, and diffuse edema. A nonobese diabetic mice model showed that proinflammatory cytokines induced both vitreal and retinal HRF and upregulated microglia cells [31].

The distinction between inflammatory HRF and other subtypes of hyperreflective material (i.e., retinal exudates, hemorrhages, and microaneurysms) on OCT B-scans include location within the inner retina, size $\leq 30 \mu\text{m}$, absence of posterior shadowing, and reflectivity similar to the retinal nerve fiber layer (Figure 1) [15,32,33]. Indeed, in a recent international consensus, these morphological characteristics were incorporated as the diagnostic criteria for HRF [17].

3.2. Clinical and Prognostic Implications of Hyperreflective Foci in Diabetic Macular Edema. The amount of HRF reflects disease severity, exhibiting direct associations with

HbA1c values and high levels of total cholesterol, triglycerides, and low-density lipoprotein [34–37]. The association with glycometabolic state has been observed even in early stages of diabetic retinopathy without DME, supporting the hypothesis of lipid extravasation conceivable in subjects with poor glycemic control [38,39].

In eyes with DME, HRF located in the outer retinal layers have been strongly associated with worse visual prognosis, disruption of the ELM, photoreceptor loss, and worse prognosis after vitrectomy [6,29,40,41]. An alternative method of studying the integrity of the photoreceptor-RPE complex in the so-called “parallelism” supported that HRF in the outer retinal layers affects photoreceptor layer continuity. “Parallelism” is a term coined to evaluate retinal layer integrity through OCT B-scans postprocessing using dedicated software for imaging analysis. In brief, this parameter measures how straight the layers are and how parallel the layers are to each other [42]. The parallelism reflected the image complexity and the retinal structural changes, and it is lower in DME eyes than normal eyes. Parallelism also indicates the integrity of photoreceptors, exhibiting a direct association with visual acuity. One of the main factors affecting the parallelism with a relationship with photoreceptor integrity and visual function is the presence of HRF in the outer retinal layers [43,44].

The number of HRF in the outer retinal layers, as a predictor of final visual acuity, was associated with different patterns of DME including diffuse macular edema, cystoid macular edema, and serous retinal detachment [45]. The detection of similar HRF within the choroidal vasculature also denoted worse disease severity and prognosis [46,47]. In this regard, treatment-naïve DME with inflammatory biomarkers (i.e., HRF and serous retinal detachment) showed a superior anatomical response and fewer injections with a dexamethasone (DEX) intravitreal implant, even if better visual acuity was achieved with intravitreal aflibercept. Lens opacity development explained the lower-than-expected functional outcome in the DEX group [48]. A theoretical advantage in favor of a DEX implant as the first-line agent over anti-VEGF therapy has been hypothesized for DME with inflammatory biomarkers [17].

Changes in intraretinal HRF distribution during DME resorption after anti-vascular growth factor (VEGF) treatment included descending migration toward outer retinal layers, supporting the role of the osmotic gradient in fluid and macromolecule clearance [49]. DME with HRF has been associated with a poorer visual outcome following treatment with intravitreal steroid and anti-VEGF agents [14]. Clusters of HRF occupying the central macular area was associated with worse visual acuity than eyes without HRF clusters before any treatment, and the functional difference was maintained following intravitreal ranibizumab and focal laser therapy for up to 5 years [50].

While the role of HRF in predicting visual outcome of DME treated with anti-VEGF agents did not reach univocal conclusions [34,45,51,52], final visual gain resulted evident in DME eyes managed with DEX implant [13,53]. Treatment with DEX implant significantly modulated the number of foci with a reduction maintained up to 12 months of follow-

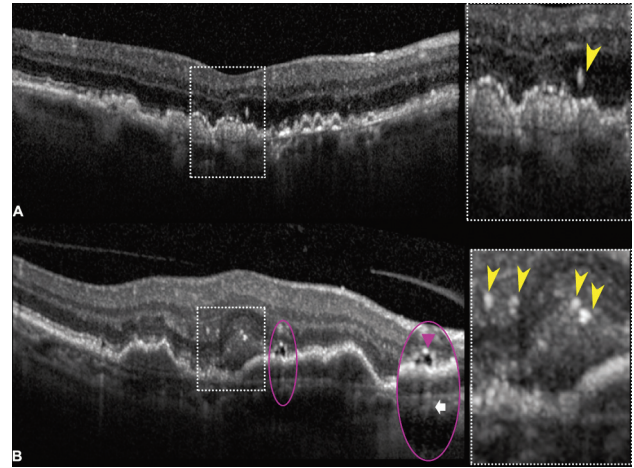


FIGURE 2: Spectral-domain optical coherence tomography (SD-OCT) B-scans illustrating hyperreflective foci (HRF) in age-related macular degeneration (AMD). (a) SD-OCT B-scan of intermediate AMD demonstrating a large HRF overlying confluent drusen located just above the external limiting membrane within the outer nuclear layer (inset, *yellow arrowhead*). HRF may represent migrating retinal pigment epithelium cells or a nascent type 3 lesion. Nascent lesions can be differentiated from type 3 macular neovascularization for the absence of exudative changes, as intraretinal fluid and cystic changes on OCT B-scans. (b) SD-OCT B-scan showing a case of macular neovascularization with multiple HRF located in the subretinal space and outer plexiform layer (inset, *yellow arrowheads*), probably of microglial origin, and more interestingly associated with a subretinal lipid globule. This novel OCT feature appears as a roundish hyporeflective structure (inset, *purple ellipse*) with a characteristic hypertransmission tail (*white arrow*), which is originated from a lensing effect produced by a lipidic content [74].

up [18]. However, the reduction of the number of HRF located in the outer retina, modulated by anti-VEGF treatment, improved visual gain [54,55]. The prognostic role of HRF has been further corroborated by the higher levels of both IL-1 β and HRF (>10) in refractory DME [56]; likewise, a high HRF number at baseline is predictive of early recurrence of DME and a shorter duration of DEX implant efficacy [57,58]. Patients with DME managed with observation exhibited a high risk of visual loss in the presence of DRIL, HRF, and ellipsoid zone disruption at baseline [11].

Evidence of HRF in the foveal region influenced post-operative visual recovery in eyes with vitreous hemorrhage due to proliferative diabetic retinopathy [59]. Nevertheless, their presence seemed to be independent of macular and peripheral retinal ischemia [60].

Recently, multiple (more than 30 in number) and diffuse HRF were considered integrant criteria of severity in the OCT grading proposed for diabetic maculopathy by an international panel of retinal experts [16].

4. Age-Related Macular Degeneration

4.1. Pathogenesis and Imaging Characterization. Khanifer et al. first reported HRF in AMD in 2008 [61] and analyzed drusen ultrastructure with spectral-domain (SD) OCT.

Interestingly, the presence of HRF was noted overlying areas of RPE elevation and often in association with calcified drusen [61–63].

It was generally believed that HRF represent anteriorly migrating RPE cells and possible disaggregated photoreceptors, as supported by the corresponding pigmentary changes visible on color photographic images [61,64,65]. However, hyperpigmentation is not detectable in all cases [61], opening different hypotheses for a non-RPE origin. The foci may represent microglia migrating from the inner to the outer retinal layers engorged by lipid droplets or cholesterol [3,4]. This alternative HRF population has variable morphological characteristics such as size, migration, and clumping. Furthermore, microglial activation was particularly related to neovascular disease as validated through histopathology [4,66].

HRF located above the external limiting membrane and ONL/OPL junction, often co-localized with a drusenoid pigment epithelial detachment (PED), can also represent the antecedents of type 3 macular neovascularization (MNV), or the so-called *nascent* type 3 [67–73]. Nascent type 3 lesions were described as associated with HRF located within the ONL, OPL, or INL on OCT B-scans with a detectable flow signal on OCTA but without evident exudation (e.g., intraretinal fluid and microcystic changes) [67]. Figure 2 illustrates the OCT appearance of HRF in the context of intermediate AMD and MNV [67,74].

Intraretinal HRF from a possible RPE source have been characterized on clinicopathological correlations as isolated or grouped pigmented, nucleated RPE cells that shadow posteriorly on OCT B-scans often associated with hypertransmission areas reflecting the atrophic and dissociated RPE cells [3,75,76]. Different RPE histological phenotypes corresponding to hyperreflective structures on OCT B-scans were described [3,75]. Among these phenotypes, the RPE plume denoted a peculiar OCT feature with a comma-shaped configuration of HRF, believed to represent grouped migrating RPE cells within the Henle fiber layer [3,75].

4.2. Clinical Relevance and Prognostic Implications. HRF can be detected in intermediate to advanced AMD, demonstrating a predictive role for AMD progression and prognostic value when macular complications occur [77–80]. HRF were associated with disease severity, particularly in eyes with intermediate AMD, where they tended to increase in number and density and migrated from the ONL to the inner retinal layers over time [9,77,81]. In intermediate AMD, retinal sensitivity assessed through microperimetry was affected by the presence of HRF that typically co-localized with alterations of the outer retinal bands and the RPE [82–84]. HRF represented markers of cellular dysfunction responsible for visual decline before the development of macular complications [85]. Hyperreflective specks (HRS) shared similar features with HRF, appearing as hyperreflective dots preferentially located in the Henle fiber and ONL associated with visual dysfunction. HRS distinctive features included smaller diameter, lower reflectivity than the RPE band, and more uniform size than HRF. Both HRF

and HRS were considered markers of cellular activity, with HRS representing lipofuscin granules, translocated inwardly within cone photoreceptors [85].

More interestingly, the increasing number of HRF was associated with RPE atrophy and considered a precursor of geographic atrophy [64,77,79]. Several factors have been implicated in macular atrophy progression, including drusen volume, HRF, HRF within a drusenoid lesion, and subretinal drusenoid deposits [86,87]. However, HRF represented the strongest predictor alone for progression to both central or any geographic atrophy [86,88,89]. In progression of geographic atrophy, the morphological features accompanying the presence of HRF were often characterized by reduced retinal thickness and volume and ONL thinning [90]. The distribution of HRF varied according to the subtype of macular complication. Eyes developing macular atrophy presented HRF co-localizing with drusen at 0.5 mm eccentricity, not at the foveal center [91]. Deep learning quantification of HRF in late AMD demonstrated their spatial localization at the atrophy border, demarcating areas subject to growth and expansion of existing atrophic lesions. Furthermore, HRF tended to accumulate in correspondence to areas developing *de novo* lesions [92].

Similarly, in eyes with drusenoid PED, the presence of HRF at baseline and their migration throughout retinal layers were directly associated with new-onset atrophy [78]. Changes in HRF preceded drusenoid PED collapse, where migrating RPE cells and subsequent RPE disintegration, responsible for hypertransmission, accompanied the PED breakpoint [93].

The prognostic role of HRF has been proven for predicting neovascular conversion. Both the presence and HRF count represented strong predictive biomarkers of neovascular progression [7]. Precursors of type 3 lesions were typically represented by HRF located in the outer retinal layers [67,72,94]. One of the possible mechanisms underlying neovascular complications was represented by increased choriocapillaris ischemic changes found to be more severe in eyes with HRF [95]. The predictive value of HRF was mostly associated with drusen growth accompanied by overlying HRF in MNV conversion, suggesting a distinctive hallmark of neovascular conversion [90,91,96].

In eyes with MNV, HRF were diffusely distributed in the neurosensory retina and their presence was associated with a poor visual outcome despite anti-VEGF treatment [97,98]. Anti-VEGF switching from ranibizumab to aflibercept demonstrated a morphological and functional improvement, including HRF reduction, associated with a decreasing central subfoveal thickness [8,99,100]. Of note, the presence of HRF was strongly correlated with intraretinal fluid [101]. HRF detection in neovascular AMD and polypoidal choroidal vasculopathy (PCV) was considered a reliable predictor of poor visual prognosis after anti-VEGF treatment [102].

5. Miscellaneous

The role of HRF has been investigated in other retinal vascular diseases, including branch retinal vein occlusion

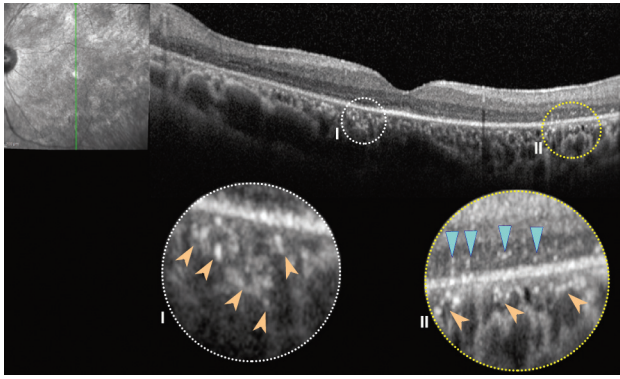


FIGURE 3: Spectral-domain optical coherence tomography B-scans showing an illustrative case of retinitis pigmentosa characterized by both choroidal hyperreflective foci (insets, peach arrowheads) and intraretinal hyperreflective foci (inset II, light blue arrowheads).

(BRVO) and central retinal vein occlusion (CRVO). In this regard, two distinct HRF populations have been identified, including fine scattered HRF probably related to extravasation of blood constituents and confluent HRF mainly located in the unaffected areas spared by the retinal occlusion. Confluent HRF were thought to be associated with the absorption of water and other molecules [103]. While fine scattered HRF cannot be visualized on fundus photographic images, confluent HRF were believed to represent retinal exudates [104]. In retinal vein occlusion, HRF were topographically scattered along the OPL and the external limiting membrane [103,105]. Similar to other retinal diseases, a poor visual outcome after anti-VEGF treatment accompanied the identification of HRF at baseline [104,106]. Furthermore, the use of intravitreal DEX implants might be privileged in eyes with numerous HRF and long-standing macular edema secondary to RVO in consideration with the inflammatory component [107].

Among degenerative retinal diseases, retinitis pigmentosa (RP) revealed HRF with specific topographic distribution and association with disease progression. Eyes with HRF distributed in the INL denote an early stage of RP with spared RPE-Bruch's membrane complex. However, eyes with HRF in the ONL designate a more advanced disease characterized by photoreceptor loss and RPE cell migration and degeneration [108]. RPE cell degeneration in RP eyes occurs secondary to proliferation, spreading, and migration of the RPE cells toward the inner retina with bone spicule formation [109]. The distribution of HRF is mainly concentrated over regions of photoreceptor disruption and associated with intraocular inflammation, further corroborating the hypothesis of RPE or microglial migration in response to photoreceptor degeneration (Figure 3) [110]. Similarly, the recognition of choroidal HRF corresponded to ELM and ellipsoid zone disruption suggesting a migration of deteriorated photoreceptors and RPE cells from the outer retina toward the choroid due to a degradation process [111].

In Stargardt disease, the evidence of choroidal HRF primarily located in the choriocapillaris and Sattler's layer was considered a biomarker of disease severity in terms of

atrophic changes and visual function [112,113]. Furthermore, the concentration of HRF was greater in atrophic areas measuring less than 5 mm^2 , hypothesizing that HRF tended to fade with atrophy enlargement [113].

In pathologic myopia, the HRF role has been investigated in myopic choroidal neovascularization and myopic macular hole [114,115]. HRF appeared to be associated with the presence of retinal edema, serous neuroretinal detachment, and hemorrhage in myopic choroidal neovascularization. All these signatures indicate an active retinal exudation, suggesting that HRF represent an additional indicator of choroidal neovascularization activity [114]. After myopic macular hole repair, the presence of HRF was associated with a worse visual acuity. The limited representation of HRF after macular hole repair with the inverted inner limiting membrane (ILM) flap technique was explained with superior sealing of the retina compartment, allowing the RPE to recover its pump function effectively [115].

HRF were recognized in uveitis and intraocular inflammatory disorders and were likely presumed to represent intraretinal exudates, lymphocytic cellular or clumping of photoreceptors or intraretinal RPE cells when related to photoreceptor loss [116–119]. In eyes with uveitic macular edema, HRF were associated with worse visual acuity [120]. After treatment, the foci decreased in number and mainly remained located to the inner retina layers [121].

6. Conclusions

Hyperreflective foci represent a univocal OCT feature revealing several possible histopathological correlates, including migrating RPE cells, microglia, precursors of exudates, or intraretinal neovascularization in the setting of AMD. HRF represent an important OCT biomarker with significant clinical and prognostic implications embracing several common macular diseases. The detection of HRF of size $\leq 30 \mu\text{m}$ without posterior shadowing and reflectivity similar to the retinal nerve fiber layer configures the inflammatory phenotype in DME that usually responds better to early intravitreal steroid implant.

Relevance as a biomarker is also observed in AMD, where the number and distribution of HRF may be predictors for progression to advanced stages of disease. The co-localization of HRF overlying drusen associated with drusen growth in the foveal center is believed to be a predictor of neovascular progression. In contrast, a high concentration of HRF distributed at 0.5 mm of eccentricity edging the foveal pit, in the absence of drusen occupying the foveal center, tends to predispose to macular atrophy. Moreover, the presence of HRF influences anti-VEGF treatment response and visual prognosis of MNV. In conclusion, HRF can be considered a critical OCT feature with substantial predictive value for disease progression and treatment response in the principal macular disorders encountered in routine clinical practice. Their prompt recognition and critical interpretation may guide clinical and therapeutic strategies.

Data Availability

Data are available upon request to the corresponding author Serena Fragiotta, MD, PhD, via e-mail (serena.fragiotta@uniroma1.it).

Conflicts of Interest

The authors declare that they have no conflicts of interest.

References

- [1] P. Massin, A. Girach, A. Erginay, and A. Gaudric, "Optical coherence tomography: a key to the future management of patients with diabetic macular oedema," *Acta Ophthalmologica Scandinavica*, vol. 84, no. 4, pp. 466–474, 2006.
- [2] M. Bolz, U. Schmidt-Erfurth, G. Deak, G. Mylonas, K. Kriechbaum, and C. Scholda, "Optical coherence tomographic hyperreflective foci," *Ophthalmology*, vol. 116, no. 5, pp. 914–920, 2009.
- [3] C. A. Curcio, E. C. Zanzottera, T. Ach, C. Balaratnasingam, and K. B. Freund, "Activated retinal pigment epithelium, an optical coherence tomography biomarker for progression in age-related macular degeneration," *Investigative Ophthalmology & Visual Science*, vol. 58, pp. BIO211–BIO226, 2017.
- [4] C. E. Pang, J. D. Messinger, E. C. Zanzottera, K. B. Freund, and C. A. Curcio, "The onion sign in neovascular age-related macular degeneration represents cholesterol crystals," *Ophthalmology*, vol. 122, no. 11, pp. 2316–2326, 2015.
- [5] C. Framme, S. Wolf, and U. Wolf-Schnurrbusch, "Small dense particles in the retina observable by spectral-domain optical coherence tomography in age-related macular degeneration," *Investigative Ophthalmology & Visual Science*, vol. 51, no. 11, pp. 5965–5969, 2010.
- [6] A. Uji, T. Murakami, K. Nishijima et al., "Association between hyperreflective foci in the outer retina, status of photoreceptor layer, and visual acuity in diabetic macular edema," *American Journal of Ophthalmology*, vol. 153, no. 4, pp. 710–717, 2012.
- [7] S. Fragiotta, T. Rossi, A. Cutini, P. L. Grenga, and E. M. Vingolo, "Predictive factors for development of neovascular age-related macular degeneration," *Retina*, vol. 38, no. 2, pp. 245–252, 2018.
- [8] K. Abri Aghdam, A. Pielen, C. Framme, and B. Junker, "Correlation between hyperreflective foci and clinical outcomes in neovascular age-related macular degeneration after switching to aflibercept," *Investigative Ophthalmology & Visual Science*, vol. 56, no. 11, pp. 6448–6455, 2015.
- [9] L. Altay, P. Scholz, T. Schick et al., "Association of hyperreflective foci present in early forms of age-related macular degeneration with known age-related macular degeneration risk polymorphisms," *Investigative Ophthalmology & Visual Science*, vol. 57, no. 10, pp. 4315–4320, 2016.
- [10] E. Borrelli, B. Zuccaro, I. Zucchiatti et al., "Optical coherence tomography parameters as predictors of treatment response to eplerenone in central serous chorioretinopathy," *Journal of Clinical Medicine*, vol. 8, no. 9, p. 1271, 2019.
- [11] C. Busch, M. Okada, D. Zur et al., "Baseline predictors for visual acuity loss during observation in diabetic macular oedema with good baseline visual acuity," *Acta Ophthalmologica*, vol. 98, no. 7, pp. e801–e806, 2020.
- [12] K. C. Chen, J. J. Jung, C. A. Curcio et al., "Intraretinal hyperreflective foci in acquired vitelliform lesions of the macula: clinical and histologic study," *American Journal of Ophthalmology*, vol. 164, pp. 89–98, 2016.
- [13] I. Chatziralli, P. Theodosiadis, E. Parikakis, E. Dimitriou, T. Xirou, and G. Theodosiadis, "Dexamethasone intravitreal implant in diabetic macular edema: real-life data from a prospective study and predictive factors for visual outcome," *Diabetes Therapy*, vol. 8, no. 6, pp. 1393–1404, 2017.
- [14] I. P. Chatziralli, T. N. Sergentanis, and S. Sivaprasad, "Hyperreflective FOCI as an independent visual outcome predictor in macular edema due to retinal vascular diseases treated with intravitreal dexamethasone or ranibizumab," *Retina*, vol. 36, no. 12, pp. 2319–2328, 2016.
- [15] S. Vujosevic, S. Bini, T. Torresin et al., "Hyperreflective retinal spots in normal and diabetic eyes," *Retina*, vol. 37, no. 6, pp. 1092–1103, 2017.
- [16] G. Panozzo, M. V. Cicinelli, A. J. Augustin et al., "An optical coherence tomography-based grading of diabetic maculopathy proposed by an international expert panel: the European School for Advanced Studies in Ophthalmology classification," *European Journal of Ophthalmology*, vol. 30, no. 1, pp. 8–18, 2020.
- [17] L. Kodjikian, D. Bellocq, F. Bandello et al., "First-line treatment algorithm and guidelines in center-involving diabetic macular edema," *European Journal of Ophthalmology*, vol. 29, no. 6, pp. 573–584, 2019.
- [18] A. Meduri, G. W. Oliverio, L. Trombetta, M. Giordano, L. Inferrera, and C. J. Trombetta, "Optical coherence tomography predictors of favorable functional response in naïve diabetic macular edema eyes treated with dexamethasone implants as a first-line agent," *Journal of Ophthalmology*, vol. 2021, Article ID 6639418, 5 pages, 2021.
- [19] G. G. Deák, M. Bolz, K. Kriechbaum et al., "Effect of retinal photocoagulation on intraretinal lipid exudates in diabetic macular edema documented by optical coherence tomography," *Ophthalmology*, vol. 117, no. 4, pp. 773–779, 2010.
- [20] Y. Yamada, K. Suzuma, A. Fujikawa, T. Kumagami, and T. Kitaoka, "Imaging of laser-photocoagulated diabetic microaneurysm with spectral domain optical coherence tomography," *Retina*, vol. 33, no. 4, pp. 726–731, 2013.
- [21] T. Horii, T. Murakami, K. Nishijima et al., "Relationship between fluorescein pooling and optical coherence tomographic reflectivity of cystoid spaces in diabetic macular edema," *Ophthalmology*, vol. 119, no. 5, pp. 1047–1055, 2012.
- [22] S. Yoshitake, T. Murakami, A. Uji et al., "Association between cystoid spaces on indocyanine green hyperfluorescence and optical coherence tomography after vitrectomy for diabetic macular oedema," *Eye*, vol. 28, no. 4, pp. 439–448, 2014.
- [23] T. Murakami, K. Suzuma, Y. Dodo et al., "Decorrelation signal of diabetic hyperreflective foci on optical coherence tomography angiography," *Scientific Reports*, vol. 8, no. 1, p. 8798, 2018.
- [24] J. Fehér, S. Taurone, M. Spoletini et al., "Ultrastructure of neurovascular changes in human diabetic retinopathy," *International Journal of Immunopathology & Pharmacology*, vol. 31, 2018.
- [25] J. Ahn, S. Han, S. M. Ahn, S.-W. Kim, and J. Oh, "Clinical implications of suspended scattering particles in motion observed by optical coherence tomography angiography," *Scientific Reports*, vol. 10, no. 1, p. 15, 2020.
- [26] A. Couturier, V. Mane, C. A. Lavia, and R. Tadayoni, "Hyperreflective cystoid spaces in diabetic macular oedema: prevalence and clinical implications," *British Journal of Ophthalmology*, vol. 2020, 2020.

- [27] S. Niu, C. Yu, Q. Chen et al., "Multimodality analysis of hyper-reflective foci and hard exudates in patients with diabetic retinopathy," *Scientific Reports*, vol. 7, no. 1, p. 1568, 2017.
- [28] L. Z. Heng, M. Pefianaki, P. Hykin, and P. J. Patel, "Inter-observer agreement in detecting spectral-domain optical coherence tomography features of diabetic macular edema," *PLoS One*, vol. 10, no. 5, Article ID e0126557, 2015.
- [29] S. Yoshitake, T. Murakami, T. Horii et al., "Qualitative and quantitative characteristics of near-infrared autofluorescence in diabetic macular edema," *Ophthalmology*, vol. 121, no. 5, pp. 1036–1044, 2014.
- [30] H. Lee, H. Jang, Y. A. Choi, H. C. Kim, and H. Chung, "Association between soluble CD14 in the aqueous humor and hyperreflective foci on optical coherence tomography in patients with diabetic macular edema," *Investigative Ophthalmology & Visual Science*, vol. 59, no. 2, pp. 715–721, 2018.
- [31] O. O. Mugisho, I. D. Rupenthal, D. M. Squirrell et al., "Intravitreal pro-inflammatory cytokines in non-obese diabetic mice: modelling signs of diabetic retinopathy," *PLoS One*, vol. 13, no. 8, Article ID e0202156, 2018.
- [32] E. Midena, E. Pilotto, and S. Bini, "Hyperreflective intraretinal foci as an OCT biomarker of retinal inflammation in diabetic macular edema," *Investigative Ophthalmology & Visual Science*, vol. 59, no. 13, p. 5366, 2018.
- [33] H. Lee and H. Chung, "Author response: hyperreflective intraretinal foci as an OCT biomarker of retinal inflammation in diabetic macular edema," *Investigative Ophthalmology & Visual Science*, vol. 59, no. 13, p. 5367, 2018.
- [34] C. Framme, P. Schweizer, M. Imesch, S. Wolf, and U. Wolf-Schnurrbusch, "Behavior of SD-OCT-detected hyperreflective foci in the retina of anti-VEGF-treated patients with diabetic macular edema," *Investigative Ophthalmology & Visual Science*, vol. 53, no. 9, pp. 5814–5818, 2012.
- [35] S. Davoudi, E. Papavasileiou, R. Roohipoor et al., "Optical coherence tomography characteristics of macular edema and hard exudates and their association with lipid serum levels in type 2 diabetes," *Retina*, vol. 36, no. 9, pp. 1622–1629, 2016.
- [36] Y.-R. Chung, S. Y. Lee, Y. H. Kim, H.-E. Byeon, J. H. Kim, and K. Lee, "Hyperreflective foci in diabetic macular edema with serous retinal detachment: association with dyslipidemia," *Acta Diabetologica*, vol. 57, no. 7, pp. 861–866, 2020.
- [37] V. Schreur, A. de Breuk, F. G. Venhuizen et al., "Retinal hyperreflective foci in type 1 diabetes mellitus," *Retina*, vol. 40, no. 8, pp. 1565–1573, 2020.
- [38] U. De Benedetto, R. Sacconi, L. Pierro, R. Lattanzio, and F. Bandello, "Optical coherence tomographic hyperreflective foci in early stages of diabetic retinopathy," *Retina*, vol. 35, no. 3, pp. 449–453, 2015.
- [39] L. Frizziero, G. Midena, E. Longhin et al., "Early retinal changes by OCT angiography and multifocal electroretinography in diabetes," *Journal of Clinical Medicine*, vol. 9, no. 11, p. 3514, 2020.
- [40] K. Nishijima, T. Murakami, T. Hirashima et al., "Hyperreflective foci in outer retina predictive of photoreceptor damage and poor vision after vitrectomy for diabetic macular edema," *Retina*, vol. 34, no. 4, pp. 732–740, 2014.
- [41] B. Li, B. Zhang, Y. Chen, and D. Li, "Optical coherence tomography parameters related to vision impairment in patients with diabetic macular edema: a quantitative correlation analysis," *Journal of Ophthalmology*, vol. 2020, Article ID 5639284, 6 pages, 2020.
- [42] A. Uji, T. Murakami, N. Unoki et al., "Parallelism as a novel marker for structural integrity of retinal layers in optical coherence tomographic images in eyes with epiretinal membrane," *American Journal of Ophthalmology*, vol. 157, no. 1, pp. 227–236, 2014.
- [43] A. Uji, T. Murakami, N. Unoki et al., "Parallelism for quantitative image analysis of photoreceptor-retinal pigment epithelium complex alterations in diabetic macular edema," *Investigative Ophthalmology & Visual Science*, vol. 55, no. 5, pp. 3361–3367, 2014.
- [44] A. Uji, T. Murakami, K. Suzuma et al., "Influence of vitrectomy surgery on the integrity of outer retinal layers in diabetic macular edema," *Retina*, vol. 38, no. 1, pp. 163–172, 2018.
- [45] J.-W. Kang, H. Chung, and H. Chan Kim, "Correlation of optical coherence tomographic hyperreflective FOCI with visual outcomes in different patterns of diabetic macular edema," *Retina*, vol. 36, no. 9, pp. 1630–1639, 2016.
- [46] R. Roy, K. Saurabh, D. Shah, M. Chowdhury, and S. Goel, "Choroidal hyperreflective foci: a novel spectral domain optical coherence tomography biomarker in eyes with diabetic macular edema," *Asia-Pacific Journal of Ophthalmology*, vol. 8, no. 4, pp. 314–318, 2019.
- [47] A. Arrigo, L. Capone, R. Lattanzio, E. Aragona, P. Zollet, and F. Bandello, "Optical coherence tomography biomarkers of inflammation in diabetic macular edema treated by fluocinolone acetonide intravitreal drug-delivery system implant," *Ophthalmology and Therapy*, vol. 9, no. 4, pp. 971–980, 2020.
- [48] C. Ozsaygili and N. Duru, "Comparison of intravitreal dexamethasone implant and aflibercept in patients with treatment-naive diabetic macular edema with serous retinal detachment," *Retina*, vol. 40, no. 6, pp. 1044–1052, 2020.
- [49] B. Pemp, G. Deák, S. Prager et al., "Distribution of intraretinal exudates in diabetic macular edema during anti-vascular endothelial growth factor therapy observed by spectral domain optical coherence tomography and fundus photography," *Retina*, vol. 34, no. 12, pp. 2407–2415, 2014.
- [50] B. Weingessel, K. Miháلتz, A. Gleiss, F. Sulzbacher, C. Schütze, and P. V. Vécsei-Marlovits, "Treatment of diabetic macular edema with intravitreal anti-vascular endothelial growth factor and prompt versus deferred focal laser during long-term follow-up and identification of prognostic retinal markers," *Journal of Ophthalmology*, vol. 2018, Article ID 3082560, 11 pages, 2018.
- [51] T. Murakami, K. Suzuma, A. Uji et al., "Association between characteristics of foveal cystoid spaces and short-term responsiveness to ranibizumab for diabetic macular edema," *Japanese Journal of Ophthalmology*, vol. 62, no. 3, pp. 292–301, 2018.
- [52] V. Schreur, L. Altay, F. van Asten et al., "Hyperreflective foci on optical coherence tomography associate with treatment outcome for anti-VEGF in patients with diabetic macular edema," *PLoS One*, vol. 13, no. 10, Article ID e0206482, 2018.
- [53] D. Zur, M. Igllicki, C. Busch et al., "OCT biomarkers as functional outcome predictors in diabetic macular edema treated with dexamethasone implant," *Ophthalmology*, vol. 125, no. 2, pp. 267–275, 2018.
- [54] S. Liu, D. Wang, F. Chen, and X. Zhang, "Hyperreflective foci in OCT image as a biomarker of poor prognosis in diabetic macular edema patients treating with conbercept in China," *BMC Ophthalmology*, vol. 19, no. 1, p. 157, 2019.
- [55] T. Yoshitake, T. Murakami, K. Suzuma, Y. Dodo, M. Fujimoto, and A. Tsujikawa, "Hyperreflective foci in the outer retinal layers as a predictor of the functional efficacy of

- ranibizumab for diabetic macular edema,” *Scientific Reports*, vol. 10, no. 1, p. 873, 2020.
- [56] M. Y. Choi, D. Jee, and J.-W. Kwon, “Characteristics of diabetic macular edema patients refractory to anti-VEGF treatments and a dexamethasone implant,” *PLoS One*, vol. 14, no. 9, Article ID e0222364, 2019.
- [57] K. T. Kim, D. Y. Kim, and J. B. Chae, “Association between hyperreflective foci on spectral-domain optical coherence tomography and early recurrence of diabetic macular edema after intravitreal dexamethasone implantation,” *Journal of Ophthalmology*, vol. 2019, Article ID 3459164, 9 pages, 2019.
- [58] Y. G. Park, M. Y. Choi, and J.-W. Kwon, “Factors associated with the duration of action of dexamethasone intravitreal implants in diabetic macular edema patients,” *Scientific Reports*, vol. 9, no. 1, p. 19588, 2019.
- [59] T. Murakami, A. Uji, K. Ogino et al., “Macular morphologic findings on optical coherence tomography after microincision vitrectomy for proliferative diabetic retinopathy,” *Japanese Journal of Ophthalmology*, vol. 59, no. 4, pp. 236–243, 2015.
- [60] N. G. Yalçın and Ş. Özdek, “The relationship between macular cyst formation and ischemia in diabetic macular edema,” *Turkish Journal of Orthodontics*, vol. 49, no. 4, pp. 194–200, 2019.
- [61] A. A. Khanifar, A. F. Koreishi, J. A. Izatt, and C. A. Toth, “Drusen ultrastructure imaging with spectral domain optical coherence tomography in age-related macular degeneration,” *Ophthalmology*, vol. 115, no. 11, pp. 1883–1890, 2008.
- [62] G. Landa, R. B. Rosen, J. Pilavas, and P. M. T. Garcia, “Drusen characteristics revealed by spectral-domain optical coherence tomography and their corresponding fundus autofluorescence appearance in dry age-related macular degeneration,” *Ophthalmic Research*, vol. 47, no. 2, pp. 81–86, 2012.
- [63] F. G. Schlanitz, S. Sacu, B. Baumann et al., “Identification of drusen characteristics in age-related macular degeneration by polarization-sensitive optical coherence tomography,” *American Journal of Ophthalmology*, vol. 160, no. 2, pp. 335–344, 2015.
- [64] S. G. Schuman, A. F. Koreishi, S. Farsiu, S.-h. Jung, J. A. Izatt, and C. A. Toth, “Photoreceptor layer thinning over drusen in eyes with age-related macular degeneration imaged in vivo with spectral-domain optical coherence tomography,” *Ophthalmology*, vol. 116, no. 3, pp. 488–496, 2009.
- [65] F. A. Folgar, J. H. Chow, S. Farsiu et al., “Spatial correlation between hyperpigmentary changes on color fundus photography and hyperreflective foci on SDOCT in intermediate AMD,” *Investigative Ophthalmology & Visual Science*, vol. 53, no. 8, pp. 4626–4633, 2012.
- [66] G. Coscas, U. De Benedetto, F. Coscas et al., “Hyperreflective dots: a new spectral-domain optical coherence tomography entity for follow-up and prognosis in exudative age-related macular degeneration,” *Ophthalmologica*, vol. 229, no. 1, pp. 32–37, 2013.
- [67] R. Sacconi, D. Sarraf, S. Garrity et al., “Nascent type 3 neovascularization in age-related macular degeneration,” *Ophthalmology Retina*, vol. 2, no. 11, pp. 1097–1106, 2018.
- [68] A. Nagiel, D. Sarraf, S. R. Sadda et al., “Type 3 neovascularization,” *Retina*, vol. 35, no. 4, pp. 638–647, 2015.
- [69] D. Su, S. Lin, N. Phasukkijwatana et al., “An updated staging system of type 3 neovascularization using spectral domain optical coherence tomography,” *Retina*, vol. 36, no. 1, pp. S40–S49, 2016.
- [70] A. C. S. Tan, K. K. Dansingani, L. A. Yannuzzi, D. Sarraf, and K. B. Freund, “Type 3 neovascularization imaged with cross-sectional and en face optical coherence tomography angiography,” *Retina*, vol. 37, no. 2, pp. 234–246, 2017.
- [71] M. Li, R. Dolz-Marco, J. D. Messinger et al., “Clinicopathologic correlation of anti-vascular endothelial growth factor-treated type 3 neovascularization in age-related macular degeneration,” *Ophthalmology*, vol. 125, no. 2, pp. 276–287, 2018.
- [72] Z. Öztaş and J. Menteş, “Retinal angiomatous proliferation: multimodal imaging characteristics and follow-up with eye-tracked spectral domain optical coherence tomography of precursor lesions,” *Türk Oftalmoloji Dergisi*, vol. 48, pp. 66–69, 2018.
- [73] N. Silva, A. Marta, P. Baptista, M. J. Furtado, and M. Lume, “Optical coherence tomography findings (SD-OCT and OCTA) in early-stage type 3 neovascularization,” *Case Reports in Ophthalmology*, vol. 11, no. 2, pp. 493–499, 2020.
- [74] P. Fernández-Avellaneda, K. B. Freund, R. K. Wang et al., “Multimodal imaging features and clinical relevance of subretinal lipid globules,” *American Journal of Ophthalmology*, vol. 222, pp. 112–125, 2021.
- [75] C. Balaratnasingam, J. D. Messinger, K. R. Sloan, L. A. Yannuzzi, K. B. Freund, and C. A. Curcio, “Histologic and optical coherence tomographic correlates in drusenoid pigment epithelium detachment in age-related macular degeneration,” *Ophthalmology*, vol. 124, no. 5, pp. 644–656, 2017.
- [76] C. Ahlers, E. Götzinger, M. Pircher et al., “Imaging of the retinal pigment epithelium in age-related macular degeneration using polarization-sensitive optical coherence tomography,” *Investigative Ophthalmology & Visual Science*, vol. 51, no. 4, pp. 2149–2157, 2010.
- [77] J. G. Christenbury, F. A. Folgar, R. V. O’Connell, S. J. Chiu, S. Farsiu, and C. A. Toth, “Progression of intermediate age-related macular degeneration with proliferation and inner retinal migration of hyperreflective foci,” *Ophthalmology*, vol. 120, no. 5, pp. 1038–1045, 2013.
- [78] Y. Ouyang, F. M. Heussen, A. Hariri, P. A. Keane, and S. R. Sadda, “Optical coherence tomography-based observation of the natural history of drusenoid lesion in eyes with dry age-related macular degeneration,” *Ophthalmology*, vol. 120, no. 12, pp. 2656–2665, 2013.
- [79] J. N. Leuschen, S. G. Schuman, K. P. Winter et al., “Spectral-domain optical coherence tomography characteristics of intermediate age-related macular degeneration,” *Ophthalmology*, vol. 120, no. 1, pp. 140–150, 2013.
- [80] V. Sitnilska, E. Kersten, L. Altay et al., “Major predictive factors for progression of early to late age-related macular degeneration,” *Ophthalmologica*, vol. 243, no. 6, pp. 444–452, 2020.
- [81] M. Miura, S. Makita, S. Sugiyama et al., “Evaluation of intraretinal migration of retinal pigment epithelial cells in age-related macular degeneration using polarimetric imaging,” *Scientific Reports*, vol. 7, no. 1, p. 3150, 2017.
- [82] Z. Wu, L. N. Ayton, C. D. Luu, and R. H. Guymer, “Relationship between retinal microstructures on optical coherence tomography and microperimetry in age-related macular degeneration,” *Ophthalmology*, vol. 121, no. 7, pp. 1445–1452, 2014.
- [83] S. Fragiotta, C. Carnevale, A. Cutini, and E. M. Vingolo, “Correlation between retinal function and microstructural foveal changes in intermediate age related macular

- degeneration," *International Journal of Retina and Vitreous*, vol. 3, no. 1, p. 8, 2017.
- [84] Z. Wu, D. Cunefare, E. Chiu et al., "Longitudinal associations between microstructural changes and microperimetry in the early stages of age-related macular degeneration," *Investigative Ophthalmology & Visual Science*, vol. 57, no. 8, pp. 3714–3722, 2016.
- [85] B. S. Echols, M. E. Clark, T. A. Swain et al., "Hyperreflective foci and specks are associated with delayed rod-mediated dark adaptation in nonneovascular age-related macular degeneration," *Ophthalmology Retina*, vol. 4, no. 11, pp. 1059–1068, 2020.
- [86] J. Lei, S. Balasubramanian, N. S. Abdelfattah, M. G. Nittala, and S. R. Sadda, "Proposal of a simple optical coherence tomography-based scoring system for progression of age-related macular degeneration," *Graefes Archive for Clinical and Experimental Ophthalmology*, vol. 255, no. 8, pp. 1551–1558, 2017.
- [87] M. Paavo, W. Lee, J. Merriam et al., "Intraretinal correlates of reticular pseudodrusen revealed by autofluorescence and en face OCT," *Investigative Ophthalmology & Visual Science*, vol. 58, no. 11, pp. 4769–4777, 2017.
- [88] K. Sleiman, M. Veerappan, K. P. Winter et al., "Optical coherence tomography predictors of risk for progression to non-neovascular atrophic age-related macular degeneration," *Ophthalmology*, vol. 124, no. 12, pp. 1764–1777, 2017.
- [89] M. Nassisi, W. Fan, Y. Shi et al., "Quantity of intraretinal hyperreflective foci in patients with intermediate age-related macular degeneration correlates with 1-year progression," *Investigative Ophthalmology & Visual Science*, vol. 59, no. 8, pp. 3431–3439, 2018.
- [90] U. Schmidt-Erfurth, S. M. Waldstein, S. Klmscha et al., "Prediction of individual disease conversion in early AMD using artificial intelligence," *Investigative Ophthalmology & Visual Science*, vol. 59, no. 8, pp. 3199–3208, 2018.
- [91] S. M. Waldstein, W.-D. Vogl, H. Bogunovic, A. Sadeghipour, S. Riedl, and U. Schmidt-Erfurth, "Characterization of drusen and hyperreflective foci as biomarkers for disease progression in age-related macular degeneration using artificial intelligence in optical coherence tomography," *JAMA Ophthalmology*, vol. 138, no. 7, pp. 740–747, 2020.
- [92] U. Schmidt-Erfurth, H. Bogunovic, C. Grechenig et al., "Role of deep learning-quantified hyperreflective foci for the prediction of geographic atrophy progression," *American Journal of Ophthalmology*, vol. 216, pp. 257–270, 2020.
- [93] C. Balaratnasingam, L. A. Yannuzzi, C. A. Curcio et al., "Associations between retinal pigment epithelium and drusen volume changes during the lifecycle of large drusenoid pigment epithelial detachments," *Investigative Ophthalmology & Visual Science*, vol. 57, no. 13, pp. 5479–5489, 2016.
- [94] A. E. Fayed and A. A. Fawzi, "Projection resolved optical coherence tomography angiography to distinguish flow signal in retinal angiomatous proliferation from flow artifact," *PLoS One*, vol. 14, no. 5, Article ID e0217109, 2019.
- [95] L. Tiosano, I. Byon, A. R. Alagorie, Y.-S. Ji, and S. R. Sadda, "Choriocapillaris flow deficit associated with intraretinal hyperreflective foci in intermediate age-related macular degeneration," *Graefes Archive for Clinical and Experimental Ophthalmology*, vol. 258, no. 11, pp. 2353–2362, 2020.
- [96] X. Hu, S. M. Waldstein, S. Klmscha et al., "Morphological and functional characteristics at the onset of exudative conversion in age-related macular degeneration," *Retina*, vol. 40, no. 6, pp. 1070–1078, 2020.
- [97] Y. Akagi-Kurashige, A. Tsujikawa, A. Oishi et al., "Relationship between retinal morphological findings and visual function in age-related macular degeneration," *Graefes Archive for Clinical and Experimental Ophthalmology*, vol. 250, no. 8, pp. 1129–1136, 2012.
- [98] O. Segal, E. Barayev, A. Y. Nemet, N. Geffen, I. Vainer, and M. Mimouni, "Prognostic value of hyperreflective foci in neovascular age-related macular degeneration treated with bevacizumab," *Retina*, vol. 36, no. 11, pp. 2175–2182, 2016.
- [99] C. Türksever, C. Prunte, and K. Hatz, "Baseline optical coherence tomography findings as outcome predictors after switching from ranibizumab to aflibercept in neovascular age-related macular degeneration following a treat-and-extend regimen," *Ophthalmologica*, vol. 238, no. 3, pp. 172–178, 2017.
- [100] C. Ebner, C. Wernigg, C. Schütze, B. Weingessel, and P.-V. Vécsei-Marlovits, "Retinal pigment epithelial characteristics in eyes with neovascular age-related macular degeneration," *Wiener Klinische Wochenschrift*, vol. 133, no. 3–4, pp. 123–130, 2020.
- [101] G. Moraes, D. J. Fu, M. Wilson et al., "Quantitative analysis of OCT for neovascular age-related macular degeneration using deep learning," *Ophthalmology*, vol. 128, no. 5, pp. 693–705, 2021.
- [102] H. Lee, B. Ji, H. Chung, and H. C. Kim, "Correlation between optical coherence tomographic hyperreflective foci and visual outcomes after anti-vegf treatment in neovascular age-related macular degeneration and polypoidal choroidal vasculopathy," *Retina*, vol. 36, no. 3, pp. 465–475, 2016.
- [103] K. Ogino, T. Murakami, A. Tsujikawa et al., "Characteristics of optical coherence tomographic hyperreflective foci in retinal vein occlusion," *Retina*, vol. 32, no. 1, pp. 77–85, 2012.
- [104] J.-W. Kang, H. Lee, H. Chung, and H. C. Kim, "Correlation between optical coherence tomographic hyperreflective foci and visual outcomes after intravitreal bevacizumab for macular edema in branch retinal vein occlusion," *Graefes Archive for Clinical and Experimental Ophthalmology*, vol. 252, no. 9, pp. 1413–1421, 2014.
- [105] A. Tsujikawa, A. Ota, T. Murakami et al., "Subfoveal serous retinal detachment associated with extramacular branch retinal vein occlusion," *Clinical Ophthalmology*, vol. 7, pp. 237–241, 2013.
- [106] M. Michl, X. Liu, A. Kaider, A. Sadeghipour, B. S. Gerendas, and U. Schmidt-Erfurth, "The impact of structural optical coherence tomography changes on visual function in retinal vein occlusion," *Acta Ophthalmologica*, vol. 99, no. 4, pp. 418–426, 2020.
- [107] J. R. Do, S. J. Park, J. P. Shin, and D. H. Park, "Assessment of hyperreflective foci after bevacizumab or dexamethasone treatment according to duration of macular edema in patients with branch retinal vein occlusion," *Retina*, vol. 41, no. 2, pp. 355–365, 2020.
- [108] M. Kuroda, Y. Hiram, M. Hata, M. Mandai, M. Takahashi, and Y. Kurimoto, "Intraretinal hyperreflective foci on spectral-domain optical coherence tomographic images of patients with retinitis pigmentosa," *Clinical Ophthalmology*, vol. 8, pp. 435–440, 2014.
- [109] K. Schuerch, M. Marsiglia, W. Lee, S. H. Tsang, and J. R. Sparrow, "Multimodal imaging of disease-associated pigmentary changes in retinitis pigmentosa," *Retina*, vol. 36, no. 1, pp. S147–S158, 2016.
- [110] Y. Nagasaka, Y. Ito, S. Ueno, and H. Terasaki, "Number of hyperreflective foci in the outer retina correlates with inflammation and photoreceptor degeneration in retinitis

- pigmentosa,” *Ophthalmology Retina*, vol. 2, no. 7, pp. 726–734, 2018.
- [111] Y. Kawaguchi, A. Takahashi, T. Nagaoka, A. Ishibazawa, S. Ishiko, and A. Yoshida, “Retinal and choroidal hyperreflective foci on spectral-domain optical coherence tomographic images in a patient with retinitis pigmentosa accompanied by diabetic retinopathy,” *American Journal of Ophthalmology Case Reports*, vol. 3, pp. 25–30, 2016.
- [112] N. Piri, B. L. W. Nesmith, and S. Schaal, “Choroidal hyperreflective foci in stargardt disease shown by spectral-domain optical coherence tomography imaging,” *JAMA Ophthalmology*, vol. 133, no. 4, pp. 398–405, 2015.
- [113] M. Battaglia Parodi, R. Sacconi, F. Romano, and F. Bandello, “Hyperreflective foci in stargardt disease: 1-year follow-up,” *Graefes Archive for Clinical and Experimental Ophthalmology*, vol. 257, no. 1, pp. 41–48, 2019.
- [114] P. Milani, A. Massacesi, S. Moschini et al., “Multimodal imaging and diagnosis of myopic choroidal neovascularization in Caucasians,” *Clinical Ophthalmology*, vol. 10, pp. 1749–1757, 2016.
- [115] X.-T. Hu, Q.-T. Pan, J.-W. Zheng, and Z.-D. Zhang, “Foveal microstructure and visual outcomes of myopic macular hole surgery with or without the inverted internal limiting membrane flap technique,” *British Journal of Ophthalmology*, vol. 103, no. 10, pp. 1495–1502, 2019.
- [116] Z. Habet-Wilner, D. Zur, M. Goldstein et al., “Macular findings on optical coherence tomography in cat-scratch disease neuroretinitis,” *Eye*, vol. 25, no. 8, pp. 1064–1068, 2011.
- [117] P. A. Keane, M. Allie, S. J. Turner et al., “Characterization of birdshot chorioretinopathy using extramacular enhanced depth optical coherence tomography,” *JAMA Ophthalmology*, vol. 131, no. 3, pp. 341–350, 2013.
- [118] R. Agrawal, R. Arora, P. A. Keane, A. Agarwal, and C. Pavesio, “Morphometric features on enhanced depth imaging optical coherence tomography scans in idiopathic posterior uveitis or panuveitis,” *International Ophthalmology*, vol. 38, no. 3, pp. 993–1002, 2018.
- [119] M. Gobuty, M. Adhi, S. P. Read, and J. S. Duker, “Visual response and anatomical changes on sequential spectral-domain optical coherence tomography in birdshot chorioretinopathy treated with local corticosteroid therapy,” *International Journal of Retina and Vitreous*, vol. 2, no. 1, p. 9, 2016.
- [120] D. S. Grewal, M. L. O’Sullivan, M. Kron, and G. J. Jaffe, “Association of disorganization of retinal inner layers with visual acuity in eyes with uveitic cystoid macular edema,” *American Journal of Ophthalmology*, vol. 177, pp. 116–125, 2017.
- [121] B. Berasategui, A. Fonollosa, J. Artaraz et al., “Behavior of hyperreflective foci in non-infectious uveitic macular edema, a 12-month follow-up prospective study,” *BMC Ophthalmology*, vol. 18, no. 1, p. 179, 2018.

Research Article

Optic Nerve Head Hemoglobin Levels in Glaucoma: A Structural and Functional Correlation Study

Janaina A. G. Rocha,^{1,2,3} Diego T. Dias,^{1,4} Maria Betânia C. Lemos,^{2,3} Fábio N. Kanadani,^{1,3,5} Augusto Paranhos Jr.,¹ Carolina P. B. Gracitelli ^{1,6} and Tiago S. Prata ^{1,2,5}

¹Department of Ophthalmology, Federal University of São Paulo, São Paulo, Brazil

²Glaucoma Unit, Opty Group Brazil, São Paulo, Brazil

³Instituto de Olhos Ciências Médicas—IOCM, Belo Horizonte, Brazil

⁴Hospital de Olhos de Sergipe—HOS, Aracaju, Brazil

⁵Department of Ophthalmology, Mayo Clinic, Jacksonville, FL, USA

⁶Centro de Estudos Alcides Hirai, Ver Mais Oftalmologia, Vinhedo, São Paulo, Brazil

Correspondence should be addressed to Tiago S. Prata; t.prata0807@gmail.com

Received 3 April 2021; Revised 25 June 2021; Accepted 16 September 2021; Published 7 October 2021

Academic Editor: Gianluca Scuderi

Copyright © 2021 Janaina A. G. Rocha et al. This is an open access article distributed under the Creative Commons Attribution License, which permits unrestricted use, distribution, and reproduction in any medium, provided the original work is properly cited.

Purpose. To investigate structural and functional correlations in glaucoma patients using optic nerve head hemoglobin (ONH Hb) measurements as determined by automated colorimetric analysis of conventional retinography. **Methods.** We prospectively enrolled healthy participants and glaucomatous patients with a wide range of disease stages. All participants underwent visual field (VF) testing (standard automated perimetry, SAP), color fundus imaging (mydriatic retinography), and peripapillary retinal nerve fiber layer (pRNFL) assessment through spectral-domain optical coherence tomography (SD-OCT). Software Laguna ONhE was used to estimate the amount of ONH Hb and to determine the glaucoma discriminant function (GDF) index. Scatter plots were constructed, and regression analysis was used to investigate the correlations between GDF, average pRNFL thickness, and VF mean deviation (VFMD) index values. A secondary analysis was performed to compare each parameter between three different glaucoma groups divided according to VFMD values (mild, >−6 dB; moderate, −6 to −12 dB; and advanced, <−12 dB). **Results.** One hundred ninety-six eyes from 123 participants (69 with glaucoma and 54 controls) were enrolled. Overall, all parameters evaluated differed significantly between glaucomatous and control eyes ($p \leq 0.001$). The comparison of each parameter according to groups of disease stages revealed significant differences between controls and each of the glaucomatous groups ($p < 0.001$). More pronounced changes in GDF values were observed in early disease stages. We found significant nonlinear correlations between GDF and VFMD values ($R^2 = 0.295$, $p < 0.001$) and between pRNFL thickness and VFMD ($R^2 = 0.598$, $p < 0.001$). A linear correlation was found between GDF and pRNFL thickness values ($R^2 = 0.195$, $p < 0.001$). **Conclusion.** Our results showed significant associations between ONH Hb values and both structural and functional damage in glaucoma obtained by SD-OCT and SAP, respectively. The nonlinear correlation we found and the GDF behavior along different disease stages suggest that ONH Hb levels' reduction may precede visual function changes in early glaucoma stages.

1. Introduction

Glaucoma consists in the main cause of irreversible blindness worldwide [1]. The disease is considered as a progressive and chronic optic neuropathy, characterized by specific changes on the optic nerve head (ONH), peripapillary retinal nerve fiber layer (pRNFL), and visual field

(VF) [2, 3]. Disease control and blindness prevention are strictly related to early diagnosis [2, 3]. However, the diagnosis of glaucoma can be challenging in the early stages of the disease, especially for general ophthalmologists [4, 5]. Taking this into account, it is essential to perform the correlation between structural and functional changes. Anatomical evaluation can be performed through

stereoscopic retinography [6] and automated quantitative exams such as optical coherence tomography (OCT) which were developed with the aim of contributing to the diagnosis of the disease [7–9]. Nevertheless, the high cost can represent a limitation to the access of the referred diagnostic tools.

Considering the pathological mechanisms of glaucoma, vascular dysfunction has been related to the optic nerve glaucomatous lesion [10]. The access to these vascular changes can be achieved through some diagnostic tests. At first, one can mention the evaluation of the ocular blood flow, through nearby vessels, using echo Doppler [11]. Other tests were developed to measure oxygen concentration in the optic nerve [12], blood flow, and vascular structure with the emergence and clinical application of OCT angiography (OCT-A) [13].

Previous studies have evaluated the hypothesis of a relationship between tissue perfusion and the level of hemoglobin (Hb) and oxygenation. Tissues with adequate perfusion demonstrate a good level of Hb, whereas low levels occur in tissue loss [14, 15]. Some studies have proposed a simple method for measuring hemoglobin levels in the ONH, assessing conventional retinography through automated colorimetric analysis, using software Laguna ONhE [16–19]. These preceding data have demonstrated that lower levels of optic nerve head hemoglobin (ONH Hb) are found in patients with established glaucoma, along with high reproducibility results, both in glaucomatous and non-glaucomatous eyes [15].

All these considered, we sought to investigate the correlation between the levels of ONH Hb, assessed by automated colorimetric analysis, and the levels of structural and functional damage, obtained by spectral-domain optical coherence tomography (SD-OCT) and standard automated perimetry (SAP), respectively, in glaucomatous patients.

2. Methods

This study protocol, according to the tenets of the Declaration of Helsinki, was approved by the ethics committee and the institutional review board of the Federal University of São Paulo (CEP: 4.055.180). Written informed consent was obtained by all participants prior to enrollment and examination.

2.1. Participants. In this observational cross-sectional study, we included consecutive healthy individuals and patients with primary open-angle glaucoma attending to the Glaucoma Sector of Hospital Medicina dos Olhos (São Paulo, Brazil) between May 2020 and January 2021.

Glaucoma was defined as the presence of glaucomatous optic neuropathy (GON) associated or not with the corresponding VF alteration. The criteria used to define the disease were the same as those used by our research group in previous studies [20, 21]. GON was considered in the presence of a vertical cup-to-disc ratio (VCDR) greater than or equal to 0.6, asymmetry of VCDR between the eyes (greater than 0.2), detection of localized or diffuse pRNFL

defects, or neuroretinal rim defects, without other pathologies that could explain these changes. We adopted VF glaucomatous defect in the SAP (Humphrey SITA—Standard 24-2, Carl Zeiss Meditec, Dublin, CA), if there were, on the pattern deviation plot, three or more points in clusters with a probability of less than 5% (points directly above and below the blind spot or on the edge of the field were excluded), a pattern standard deviation index with a probability of less than 5%, or the result outside the normal limits on glaucoma hemifield test.

The following exclusion criteria were adopted: age ≤ 18 years, previous ocular trauma or posterior segment intraocular surgery, significant media opacity, difficulty in performing the exams, diagnosis of primary angle closure or secondary glaucoma, and presence of ocular diseases other than glaucoma that could influence the results, such as diabetic or hypertensive retinopathy and macular edema.

Regarding the control group, nonglaucomatous patients were included, demonstrating normal appearance of the optic disc, such as a VCDR less than 0.6, absence of defects on the neuroretinal rim or pRNFL, and intraocular pressure (IOP) less than 21 mmHg, without treatment [20].

2.2. Study Protocol. Complete ophthalmological examination was performed in all participants. This evaluation included clinical history, best-corrected visual acuity, slit-lamp biomicroscopy, IOP measurement with Goldmann applanation tonometry, gonioscopy, ultrasound pachymetry, dilated fundus examination, VF testing (Humphrey SITA—Standard 24-2, Carl Zeiss Meditec, Dublin, CA), color fundus imaging (mydriatic fundus retinography Canon CR-2; Canon, Tokyo, Japan), and pRNFL and topographic ONH measurements based on SD-OCT (RTVue-100 OCT; Optovue Inc., Fremont, CA).

Accepted reliability indices for this protocol include patients' experience in performing VF testing (at least 3 previous exams). Patients were excluded from the study if the exams presented $>15\%$ false positives or $>33\%$ loss of fixation or false negative. Additionally, during SAP review, the exam was eliminated in the presence of some artifacts such as edge defects, inattention or loss of fixation, fatigue effect, or alterations indicative of pathologies other than glaucoma.

The color fundus retinography was then analyzed by Laguna ONhE software. The full description of the program was presented in a previous study [16]. Summarizing, Laguna ONhE analyzes conventional fundus photographs to measure the amount of ONH Hb. Software considers three spectral components of ONH photographs: red, green, and blue. The red component is reflected by ONH areas with a high Hb content. On the contrary, a smaller proportion of the red light, compared to green and blue components, is reflected in areas with low Hb content. The analysis of various formulas, based on the reflected amounts of red, green, and blue light, was almost linearly proportional to the amount of Hb present [16]. Figure 1 demonstrates examples of patients with normal and glaucomatous papilla and the respective pseudo-images indicating the Hb levels. Finally,

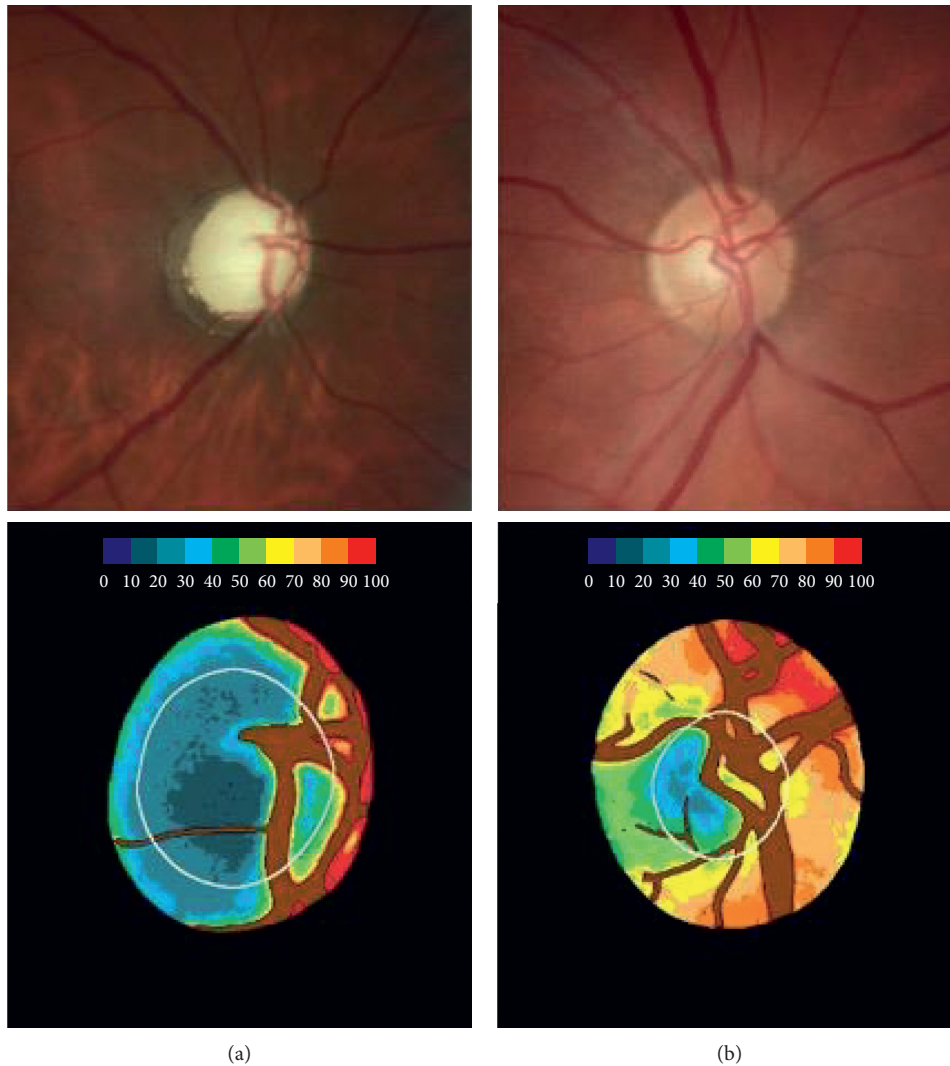


FIGURE 1: Examples of the optic nerve head: glaucomatous (a) and normal (b). Retinographies of the optic disc are represented in the upper images, and their pseudo-images referring the amount of hemoglobin are present in the lower images. A colorimetric scale (at the top of the lower images) indicates the amount of hemoglobin correspondent.

software determines an index of glaucoma discriminant function (GDF), based on colorimetric analysis and OHN Hb levels [16]. This index was performed by dividing the ONH into 3 concentric rings, and each one of them was divided into 8 parts, a total of 24 sectors. The sectors that showed the greatest difference in the amount of Hb, between eyes of patients with glaucoma and control, were those located in the vertical region, especially sectors 8 and 20, as shown in a previous study. From this, the GDF takes into account the slope of the Hb amount with the mean of these specific sectors (8 and 20) presenting 89% sensitivity at 95% specificity [16].

2.3. Sampling and Statistical Analysis. The sample size was calculated to estimate the correlation between GDF and pRNFL/VF mean deviation (VFMD). At the significance level of 5% and minimum power of 90% and considering a minimum value of 0.5 for correlation, 39 individuals are required in the sample.

Clinical and demographic data were demonstrated through descriptive analysis. The Shapiro–Wilk test was used to assess whether the data had a normal distribution. Normally distributed data were presented as mean and standard deviation, and nonnormally distributed data were presented as median and interquartile intervals. Regarding the comparison between groups, for continuous normally distributed variables, the independent samples *t*-test was performed, while for those nonnormally distributed, the Mann–Whitney test was used. The χ^2 test was performed to compared categorical data. For structure-functional relationship evaluation, data of the glaucoma patients were analyzed, scatter plots were constructed, and regression analysis was used to investigate the correlations between GDF, SD-OCT average pRNFL thickness, and VFMD index values. Additionally, a correlation subanalysis considering disease stage was performed. Taking into consideration VFMD index values, patients were divided into 3 groups, mild (>-6 dB), moderate (-6 to -12 dB), and advanced

glaucoma (<-12 dB), according to Hoddap et al. [22]. Computerized analysis was performed using R version 4.0.2. p value <0.05 was considered significant.

3. Results

A total of 196 eyes from 123 participants (69 patients with glaucoma and 54 controls) were included in this study. Twenty-four eyes from 16 patients were excluded from the analysis due to low reliability in the VF test or poor-quality images on retinography. There was no significant difference in age, gender, race, and IOP between the two groups ($p \geq 0.10$ for all comparisons). Glaucoma patients present thinner central corneal thickness (CCT) compared to the control group ($p = 0.004$). Visual field index (VFI), VFMD, and average pRNFL thickness differed significantly between patients and controls ($p < 0.001$ for all comparisons), as expected. Table 1 provides clinical and ocular characteristics of included patients.

Analyzing the history of systemic comorbidities, especially the presence of cardiovascular risk factors (arterial hypertension and/or diabetes mellitus), patients with glaucoma and control did not show differences ($p = 0.32$). There was no statistical difference related to GDF values in the presence or absence of these comorbidities, both in control patients ($p = 0.85$) and in those with glaucoma ($p = 0.33$). In concern to the use of topical hypotensive medications and GDF index values, we did not find any statistical difference between patients using beta-blockers and those who did not use them ($p = 0.10$), as well as for the use of prostaglandin analogues ($p = 0.38$) or alpha-adrenergic agonists ($p = 0.37$).

Regarding the structure-function correlations we investigated in the glaucoma group, we found significant nonlinear correlations between GDF and VFMD values ($R^2 = 0.295$, $p < 0.001$; Figure 2) and between OCT's pRNFL thickness and VFMD values ($R^2 = 0.598$, $p < 0.001$; Figure 3). Additionally, a linear correlation was found between GDF and OCT's RNFL thickness values ($R^2 = 0.195$, $p < 0.001$), as demonstrated in Figure 4.

The comparison of ONH Hb, pRNFL, and functional measurements between controls and glaucomatous eyes (divided according to disease stage; Table 2) revealed significant differences between controls and each of the glaucomatous groups ($p < 0.001$). In addition, although there was a significant difference regarding pRNFL thickness between eyes with moderate and advanced glaucoma, GDF values did not differ significantly between these two groups.

4. Discussion

Improved understanding of the structure-function relationship in patients with glaucoma is essential for diagnosis and monitoring of the disease. Within this scenario, in the last decades, the evolution of OCT imaging devices plays an important role in objective structural assessment. This approach provided significant information, especially regarding the description of both ONH and pRNFL parameters. Nonetheless, in some clinical situations related

to intrinsic ocular characteristics or even technical difficulties (for example, high myopia, tilted discs, advanced glaucoma, or peripapillary atrophies), the use of conventional pRNFL analysis is limited [23–25]. Additionally, cost issues and portability often restrict access to this technology. In our study, we evaluated the relationship between the levels of structural and functional damage in glaucomatous patients, obtained by SD-OCT and SAP, respectively, and ONH Hb values, assessed in a low-cost, noninvasive manner by automated colorimetric analysis. Our results showed a significant association between the evaluated parameters.

There are scant data in the literature regarding structure-functional correlations using ONH Hb values. A previous study has demonstrated a significant correlation between anatomical damage (RNFL thickness) and hemoglobin content in specific sectors of the ONH [19]. In addition, considering functional findings, Gonzalez de la Rosa et al. showed a significant agreement between the GDF index and OCT parameters and perimetry results (Easyfield perimeter) [16]. Mendez-Hernandez et al. also found that the GDF index correlated well with Octopus perimetry indices and Spectralis OCT metrics [26]. It must be highlighted that Gonzalez-Hernandez and Saavedra not only reaffirmed the significant linear correlation between GDF and OCT parameters but also demonstrated the relationship between the indices obtained by Laguna ONhE to be curvilinear when compared to retinal function measured by VF testing [27]. We believe that our findings not only corroborate these initial structure-functional correlation results reported by Gonzalez-Hernandez and Saavedra [27] but also add significant information about different behaviors of each parameter along the disease spectrum. One may perceive (Table 2) that while mean pRNFL thickness gradually diminishes as the disease advances, most changes on GDF values were observed in the early stages of the disease (between controls and mild glaucoma). Conversely, functional status as determined by the VFMD tends to decay in the latter stages (moderate and advanced glaucoma) of the disease. Although this assumption needs further confirmation, it suggests that GDF performance would be more suitable in early disease stages.

We believe it is important to discuss the nature of our main findings. More specifically, what would be the reasons for the nonlinear relationship between ONH Hb measurements and functional status? Initially, the intrinsic evolution of structural-functional glaucomatous damage could partially explain this relationship. It is well known that axonal loss (structural changes) precedes VF loss (functional changes). As a result, especially in the early stages of the disease, structural deterioration may occur without VF correspondence [28–31]. Since the GDF index is an estimation of a more structural parameter, it could lead to the nonlinear structure-functional correlations as we found. It should also be considered that the VFMD index, which is derived from retinal sensitivity measurements, is based on a logarithmic scale, which also contributes to this curvilinear pattern.

At this point, it is important to discuss the main clinical implications of our findings. The knowledge of the

TABLE 1: Demographic and ocular characteristics of study patients.

Variables	Control group	Glaucoma group	<i>p</i> value
Age \pm SD (years)	60.60 \pm 14.21	63.54 \pm 10.46	0.100
Gender (% , W/M)	68.5/31.5	59.4/40.6	0.300
Race (% , C/AD/O)	74.0/3.8/22.2	70.3/9.4/20.3	0.470
Intraocular pressure (mmHg)	13.00 (12.25, 15.00)	13.00 (12.00, 15.00)	0.950
Central corneal thickness (μ m)	537 (517, 553)	506 (482, 528)	0.004
pRNFL thickness (μ m)	103.74 \pm 8.67	83.47 \pm 13.06	<0.001
VFMD index (dB)	-0.76 \pm 2.05	-7.23 \pm 8.02	<0.001
VFI (%)	99 (98, 99)	95 (79.5, 97.5)	0.001
Spherical equivalent (D)	0.5 (-0.5, 2.0)	0.0 (-1.12, 1.37)	0.033
GDF index	16.25 \pm 14.17	-28.02 \pm 19.08	0.0001
VCDR	0.40 \pm 0.18	0.75 \pm 0.13	0.0001

Data are given as mean \pm standard deviation whenever indicated. W: women; M: men; C: Caucasian; AD: African descendants; O: others; pRNFL: peripapillary retinal nerve fiber layer; VFMD: visual field mean deviation; VFI: visual field index; GDF: glaucoma discriminant function; VCDR: vertical cup-to-disc ratio.

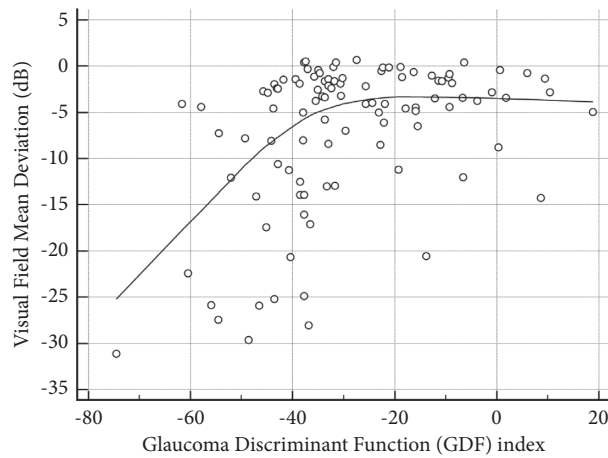


FIGURE 2: Significant nonlinear correlation between the glaucoma discriminant function (GDF) index and visual field mean deviation index values ($R^2 = 0.295$; $p < 0.001$). A LOESS (local regression smoothing) trendline is plotted with a degree of smoothing of 80%.

relationship of glaucoma with some vasospasm phenomena [32, 33], such as migraines [34, 35], syndrome of Raynaud, and peripheral vascular dysregulation [36], and also with sleep apnea [37, 38], supports the idea of the participation of vascular dysfunction in the pathogenesis of glaucoma. However, despite the recent evolution in studies that assess blood flow in the ONH and especially vascular density through OCT-A, the high cost of this technology represents a limitation of its widespread use [12, 39–44]. Within this context, as previously described, the Laguna ONhE program represents a feasible lower cost option, analyzing conventional color retinography, to evaluate the vascular component by estimating Hb levels at the ONH. Although our study does not provide a direct comparison with other methods focusing specifically on vascular changes in the ONH, a recent study comparing the Laguna ONhE program and OCT-A demonstrated that the technologies showed similar performance in diagnosing patients with open-angle glaucoma. The area under the receiver operating characteristic curve for discriminating between glaucomatous and healthy eyes was 0.93 (95% CI: 0.86 to 0.97) for a specific OCT-A parameter and 0.92 (95% CI: 0.86 to 0.97) for the GDF index [45]. We believe the results of our study along

with the existing literature support ONH Hb measurement as a viable and accessible tool for assessing structural damage in glaucoma, likely more related to the vascular component.

Our study presents some limitations and characteristics that should be mentioned. First, our findings should only be extrapolated to this specific population and therefore should not be applied to glaucomatous patients with different patterns. Second, we performed a cross-sectional study. Therefore, we were not able to evaluate the prognostic value of the GDF index nor investigate cause-effect relationships. Third, although it has been shown that age does not seem to significantly influence ONH Hb levels [17], it certainly impacts pRNFL thickness throughout life. This fact may have influenced, in part, our correlation analyses. Finally, some study patients had both eyes included in the analysis without any specific statistical adjustment. Even though this should be considered while interpreting our findings, we believe that such an adjustment would be more indicated for surgical studies, longitudinal analyses, or risk factor studies, rather than a cross-sectional structure-functional analysis as we present herein.

In conclusion, our results showed significant associations between ONH Hb values and both structural and

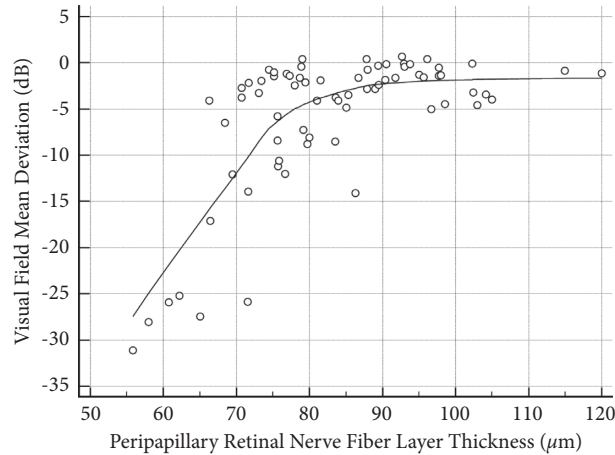


FIGURE 3: Significant nonlinear correlation between peripapillary retinal nerve fiber layer thickness and visual field mean deviation index values ($R^2 = 0.598$; $p < 0.001$). A LOESS (local regression smoothing) trendline is plotted with a degree of smoothing of 80%.

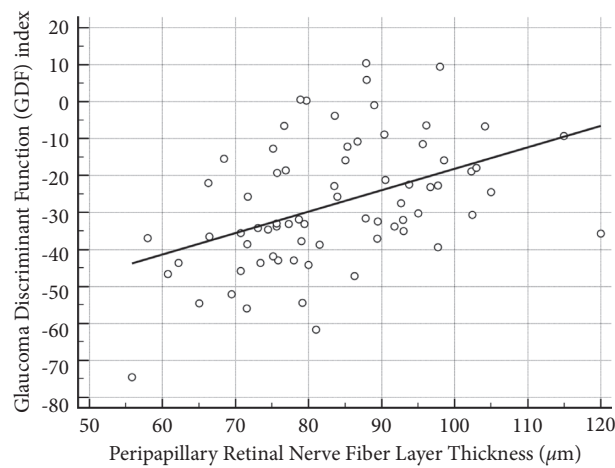


FIGURE 4: Significant linear correlation between peripapillary retinal nerve fiber layer thickness and glaucoma discriminant function (GDF) index values ($R^2 = 0.195$; $p = 0.001$).

TABLE 2: Glaucoma discriminant function index and average peripapillary retinal nerve fiber layer thickness by disease stage.

Variables ^a	Control group ($n = 90$)	Mild glaucoma ($n = 66$)	Moderate glaucoma ($n = 13$)	Advanced glaucoma ($n = 25$)	p value
GDF index	16.25 ± 14.17	-24.59 ± 16.50	-31.65 ± 15.40	-34.26 ± 24.90	$<0.001^b$
pRNFL thickness (μm)	102.27 ± 14.40	87.79 ± 11.68	77.24 ± 4.50	67.60 ± 8.84	$<0.001^c$
VFMD index (dB)	-0.76 ± 2.05	-2.21 ± 1.67	-8.43 ± 1.67	-19.62 ± 6.17	$<0.001^c$

^aData are given as mean \pm SD. ^bEach glaucoma group differed significantly from controls. There was also a significant difference between eyes with mild and advanced glaucoma. ^cEach glaucoma group differed significantly from controls. There were also significant differences between eyes with mild and advanced glaucoma and between eyes with moderate and advanced glaucoma.

functional damage in glaucoma obtained by SD-OCT and SAP, respectively. The nonlinear structure-functional findings and the GDF behavior along different disease stages suggest that ONH Hb levels' reduction may precede visual

function changes in early glaucoma stages. Further longitudinal studies are warranted to evaluate the diagnostic performance of this technique in different types of glaucoma and as a tool for longitudinal monitoring of these patients.

Data Availability

The data used to support the findings of this study are included within the supplementary information file (Excel sheet).

Conflicts of Interest

The authors declare no conflicts of interest.

Supplementary Materials

ONH Hb and VFMD DATA_JO experimental data of the manuscript are included in the supplementary file. (*Supplementary Materials*)

References

- [1] S. Kingman, "Glaucoma is second leading cause of blindness globally," *Bulletin of the World Health Organization*, vol. 82, no. 11, pp. 887-888, 2004.
- [2] J. S. Schuman, M. R. Hee, A. V. Arya et al., "Optical coherence tomography: a new tool for glaucoma diagnosis," *Current Opinion in Ophthalmology*, vol. 6, no. 2, pp. 89-95, 1995.
- [3] R. N. Weinreb, T. Aung, and F. A. Medeiros, "The pathophysiology and treatment of glaucoma: a review," *Journal of the American Medical Association*, vol. 311, no. 18, pp. 1901-1911, 2014.
- [4] R. M. Vessani, R. Moritz, L. Batis, R. B. Zagui, S. Bernardoni, and R. Susanna, "Comparison of quantitative imaging devices and subjective optic nerve head assessment by general ophthalmologists to differentiate normal from glaucomatous eyes," *Journal of Glaucoma*, vol. 18, no. 3, pp. 253-261, 2009.
- [5] C. G. V. S. Franco, M. P. Ávila, and L. Magacho, "Use of computerized campimetry and/or optical coherence tomography for glaucoma diagnosis by non-glaucoma specialists," *Arquivos Brasileiros de Oftalmologia*, vol. 84, no. 2, pp. 113-120, 2021.
- [6] A. Azuara-Blanco, L. J. Katz, G. L. Spaeth, S. A. Vernon, F. Spencer, and I. M. Lanzl, "Clinical agreement among glaucoma experts in the detection of glaucomatous changes of the optic disk using simultaneous stereoscopic photographs," *American Journal of Ophthalmology*, vol. 136, no. 5, pp. 949-950, 2003.
- [7] C. P. B. Gracitelli, R. Y. Abe, and F. A. Medeiros, "Spectral-domain optical coherence tomography for glaucoma diagnosis," *The Open Ophthalmology Journal*, vol. 9, no. 1, pp. 68-77, 2015.
- [8] T. S. Prata, F. S. Lopes, V. G. Prado et al., "In vivo analysis of glaucoma-related features within the optic nerve head using enhanced depth imaging optical coherence tomography," *PLoS One*, vol. 12, no. 7, Article ID e0180128, 2017.
- [9] C. P. B. Gracitelli, P. A. Moreno, M. T. Leite, and T. S. Prata, "Identification of the most accurate spectral-domain optical coherence tomography parameters in eyes with early high-tension and low-tension glaucoma," *Journal of Glaucoma*, vol. 25, no. 10, pp. 854-859, 2016.
- [10] J. Flammer, I. O. Haefliger, S. Orgul, and T. Resink, "Vascular dysregulation: a principal risk factor for glaucomatous damage?" *Journal of Glaucoma*, vol. 8, no. 3, pp. 212-219, 1999.
- [11] A. Harris, R. C. Sergott, G. L. Spaeth, J. L. Katz, J. A. Shoemaker, and B. J. Martin, "Color doppler analysis of ocular vessel blood velocity in normal-tension glaucoma," *American Journal of Ophthalmology*, vol. 118, no. 5, pp. 642-649, 1994.
- [12] J. B. Hickam, H. O. Sieker, and R. Frayser, "Studies of retinal circulation and A-V oxygen difference in man," *Transactions of the American Clinical and Climatological Association*, vol. 71, pp. 34-44, 1959.
- [13] Y. Jia, J. C. Morrison, J. Tokayer et al., "Quantitative OCT angiography of optic nerve head blood flow," *Biomedical Optics Express*, vol. 3, no. 12, pp. 3127-3137, 2012.
- [14] G. Tezel, X. Yang, C. Luo et al., "Hemoglobin expression and regulation in glaucoma: insights into retinal ganglion cell oxygenation," *Investigative Ophthalmology & Visual Science*, vol. 51, no. 2, pp. 907-919, 2010.
- [15] C. Mendez-Hernandez, J. Garcia-Feijoo, P. Arribas-Pardo et al., "Reproducibility of optic nerve head hemoglobin measures," *Journal of Glaucoma*, vol. 25, no. 4, pp. 348-354, 2016.
- [16] M. Gonzalez de la Rosa, M. Gonzalez-Hernandez, J. Sigut et al., "Measuring hemoglobin levels in the optic nerve head: comparisons with other structural and functional parameters of glaucoma," *Investigative Ophthalmology & Visual Science*, vol. 54, no. 1, pp. 482-489, 2013.
- [17] C. Pena-Betancor, M. Gonzalez-Hernandez, F. Fumero-Batista et al., "Estimation of the relative amount of hemoglobin in the cup and neuroretinal rim using stereoscopic color fundus images," *Investigative Ophthalmology & Visual Science*, vol. 56, no. 3, pp. 1562-1568, 2015.
- [18] E. Medina-Mesa, M. Gonzalez-Hernandez, J. Sigut et al., "Estimating the amount of hemoglobin in the neuroretinal rim using color images and OCT," *Current Eye Research*, vol. 41, no. 6, pp. 798-805, 2016.
- [19] M. Gonzalez-Hernandez, J. S. Saavedra, and M. Gonzalez de la Rosa, "Relationship between retinal nerve fiber layer thickness and hemoglobin present in the optic nerve head in glaucoma," *Journal of Ophthalmology*, vol. 2017, Article ID 2340236, 10 pages, 2017.
- [20] F. S. Lopes, S. Dorairaj, D. L. Junqueira, R. L. Furlanetto, L. G. Biteli, and T. S. Prata, "Analysis of neuroretinal rim distribution and vascular pattern in eyes with presumed large physiological cupping: a comparative study," *BMC Ophthalmology*, vol. 14, no. 1, 72 pages, 2014.
- [21] F. S. Lopes, I. Matsubara, I. Almeida et al., "Structure-function relationships in glaucoma using enhanced depth imaging optical coherence tomography-derived parameters: a cross-sectional observational study," *BMC Ophthalmology*, vol. 19, no. 52, pp. 52-58, 2019.
- [22] E. Hodapp, R. K. Parrish, and D. R. Anderson, *Clinical Decisions in Glaucoma*, Mosby, Maryland Heights, MO, USA, 1993.
- [23] F. M. Rauscher, N. Sekhon, W. J. Feuer, and D. L. Budenz, "Myopia affects retinal nerve fiber layer measurements as determined by optical coherence tomography," *Journal of Glaucoma*, vol. 18, no. 7, pp. 501-505, 2009.
- [24] N. R. Kim, H. Lim, J. H. Kim, S. S. Rho, G. J. Seong, and C. Y. Kim, "Factors associated with false positives in retinal nerve fiber layer color codes from spectral-domain optical coherence tomography," *Ophthalmology*, vol. 118, no. 9, pp. 1774-1781, 2011.
- [25] G. T. Chong and R. K. Lee, "Glaucoma versus red disease: imaging and glaucoma diagnosis," *Current Opinion in Ophthalmology*, vol. 23, no. 2, pp. 79-88, 2012.
- [26] C. Mendez-Hernandez, I. Rodriguez-Uña, M. Gonzalez-de-la Rosa, P. Arribas-Pardo, and J. Garcia-Feijoo, "Glaucoma

- diagnostic capacity of optic nerve head haemoglobin measures compared with spectral domain OCT and HRT III confocal tomography,” *Acta Ophthalmologica*, vol. 94, no. 7, pp. 697–704, 2016.
- [27] M. Gonzalez-Hernandez and J. F. S. Saavedra, “Reproducibilidad de la aplicación laguna ONhE con segmentación automática de los límites de la cabeza del nervio óptico, excavación y anillo euroretiniano: validación de nuevos algoritmos,” Doctoral Dissertation, University of La Laguna, San Cristóbal de La Laguna, Spain, 2017.
- [28] N. A. Lutaka, R. A. Grochowski, and N. Kasahara, “Correlation between visual field index and other functional and structural measures in glaucoma patients and suspects,” *Journal of Ophthalmic and Vision Research*, vol. 12, pp. 53–57, 2017.
- [29] A. Rao, “Comparison of relation between visual function index and retinal nerve fiber layer structure by optical coherence tomography among primary open angle glaucoma and primary angle closure glaucoma eyes,” *Oman Journal of Ophthalmology*, vol. 7, no. 1, pp. 9–12, 2014.
- [30] G. Wollstein, L. Kagemann, R. A. Bilonick et al., “Retinal nerve fibre layer and visual function loss in glaucoma: the tipping point,” *British Journal of Ophthalmology*, vol. 96, no. 1, pp. 47–52, 2012.
- [31] S. A. Banegas, A. Antón, A. Morilla et al., “Evaluation of the retinal nerve fiber layer thickness, the mean deviation, and the visual field index in progressive glaucoma,” *Journal of Glaucoma*, vol. 25, no. 3, pp. e229–e235, 2016.
- [32] P. Gasser, J. Flammer, U. Guthauser, and F. Mahler, “Do vasospasms provoke ocular diseases?” *Angiology*, vol. 41, no. 3, pp. 213–220, 1990.
- [33] D. C. Broadway and S. M. Drance, “Glaucoma and vasospasm,” *British Journal of Ophthalmology*, vol. 82, no. 8, pp. 862–870, 1998.
- [34] G. Gramer, B. H. F. Weber, and E. Gramer, “Migraine and vasospasm in glaucoma: age-related evaluation of 2027 patients with glaucoma or ocular hypertension,” *Investigative Ophthalmology & Visual Science*, vol. 56, no. 13, pp. 7999–8007, 2015.
- [35] C. Cursiefen, M. Wisse, S. Cursiefen, A. Jünemann, P. Martus, and M. Korth, “Migraine and tension headache in high-pressure and normal-pressure glaucoma,” *American Journal of Ophthalmology*, vol. 129, no. 1, pp. 102–104, 2000.
- [36] J. Mallick, L. Devi, P. Malik, and J. Mallick, “Update on normal tension glaucoma,” *Journal of Ophthalmic and Vision Research*, vol. 11, no. 2, pp. 204–208, 2016.
- [37] O. Faridi, S. C. Park, J. M. Liebmann, and R. Ritch, “Glaucoma and obstructive sleep apnoea syndrome,” *Clinical & Experimental Ophthalmology*, vol. 40, no. 4, pp. 408–419, 2012.
- [38] P.-W. Lin, M. Friedman, H.-C. Lin, H.-W. Chang, M. Wilson, and M.-C. Lin, “Normal tension glaucoma in patients with obstructive sleep apnea/hypopnea syndrome,” *Journal of Glaucoma*, vol. 20, no. 9, pp. 553–558, 2011.
- [39] J. Wu, R. T. Sebastian, C. J. Chu, F. McGregor, A. D. Dick, and L. Liu, “Reduced macular vessel density and capillary perfusion in glaucoma detected using OCT angiography,” *Current Eye Research*, vol. 44, no. 5, pp. 533–540, 2019.
- [40] L. Liu, Y. Jia, H. L. Takusagawa et al., “Optical coherence tomography angiography of the peripapillary retina in glaucoma,” *JAMA Ophthalmology*, vol. 133, no. 9, pp. 1045–1052, 2015.
- [41] R. Igarashi, S. Ochiai, T. Togano et al., “Foveal avascular zone measurement via optical coherence tomography angiography and its relationship with the visual field in eyes with open-angle glaucoma,” *Journal of Glaucoma*, vol. 29, no. 6, pp. 492–497, 2020.
- [42] L. Van Melkebeke, J. Barbosa-Breda, M. Huygens, and I. Stalmans, “Optical coherence tomography angiography in glaucoma: a review,” *Ophthalmic Research*, vol. 60, no. 3, pp. 139–151, 2018.
- [43] Y. Jia, E. Wei, X. Wang et al., “Optical coherence tomography angiography of optic disc perfusion in glaucoma,” *Ophthalmology*, vol. 121, no. 7, pp. 1322–1332, 2014.
- [44] S. Moghimi, C. Bowd, L. M. Zangwill et al., “Measurement floors and dynamic ranges of OCT and OCT angiography in glaucoma,” *Ophthalmology*, vol. 126, no. 7, pp. 980–988, 2019.
- [45] C. Mendez-Hernandez, S. Wang, P. Arribas-Pardo et al., “Diagnostic validity of optic nerve head colorimetric assessment and optical coherence tomography angiography in patients with glaucoma,” *British Journal of Ophthalmology*, vol. 105, no. 7, pp. 957–963, 2020.

Review Article

Near-Infrared Reflectance Imaging in Retinal Diseases Affecting Young Patients

Solmaz Abdolrahimzadeh , **Chiara Ciancimino** , **Flaminia Grassi** , **Edoardo Sordi** ,
Serena Fragiotta , and **Gianluca Scuderi** 

Ophthalmology Unit, "Sapienza" University of Rome, NESMOS Department, St. Andrea Hospital, Via di Grottarossa 1035/1039, Rome, Italy

Correspondence should be addressed to Serena Fragiotta; serena.fragiotta@uniroma1.it

Received 5 January 2021; Revised 4 June 2021; Accepted 13 July 2021; Published 31 July 2021

Academic Editor: Mário Monteiro

Copyright © 2021 Solmaz Abdolrahimzadeh et al. This is an open access article distributed under the Creative Commons Attribution License, which permits unrestricted use, distribution, and reproduction in any medium, provided the original work is properly cited.

Near-infrared reflectance (NIR) is a noninvasive, contactless, and rapid in vivo imaging technique for visualizing subretinal alterations in the photoreceptor layer, retinal pigment epithelium, and choroid. The present report describes the application of this imaging method in retinal and choroidal pathologies affecting young patients where scarce cooperation, poor fixation, and intense glare sensation can result in a challenging clinical examination. A literature search of the MEDLINE database was performed using the terms "near-infrared reflectance" and "spectral-domain optical coherence tomography." Articles were selected if they described the diagnostic use of NIR in children or young adults. Of 700 publications, 42 manuscripts published between 2005 and 2020 were inherent to children or young adults and were considered in this narrative literature review. The first disease category is the phakomatoses where NIR is essential in visualizing choroidal alterations recognized as cardinal biomarkers in neurofibromatosis type 1, microvascular retinal alterations, and retinal astrocytic hamartomas. Another diagnostic application is the accurate visualization of crystals of various nature, including the glistening crystals that characterize Bietti crystalline dystrophy. Acute macular neuropathy and paracentral acute middle maculopathy represent a further disease category with young adulthood onset where NIR is not only diagnostic but also essential to monitor disease progression. A further interesting clinical application is to facilitate the detection of laser-induced maculopathy where funduscopy examination can be normal or subnormal. In conclusion, NIR imaging has a noninterchangeable role in diagnosing certain retinal diseases, especially in children and young adults where there is scarce collaboration and a lack of evident clinical findings. Moreover, this technique can reveal unique retinal and choroidal biomarkers highly specific to rare conditions.

1. Introduction

Near-infrared reflectance (NIR) imaging is a noninvasive, noncontact, and rapid in vivo examination currently extensively available for ophthalmologists. Most images are acquired simultaneously with cross-sectional spectral-domain optical coherence tomography (SDOCT) in routine clinical practice. Specifically, the technique enables visualizing subretinal alterations located in the retinal photoreceptor layer, the retinal pigmented epithelium (RPE), and choroid [1]. The basis is a long excitation wavelength (~820 nm diode laser) that penetrates the optic media and

enables visualizing the retina and choroid in detail [2]. Changes in reflection and absorption of light through retinal tissues enhance visualization of structures beneath the retinal pigment epithelium (RPE) and melanin [1, 3]. Images often correlate with blue-light fundus autofluorescence (FAF); however, NIR demonstrates superiority in revealing sub-RPE lesions. This is due to a more substantial absorbance of monochromatic light of a shorter wavelength (480 nm) by melanin and lipofuscin granules at the RPE level [3, 4]. Highly reflective structures at the subretinal and sub-RPE level are enhanced and better recognized. For instance, hyperreflective crystalline deposits representing cholesterol

crystals appear as intensely reflective plaques, while calcifications or calcified drusen are appreciated as roundish lesions with a glistening appearance [5–7]. The glistening appearance is also characteristic of crystalline deposits in Bietti crystalline dystrophy [8]. Such similarities in reflectance between inherited retinal dystrophy and age-related changes can also be seen in retinitis punctata albescens and reticular pseudodrusen [9].

NIR has gained widespread use in ophthalmology in the last decade. The present report underlines the importance of this imaging method in retinal and choroidal pathologies affecting young patients where scarce cooperation, poor fixation, and intense glare sensation can make fundus examination challenging.

2. Methods

A literature search of the MEDLINE database was performed using the terms “near-infrared reflectance (NIR)” and “spectral-domain optical coherence tomography” for articles in English accessed through December 2020. The articles were selected if they described the diagnostic use of NIR in children or young adults. Of 700 publications, 42 manuscripts published between 2005 and 2020 were inherent to children or young adults and are described in this narrative literature review. Reference lists of the selected manuscripts were also analysed to retrieve other relevant studies.

3. Neuro-Oculocutaneous Syndromes/ Phakomatosis

Neurofibromatosis type 1 (NF1), tuberous sclerosis complex (TSC), and Sturge–Weber syndrome (SWS) are neuro-oculocutaneous diseases often classified among the phakomatoses [10]. Multimodal imaging methods enable facilitated visualization of retinal and choroidal changes and have improved diagnostic and management strategies in these diseases.

3.1. Neurofibromatosis Type 1. NF1 is the most common disease in the phakomatoses, with a prevalence of 1:4000 individuals. This autosomal dominant disorder is diagnosed based on clinical findings established in 1988 by the National Institute of Health (NIH) consensus development statement. A minimum of 2 of the following major criteria are required for diagnosis: 6 or more café au lait spots, axillary or inguinal freckling, 2 or more cutaneous neurofibromas, 1 plexiform neurofibroma, distinctive osseous lesions, optic glioma, 2 or more iris Lisch nodules, and a first-degree relative with NF1 [11]. From the early 2000s, a few reports underlined the detection of choroidal abnormalities in this disorder using imaging methods [12, 13] and the first large cohort study was conducted in 2012 by Viola et al. [14]. Through the concomitant use of NIR imaging and SDOCT, hyperreflective rounded or patchy nodules were associated with hyperreflective signals in choroidal tissue, respectively (Figures 1 and 2). The prevalence of choroidal nodules detected by NIR was 71% in the paediatric population, a much higher

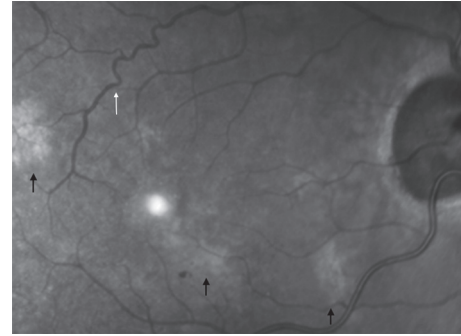


FIGURE 1: Near-infrared reflectance fundus image in neurofibromatosis type 1 (NF1). Hyperreflective choroidal alterations typical of NF1 are shown with black arrows, corkscrew retinal vascular alteration is shown with a white arrow.

frequency than the NIH ophthalmic diagnostic criteria of 43% for iris Lisch nodules [14]. Subsequent literature published on the topic confirmed NIR as a valid and reliable diagnostic imaging method in revealing choroidal abnormalities with a very high interobserver agreement in NF1 patients [15–17].

In recent years, Abdolrahimzadeh et al. described retinal microvasculature abnormalities (RVA) in NF1 using NIR imaging (Figure 1) [18]. These lesions were later confirmed in further studies on larger patient populations [16, 19]. RVA in NF1 are characterized by corkscrew and moyamoya-like vessel configurations with a tendency to increase with age. RVA have high diagnostic specificity with a positive predictive value of 100% [16]. A recently reported additional feature detected with NIR in NF1 patients is prominent choroidal vessels (Figure 2) [20].

NIR imaging is a sensitive, noninvasive, and reproducible examination that enables the detection of choroidal alterations, RVA, and enlarged choroidal vessels in NF1 patients. Choroidal alterations, detected with NIR, have been proposed as an additional diagnostic criterion in NF1 along with the original NIH criteria.

3.2. Tuberous Sclerosis Complex. Tuberous sclerosis complex (TSC), classified in the phakomatoses, is a multisystemic disease characterized by hamartomas that involve the central nervous system, eye, skin, heart, kidneys, liver, and lung. The estimated incidence and prevalence are 1/6800 and 1/15000, respectively, with 50% to 84% of sporadic cases [21]. Retinal astrocytic hamartoma (RAH) may be the first clinical sign and is a hallmark of TSC reported in 44% to 48% in two large case series [22, 23]. Diagnosis of typical RAH has traditionally been through fundus examination, but recent advances in imaging facilitate the detection of lesions using NIR and SDOCT [24].

On ophthalmoscopic examination, RAH are divided into type 1 lesions that are flat and translucent or type 2 lesions that are elevated and multilobar with a “mulberry-like” appearance commonly associated with calcifications [23, 25]. Nyboer et al. reported 116 patients with TSC and described that translucent lesions could be easily overlooked

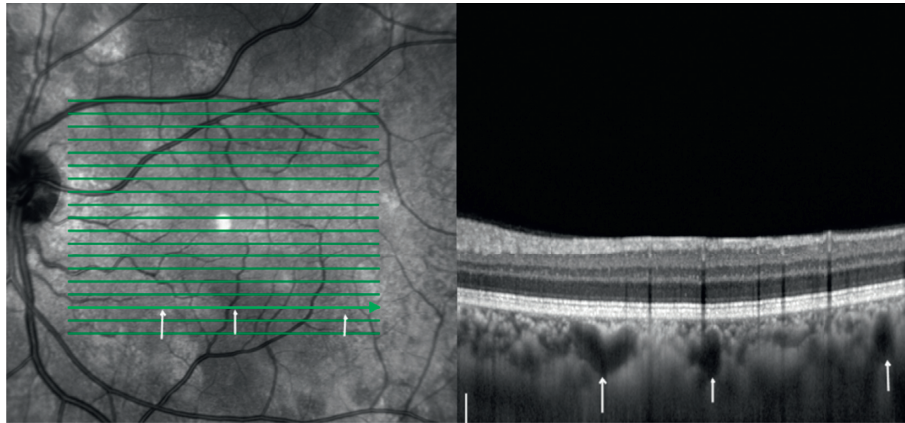


FIGURE 2: Near-infrared reflectance (NIR) and cross-sectional enhanced-depth imaging spectral-domain optical coherence tomography (SDOCT) image in neurofibromatosis type 1. On the NIR image, white/grey rounded or patchy choroidal alterations typical of NF1 are evident and arrows indicate faint hyperreflective choroidal vessels. On the SDOCT cross-sectional image, arrows indicate dilated choroidal vessels.

on ophthalmoscopic examination due to only a slight difference in the background fundus color compared to lesions [23]. This difficulty in the detection of RAH can be overcome with NIR imaging, which reveals areas of hyperreflectivity that correspond to subtle thickening of the retinal nerve fiber layer (RNFL) or elevated honeycomb-like multicavitary intraretinal masses within the RNFL on SDOCT (Figure 3) [26–28].

Therefore, NIR and SDOCT are sensitive imaging modalities that enable detecting and localizing even small translucent RAH that are not readily visible on fundus ophthalmoscopy. This facilitates the diagnosis and follow-up of TSC patients where the examination is hindered by uncooperative patients or concomitant neurological or psychological conditions that characterize the disease.

3.3. Sturge–Weber Syndrome. The Sturge–Weber syndrome (SWS) is a neuro-oculocutaneous disease characterized by leptomeningeal angiomas, ipsilateral facial naevus flammeus, congenital glaucoma, and diffuse choroidal hemangioma. SWS is diagnosed during infancy or childhood, where ophthalmological examination of patients is challenging and a fast and efficient imaging technique is fundamental. Enhanced-depth imaging SDOCT penetrates the RPE and enables assessing choroidal hemangiomas and correlated retinal complications. A recent report of an 8-year-old patient revealed a diffuse choroidal hemangioma characterized by multiple hyperreflective dots surrounded by hyporefective rings on NIR. These alterations corresponded to focal alterations of the RPE-photoreceptor layer on SDOCT images and the white dot-shaped “microdrusen-like” alterations of the retina (Figure 4) [29].

3.4. Congenital Hamartomas. The congenital simple hamartoma of the RPE (CSHRPE) is a rare benign pigmented lesion found in phakomatoses [30]. The existing literature shows the role of NIR in delineating a hyperreflective lesion otherwise not clearly detectable on color

fundus photography [31, 32]. Gass described this alteration as a hamartomatous malformation involving the RPE, retina, retinal vasculature, and overlying vitreous [33]. SDOCT enables appreciating the structure of these tumours in great detail. Furthermore, as the boundaries of combined hamartomas can be hard to distinguish clinically, NIR imaging facilitates delineating both the edges of the tumour and the extent of macular involvement in view of possible surgical management [34].

4. Hereditary Fundus Dystrophies

Hereditary fundus dystrophies commonly manifest during childhood and young adulthood resulting in profound visual impairment. As these diseases affect the RPE, photoreceptors, and the choriocapillaris complex, multimodal imaging is essential in the diagnostic work-up. NIR imaging is particularly indicated in patients with Bietti crystalline dystrophy (BCD) [8] and occult macular dystrophy, whereas NIR-autofluorescence (NIR-AF), with 787 nm excitation and 830 nm emission wavelength, is preferred in Best vitelliform and Stargardt dystrophy [35, 36].

4.1. Bietti Crystalline Dystrophy. Bietti crystalline dystrophy (BCD) is a rare autosomal recessive disease characterized by the deposition of crystalline material in the cornea, retina, RPE, and the choroid. CYP4V2 was identified as the causative gene in 2004 [37]. Retinal crystalline deposits are a characteristic feature in BCD; however, it is not always easy to differentiate these from other small deposits associated with other diseases. Diagnosis is particularly challenging when chorioretinal atrophy has progressed and only a few deposits are observed. Oishi et al. [8] considered NIR as the most practical imaging method in differentiating patients with BCD and CYP4V2 mutations from other chorioretinal dystrophies with crystalline-like retinal deposits. Although genetic testing is necessary to confirm the diagnosis, NIR is an essential first-step methodology with a sensitivity and specificity of 100% in identifying CYP4V2 mutation-positive

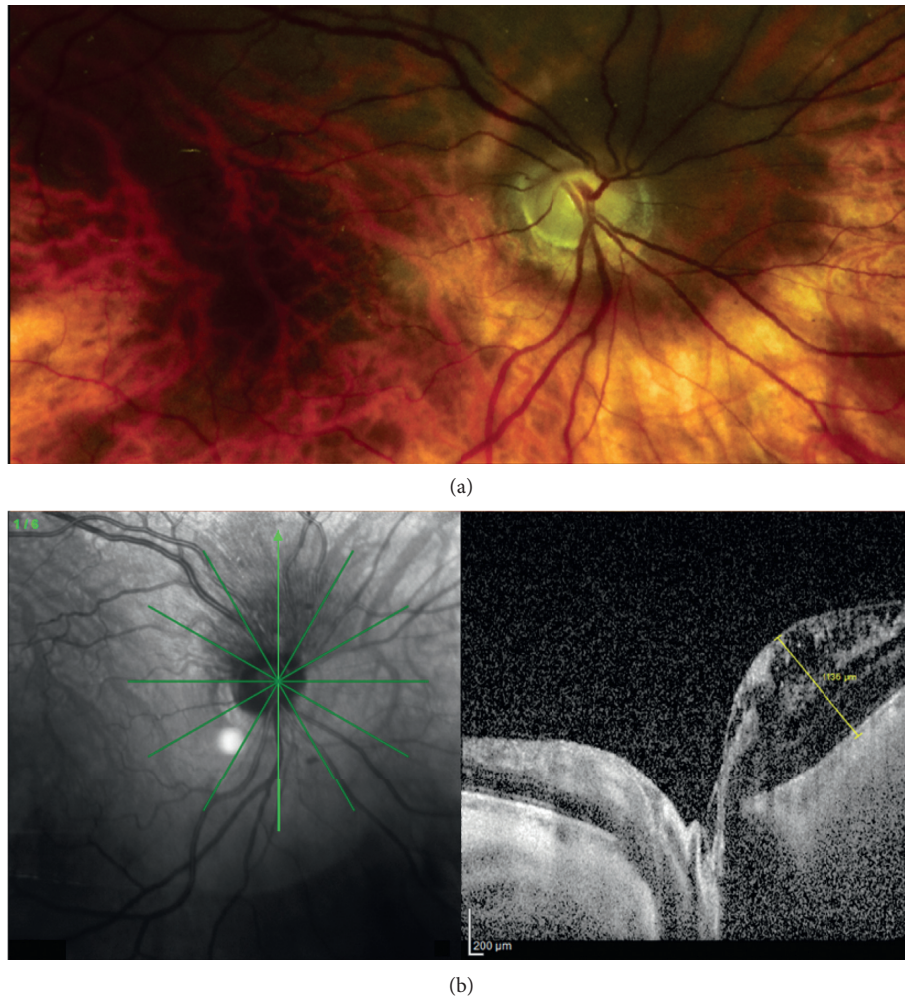


FIGURE 3: (a) Fundus image of the right eye. The fundus appearance is unremarkable, and retinal astrocytic hamartoma is not evident. (b) Near-infrared reflectance (NIR) and cross-sectional spectral-domain optical coherence tomography (SDOCT) image features of a peripapillary retinal astrocytic hamartoma (RAH) in the right eye of a patient with neurofibromatosis type 1. (a) NIR shows a shadowed area in the superior peripapillary margin of the optic disc; (b) SDOCT image at presentation shows the origin and expansion of a RAH in the retinal nerve fiber layer with numerous pinpoint and larger optically empty spaces within the mass; there is prominent outward bowing. The retinal nerve fiber layer, ganglion cell layer, and inner plexiform layer have considerable disorganization. The inner nuclear layer seems thickened. An initial splitting located in the outer plexiform layer is visible. The outer nuclear layer, external limiting membrane, and retinal epithelium are present. No calcification is present in the mass as there is no shadowing. The height of the mass is 1136 microns (modified with permission from Abdolrahimzadeh et al. [27]).

patients. Histopathological studies show that the deposits in BCD originate from lipid crystallization [38] and hyper-reflective crystalline formations are considered the SDOCT hallmark of cholesterol crystals as they present intense reflectivity with strong light scattering [5].

4.2. Occult Macular Dystrophy. Occult macular dystrophy (OMD) is hereditary dystrophy described by Miyake et al. in 1989 in patients with a bilateral progressive visual decline in the context of a normal fundus, fluorescein angiograms, and full-field electroretinogram (ERG) [39]. Retinitis pigmentosa 1-like 1 gene (RP1L1, OMIM 608581) is the only confirmed associated gene and dominant mutations in RP1L1 are responsible for occult macular dystrophy [40]. Focal macular and multifocal ERG are severely attenuated, indicating localized macular dysfunction [39]. NIR imaging

reveals macular hyporeflexive lesions easily discernible from the surrounding reflectance that correspond to an abnormal interdigitation and ellipsoid zone on SDOCT cross-sectional images. The hyporeflexive alterations on NIR are confirmed in 66.7% of cases and are fundamental in diagnosis and monitoring disease progression [41].

4.3. Recessive Stargardt Disease. Recessive Stargardt disease occurs due to a deficiency of ABCA4 activity that accelerates the formation and accumulation of toxic bisretinoid molecules in RPE and photoreceptor cells. Multimodal imaging is central to this pathology and NIR-autofluorescence (NIR-AF) images, acquired using the indocyanine-green angiography mode (787 nm excitation), are particularly helpful in visualizing the RPE, which is commonly the first site of damage [35]. Figure 5 shows diffuse RPE atrophy visible on

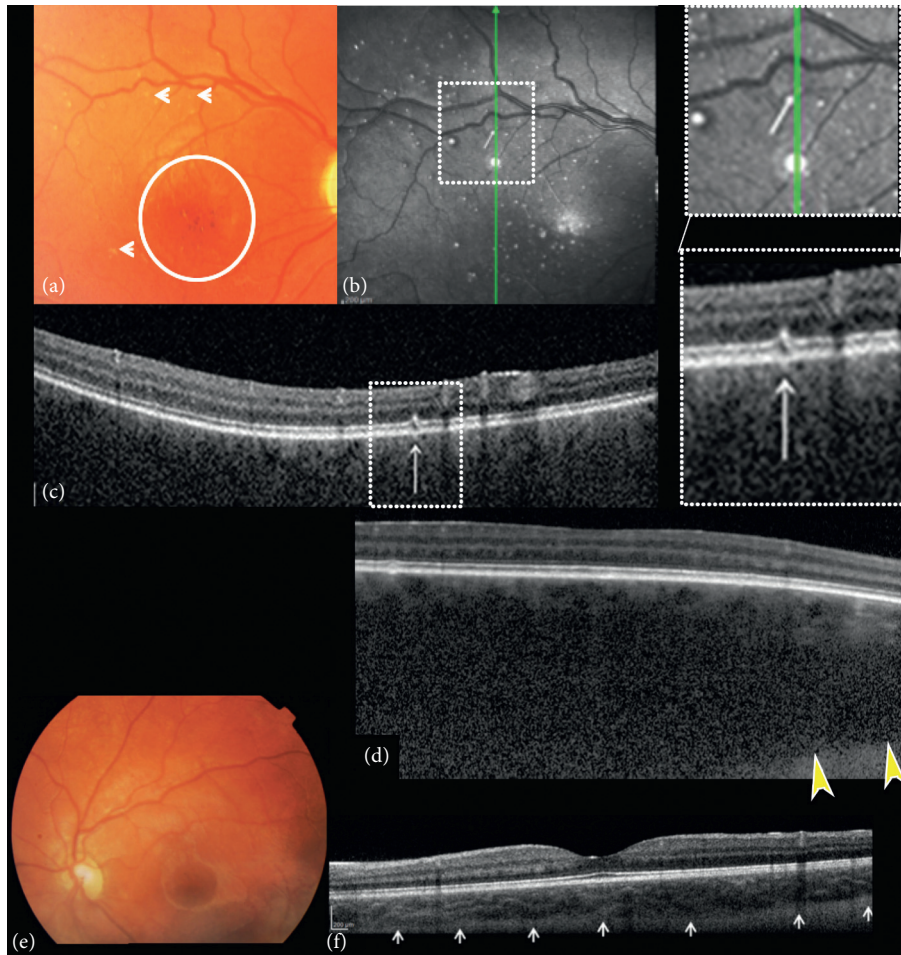


FIGURE 4: Composite of fundus color photographs and spectral-domain optical coherence (SDOCT) of the right and left eye. (a) The right fundus image shows excavation and pallor of the optic disk, absence of tessellation, diffuse choroidal hemangioma, hypo-hyper pigmentation of the foveal area with absent foveal reflex (circle), and small white dot shaped “microdrusen-like” alterations (arrows). (b) Near-infrared reflectance (NIR) of the right eye shows multiple hyperreflective dots surrounded by a hypo-reflective ring corresponding to the small white dot shaped “microdrusen-like” alterations of the posterior pole observed with ophthalmoscopy corresponded. B-scan cross-sectional SDOCT scan (c) on the hyperreflective dots shows focal alterations of the retinal pigment epithelial (RPE)-photoreceptor layer (involving the RPE, interdigital, ellipsoid and myoid zone), better seen on magnifications. (d) Enhanced-depth image (EDI) of the right eye shows choroidal thickness above $1000\ \mu\text{m}$ (yellow arrowheads indicate chorioscleral junction). (e) Left fundus image shows slightly increased excavation of the optic disc and absence of fundus tessellation. (f) EDI of the left eye shows no remarkable alterations; subfoveal choroidal thickness is $301\ \mu\text{m}$ (modified with permission from Abdolrahimzadeh et al [29]).

both short-wavelength (SW-AF) and near-infrared autofluorescence (NIR-AF) where lesions are more evident with NIR-AF in a 19-year-old female diagnosed with recessive Stargardt disease.

5. Other Macular Disorders

5.1. Acute Macular Neuropathy and Paracentral Acute Middle Maculopathy. Acute macular neuropathy (AMN) and paracentral acute middle maculopathy (PAMM) share similar clinical and multimodal imaging characteristics and NIR imaging represents the principle modality for diagnosis [42–44].

AMN is a rare acute pathology of uncertain aetiology presenting with a paracentral scotoma and characteristic wedge-shaped macular lesions, probably linked to oral

contraceptive use in young women, prodromal viral infections, and shock [45]. On fundus photography, lesions appear as multiple dark brown areas pointing toward the fovea; however, these are often very faded and difficult to recognize. NIR clearly identifies hyporeflexive, well-defined lesions that facilitate accurately monitoring lesion progression over time [46]. These hyporeflexive lesions appear to correlate with SDOCT-hyperreflective alterations involving the outer plexiform/outer nuclear layer junction that precede outer segment abnormalities. Fawzi et al. hypothesized that optimal visualization of these lesions with NIR depends on persistent RPE melanin abnormalities [47].

The pathogenesis of AMN is still unclear; however, a microvascular ischemic insult is thought to be the precipitating risk factor [47] although the localization of the ischemic injury is still a matter of debate. In a study conducted

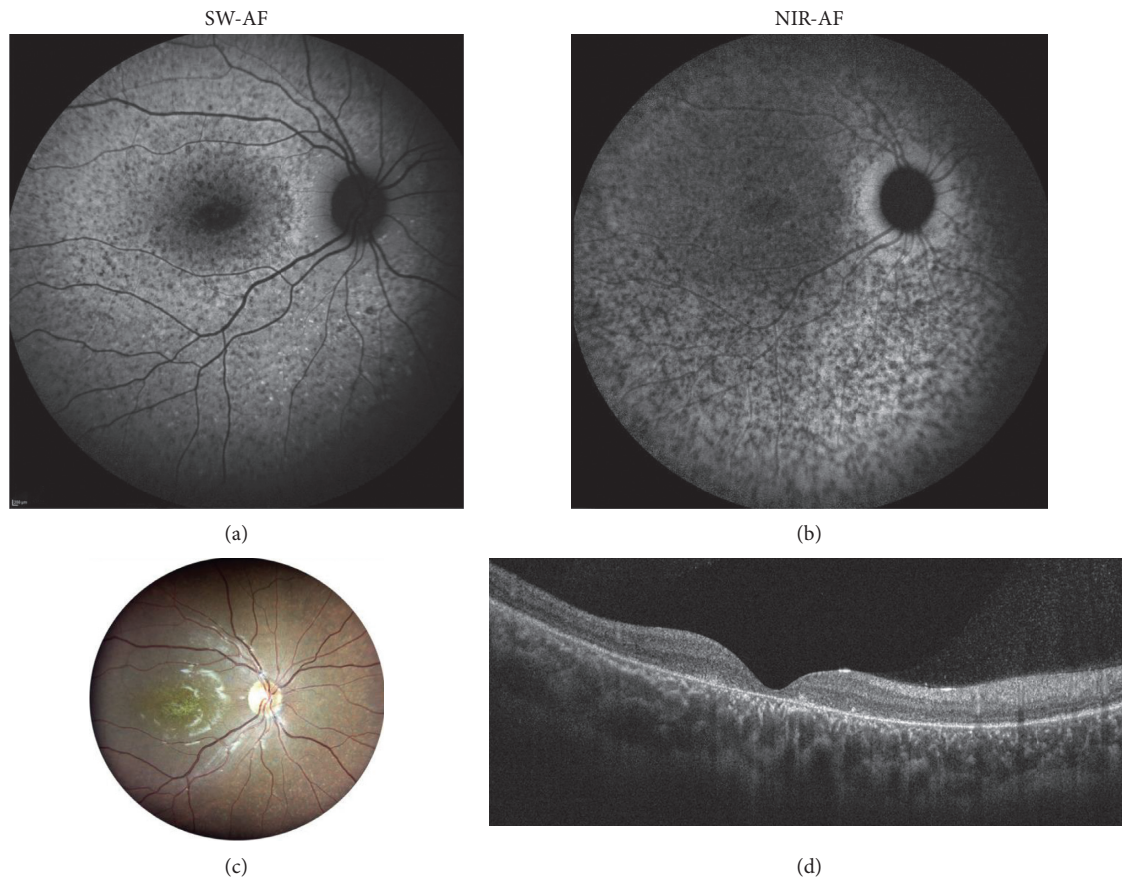


FIGURE 5: Composite images in a 19-year-old female with Stargardt disease. (a) Short-wavelength autofluorescence (SW-AF); (b) near-infrared autofluorescence (NIR-AF); (c) fundus photograph; (d) spectral-domain optical coherence tomography subfoveal b scan. Diffuse retinal pigment epithelium (RPE) atrophy is visible on both SW-AF and NIR-AF. RPE atrophy is more evident with NIR-AF exceeding the areas visible on SW-AF.

by Thanos et al. [48], comparing NIR, SDOCT, and OCT angiography (OCTA), flow deficits were reported to be distributed at choriocapillaris level colocalizing with the hyporeflective lesions on NIR. Other authors hypothesized the deep capillary plexus as the prominent microvascular plexus affected in this condition [43, 49].

PAMM lesions can be associated with retinal vascular diseases. In young patients, a causative event may be represented by sickle cell crisis presenting with bilateral vision loss [42]. Color fundus photography shows nasal parafoveal whitening, NIR imaging reveals nasal parafoveal hyporeflective lesions, and SDOCT demonstrates hyperreflective changes affecting the middle retinal layers above the outer plexiform layer corresponding to the hyporeflective lesions on NIR [42, 50]. Similar to AMN, PAMM lesions correspond to hyperreflective bands localized in the inner plexiform and inner nuclear layers, accompanied by reduced flow in the intermediate and deep capillary plexuses [43, 50, 51].

5.2. Acute Idiopathic Maculopathy. In a case of acute idiopathic maculopathy presenting a bacillary layer detachment, NIR showed a hyperreflective perifoveal ring in the acute phase corresponding to subretinal fluid. Some residual central

hyperreflectivity surrounded by a hyporeflective ring persisted following bacillary detachment resolution. This aspect has been related to a central thickening of the RPE/Bruch's membrane with adjacent ellipsoid and interdigitation zone disruption. In the case reported, NIR abnormalities persisted for months, even after fundus AF normalized [52].

5.3. Iatrogenic Laser-Induced Maculopathy. Retinal injuries secondary to laser pointers are increasingly frequent and different reviews have underlined how this has become a worrisome phenomenon. In 2017, Birtel et al. reported 111 cases of retinal injury due to laser pointers [53]. In 2018, Linton et al. documented 84 cases of handheld laser burns, where young boys represented the category most at risk [54]. The commonly reported symptoms following laser accidents include blurry vision, central scotomas, and reduced visual acuity. At fundoscopy, a multitude of retinal abnormalities can be observed spacing from circumscribed yellowish lesions, haemorrhage, pigment changes, and macular holes [53, 55]. However, lesions can be very subtle and easily missed, especially if the patient has difficulty in cooperating during the clinical examination or is reluctant to disclose the event and correlated symptoms. As laser-induced lesions

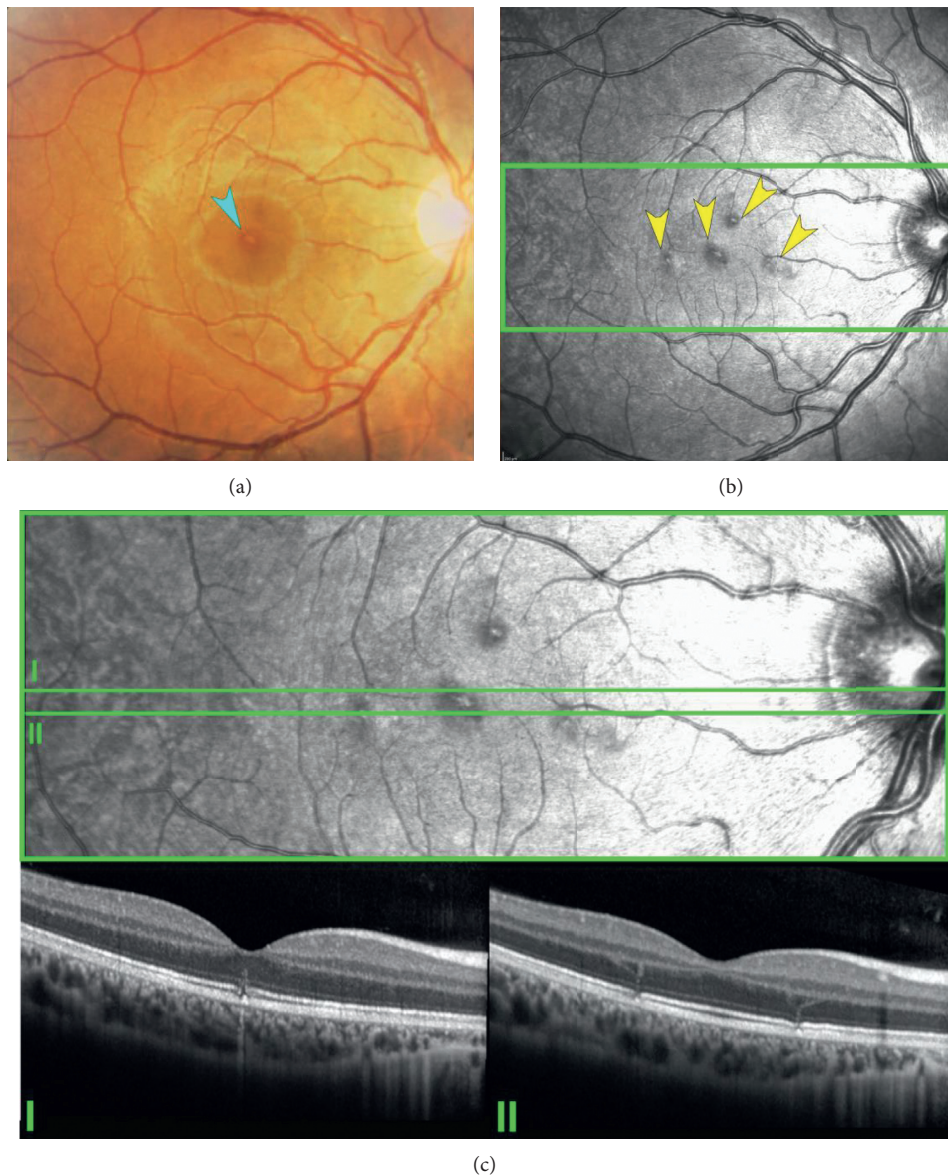


FIGURE 6: Multimodal imaging in a young patient with handheld laser-induced maculopathy. (a) Color fundus photograph shows a subtle focal yellowish-orange lesion in the foveolar area (light blue arrowhead). (b) Near-infrared reflectance demonstrates multiple roundish lesions with perilesional hyporeflective borders (yellow arrowheads). (c) SDOCT cross-sectional image scans through the lesions. (I-II) show defects of the ellipsoid zone and external limiting membrane with curvilinear hyperreflective tracts that appear to follow Henle fibers ascending toward the outer plexiform layer.

primarily affect the photoreceptors in the interdigitation and ellipsoid zones with various degrees of RPE involvement, NIR is particularly useful in detecting these lesions [56].

Herein, we report an illustrative case of a 16-year-old boy with a history of handheld laser misuse in his right eye for 15–20 seconds at 10 centimeters of distance. His best-corrected visual acuity was 20/20, and he denied visual disturbances. Clinical examination showed subtle macular changes. However, NIR enabled the identification of various parafoveal lesions with increased central reflectivity and hyporeflective borders that, on SDOCT cross-sectional images, corresponded to defects of the ellipsoid zone and external limiting membrane with curvilinear hyperreflective tracts (Figure 6).

A multimodal imaging approach including both NIR and SDOCT imaging in patients with suspected laser injury is imperative for diagnosis. Patients and parents benefit from counselling on the risks related to laser misuse in order to avoid exposure and repeated, possibly sight-threatening, damage.

6. Miscellaneous

Within the articles of this literature research a case of acute zonal cone photoreceptor outer segment loss in an adolescent boy was reported. Fundus examination, short-wavelength, and near-infrared FAF imaging were normal in

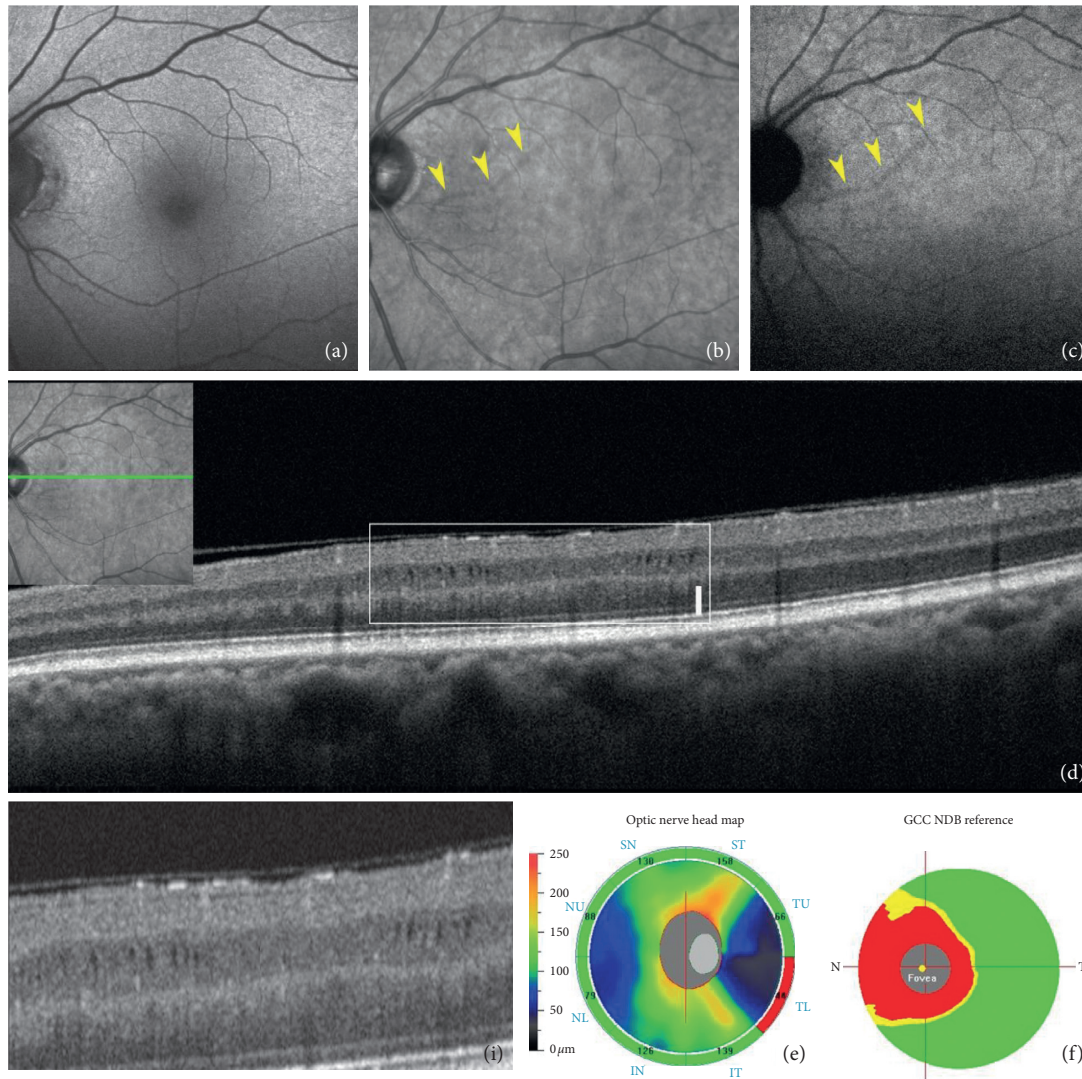


FIGURE 7: Microcystic edema. (a) Short-wavelength fundus autofluorescence (FAF) does not show alterations. (b) Infrared reflectance demonstrates a linear lesion of reduced reflectivity (yellow arrowheads), visible also at near-infrared FAF (yellow arrowheads (c)). (d) Spectral-domain optical coherence tomography b scan through the lesion as detailed in the miniature, the inset I reports a magnification of the microcystic spaces occupying the inner nuclear layer. (e) Retinal nerve fiber layer map confirming a defect in the inferior temporal sector and a diffuse defect in the ganglion cell layer map (f).

both eyes, whereas NIR imaging showed a region of hyporeflectance that corresponded to a dense cone scotoma [57].

In early-onset cobalamin C (cblC) disease, patients show an early-onset, fast-progressing maculopathy with severe central outer nuclear and ganglion cell layer loss. In the context of multimodal imaging techniques, NIR showed bulls-eye maculopathy in a 14-month boy and was crucial for the interpretation of the SDOCT images that were acquired simultaneously [58].

Recent studies on dengue fever ocular manifestations demonstrated that the RPE is a target for the dengue virus and alterations in intercellular junctions following infection of RPE cells promote leakage of extracellular fluid into the retina. These lesions appear as crescent-shaped defects and are helpful in detecting subtle alterations on fundus examination [59, 60].

Microcystic macular edema occurring with optic neuropathies can be studied with multiple imaging techniques. NIR highlights well-circumscribed perifoveal retinal atrophic arcuate dark zones, which proved to have a very good correspondence both with cystic lesions in the inner nuclear layer on SDOCT scans and to scotomas detected with visual field examination (Figure 7) [61].

7. Conclusions

Near-infrared reflectance represents an optimal noninvasive imaging technique to visualize and enhance subretinal and sub-RPE alterations. This method can be combined with SDOCT cross-sectional scans to further improve diagnostic evaluation. The fast and straightforward acquisition mode is

particularly useful in children who do not collaborate easily during ophthalmological examination. The role of NIR is essential in diagnosing several retinal diseases with onset from infancy to young adulthood. Beyond the difficulties in examining young patients, most of the alterations localized in the subretinal and sub-RPE space may be overlooked during a routine clinical examination. NIR is crucial in phakomatoses and facilitates the detection of choroidal alterations that are cardinal biomarkers in NF1. Another diagnostic application is the accurate visualization of the glistening crystals characterizing Bietti crystalline dystrophy. In AMN and PAMM lesions with young adulthood onset, NIR is not only diagnostic but also essential to monitor disease progression. An interesting clinical application is also the prompt recognition of laser-induced maculopathy where funduscopy examination can appear normal or subnormal.

In conclusion, NIR has a noninterchangeable role in the diagnosis of certain retinal and choroidal alterations, especially in children and young adults where a clinical examination is hindered owing to poor collaboration and lack of evident funduscopy findings. Moreover, this imaging method can reveal unique retinal biomarkers highly specific to rare conditions, which are otherwise difficult to recognize.

Data Availability

The data supporting this narrative review were taken from previously reported studies and datasets, which have been cited. The processed data are available from the corresponding author upon request, e-mail: serena.fragiotta@uniroma1.it.

Conflicts of Interest

The authors declare that there are no conflicts of interest.

References

- [1] A. E. Elsner, S. A. Burns, J. J. Weiter, and F. C. Delori, "Infrared imaging of sub-retinal structures in the human ocular fundus," *Vision Research*, vol. 36, no. 1, pp. 191–205, 1996.
- [2] A. Hassenstein and C. H. Meyer, "Clinical use and research applications of Heidelberg retinal angiography and spectral-domain optical coherence tomography—a review," *Clinical and Experimental Ophthalmology*, vol. 37, no. 1, pp. 130–143, 2009.
- [3] A. W. A. Weinberger, A. Lappas, T. Kirschkamp et al., "Fundus near infrared fluorescence correlates with fundus near infrared reflectance," *Investigative Ophthalmology and Visual Science*, vol. 47, no. 7, pp. 3098–3108, 2006.
- [4] P. Charbel Issa, R. P. Finger, F. G. Holz, and H. P. N. Scholl, "Multimodal imaging including spectral domain OCT and confocal near infrared reflectance for characterization of outer retinal pathology in pseudoxanthoma elasticum," *Investigative Ophthalmology and Visual Science*, vol. 50, no. 12, pp. 5913–5918, 2009.
- [5] S. Fragiotta, P. Fernandez-Avellaneda, M. P. Breazzano, L. A. Yannuzzi, C. A. Curcio, and K. B. Freund, "Linear and planar reflection artifacts on swept-source and spectral-domain optical coherence tomography due to hyperreflective crystalline deposits," *Graefe's Archive for Clinical and Experimental Ophthalmology*, vol. 258, 2019.
- [6] S. Fragiotta, P. Fernandez-Avellaneda, M. P. Breazzano et al., "The fate and prognostic implications of hyperreflective crystalline deposits in nonneovascular age-related macular degeneration," *Investigative Ophthalmology and Visual Science*, vol. 60, no. 8, pp. 3100–3109, 2019.
- [7] A. C. S. Tan, M. G. Pilgrim, S. Fearn et al., "Calcified nodules in retinal drusen are associated with disease progression in age-related macular degeneration," *Science Translational Medicine*, vol. 10, no. 466, 2018.
- [8] A. Oishi, M. Oishi, M. Miyata et al., "Multimodal imaging for differential diagnosis of Bietti crystalline dystrophy," *Ophthalmology Retina*, vol. 2, no. 10, pp. 1071–1077, 2018.
- [9] M. Suzuki, T. Sato, and R. F. Spaide, "Pseudodrusen subtypes as delineated by multimodal imaging of the fundus," *American Journal of Ophthalmology*, vol. 157, no. 5, pp. 1005–1012, 2014.
- [10] S. Abdolrahimzadeh, V. Fameli, R. Mollo, M. T. Contestabile, A. Perdicchi, and S. M. Recupero, "Rare diseases leading to childhood glaucoma: epidemiology, pathophysiology, and management," *BioMed Research International*, vol. 2015, Article ID 781294, 2015.
- [11] "National institutes of Health consensus development conference statement on acoustic neuroma, december 11-13, 1991. The consensus development panel," *Archives of Neurology*, vol. 51, no. 2, pp. 201–207, 1994.
- [12] T. Yasunari, K. Shiraki, H. Hattori, and T. Miki, "Frequency of choroidal abnormalities in neurofibromatosis type 1," *The Lancet*, vol. 356, no. 9234, pp. 988–992, 2000.
- [13] S. Nakakura, K. Shiraki, T. Yasunari, Y. Hayashi, S. Ataka, and T. Kohno, "Quantification and anatomic distribution of choroidal abnormalities in patients with type I neurofibromatosis," *Graefe's Archive for Clinical and Experimental Ophthalmology*, vol. 243, no. 10, pp. 980–984, 2005.
- [14] F. Viola, E. Villani, F. Natacci et al., "Choroidal abnormalities detected by near-infrared reflectance imaging as a new diagnostic criterion for neurofibromatosis 1," *Ophthalmology*, vol. 119, no. 2, pp. 369–375, 2012.
- [15] T. Ueda-Consolvo, A. Miyakoshi, H. Ozaki, S. Houki, and A. Hayashi, "Near-infrared fundus autofluorescence-visualized melanin in the choroidal abnormalities of neurofibromatosis type 1," *Clinical Ophthalmology*, vol. 6, pp. 1191–1194, 2012.
- [16] A. Moramarco, E. Miraglia, F. Mallone et al., "Retinal microvascular abnormalities in neurofibromatosis type 1," *British Journal of Ophthalmology*, vol. 103, no. 11, pp. 1590–1594, 2019.
- [17] A. Moramarco, S. Giustini, I. Nofroni et al., "Near-infrared imaging: an in vivo, non-invasive diagnostic tool in neurofibromatosis type 1," *Graefe's Archive for Clinical and Experimental Ophthalmology*, vol. 256, no. 2, pp. 307–311, 2018.
- [18] S. Abdolrahimzadeh, L. Felli, D. C. Piraino, R. Mollo, S. Calvieri, and S. M. Recupero, "Retinal microvascular abnormalities overlying choroidal nodules in neurofibromatosis type 1," *BMC Ophthalmology*, vol. 14, no. 1, p. 146, 2014.
- [19] R. Parrozzani, L. Frizziero, S. Trainiti et al., "Retinal vascular abnormalities related to neurofibromatosis type 1: natural history and classification by OCT angiography in 473 patients," *Retina*, vol. 41, 2020.
- [20] S. Abdolrahimzadeh, F. Parisi, B. Abdolrahimzadeh, and F. Cruciani, "Unusual choroidal vessels in neurofibromatosis type 1 observed with near-infrared reflectance and spectral domain optical coherence tomography," *Acta Ophthalmologica*, vol. 94, no. 8, pp. e815–e816, 2016.











- [21] W. C. Wiederholt, M. R. Gomez, and L. T. Kurland, "Incidence and prevalence of tuberous sclerosis in Rochester, Minnesota, 1950 through 1982," *Neurology*, vol. 35, no. 4, p. 600, 1985.
- [22] S. A. Rowley, F. J. O'Callaghan, and J. P. Osborne, "Ophthalmic manifestations of tuberous sclerosis: a population based study," *British Journal of Ophthalmology*, vol. 85, no. 4, pp. 420–423, 2001.
- [23] J. H. Nyboer, D. M. Robertson, and M. R. Gomez, "Retinal lesions in tuberous sclerosis," *Archives of Ophthalmology*, vol. 94, no. 8, pp. 1277–1280, 1976.
- [24] S. Abdolrahimzadeh, A. M. Plateroti, S. M. Recupero, and A. Lambiase, "An update on the ophthalmologic features in the phakomatoses," *Journal of Ophthalmology*, vol. 2016, Article ID 3043026, 2016.
- [25] C. L. Shields, E. A. T. Say, T. Fuller, S. Arora, W. A. Samara, and J. A. Shields, "Retinal astrocytic hamartoma arises in nerve fiber layer and shows "Moth-Eaten" optically empty spaces on optical coherence tomography," *Ophthalmology*, vol. 123, no. 8, pp. 1809–1816, 2016.
- [26] S. Abdolrahimzadeh, M. Formisano, L. Scuderi, and S. Rahimi, "Long-term follow-up of adult patient with neurofibromatosis type 1 with retinal astrocytic hamartoma using spectral-domain optical coherence tomography: a review of the literature and a report of a case," *Ophthalmic Genetics*, vol. 42, pp. 1–7, 2020.
- [27] L. Xu, T. R. Burke, J. P. Greenberg, V. B. Mahajan, and S. H. Tsang, "Infrared imaging and optical coherence tomography reveal early-stage astrocytic hamartomas not detectable by funduscopy," *American Journal of Ophthalmology*, vol. 153, no. 5, pp. 883–889, 2012, e882.
- [28] P. L. Mellen, K. Sioufi, J. A. Shields, and C. L. Shields, "Invisible, honeycomb-like, cavitory retinal astrocytic hamartoma," *Retinal Cases and Brief Reports*, vol. 14, no. 3, pp. 211–214, 2020.
- [29] S. Abdolrahimzadeh, F. Parisi, F. Mantelli, A. Perdicchi, and G. Scuderi, "Retinal pigment epithelium-photoreceptor layer alterations in a patient with Sturge-Weber syndrome with diffuse choroidal hemangioma," *Ophthalmic Genetics*, vol. 38, no. 6, pp. 567–569, 2017.
- [30] C. L. Shields, J. A. Shields, B. P. Marr, D. E. Sperber, and J. D. M. Gass, "Congenital simple hamartoma of the retinal pigment epithelium," *Ophthalmology*, vol. 110, no. 5, pp. 1005–1011, 2003.
- [31] P. Arjmand, E. B. Elimimian, E. A. T. Say, and C. L. Shields, "Optical coherence tomography angiography of congenital simple hamartoma of the retinal pigment epithelium," *Retinal Cases and Brief Reports*, vol. 13, no. 4, pp. 357–360, 2019.
- [32] M. W. Rodrigues, D. B. Cavallini, C. Dalloul, C. L. Shields, and R. Jorge, "Retinal sensitivity and photoreceptor arrangement changes secondary to congenital simple hamartoma of retinal pigment epithelium," *International Journal of Retina and Vitreous*, vol. 5, no. 1, p. 5, 2019.
- [33] J. D. Gass, "An unusual hamartoma of the pigment epithelium and retina simulating choroidal melanoma and retinoblastoma," *Retina*, vol. 23, no. 6 Suppl, pp. 171–183, discussion 184–175, 1973.
- [34] K. Kaprinis, H. Bobat, and G. De Salvo, "MultiColor™ imaging in combined hamartoma of the retina and retinal pigment epithelium," *Eye*, vol. 32, no. 9, pp. 1478–1482, 2018.
- [35] J. R. Lima de Carvalho Jr., M. Paavo, L. Chen, J. Chiang, S. H. Tsang, and J. R. Sparrow, "Multimodal imaging in best vitelliform macular dystrophy," *Investigative Ophthalmology and Visual Science*, vol. 60, no. 6, pp. 2012–2022, 2019.
- [36] M. Paavo, W. Lee, R. Allikmets, S. Tsang, and J. R. Sparrow, "Photoreceptor cells as a source of fundus autofluorescence in recessive Stargardt disease," *Journal of Neuroscience Research*, vol. 97, no. 1, pp. 98–106, 2019.
- [37] A. Mataftsi, L. Zografos, E. Millá, M. Secrétan, and F. L. Munier, "Bietti's crystalline corneoretinal dystrophy: a cross-sectional study," *Retina*, vol. 24, no. 3, pp. 416–426, 2004.
- [38] D. J. Wilson, R. G. Weleber, M. L. Klein, R. B. Welch, and W. R. Green, "Bietti's crystalline dystrophy," *Archives of Ophthalmology*, vol. 107, no. 2, pp. 213–221, 1989.
- [39] Y. Miyake and K. Tsunoda, "Occult macular dystrophy," *Japanese Journal of Ophthalmology*, vol. 59, no. 2, pp. 71–80, 2015.
- [40] M. Akahori, K. Tsunoda, Y. Miyake et al., "Dominant mutations in RP1L1 are responsible for occult macular dystrophy," *The American Journal of Human Genetics*, vol. 87, no. 3, pp. 424–429, 2010.
- [41] D.-D. Wang, F.-J. Gao, J.-K. Li et al., "Clinical and genetic characteristics of Chinese patients with occult macular dystrophy," *Investigative Ophthalmology and Visual Science*, vol. 61, no. 3, p. 10, 2020.
- [42] X. Chen, E. Rahimy, R. C. Sergott et al., "Spectrum of retinal vascular diseases associated with paracentral acute middle maculopathy," *American Journal of Ophthalmology*, vol. 160, no. 1, pp. 26–34, 2015.
- [43] S. Chu, P. L. Nesper, B. T. Soetikno, S. J. Bakri, and A. A. Fawzi, "Projection-resolved OCT angiography of microvascular changes in paracentral acute middle maculopathy and acute macular neuroretinopathy," *Investigative Ophthalmology and Visual Science*, vol. 59, no. 7, pp. 2913–2922, 2018.
- [44] J. Sridhar, A. Shahlaee, E. Rahimy et al., "Optical coherence tomography angiography and en face optical coherence tomography features of paracentral acute middle maculopathy," *American Journal of Ophthalmology*, vol. 160, no. 6, pp. 1259–1268, 2015, e1252.
- [45] S. Mrejen, C. E. Pang, D. Sarraf et al., "Adaptive optics imaging of cone mosaic abnormalities in acute macular neuroretinopathy," *Ophthalmic Surgery, Lasers and Imaging Retina*, vol. 45, no. 6, pp. 562–569, 2014.
- [46] G. De Salvo, S. Vaz-Pereira, R. Arora, and A. J. Lotery, "Multicolor imaging in the diagnosis and follow up of type 2 acute macular neuroretinopathy," *Eye*, vol. 31, no. 1, pp. 127–131, 2017.
- [47] A. A. Fawzi, R. R. Pappuru, D. Sarraf et al., "Acute macular neuroretinopathy," *Retina*, vol. 32, no. 8, pp. 1500–1513, 2012.
- [48] A. Thanos, L. J. Faia, Y. Yonekawa, and S. Randhawa, "Optical coherence tomographic angiography in acute macular neuroretinopathy," *JAMA Ophthalmology*, vol. 134, no. 11, pp. 1310–1314, 2016.
- [49] J. Nemirow, D. Sarraf, J. P. Davila, and D. Rodger, "Optical coherence tomography angiography of acute macular neuroretinopathy reveals deep capillary ischemia," *Retinal Cases and Brief Reports*, vol. 12, no. Suppl 1, pp. S12–S15, 2018.
- [50] D. Sarraf, E. Rahimy, A. A. Fawzi et al., "Paracentral acute middle maculopathy," *JAMA Ophthalmology*, vol. 131, no. 10, pp. 1275–1287, 2013.
- [51] F. Pichi, S. Fragiotta, K. B. Freund et al., "Cilioretinal artery hypoperfusion and its association with paracentral acute middle maculopathy," *British Journal of Ophthalmology*, vol. 103, no. 8, pp. 1137–1145, 2019.
- [52] P. Fernandez-Avellaneda, M. P. Breazzano, S. Fragiotta et al., "Bacillary layer detachment overlying reduced

choriocapillaris flow in acute idiopathic maculopathy,” *Retinal Cases and Brief Reports*, 2019.

- [53] J. Birtel, W. M. Harmening, T. U. Krohne, F. G. Holz, P. Charbel Issa, and P. Herrmann, “Retinal injury following laser pointer exposure,” *Deutsches Aerzteblatt Online*, vol. 114, no. 49, pp. 831–837, 2017.
- [54] E. Linton, A. Walkden, L. R. Steeples et al., “Retinal burns from laser pointers: a risk in children with behavioural problems,” *Eye*, vol. 33, no. 3, pp. 492–504, 2019.
- [55] S. M. Alsulaiman, A. A. Alrushood, J. Almasaud et al., “High-power handheld blue laser-induced maculopathy,” *Ophthalmology*, vol. 121, no. 2, pp. 566–572, 2014.
- [56] E. Dhrami-Gavazi, W. Lee, C. Balaratnasingam, L. Kayserman, L. A. Yannuzzi, and K. B. Freund, “Multimodal imaging documentation of rapid evolution of retinal changes in handheld laser-induced maculopathy,” *International Journal of Retina and Vitreous*, vol. 1, no. 1, p. 14, 2015.
- [57] T. S. Aleman, H. S. Sandhu, L. W. Serrano et al., “Acute zonal cone photoreceptor outer segment loss,” *JAMA Ophthalmology*, vol. 135, no. 5, pp. 487–490, 2017.
- [58] L. Bonafede, C. H. Ficioglu, L. Serrano et al., “Cobalamin C deficiency shows a rapidly progressing maculopathy with severe photoreceptor and ganglion cell loss,” *Investigative Ophthalmology & Visual Science*, vol. 56, no. 13, pp. 7875–7887, 2015.
- [59] J. Carr, L. Ashander, J. Calvert et al., “Molecular responses of human retinal cells to infection with dengue virus,” *Mediators of Inflammation*, vol. 1–16, 2017.
- [60] T. Somkijrunroj and W. Kongwattananon, “Ocular manifestations of dengue,” *Current Opinion in Ophthalmology*, vol. 30, no. 6, pp. 500–505, 2019.
- [61] N. Voide and F. Borruat, “Microcystic macular edema in optic nerve atrophy: case series,” *Acta Ophthalmologica*, vol. 92, 2014.

Review Article

OCT Biomarkers in Neovascular Age-Related Macular Degeneration: A Narrative Review

Cristian Metrangolo ¹, **Simone Donati** ^{1,2}, **Marco Mazzola** ³, **Liviana Fontanel** ²,
Walter Messina ², **Giulia D'alterio** ¹, **Marisa Rubino** ¹, **Paolo Radice** ¹,
Elias Premi ^{1,2} and **Claudio Azzolini** ²

¹Ophthalmology Unit, Ospedale di Circolo e Fondazione Macchi, ASST Sette Laghi, Varese, Italy

²Department of Medicine and Surgery, University of Insubria, Varese, Italy

³Multizonal Unit of Ophthalmology of Autonomous Province of Trento, Rovereto, Italy

Correspondence should be addressed to Simone Donati; simone.donati@uninsubria.it

Received 12 March 2021; Accepted 13 July 2021; Published 19 July 2021

Academic Editor: Serena Fragiotta

Copyright © 2021 Cristian Metrangolo et al. This is an open access article distributed under the Creative Commons Attribution License, which permits unrestricted use, distribution, and reproduction in any medium, provided the original work is properly cited.

Age-related macular degeneration (AMD) is the leading cause of legal blindness in elderly people. Neovascular AMD (nAMD) is responsible for the majority of cases of severe visual loss in eyes with AMD. Optical coherence tomography (OCT) is the most widely used technology for the diagnosis and follow-up of nAMD patients, which is widely used to study and guide the clinical approach, as well as to predict and evaluate treatment response. The aim of this review is to describe and analyze various structural OCT-based biomarkers, which have practical value during both initial assessment and treatment follow-up of nAMD patients. While central retinal thickness has been the most common and one of the first OCT identified biomarkers, today, other qualitative and quantitative biomarkers provide novel insight into disease activity and offer superior prognostic value and better guidance for tailored therapeutic management. The key importance of retinal fluid compartmentalization (intraretinal fluid, subretinal fluid, and subretinal pigment epithelium (RPE) fluid) will be discussed firstly. In the second part, the structural alterations of different retinal layers in various stages of the disease (photoreceptors layer integrity, hyperreflective dots, outer retinal tubulations, subretinal hyperreflective material, and retinal pigment epithelial tears) will be analyzed in detail. The last part of the review will focus on how alterations of the vitreoretinal interface (vitreomacular adhesion and traction) and of the choroid (sub-RPE hyperreflective columns, prechoidal clefts, choroidal caverns, choroidal thickness and choroidal volume, and choroidal vascular index) interact with nAMD progression. OCT technology is evolving very quickly, and new retinal biomarkers are continuously described. This up-to-date review article provides a comprehensive description on how structural OCT-based biomarkers provide a valuable tool to monitor the progression of the disease and the treatment response in nAMD patients. Thus, in this perspective, clinicians will be able to allocate hospital resources in the best possible way and tailor treatment to the individual patient's needs.

1. Introduction

Age-related macular degeneration (AMD) is the leading cause of legal blindness in elderly people, especially in developed countries. Its prevalence increases significantly after the age of 50 in each decade, and it affects up to 18% of adults aged over 85 years [1, 2]. In 2020, about 200 million people were affected by AMD worldwide, and the incidence is constantly increasing as a consequence of exponential population aging. The AMD population is expected to be 288 million by 2040 [3, 4].

Neovascular AMD (nAMD) represents a small subset (less than 10%) of total AMD cases; however, the neovascular form is responsible for the majority of cases of severe visual loss in eyes with AMD [5]. It can lead to a progressive and irreversible central visual loss, with severe impairment in daily life. For this reason, appropriate management of this disease is essential.

A multimodal imaging approach should be used in the diagnosis of nAMD, including fluorescein angiography (FA), indocyanine green angiography (ICG), optical

coherence tomography (OCT), and OCT angiography. However, OCT can be extremely useful in the follow-up of these patients to predict and evaluate treatment response, as well as to guide treatments [6]. Indeed, it is a widely diffused, user-friendly, quick, and noninvasive device that provides high-resolution in vivo imaging of chorioretinal anatomy and vasculature [7].

Today, with the word “biomarker,” we mean morphological and structural alterations that can provide important information about the stage of a disease [7]. OCT allows to identify specific retinal biomarkers associated with visual acuity (VA) at baseline and to provide information about the patient’s visual recovery after anti-Vascular Endothelial Growth Factor (anti-VEGF) treatment, to offer an efficient and personalized management of nAMD.

OCT biomarkers in nAMD can be divided into two different categories. On the one hand, biomarkers based on the retinal distribution of fluids and, on the other, structural biomarkers based on the presence or absence of specific features can be observed in the retinal layers, choroid, or vitreomacular interface. Retinal fluids are observed in exudative AMD and underline the presence of macular neovascularization (MNV), while structural biomarkers can be observed in both exudative and dry AMD as merely manifestations of the progression of the disease.

The measurement of central retinal thickness (CRT) is the most common and one of the first OCT biomarkers identified in the literature [8].

Furthermore, several studies found that fluctuation in retinal thickness due to the activity of the lesion has negative effects on the final VA in patients with nAMD treated with anti-VEGF therapy. Although fluctuation in any retinal tissue compartments has a negative impact on VA, intraretinal cystoid fluid has the worst influence [9]. CRT should be measured in patients with nAMD, because it seems to be correlated with VA both at baseline and after treatment [10], and it is considered the most available and intuitive morphological parameter that can be evaluated from OCT scans. However, studies revealed different results about this correlation, and CRT appears to be not so valuable predictor of visual function. Indeed, studies that consider other parameters such as fluid location, fibrosis, and integrity of individual retinal layers may be more accurate [11]. This is because CRT considers different retinal layers that alone could influence functional outcomes [12, 13]. In particular, intraretinal cystoid fluid has been shown to have the greatest impact on CRT compared with the other fluid features [14]. Intraretinal cysts at baseline may indicate preexisting retinal damage or a more aggressive form of nAMD, reducing visual acuity recovery [15]. For these reasons, we highlight the importance of recognizing the distribution of fluids in retinal layers in nAMD. Specifically, we can distinguish intraretinal cystoid fluid (IRC), subretinal fluid (SRF), and pigment epithelial detachment (PED).

The aim of this narrative review is to describe and analyze various OCT-based biomarkers, which have practical value during both initial assessment and treatment follow-up of patients affected by nAMD.

2. Distribution of Retinal Fluids as OCT Biomarker

Neovascular AMD is characterized by the growth of abnormal choroidal vessels, breaking through the Bruch membrane (BM) and proliferating into the subretinal pigment epithelium (RPE) space. These vessels are also defined macular neovascularization (MNV) and can further expand beyond the RPE into the subretinal and intraretinal layers. Exudation due to the immaturity of these vessels often results in fluid accumulation in different layers depending on MNV extension and on retinal tissue ability to solve it [16, 17].

2.1. Intraretinal Cystoid Fluid. Intraretinal cystoid fluid (IRC) can be defined as a cystoid accumulation of fluid within the inner retinal layers, typically associated with increased retinal thickening (Figure 1). IRC is usually related to type 2 and type 3 MNV, but it can also be found in type 1 MNV, in later stages of disease [16]. Many comprehensive literature reviews qualify IRC as the most important negative prognostic biomarker in AMD, associated with a higher risk of visual loss and development of fibrosis or atrophy [7, 18].

IRC presence at baseline is often associated with both poor baseline VA and lower visual improvement after anti-VEGF treatment [6, 19].

In a post hoc analysis of a prospective, randomized multicenter clinical trial including 1240 patients with nAMD treated with intravitreal ranibizumab or aflibercept, Schmidt-Erfurth et al. showed that IRC was the only feature statistically correlated with baseline visual function, with low best-corrected visual acuity (BCVA) values at baseline and during the treatment. When IRC persisted throughout the initial three-month loading phase, there was a further decrease in BCVA, and these degenerative cysts showed the worst prognosis in visual outcomes [20]. Moreover, patients with persistent IRC, despite twelve anti-VEGF injections monthly, showed a higher risk of fibrosis and RPE atrophy [16].

The negative effect of IRC on VA was confirmed in the CATT study at all time points examined in a two-year period. This correlation was stronger in the second year, and the authors postulated that the small hyporeflective cystoid structures persisting after anti-VEGF therapy at the conclusion of the first year may have been due to non-VEGF mechanisms, such as cell death [14].

Finally, we can conclude that IRC is always a negative prognostic biomarker, and, whenever it occurs at baseline or during anti-VEGF therapy, VA would be significantly compromised [20].

2.2. Subretinal Fluid. Subretinal fluid (SRF) is described as an exudation occurring between the outer border of photoreceptors and the inner border of the RPE (Figure 1). SRF is the most frequent fluid localization in type 1 MNV, and it can also occur in the context of type 2 MNV. In type 3 MNV, SRF is commonly found in association with IRC overlying PED [16]. The presence of SRF is often associated

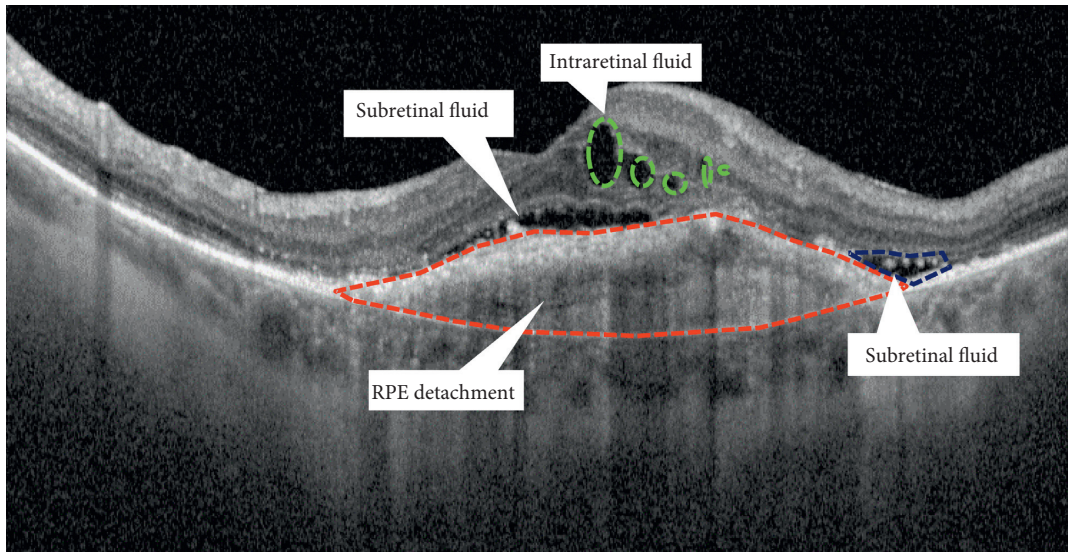


FIGURE 1: Fluid distribution in neovascular AMD.

with higher visual outcomes and lower rates of atrophy, regardless of intravitreal treatment frequency, respect to IRC [16].

A post hoc analysis of prospective, randomized VIEW trials stated that nAMD patients who presented SRF at baseline were shown to have a higher mean BCVA both at baseline and through the duration of anti-VEGF treatment than patients without SRF [19]. A post hoc analysis of prospective, randomized VIEW trials stated that nAMD patients who presented SRF at baseline were shown to have a higher mean BCVA both at baseline and through the duration of anti-VEGF treatment than patients without SRF [19].

Schmidt-Erfurth et al. found that visual prognosis worsened progressively when SRF was associated with retinal Pigmented Epithelium Detachment (SRF + PED) and with IRC (SRF + IRC), with the worst VA in patients with SRF associated with both IRC and PED (SRF + IRC + PED) [20]. Furthermore, refractory SRF may have not a significant negative effect on VA [16, 21], and it was associated with better anatomical and functional outcome than refractory IRC [22].

The FLUID study reported the visual outcomes of nAMD patients treated for 24 months with ranibizumab intravitreal injections in two different treat-and-extend protocols, differing only in the tolerance level of SRF. Patients treated with a protocol that tolerates a small amount of SRF ($\leq 200 \mu\text{m}$ under the fovea center) achieved a mean BCVA that was noninferior to the group, in which SRF had to be completely resolved [23, 24].

However, the use of microperimetry in the eyes with SRF revealed a progressive decrease in retinal sensitivity over time, expression of functional changes [25].

In the post hoc analysis of the prospective, randomized HARBOR study, baseline SRF absence was associated with an increased risk of macular atrophy (MA) and low VA. The authors provided two different interpretations of these results: SRF itself could be protective against the development

of MA; otherwise, SRF may have been related to the presence of a low-activity persistent MNV that limited atrophy, supporting the metabolism of the RPE [18]. However, Sadda et al., disagreeing with the protective role of SRF, emphasized that patients with persistent SRF in the HARBOR study achieved a good visual outcome, because they had been treated continuously during the study [26].

The CATT study showed that eyes with foveal SRF at baseline had higher BCVA at 5 years of follow-up, and this effect was even more evident than at the two-year follow-up. The protective role of SRF was also explained in the CATT study, hypothesizing that SRF might protect retinal photoreceptors from potential toxicity related to direct contact with the underlying diseased RPE. SRF may contain neuroprotective factors providing trophic support to the overlying retina [27].

2.3. Sub-RPE Fluid. Serous retinal pigment epithelium detachment (PED) is defined as a separation of the RPE from the inner collagenous layer of Bruch's membrane (Figure 1). Its finding on OCT seems to be less important for the visual prognosis of patients with nAMD than the presence of IRC or SRF.

Previous studies reported inconsistent results regarding the relationship between PED and VA. While some studies associated the presence of PEDs with less favorable visual outcomes, others reported no significant relationships [28].

PED appeared to affect visual recovery only when combined with IRC or SRF, and it is associated with an increase in retreatment frequency [16, 20, 29, 30].

In the post hoc analysis of prospective VIEW trials, 1353 eyes with PED at baseline presented a slightly higher mean BCVA at baseline than patients without PED, but over time, the correlation became less strong and showed a minimal impact of PED on VA [19]. In the post hoc analysis of prospective VIEW trials, 1353 eyes with PED at baseline presented a slightly higher mean BCVA at baseline than

patients without PED, but over time, the correlation became less strong and showed a minimal impact of PED on VA [19].

Similarly, in the post hoc analysis of the HARBOR study, patients with PED had better VA at baseline and at month 24 than patients without PED. Indeed, patients who started treatment with higher VA maintained these values until the end of the study. Nevertheless, at year two, there was no statistically significant difference between BCVA increase in patients with PED and patients without PED ($p = 0.08$).

A similar rate of MA was seen at month 24 in eyes with and without PED at baseline; however, patients with complete resolution of PED generally developed MA at month 24, regardless of PED size at baseline [31].

In the CATT study, foveal PED was associated with higher VA at year 5. The reason for higher VA in these eyes is unclear, and the authors suggested that sub-RPE fluid provides a trophic support to the retina [27]. Nevertheless, several studies reported a lack of correlation between visual improvement and resolution of PED [31, 32]. Moreover, OCT PED morphology (height, width, volume, dome shape versus peak, presence of RPE tear, or cholesterol bands) was not related to the visual outcome [28].

Finally, PED height reduction was not associated with an increase in VA, suggesting that complete resolution of PED may not influence the final VA, compared to IRC and SRF [33].

3. Structural OCT Biomarkers

3.1. Retinal Features

3.1.1. Photoreceptor Layer Integrity. Photoreceptor degeneration and loss are well-known features in nAMD and are considered key factors of visual decrease in this disease [34] (Figure 2).

Thanks to OCT imaging, it is possible to identify three hyperreflective bands in the photoreceptor layer: External Limiting Membrane (ELM), Ellipsoid Zone (EZ), and Interdigitation Zone (IZ).

Various studies showed that foveal photoreceptor layer integrity is strongly correlated with visual acuity in several retinal diseases [35–40]. In nAMD, the disruption of the foveal ELM band [41–43] and the foveal EZ band [41, 43–45] has been associated with compromised BCVA at baseline and after anti-VEGF therapy.

Restoration of the foveal ELM band and the foveal EZ band after anti-VEGF therapy in nAMD has been described [40, 42, 44]. Restoration of the foveal ELM band after anti-VEGF therapy showed a correlation with better final BCVA. [42].

In a post hoc analysis of the OCTAVE trial, Riedl and colleagues analyzed 185 eyes of 185 newly diagnosed treatment-naïve nAMD patients. They showed a slight positive correlation between foveal EZ integrity and BCVA at baseline [44]. However, within the same study, BCVA variations and modifications in EZ integrity after anti-VEGF treatment did not show a meaningful correlation. Furthermore, Riedl described a correlation between the

presence of subretinal fluid and EZ integrity at baseline and the EZ damage with SRF resolution after anti-VEGF treatment.

Coscas and coworkers [42], in a retrospective analysis on 50 eyes with nAMD, described that baseline foveal ELM and EZ integrity showed a predictive value correlating with final photoreceptor layer integrity and final BCVA.

3.1.2. Hyperreflective Dots. Hyperreflective Dots (HRD) are well-defined and circumscribed retinal lesions of approximately 20–40 μm in diameter with equivalent or higher reflectivity than the RPE band on OCT [46] (Figure 3).

HRDs have been described in several retinal diseases such as AMD, diabetic retinopathy, retinal vein occlusion, and central serous chorioretinopathy. In nAMD patients, these lesions are scattered throughout all retinal layers, in particular, around intraretinal cystoid spaces [47].

Since the histopathology of HRDs is unknown, different authors made hypotheses about the structure of this OCT feature.

Curcio and colleagues hypothesized that HRD in nAMD could be composed of two different cell populations: activated migrating RPE cells and lipid-filled microglia cells [48].

Activated migrating RPE cells have been described as discrete hyperreflective lesions in an ex vivo Spectral Domain OCT (SD-OCT) imaging-histology study of two neovascular and two nonneovascular PED. In this study, migrating RPE cells have been found throughout all retinal layers, even surrounding inner retinal capillaries. Furthermore, migrating RPE cells have been found solitarily, as punctate reflective lesions, or in swarms as large irregular lesions [49].

In the same study, a different type of hyperreflective cells was found to be associated with intraretinal cysts in the neovascular PEDs. These cells were larger than RPE, spherical, and full of lipid droplets different from RPE organelles. The authors hypothesized that this cell population could be constituted by microglia [48, 49].

Another study evaluating the association of HRDs with known AMD risk polymorphisms in early forms of AMD showed an association with polymorphisms in genes involved in extracellular matrix interactions, lipid metabolism, and complement activation, suggesting a role of the inflammation in the onset of HRDs [50].

Coscas and colleagues analyzed the prognostic value of HRDs in eyes with neovascular AMD. This study showed that poor BCVA at baseline was significantly associated with persistence of HRDs after anti-VEGF therapy. Moreover, they studied this biomarker after anti-VEGF therapy and showed the persistence of a high number of HRDs in nonresponder patients, while, in responder patients, HRDs quickly decreased after the first injection [51].

3.1.3. Outer Retinal Tubulation. Outer Retinal Tubulations (ORT) are intraretinal tubular biomarkers located more frequently in the outer nuclear layer, whose OCT aspect was first described by Zweifel et al. in 2009 [52] (Figure 4).

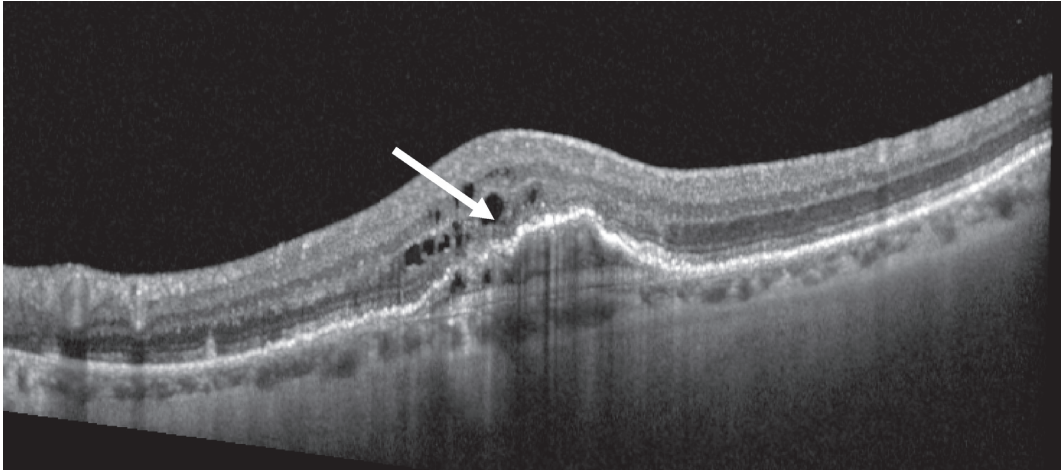


FIGURE 2: Structural OCT biomarkers: photoreceptors layer degeneration (white arrow).

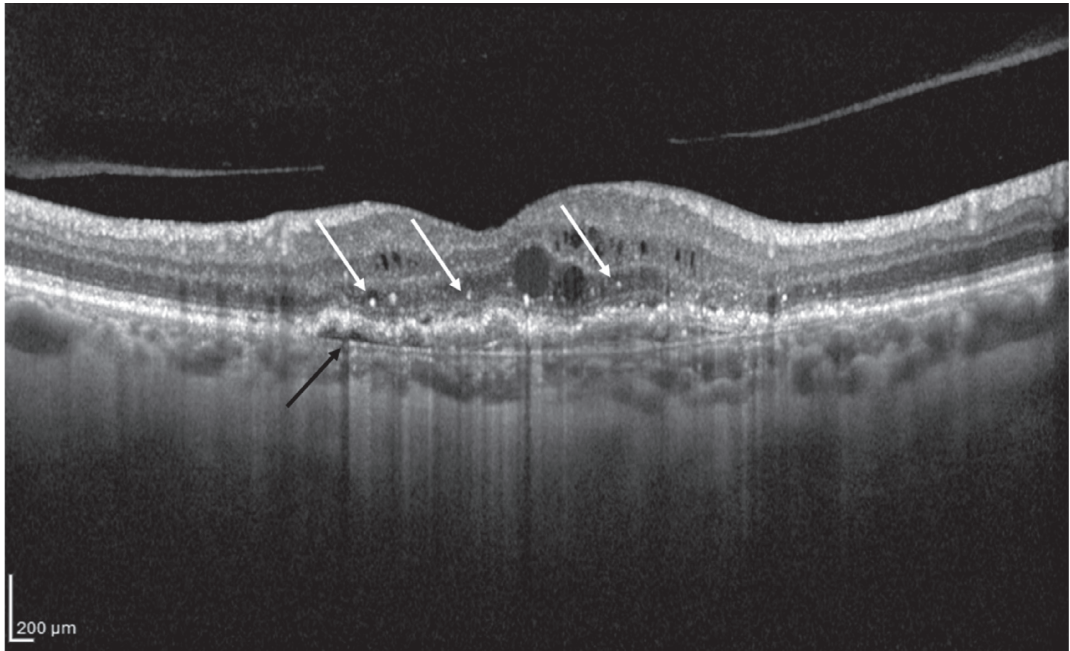


FIGURE 3: Structural OCT biomarkers: hyperreflective dots (HRD; white arrows) and RPE detachment (black arrow).

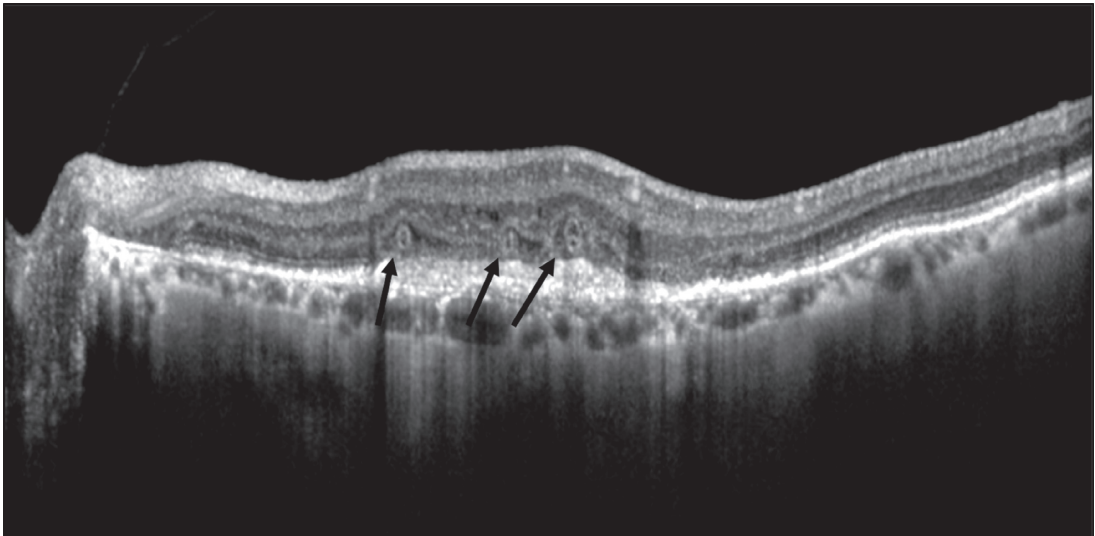


FIGURE 4: Structural OCT biomarkers: outer retinal tubulations (black arrows).

ORTs have been documented in various retinal diseases, including nAMD. The prevalence of ORTs in nAMD is low at the time of first diagnosis but increases over time during anti-VEGF therapy [53, 54].

ORTs are identified as hyporeflective structures surrounded by a hyperreflective band on OCT B scans. Their tubular appearance can be better appreciated in *en face* OCT images.

The hyperreflective outer border of ORTs has been correlated with external limiting membrane and photoreceptor inner segment mitochondria [55].

These lesions can be divided in forming ORTs, without a lumen and with ELM scrolling over a free edge, and formed ORTs. Formed ORTs can be divided in two categories: close ORTs when they have 360° well-defined hyperreflective borders and open ORTs when they show incomplete hyperreflective borders [56].

Preti et al. described a sequential evolution of ORTs; that is, forming ORTs evolve into large open ORTs, which tend to bifurcate into multiple smaller open ORTs. Smaller open ORTs tend to evolve into closed ORTs [57].

Outer retinal tubulations characteristically develop in advanced stages of AMD and are associated with the presence of MNV and geographic atrophy (GA) [56].

Finally, ORTs can be considered as a rearrangement of photoreceptors as a consequence of retinal injury, and their presence has been associated with worse visual prognosis in nAMD patients [53].

Anti-VEGF treatment seems not to decrease the development of newer ORTs neither to enhance the regression of preexisting ORTs [53, 54, 58].

3.1.4. Subretinal Hyperreflective Material. Subretinal hyperreflective material (SHRM) is a tomographic feature seen on OCT as a hyperreflective material located between the neurosensory retina and RPE [59] (Figure 5).

In eyes with nAMD, SHRM is common and often persists after anti-VEGF treatment [60, 61]. The nature of SHRM is still not known, as the literature is lacking direct histopathological studies. Authors suggest that SHRM could be made up of fluid, fibrin, blood, scar, and MNV, even though it could change over time [59, 62].

Willoughby and coworkers, in a post hoc analysis of the CATT study, demonstrated that the presence of SHRM was associated with worse VA in any position, regardless of its size. Furthermore, central fovea position and greater SHRM height and width were correlated with worse BCVA.

Moreover, the persistence of SHRM from baseline to follow-up visits was associated with a lower increase in VA [59].

Pokroy and coworkers, in a retrospective study on 73 eyes treated with three intravitreal bevacizumab injections monthly followed by PRN regimen, showed that the presence of any SHRM within the 1 mm² central fovea predicted a worse visual outcome after twelve months of treatment, especially if well-defined SHRM borders and thicker SHRM were present [63].

Optical coherence tomography angiography (OCTA) can recognize vascular from avascular SHRM components

[64]. Dansingani and colleagues identified SHRM subtypes in a cohort of 33 patients. They found that 3 patients showed a type 2 MNV, 4 patients fibrosis or disciform scar, 5 patients macular hemorrhage, 10 patients subretinal hyperreflective exudation, and 17 patients vitelliform lesions [64]. Kawashima and colleagues, in a prospective consecutive interventional case series on 44 treatment-naïve nAMD eyes, showed that vascular SHRM still remains after treatment with three intravitreal aflibercept injections monthly. Based on these findings, the authors suggested that vascular SHRM underlies a lower response to anti-VEGF therapy [65].

Kumar and colleagues, in a retrospective analysis on 499 treatment-naïve nAMD patients enrolled in randomized anti-VEGF and antiplatelet derived growth factor (PDGF) clinical trials, showed that baseline SHRM characteristics, such as layered appearance, hyperreflective spots, SHRM separation from the outer retina, and larger size, had a negative impact on subsequent visual acuity. Furthermore, in the same study, Kumar et al. described that decreasing reflectivity of SHRM lesions at follow-up visits correlated with better visual acuity [66].

3.1.5. Retinal Pigment Epithelial Tears. Retinal pigment epithelial (RPE) tears, also known as RPE rips, represent a disruption of the RPE monolayer (Figure 6). RPE tears are a well-known complication of nAMD [67]. In the large majority of cases (86.2%–100%), RPE tears occur in patients with preexisting PEDs [68]. RPE tears could occur spontaneously or as a consequence of thermal laser treatment, photodynamic therapy, or anti-VEGF therapy. The size and recent onset (<4.5 months) of PED are potential risk factors for developing RPE tears [68]. Moreover, different morphologies of PED additionally increase the risk of developing an RPE tear. Indeed, 80.6% of tears come from a fibrovascular PED, 16.2% after a hemorrhagic PED, and 3.2% from serous PEDs [69]. The PED height is a predictive factor according to several authors. Chan et al. reported that PED height greater than 400 μm is the only significant risk factor for an RPE tear after bevacizumab injection, and with PED height over 600 μm, the risk increases [70]. Sarraf et al. described that a height >550 microns is a high-risk factor for the development of RPE tears with ranibizumab therapy [71]. Indeed, this value is considered by a large consensus as the only predictive value for RPE tears occurrence. Chiang et al. noted that, in addition to PED height, a large PED basal diameter on fluorescein angiography was also a risk factor [72]. In addition, a small MNV size/PED size ratio (<50%) has been suggested as a risk factor by Chan et al. [73]. RPE irregularities along the PED borders, such as RPE thinning, RPE indentations, and small interruptions in the PED on OCT, have also been reported as predictors of impending RPE tears in patients with exudative AMD treated with anti-VEGF therapy [74, 75]. Otherwise, Musashi et al. observed microrips at the margin of the PED in 11 patients with polypoidal choroidal vasculopathy treated with photodynamic therapy and noted that no one progressed to a tear. Ten of these microrips disappeared spontaneously [76]. This difference between the studies may be due to different etiologies and treatments [77].

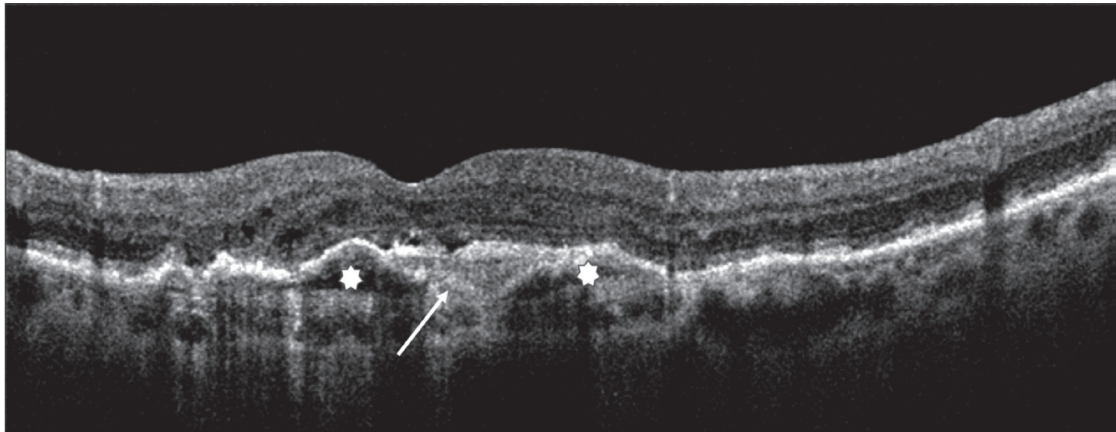


FIGURE 5: Structural OCT biomarkers: subretinal hyperreflective material (SRHM; white arrow) and pigment epithelium detachment (white stars).

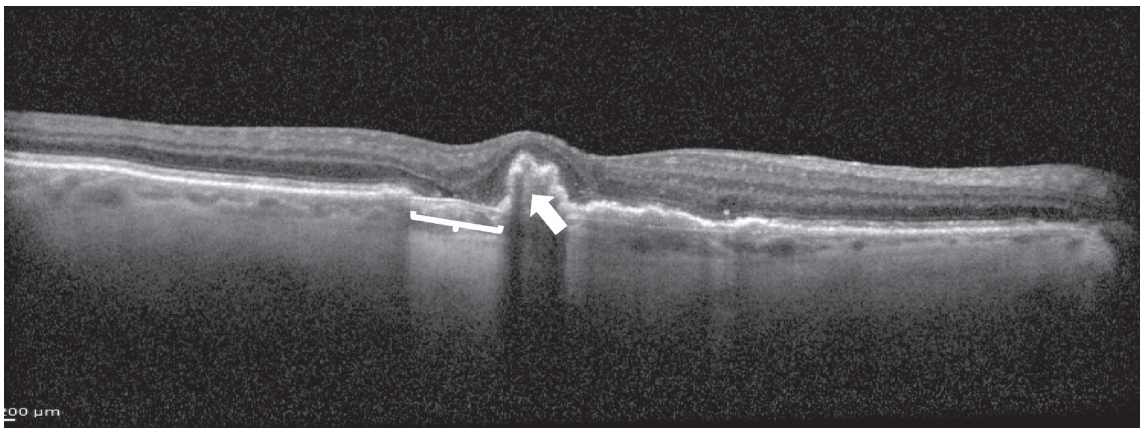


FIGURE 6: Structural OCT biomarkers: RPE tear (white bracket) and RPE layer retraction (white arrow).

The RPE rip in OCT imaging looks like an area of RPE disruption, usually located between the normal retinal architecture and the border of the PED. Small RPE ruptures appear as a tented up or peaked PED with a microscopic RPE defect. As the grade of the RPE rip increases, OCT shows a wider patch of RPE loss with the redundant RPE taking on a dome-shaped configuration [78]. The retracted RPE is observed with an irregular contour, dense hyperreflectivity from duplication of the RPE, and a shadowing effect beneath it [68, 77]. The overlying neurosensory retina remains intact with or without neurosensory detachment. In the area, where the RPE layer is absent, the bare choroid shows hyperreflectivity and deeper signal penetration [79].

RPE tears must be differentiated from RPE apertures described by Querques et al. in avascular PEDs secondary to AMD. RPE apertures are defined as round discontinuities that can be located not only at the base of an avascular PED, but also at its apex. Importantly, they do not show the rippling or retraction seen in RPE tears. The authors suggested that focal atrophic progression of drusenoid material plays role in their pathogenesis [80].

RPE tear development seems to be due to several factors: firstly, the presence of the PED applies hydrostatic pressure to the RPE and stretches it. The contractile capacity of the MNV

adds tangential forces to the RPE monolayer [77]. These processes together create a weak point at the junction of the detached and flat RPE, where the tear occurs. The tear is followed by retraction of the pigment epithelium, revealing bare Bruch's membrane [78]. Several authors propose that intravitreal anti-VEGF treatment could increase the risk of early tearing, possibly by shrinking the neovascular complex, thereby creating an extra contraction force in a PED at risk and triggering the tear of the RPE [2]. Despite multiple reports, not all studies support these conclusions [78]. There is still no evidence that any anti-VEGF agent is safer than the others [78]. In eyes with high-risk, alternative anti-VEGF treatment protocols such as low-dose and frequent injection treatments have been proposed. However, there is no proven method to foresee the development of RPE tears [78].

The visual acuity outcome after an RPE tear is variable and is determined not only by control of neovascularization, but also by tissue remodeling. Poor visual acuity is more frequently observed in cases of foveal involvement [78]. Mukai et al. observed two different repair mechanisms in the area, where RPE tears developed. When the subretinal fluid persists for more than 6 months, the denuded area is covered with thickened proliferative tissue. With an early resolution of the subretinal fluid, the outer retina appeared to be

directly attached to Bruch's membrane [81]. Oishi et al. [82] describe that, after an RPE tear, a thinning of the outer nuclear layer occurs in the area devoid of the RPE and in adjacent areas. This means that photoreceptors are lost progressively after the development of an RPE tear.

Once the RPE tear has developed, there are no clinical practice guidelines on the management of these patients. However, the evidence points to continuing (or starting) anti-VEGF treatment, which seems to reduce the development of fibrosis and decreases the risk of disciform scar development. In the presence of an active CNV, anti-VEGF injections should be repeated until the underlying disease has been resolved [68, 77, 83]. Invernizzi et al. suggested that long-term visual outcomes in eyes affected by an RPE tear may be mostly related to the patient's response to therapy than to the tear itself [67].

3.1.6. Vitreomacular Interface Alterations. The development and progression of AMD has been related to different risk factors. Recently, vitreomacular alterations have been identified as new risk factors for AMD [84]. In particular, thanks to the recent OCT imaging definition of vitreomacular adhesion (VMA) and traction (VMT), many papers describe the role of the vitreous in different aspects of exudative AMD [85]. VMA is characterized by an elevation of the cortical vitreous above the retinal surface, with the posterior hyaloid remaining attached within a 3 mm radius of the fovea without retinal abnormalities; VMT presents perifoveal vitreous cortex detachment from the retinal surface with macular attachment of the posterior hyaloid within a 3 mm radius of the fovea and distortion of the foveal surface [86] (Figures 7(a) and 7(b)).

In recent studies, there was no significant difference in the prevalence of VMA between eyes affected by AMD and age-matched controls [87]. VMA has been evaluated and described in a wide percentage of exudative AMD. Particularly, the adhesion area matched to the site of MNV.

The relation between adhesion and development of exudative MNV has been described not to be causative but correlated: the exudative, fibrotic, and proliferative events make the vitreal adhesion stronger and stabler to the retinal surface [88, 89]. For this reason, the higher prevalence of VMA reported in previous literature might be considered as a consequence of MNV, rather than a causative factor.

While the extension of the neovascular lesion is associated with the presence of VMA, the area of vitreomacular adhesion is not related to the angiographic subtype of the neovascular lesion [90–92]. Even though different opinions describe the role of a preexisting VMA and MNV development [93], the possibility to resolve the VMA may not represent a protective factor in high-risk patients [94].

Several authors describe a higher number of intravitreal injections to treat nAMD in patients presenting VMA compared to patients with complete PVD. The reasons are not fully understood, but VMA seems to make the exudative lesion more extensive and resistant to intravitreal treatment. This fact could be also due to the partial vitreous detachment influencing the achievement of the anti-VEGF therapy target [30, 95–97].

Vitreomacular traction may present a different behavior. As it could be symptomatic by causing alterations to inner and outer retinal layer for its persistent and tractive action on the macular surface, it could lead to the development of a chronic inflammation influencing the progression of exudative AMD, more than VMA [97, 98].

The presence of VMT reduces the functional and morphological improvement at two years in patients treated with anti-VEGF, requiring more injections in a ProReNata (PRN) regimen. Several authors describe the beneficial effects of surgical VMT removal on exudative AMD response to anti-VEGF. It could be due to the reduction of chronic traction and inflammatory effects, as well as to the diffusion of cytokines and VEGF from the macula into the vitreous [99–101].

3.2. Choroidal Features

3.2.1. Sub-RPE Hyperreflective Columns. Sub-RPE Hyperreflective Columns are OCT biomarkers that look like narrow columns of hyperreflectivity beneath the RPE. They have been considered as a sign of a weakened or cracked RPE layer, where fluid, blood, and/or vessels can more easily break into the subretinal space. It has been described in 27% of eyes with neovascular AMD. These sub-RPE columns are different from the regions of the increased backscattering effect observable in geographic atrophy, which look like large spans of sub-RPE hyperreflectivity [102, 103].

3.2.2. Prechoroidal Clefts. Prechoroidal Clefts are outwardly bowed hyporeflective cavities between the deeper fibrous component and the underlying hyperreflective choroid characterizing the multilayered PED (Figure 8). In eyes with exudative AMD receiving serial intravitreal anti-VEGF injections, chronic fibrovascular PEDs appear to develop through a sequential layering of hyperreflective bands beneath the RPE. Near the base of the PED (adjacent to the choroid), a fusiform complex of homogenous hyperreflective lamella surrounds the main body of this internal structure showing contractile properties, resulting in the spindle-shaped appearance. The progressive modification of sub-RPE neovascular lesions causes a delamination of RPE-Bruch's membrane complex and of the choroidal tissue due to retractive but also exudative forces [104, 105]. A similar lesion has been described by Khan in patients with polypoidal choroidal vasculopathy as one component of a "triple-layer" sign. In the literature, different authors described that these eyes surprisingly maintain a good to excellent visual acuity, probably because the neovascular and cicatricial process is confined to the sub-RPE space and effectively inhibited by continued anti-VEGF therapy. A second hypothesis considered neovascular tissue as a surrogate of the choriocapillaris and provided oxygenation or nutritional support to the outer retinal layers and the RPE, thereby protecting against involution and geographic atrophy [104–108].

The multilayered PED may be at lower risk of developing a high-grade RPE tear due to the stabilizing effect of a

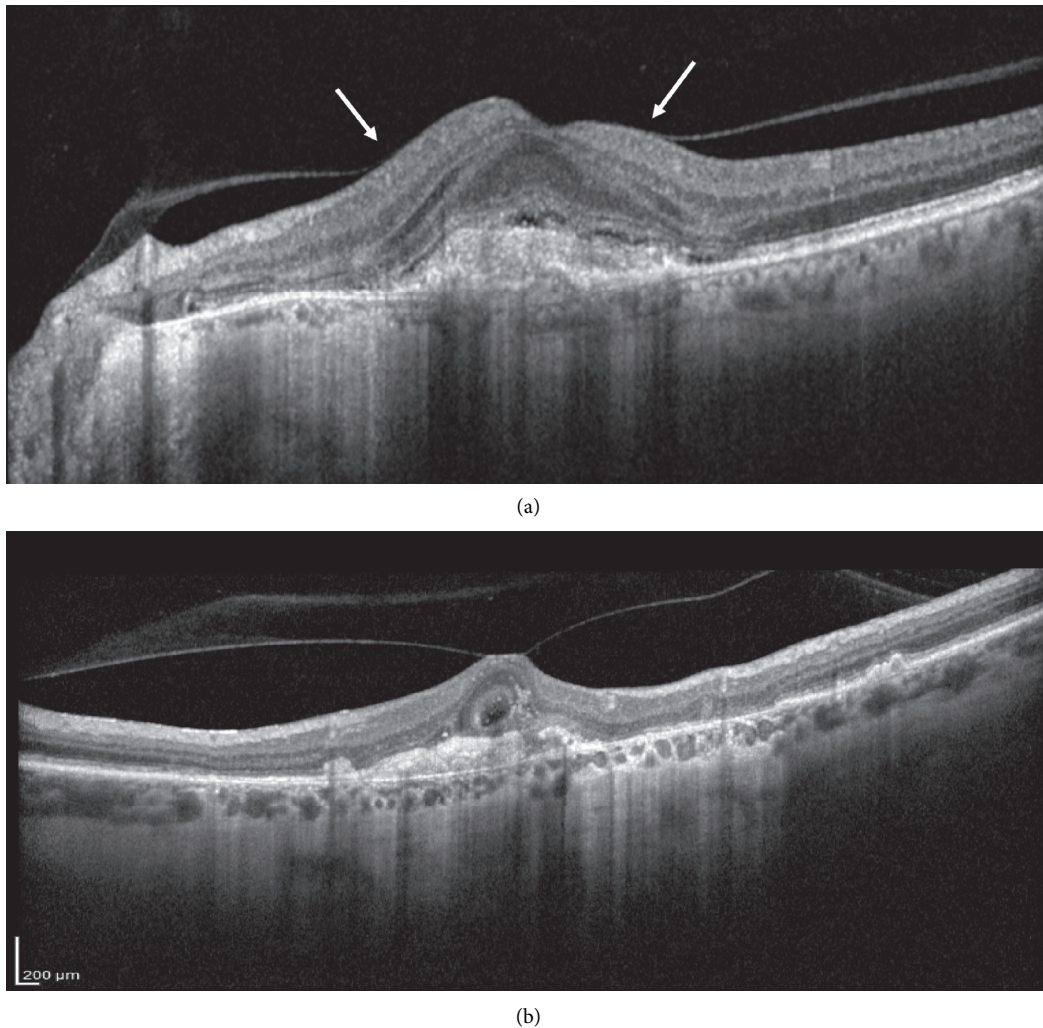


FIGURE 7: Structural OCT biomarker: (a) vitreomacular adhesion (VMA, white arrows). The posterior hyaloid is partially detached, with a continuous adhesion on the foveal surface; (b) vitreomacular traction. The posterior hyaloid is fully detached but a foveal adhesion is present on the fovea with an evident traction.

fibrovascular tissue complex that fills the sub-RPE space and anchors the PED to the underlying Bruch's complex. The early presentation in the first six months of treatment could have a negative prognostic value, probably due to the associated complications like RPE hemorrhage and RPE rips [106].

3.2.3. Choroidal Caverns. Choroidal caverns have been described with the following morphological features: (1) nonreflective spherical to polyhedral structures visible on en face and cross-sectional OCT; (2) posterior tail of hypertransmission on cross-sectional OCT (B-scan); (3) in case of RPE loss, frequently hyperreflective on Near Infrared Imaging and rarely reflective on color photographs or hyperfluorescent on ICGA; (4) not visible on FA or fundus autofluorescence imaging; (5) no evidence of flow signal on en face or cross-sectional OCT-A [109] (Figure 9).

A recent histological and clinical imaging study characterized and defined the morphology of these lesions. They

could be present in healthy subjects, as well as in different degenerative retinal pathologies, characterized by retinal and RPE atrophy. [8] Choroidal caverns were first hypothesized to be nonperfused ghost vessels with preserved stromal pillars at sites of preexisting choroidal vessels [110]. Subsequent studies proposed them as OCT correlates of Friedman lipid-rich globules [111].

In AMD, these lesions have been described in association with geographic atrophy, as well as related to neovascular tissue. In this latter case, lipid globules can be found in the sub-RPE space, intramembrane, or now described in subretinal space, to be distinguished from subretinal fluid [112, 113].

Since sub-RPE caverns have not been associated with pathological significance, no clinical intervention is needed.

3.2.4. Choroidal Thickness: Subfoveal Choroidal Thickness and Choroidal Volume. The evaluation of morphological parameters of the choroid has been enhanced with the latest

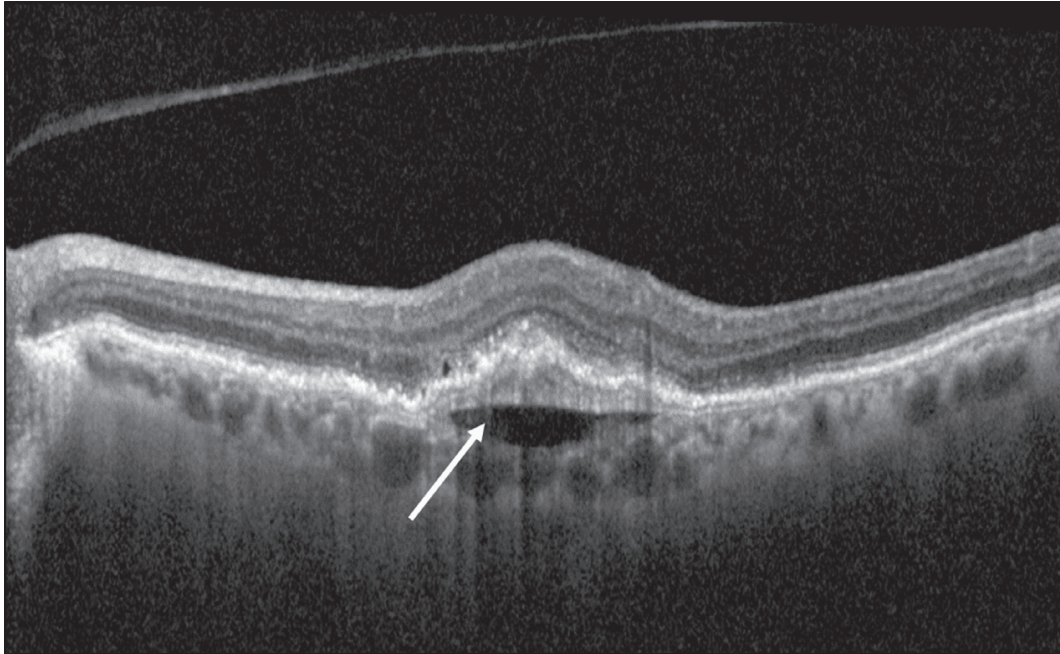


FIGURE 8: Structural biomarker: prechoroidal clefts (white arrow).

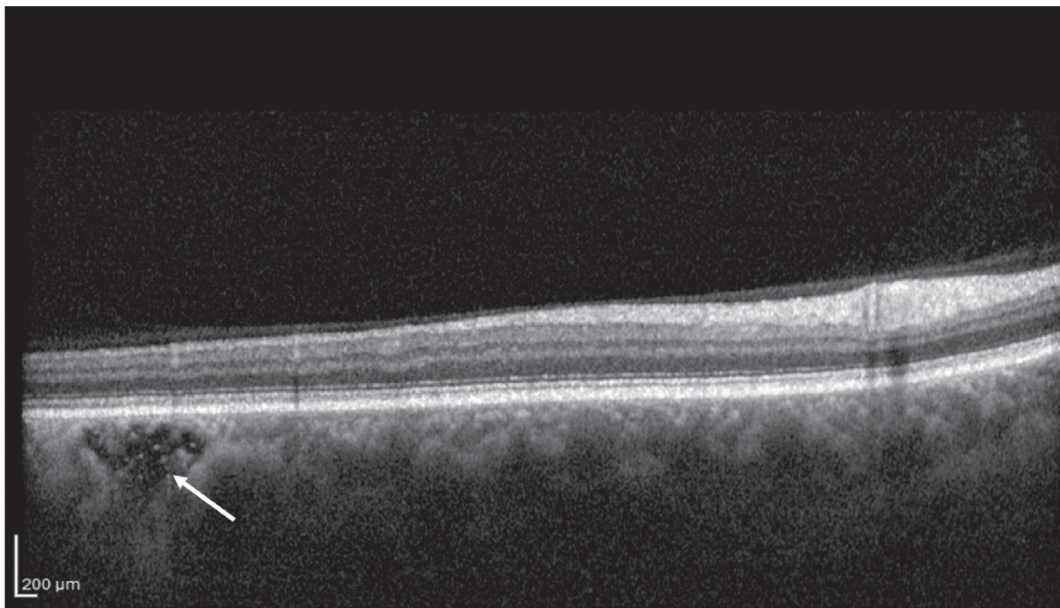


FIGURE 9: Structural biomarker: choroidal caverns (white arrow).

Swept Source OCTs enabling the analysis beyond the RPE through a strong signal identifying the vascular layer boundaries [114]. The reproducibility of the measurement is still uncertain, probably due to the circadian variation of choroidal thickness, its sensibility to systemic pressure, and different ocular variables like pre- and post-anti-VEGF injection conditions [115].

A condition of choroidal hypoperfusion may be considered as an etiological factor for the development and progression of exudative AMD. This fact is still debated, considering the role of outer retina and RPE in choriocapillary vascular sclerosis [116].

All choroidal parameters, in particular the widely studied subfoveal choroidal thickness (Figure 10), did not demonstrate a correlation with visual acuity recovery in treated patients, nor a different response to intravitreal anti-VEGF therapy. Choroidal volume, trying to avoid biases in choroidal boundary measurements, still does not show interesting clinical correlations [114, 117, 118].

A well-defined morphological entity has been identified in the pachychoroid condition. Pachychoroid is characterized by the presence of increased choroidal thickness associated with a dilation of the outer choroidal layer.

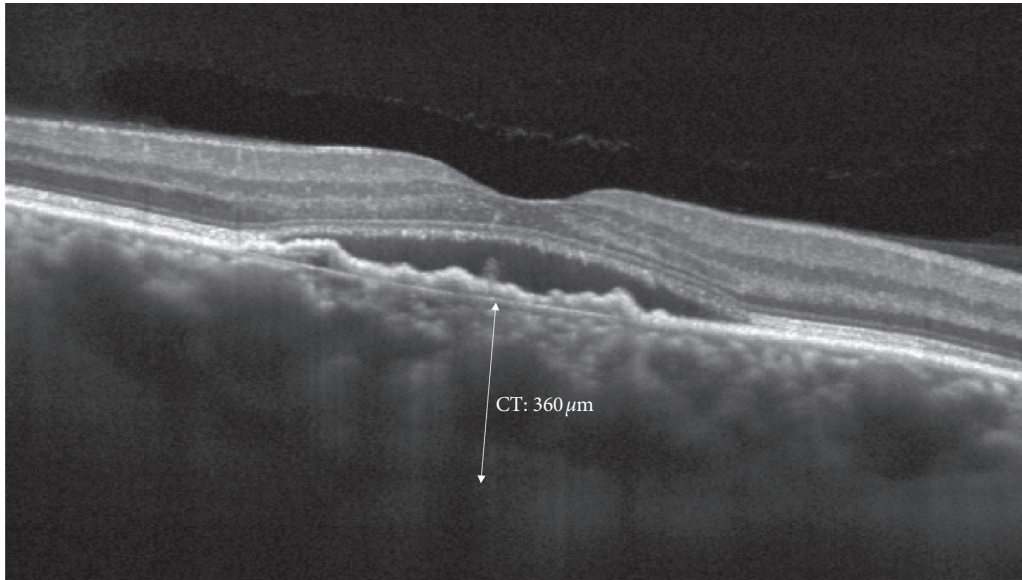


FIGURE 10: Structural biomarker: manual caliper to measure choroidal thickness (CT).

TABLE 1: Summary of OCT biomarkers and prognostic value.

Biomarker	Role
Central retinal thickness	Limited prognostic value for visual acuity If increased correlation with lesion activity is higher
Intraretinal fluids (IRC)	Negative prognostic value for VA Role debated
Distribution of retinal fluids	Protective for VA if chronic Related to a stable disease More treatments needed
Subretinal fluids (SRF)	No prognostic value for VA
Sub-RPE fluids	
Subretinal hyperreflective material (SRHM)	Negative prognostic value, in particular if persistent after anti-VEGF therapy
Outer retinal tubulation (ORT)	Associated to worse visual prognosis
Photoreceptor layer damage	Negative prognosis on visual acuity
Structural alterations	VMA and VMT: more intravitreal treatments needed
Vitreomacular interface	No prognostic value for visual acuity
Hyperreflective dots	Related to activity of the lesion and its recurrences
RPE rips	Negative prognostic value in particular if subfoveal
Choroidal morphology	Choroidal thickness: no prognostic value on VA Prechoroidal clefts: risk for REP rips

Pachychoroid has been associated with a spectrum of clinical conditions, in particular central serous chorioretinopathy, and choroidal neovascularization (called pachychoroid neovascularopathy). These features differ from nAMD, even though polypoidal choroidal neovascularization may represent a common complication [119, 120].

3.2.5. *Choroidal Vascular Index (CVI)*. Choroidal Vascular Index (CVI) has been elaborated with a binarization method using choroidal OCT B-scan to quantify the vascular component in the context of choroidal tissue overall. The imaging evaluation defined two components considering the tissue and the vascular lumen. The index is defined as the proportion of the lumen area over the total analyzed area of the scan. This parameter seems to be more stable than choroidal thickness measurements [121]. Indeed,

considering the hypoxic hypothesis for AMD progression towards choroidal neovascularization, several studies correlated the reduction of CVI with the decrease of the vascular lumen area compared to the stromal area of the choroid [122, 123]. These preliminary data may have to be further verified comparing both eyes in the same patient or different cohorts of healthy and AMD patients, to enable a risk assessment for AMD development and progression.

4. Conclusions

OCT biomarkers are becoming even more useful in the management of patients affected by nAMD, for several reasons (Table 1).

Firstly, the identification of specific biomarkers at baseline foresees the visual prognosis of these patients, even

before anti-VEGF treatment has started. Furthermore, biomarkers can provide information about the expected treatment response. In this regard, it is important to identify predictive factors associated with visual outcomes, since it could help the physician manage patients' expectations and make treatment decisions [124].

Secondly, biomarkers enable the evaluation of the progression of the disease and the treatment response, regardless of any VA alterations. In particular, the arrangement of retinal fluids can steer therapeutic decisions, with SRF being better tolerated than IRC. Indeed, OCT allows obtaining valuable information easily and quickly for an adequate course of treatment of nAMD patients, which cannot be ignored.

Moreover, OCT biomarkers can be useful to reduce the therapeutic burden of anti-VEGF treatments and to tailor the approach to each patient with nAMD.

Currently, hospital resources are not unlimited, even though there are a large number of patients needing anti-VEGF treatment. For this reason, resources must be allocated in the best possible way, ensuring an appropriate treatment to each patient [125]. Thus, for instance, it is worth prioritizing intravitreal treatment to those patients presenting biomarkers predicting good visual recovery.

Finally, biomarkers can help identify the right moment to stop intravitreal treatment for those patients having no further improvement. When OCT evaluation shows negative biomarkers, such as the disruption of the foveal photoreceptor layer, the presence of ORTs, and/or persistent IRC associated with persistent low visual acuity, physicians should stop anti-VEGF treatment, reallocating resources to other patients. On the contrary, when OCT shows positive biomarkers such as the disappearance of IRC, associated with persistent SRF or PED correlated to a good VA, the physician should continue anti-VEGF treatment.

In conclusion, OCT biomarkers are suitable to predict VA in patients with nAMD, and to guide the treatment and follow-up of these patients, improving the quality of nAMD management.

Data Availability

Research data will be available upon request from the corresponding author.

Conflicts of Interest

Authors declare no conflicts of interest.

Acknowledgments

The authors thank Mrs. Isabella Centonze for English language revision.

References

[1] D. Branisteanu, D. Branisteanu, C. Feraru et al., "Influence of unilateral intravitreal bevacizumab injection on the incidence of symptomatic choroidal neovascularization in the fellow eye in patients with neovascular age-related macular

degeneration (review)," *Experimental and Therapeutic Medicine*, vol. 20, no. 6, p. 182, 2020.

[2] V. Daien, R. P. Finger, J. S. Talks et al., "Evolution of treatment paradigms in neovascular age-related macular degeneration: a review of real-world evidence," *British Journal of Ophthalmology*, vol. 2020, Article ID bjophthalmol-2020-317434, , 2020.

[3] A. Stahl, "The diagnosis and treatment of age-related macular degeneration," *Deutsches Aerzteblatt Online*, vol. 117, no. 29-30, pp. 513–520, 2020.

[4] W. L. Wong, X. Su, X. Li et al., "Global prevalence of age-related macular degeneration and disease burden projection for 2020 and 2040: a systematic review and meta-analysis," *The Lancet Global Health*, vol. 2, no. 2, pp. e106–e116, 2014.

[5] S. R. Singh, M. Lupidi, S. B. Mishra, M. Paez-Escamilla, G. Querques, and J. Chhablani, "Unique optical coherence tomographic features in age-related macular degeneration," *Survey of Ophthalmology*, vol. 65, no. 4, pp. 451–457, 2020.

[6] T.-T. Lai, Y.-T. Hsieh, C.-M. Yang, T.-C. Ho, and C.-H. Yang, "Biomarkers of optical coherence tomography in evaluating the treatment outcomes of neovascular age-related macular degeneration: a real-world study," *Scientific Reports*, vol. 9, no. 1, p. 529, 2019.

[7] P. Phadikar, S. Saxena, S. Ruia, T. Y. Y. Lai, C. H. Meyer, and D. Elliott, "The potential of spectral domain optical coherence tomography imaging based retinal biomarkers," *International Journal of Retina and Vitreous*, vol. 3, no. 1, pp. 1–10, 2017.

[8] U. Schmidt-Erfurth and S. M. Waldstein, "A paradigm shift in imaging biomarkers in neovascular age-related macular degeneration," *Progress in Retinal and Eye Research*, vol. 50, pp. 1–24, 2016.

[9] U. Chakravarthy, M. Havelio, A. Syntosi et al., "Impact of macular fluid volume fluctuations on visual acuity during anti-VEGF therapy in eyes with nAMD," *Eye*, 2021.

[10] A. C. Ho, N. Saroj, K. Baker et al., "Impact of baseline characteristics on treatment response to intravitreal aflibercept injection for wet age-related macular degeneration," *Ophthalmology Retina*, vol. 2, no. 7, pp. 676–683, 2018.

[11] W. C. Ou, D. M. Brown, J. F. Payne, and C. C. Wyckoff, "Relationship between visual acuity and retinal thickness during anti-vascular endothelial growth factor therapy for retinal diseases," *American Journal of Ophthalmology*, vol. 180, pp. 8–17, 2017.

[12] G. Moraes, D. J. Fu, M. Wilson et al., "Quantitative analysis of OCT for neovascular age-related macular degeneration using deep learning," *Ophthalmology*, vol. 128, no. 5, pp. 693–705, 2021.

[13] G. J. Jaffe, D. F. Martin, C. A. Toth et al., "Macular morphology and visual acuity in the comparison of age-related macular degeneration treatments trials," *Ophthalmology*, vol. 120, no. 9, pp. 1860–1870, 2013.

[14] S. Sharma, C. A. Toth, E. Daniel et al., "Macular morphology and visual acuity in the second year of the comparison of age-related macular degeneration treatments trials," *Ophthalmology*, vol. 123, no. 4, pp. 865–875, 2016.

[15] M. Ritter, C. Simader, M. Bolz et al., "Intraretinal cysts are the most relevant prognostic biomarker in neovascular age-related macular degeneration independent of the therapeutic strategy," *British Journal of Ophthalmology*, vol. 98, no. 12, pp. 1629–1635, 2014.

[16] S. R. Sadda, L. L. Tuomi, B. Ding, A. E. Fung, and J. J. Hopkins, "Macular atrophy in the HARBOR study for

- neovascular age-related macular degeneration,” *Ophthalmology*, vol. 125, no. 6, pp. 878–886, 2018.
- [17] R. F. Spaide, G. J. Jaffe, D. Sarraf et al., “Consensus nomenclature for reporting neovascular age-related macular degeneration data: consensus on neovascular age-related macular degeneration nomenclature study group,” *Ophthalmology*, vol. 127, no. 5, pp. 616–636, 2020.
- [18] S. M. Waldstein, C. Simader, G. Staurenghi et al., “Morphology and visual acuity in aflibercept and ranibizumab therapy for neovascular age-related macular degeneration in the VIEW trials,” *Ophthalmology*, vol. 123, no. 7, pp. 1521–1529, 2016.
- [19] U. Schmidt-Erfurth, S. M. Waldstein, G.-G. Deak, M. Kundi, and C. Simader, “Pigment epithelial detachment followed by retinal cystoid degeneration leads to vision loss in treatment of neovascular age-related macular degeneration,” *Ophthalmology*, vol. 122, no. 4, pp. 822–832, 2015.
- [20] U. Schmidt-Erfurth, S. Klimscha, S. M. Waldstein, and H. Bogunović, “A view of the current and future role of optical coherence tomography in the management of age-related macular degeneration,” *Eye*, vol. 31, no. 1, pp. 26–44, 2017.
- [21] H. Hosseini, G. Rabina, M. Pettenkofer et al., “Clinical characteristics and visual outcomes of non-resolving subretinal fluid in neovascular AMD despite continuous monthly anti-VEGF injections: a long-term follow-up,” *Graefe’s Archive for Clinical and Experimental Ophthalmology*, vol. 259, no. 5, pp. 1153–1160, 2020.
- [22] C. Gianniou, A. Dirani, L. Jang, and I. Mantel, “Refractory intraretinal or subretinal fluid in neovascular age-related macular degeneration treated with intravitreal ranibizumab: functional and structural outcome,” *Retina*, vol. 35, no. 6, pp. 1195–1201, 2015.
- [23] J. J. Arnold, C. M. Markey, N. P. Kurstjens, and R. H. Guymer, “The role of sub-retinal fluid in determining treatment outcomes in patients with neovascular age-related macular degeneration—a phase IV randomised clinical trial with ranibizumab: the FLUID study,” *BMC Ophthalmology*, vol. 16, no. 1, p. 31, 2016.
- [24] R. H. Guymer, C. M. Markey, I. L. McAllister, M. C. Gillies, A. P. Hunyor, and J. J. Arnold, “Tolerating subretinal fluid in neovascular age-related macular degeneration treated with ranibizumab using a treat-and-extend regimen: FLUID study 24-month results,” *Ophthalmology*, vol. 126, no. 5, pp. 723–734, 2019.
- [25] M. Roh, I. Láins, H. J. Shin et al., “Microperimetry in age-related macular degeneration: association with macular morphology assessed by optical coherence tomography,” *British Journal of Ophthalmology*, vol. 103, no. 12, pp. 1769–1776, 2019.
- [26] S. R. Sadda, R. Guymer, J. M. Monés, A. Tufail, and G. J. Jaffe, “Anti-vascular endothelial growth factor use and atrophy in neovascular age-related macular degeneration: systematic literature review and expert opinion,” *Ophthalmology*, vol. 127, no. 5, pp. 648–659, 2020.
- [27] G. J. Jaffe, G.-S. Ying, C. A. Toth et al., “Macular morphology and visual acuity in year five of the comparison of age-related macular degeneration treatments trials,” *Ophthalmology*, vol. 126, no. 2, pp. 252–260, 2019.
- [28] K. X. Cheong, D. S. Grewal, K. Y. C. Teo, A. T. L. Gan, G. J. Jaffe, and G. C. M. Cheung, “The relationship between pigment epithelial detachment and visual outcome in neovascular age-related macular degeneration and polypoidal choroidal vasculopathy,” *Eye*, vol. 34, no. 12, pp. 2257–2263, 2020.
- [29] C. Simader, M. Ritter, M. Bolz et al., “Morphologic parameters relevant for visual outcome during anti-angiogenic therapy of neovascular age-related macular degeneration,” *Ophthalmology*, vol. 121, no. 6, pp. 1237–1245, 2014.
- [30] M. Ashraf, A. Souka, and R. A. Adelman, “Age-related macular degeneration: using morphological predictors to modify current treatment protocols,” *Acta Ophthalmologica*, vol. 96, no. 2, pp. 120–133, 2018.
- [31] D. Sarraf, N. J. S. London, R. N. Khurana et al., “Ranibizumab treatment for pigment epithelial detachment secondary to neovascular age-related macular degeneration: post hoc analysis of the HARBOR study,” *Ophthalmology*, vol. 123, no. 10, pp. 2213–2224, 2016.
- [32] M. Karampelas, P. Malamos, P. Petrou, I. Georgalas, D. Papaconstantinou, and D. Brouzas, “Retinal pigment epithelial detachment in age-related macular degeneration,” *Ophthalmology and Therapy*, vol. 9, no. 4, pp. 739–756, 2020.
- [33] T. Ach, A. E. Hoeh, M. Ruppenstein, F. T. A. Kretz, and S. Dithmar, “Intravitreal bevacizumab in vascular pigment epithelium detachment as a result of subfoveal occult choroidal neovascularization in age-related macular degeneration,” *Retina*, vol. 30, no. 9, pp. 1420–1425, 2010.
- [34] C. A. Curcio, N. E. Medeiros, and C. L. Millican, “Photoreceptor loss in age-related macular degeneration,” *Investigative Ophthalmology & Visual Science*, vol. 37, no. 7, pp. 1236–1249, 1996.
- [35] T. Otani, Y. Yamaguchi, and S. Kishi, “Correlation between visual acuity and foveal microstructural changes in diabetic macular edema,” *Retina*, vol. 30, no. 5, pp. 774–780, 2010.
- [36] H. J. Shin, S. H. Lee, H. Chung, and H. C. Kim, “Association between photoreceptor integrity and visual outcome in diabetic macular edema,” *Graefe’s Archive for Clinical and Experimental Ophthalmology*, vol. 250, no. 1, pp. 61–70, 2012.
- [37] J. K. Chhablani, J. S. Kim, L. Cheng, I. Kozak, and W. Freeman, “External limiting membrane as a predictor of visual improvement in diabetic macular edema after pars plana vitrectomy,” *Graefe’s Archive for Clinical and Experimental Ophthalmology*, vol. 250, no. 10, pp. 1415–1420, 2012.
- [38] A. Oishi, A. Tsujikawa, K. Yamashiro et al., “One-year result of aflibercept treatment on age-related macular degeneration and predictive factors for visual outcome,” *American Journal of Ophthalmology*, vol. 159, no. 5, pp. 853.e1–860.e1, 2015.
- [39] A. Oishi, M. Shimozone, M. Mandai, M. Hata, A. Nishida, and Y. Kurimoto, “Recovery of photoreceptor outer segments after anti-VEGF therapy for age-related macular degeneration,” *Graefe’s Archive for Clinical and Experimental Ophthalmology*, vol. 251, no. 2, pp. 435–440, 2013.
- [40] Y. Itoh, M. Inoue, T. Rii, K. Hirota, and A. Hirakata, “Correlation between foveal cone outer segment tips line and visual recovery after epiretinal membrane surgery,” *Investigative Ophthalmology & Visual Science*, vol. 54, no. 12, pp. 7302–7308, 2013.
- [41] M. Woronkiewicz, S. Lightman, and O. Tomkins-Netzer, “The prognostic value of total macular external limiting membrane and ellipsoid zone damage for clinical outcome in treatment-resistant neovascular age-related macular degeneration,” *Graefe’s Archive for Clinical and Experimental Ophthalmology*, vol. 258, no. 11, pp. 2373–2378, 2020.
- [42] F. Coscas, G. Coscas, M. Lupidi et al., “Restoration of outer retinal layers after aflibercept therapy in exudative AMD: prognostic value,” *Investigative Ophthalmology & Visual Science*, vol. 56, no. 6, pp. 4129–4134, 2015.

- [43] H. J. Shin, H. Chung, and H. C. Kim, "Association between foveal microstructure and visual outcome in age-related macular degeneration," *Retina*, vol. 31, no. 8, pp. 1627–1636, 2011.
- [44] S. Riedl, L. Cooney, C. Grechenig et al., "Topographic analysis of photoreceptor loss correlated with disease morphology in neovascular age-related macular degeneration," *Retina*, vol. 40, no. 11, pp. 2148–2157, 2020.
- [45] Y. M. Kim, J. H. Kim, and H. J. Koh, "Improvement of photoreceptor integrity and associated visual outcome in neovascular age-related macular degeneration," *American Journal of Ophthalmology*, vol. 154, no. 1, pp. 164.e1–173.e1, 2012.
- [46] H. S. Hwang, J. B. Chae, J. Y. Kim, and D. Y. Kim, "Association between hyperreflective dots on spectral-domain optical coherence tomography in macular edema and response to treatment," *Investigative Ophthalmology & Visual Science*, vol. 58, no. 13, pp. 5958–5967, 2017.
- [47] G. Coscas, F. Coscas, S. Vismara, A. Zourdani, and C. Li Calzi, "Clinical features and natural history of AMD on OCT," *Optical Coherence Tomography in Age-Related Macular Degeneration*, Springer, Berlin, Germany, 2009.
- [48] C. A. Curcio, E. C. Zanzottera, T. Ach, C. Balaratnasingam, and K. B. Freund, "Activated retinal pigment epithelium, an optical coherence tomography biomarker for progression in age-related macular degeneration," *Investigative Ophthalmology & Visual Science*, vol. 58, no. 6, pp. BIO211–BIO226, 2017.
- [49] C. Balaratnasingam, J. D. Messinger, K. R. Sloan, L. A. Yannuzzi, K. B. Freund, and C. A. Curcio, "Histologic and optical coherence tomographic correlates in drusenoid pigment epithelium detachment in age-related macular degeneration," *Ophthalmology*, vol. 124, no. 5, pp. 644–656, 2017.
- [50] L. Altay, P. Scholz, T. Schick et al., "Association of hyperreflective foci present in early forms of age-related macular degeneration with known age-related macular degeneration risk polymorphisms," *Investigative Ophthalmology & Visual Science*, vol. 57, no. 10, pp. 4315–4320, 2016.
- [51] G. Coscas, U. De Benedetto, F. Coscas et al., "Hyperreflective dots: a new spectral-domain optical coherence tomography entity for follow-up and prognosis in exudative age-related macular degeneration," *Ophthalmologica*, vol. 229, no. 1, pp. 32–37, 2013.
- [52] S. A. Zweifel, M. Engelbert, K. Laud, R. Margolis, R. F. Spaide, and K. B. Freund, "Outer retinal tubulation: a novel optical coherence tomography finding," *Archives of Ophthalmology*, vol. 127, no. 12, pp. 1596–1602, 2009.
- [53] J. Y. Lee, F. A. Folgar, M. G. Maguire et al., "Outer retinal tubulation in the comparison of age-related macular degeneration treatments trials (CATT)," *Ophthalmology*, vol. 121, no. 12, pp. 2423–2431, 2014.
- [54] A. Dirani, C. Gianniou, L. Marchionno, D. Decugis, and I. Mantel, "Incidence of outer retinal tubulation in ranibizumab-treated age-related macular degeneration," *Retina*, vol. 35, no. 6, pp. 1166–1172, 2015.
- [55] K. M. Litts, J. D. Messinger, K. Dellatorre, L. A. Yannuzzi, K. B. Freund, and C. A. Curcio, "Clinicopathological correlation of outer retinal tubulation in age-related macular degeneration," *JAMA Ophthalmology*, vol. 133, no. 5, pp. 609–612, 2015.
- [56] K. B. Schaal, K. B. Freund, K. M. Litts, Y. Zhang, J. D. Messinger, and C. A. Curcio, "Outer retinal tubulation in advanced age-related macular degeneration: optical coherence tomographic findings correspond to histology," *Retina*, vol. 35, no. 7, pp. 1339–1350, 2015.
- [57] R. C. Preti, A. Govetto, R. G. A. Filho et al., "Optical coherence tomography analysis of outer retinal tubulations: sequential evolution and pathophysiological insights," *Retina*, vol. 38, no. 8, pp. 1518–1525, 2018.
- [58] A. Kovacs, T. Kiss, F. Rarosi, G. M. Somfai, A. Facsko, and R. Degi, "The effect of ranibizumab and aflibercept treatment on the prevalence of outer retinal tubulation and its influence on retreatment in neovascular age-related macular degeneration," *BMC Ophthalmology*, vol. 18, no. 1, p. 298, 2018.
- [59] A. S. Willoughby, G. S. Ying, C. A. Toth et al., "Subretinal hyperreflective material in the comparison of age-related macular degeneration treatments trials," *Ophthalmology*, vol. 122, no. 9, pp. 1846.e5–1853.e5, 2015.
- [60] G.-s. Ying, B. J. Kim, M. G. Maguire et al., "Sustained visual acuity loss in the comparison of age-related macular degeneration treatments trials," *JAMA Ophthalmology*, vol. 132, no. 8, pp. 915–921, 2014.
- [61] T. Ristau, P. A. Keane, A. C. Walsh et al., "Relationship between visual acuity and spectral domain optical coherence tomography retinal parameters in neovascular age-related macular degeneration," *Ophthalmologica*, vol. 231, no. 1, pp. 37–44, 2014.
- [62] W. Charafeddin, M. G. Nittala, A. Oregon, and S. R. Sadda, "Relationship between subretinal hyperreflective material reflectivity and volume in patients with neovascular age-related macular degeneration following anti-vascular endothelial growth factor treatment," *Ophthalmic Surgery, Lasers and Imaging Retina*, vol. 46, no. 5, pp. 523–530, 2015.
- [63] R. Pokroy, M. Mimouni, E. Barayev et al., "Prognostic value of subretinal hyperreflective material in neovascular age-related macular degeneration treated with bevacizumab," *Retina*, vol. 38, no. 8, pp. 1485–1491, 2018.
- [64] K. K. Dansingani, A. C. S. Tan, F. Gilani et al., "Subretinal hyperreflective material imaged with optical coherence tomography angiography," *American Journal of Ophthalmology*, vol. 169, pp. 235–248, 2016.
- [65] Y. Kawashima, M. Hata, A. Oishi et al., "Association of vascular versus avascular subretinal hyperreflective material with aflibercept response in age-related macular degeneration," *American Journal of Ophthalmology*, vol. 181, pp. 61–70, 2017.
- [66] J. B. Kumar, S. Stinnett, J. I. L. Han, and G. J. Jaffe, "Correlation of subretinal hyperreflective material morphology and visual acuity in neovascular age-related macular degeneration," *Retina*, vol. 40, no. 5, pp. 845–856, 2020.
- [67] A. Invernizzi, V. Nguyen, J. Arnold, S. Young, D. Barthelmes, and M. C. Gillies, "Early and late retinal pigment epithelium tears after anti-vascular endothelial growth factor therapy for neovascular age-related macular degeneration," *Ophthalmology*, vol. 125, no. 2, pp. 237–244, 2018.
- [68] M. Sastre-Ibáñez, C. Martínez-Rubio, R. Molina-Pallete et al., "Retinal pigment epithelial tears," *Journal Français d'Ophthalmologie*, vol. 42, no. 1, pp. 63–72, 2019.
- [69] H. J. Cho, H. S. Kim, S. G. Yoo et al., "Retinal pigment epithelial tear after intravitreal ranibizumab treatment for neovascular age-related macular degeneration," *Retina*, vol. 36, no. 10, pp. 1851–1859, 2016.
- [70] C. K. Chan, P. Abraham, C. H. Meyer et al., "Optical coherence tomography-measured pigment epithelial detachment height as a predictor for retinal pigment epithelial tears associated with intravitreal bevacizumab injections," *Retina*, vol. 30, no. 2, pp. 203–211, 2010.

- [71] D. Sarraf, C. Chan, E. Rahimy, and P. Abraham, "Prospective evaluation of the incidence and risk factors for the development of RPE tears after high- and low-dose ranibizumab therapy," *Retina*, vol. 33, no. 8, pp. 1551–1557, 2013.
- [72] A. Chiang, L. K. Chang, F. Yu, and D. Sarraf, "Predictors of anti-VEGF-associated retinal pigment epithelial tear using FA and OCT analysis," *Retina*, vol. 28, no. 9, pp. 1265–1269, 2008.
- [73] C. K. Chan, C. H. Meyer, J. G. Gross et al., "Retinal pigment epithelial tears after intravitreal bevacizumab injection for neovascular age-related macular degeneration," *Retina*, vol. 27, no. 5, pp. 541–551, 2007.
- [74] I. Moroz, J. Moisseiev, and A. Alhalel, "Optical coherence tomography predictors of retinal pigment epithelial tear following intravitreal bevacizumab injection," *Ophthalmic Surgery, Lasers and Imaging Retina*, vol. 40, no. 6, pp. 570–575, 2009.
- [75] K. Shiraki, T. Kohno, S. Ataka, K. Abe, K. Inoue, and T. Miki, "Thinning and small holes at an impending tear of a retinal pigment epithelial detachment," *Graefe's Archive for Clinical and Experimental Ophthalmology*, vol. 239, no. 6, pp. 430–436, 2001.
- [76] K. Musashi, A. Tsujikawa, Y. Hirami et al., "Microrips of the retinal pigment epithelium in polypoidal choroidal vasculopathy," *American Journal of Ophthalmology*, vol. 143, no. 5, pp. 883–885, 2007.
- [77] M. G. Ersoz, M. Karacorlu, S. Arf, I. Sayman Muslubas, and M. Hocaoglu, "Retinal pigment epithelium tears: classification, pathogenesis, predictors, and management," *Survey of Ophthalmology*, vol. 62, no. 4, pp. 493–505, 2017.
- [78] A. V. Rachitskaya and R. Goldhardt, "Retinal pigment epithelium tear," *Current Ophthalmology Reports*, vol. 3, no. 1, pp. 26–33, 2015.
- [79] M. Nicolò, D. Ghiglione, and G. Calabria, "Retinal pigment epithelial tear following intravitreal injection of bevacizumab (avastin)," *European Journal of Ophthalmology*, vol. 16, no. 5, pp. 770–773, 2006.
- [80] G. Querques, V. Capuano, E. Costanzo et al., "Retinal pigment epithelium aperture: a previously unreported finding in the evolution of avascular pigment epithelium detachment," *Retina*, vol. 36, no. 1, pp. S65–S72, 2016.
- [81] R. Mukai, T. Sato, and S. Kishi, "Repair mechanism of retinal pigment epithelial tears in age-related macular degeneration," *Retina*, vol. 35, no. 3, pp. 473–480, 2015.
- [82] A. Oishi, P. P. Fang, S. Thiele, F. G. Holz, and T. U. Krohne, "Longitudinal change of outer nuclear layer after retinal pigment epithelial tear secondary to age-related macular degeneration," *Retina*, vol. 38, no. 7, pp. 1331–1337, 2018.
- [83] C. Vazquez-Alfageme, L. Nicholson, R. D. Hamilton, and P. J. Patel, "Incidence and long-term visual acuity outcomes of retinal pigment epithelium tears after intravitreal anti-vascular endothelial growth factor treatment of neovascular age-related macular degeneration," *Retina*, vol. 39, no. 4, pp. 664–669, 2019.
- [84] M. Maier, S. Pfrommer, S. Burzer, N. Feucht, C. Winkler von Mohrenfels, and C. Lohmann, "Vitreomacular interface and posterior vitreomacular adhesion in exudative age-related macular degeneration (AMD): an OCT-based comparative study," *Klinische Monatsblätter für Augenheilkunde*, vol. 229, no. 10, pp. 1030–1035, 2012.
- [85] M. Ashraf, A. Souka, and R. A. Adelman, "Association between the vitreomacular interface and optical coherence tomography characteristics in wet age-related macular degeneration," *Retina*, vol. 37, no. 9, pp. 1738–1745, 2017.
- [86] S. Gattoussi, G. H. S. Buitendijk, T. Peto et al., "The European eye epidemiology spectral-domain optical coherence tomography classification of macular diseases for epidemiological studies," *Acta Ophthalmologica*, vol. 97, no. 4, pp. 364–371, 2019.
- [87] E. Maggio, A. Polito, M. Guerriero, G. Prigione, B. Parolini, and G. Pertile, "Vitreomacular adhesion and the risk of neovascular age-related macular degeneration," *Ophthalmology*, vol. 124, no. 5, pp. 657–666, 2017.
- [88] E. C. Kang and H. J. Koh, "Effects of vitreomacular adhesion on age-related macular degeneration," *Journal of Ophthalmology*, vol. 2015, Article ID 865083, 7 pages, 2015.
- [89] T. C. M. Kanadani, C. E. Dos Reis Veloso, S. Dorairaj, and M. B. Nehemy, "Influence of vitreomacular adhesion on anti-vascular endothelial growth factor treatment for neovascular age-related macular degeneration," *Ophthalmic Research*, vol. 58, no. 1, pp. 18–26, 2017.
- [90] S. Gattoussi, A. Cougnard-Grégoire, M.-N. Delyfer et al., "Vitreomacular adhesion and its association with age-related macular degeneration in a population-based setting: the alienor study," *Investigative Ophthalmology & Visual Science*, vol. 58, no. 4, pp. 2180–2186, 2017.
- [91] T. L. Jackson, E. Nicod, A. Angelis et al., "Vitreous attachment in age-related macular degeneration, diabetic macular edema, and retinal vein occlusion: a systematic review and metaanalysis," *Retina*, vol. 33, no. 6, pp. 1099–1108, 2013.
- [92] M. A. El-Hifnawy, H. A. Ibrahim, A. R. Gooma, and M. A. Elmasry, "The vitreomacular interface in different types of age-related macular degeneration," *International Journal of Ophthalmology*, vol. 10, no. 2, pp. 246–253, 2017.
- [93] S. Jun Lee, C. S. Lee, and H. Jun Koh, "Posterior vitreomacular adhesion and risk of exudative age-related macular degeneration: paired eye study," *American Journal of Ophthalmology*, vol. 147, no. 4, pp. 621.e1–626.e1, 2009.
- [94] R. L. Novack, G. Staurengi, A. Girach, N. Narendran, and M. Tolentino, "Safety of intravitreal ocriplasmin for focal vitreomacular adhesion in patients with exudative age-related macular degeneration," *Ophthalmology*, vol. 122, no. 4, pp. 796–802, 2015.
- [95] S. J. Lee and H. J. Koh, "Effects of vitreomacular adhesion on anti-vascular endothelial growth factor treatment for exudative age-related macular degeneration," *Ophthalmology*, vol. 118, no. 1, pp. 101–110, 2011.
- [96] M. Gao, L. Liu, X. Liang, Y. Yu, X. Liu, and W. Liu, "Influence of vitreomacular interface on anti-vascular endothelial growth factor treatment outcomes in neovascular age-related macular degeneration: a MOOSE-compliant meta-analysis," *Medicine*, vol. 96, no. 50, Article ID e9345, 2017.
- [97] P. Xie, X. Zheng, Y. Yu et al., "Vitreomacular adhesion or vitreomacular traction may affect anti-vascular endothelial growth factor treatment for neovascular age-related macular degeneration," *British Journal of Ophthalmology*, vol. 101, no. 8, pp. 1003–1010, 2017.
- [98] A. E. Green-Simms and S. J. Bakri, "Vitreomacular traction and age-related macular degeneration," *Seminars in Ophthalmology*, vol. 26, no. 3, pp. 137–138, 2011.
- [99] S. Kimura, Y. Morizane, S. Tushima et al., "Efficacy of vitrectomy and inner limiting membrane peeling in age-related macular degeneration resistant to anti-vascular endothelial growth factor therapy, with vitreomacular traction or epiretinal membrane," *Graefe's Archive for Clinical and Experimental Ophthalmology*, vol. 254, no. 9, pp. 1731–1736, 2016.

- [100] K. H. Lee, H. S. Chin, N. R. Kim, and Y. S. Moon, "Effects of vitreomacular traction on ranibizumab treatment response in eyes with neovascular age-related macular degeneration," *Korean Journal of Ophthalmology*, vol. 29, no. 6, pp. 396–403, 2015.
- [101] R. Krishnan, R. Arora, G. De Salvo et al., "Vitreomacular traction affects anti-vascular endothelial growth factor treatment outcomes for exudative age-related macular degeneration," *Retina*, vol. 35, no. 9, pp. 1750–1756, 2015.
- [102] L. Padnick-Silver, A. B. Weinberg, F. P. Lafranco, and M. S. Macsai, "Pilot study for the detection of early exudative age-related macular degeneration with optical coherence tomography," *Retina*, vol. 32, no. 6, pp. 1045–1056, 2012.
- [103] R. Silva, M. L. Cachulo, P. Fonseca et al., "Age-related macular degeneration and risk factors for the development of choroidal neovascularisation in the fellow eye: a 3-year follow-up study," *Ophthalmologica*, vol. 226, no. 3, pp. 110–118, 2011.
- [104] E. Rahimy, K. B. Freund, M. Larsen et al., "Multilayered pigment epithelial detachment in neovascular age-related macular degeneration," *Retina*, vol. 34, no. 7, pp. 1289–1295, 2014.
- [105] J. M. Kim, S. W. Kang, D. y. Son, and K. Bae, "Risk factors and clinical significance of prechoroidal cleft in neovascular age-related macular degeneration," *Retina*, vol. 37, no. 11, pp. 2047–2055, 2017.
- [106] A. Nagiel, K. B. Freund, R. F. Spaide, I. C. Munch, M. Larsen, and D. Sarraf, "Mechanism of retinal pigment epithelium tear formation following intravitreal anti-vascular endothelial growth factor therapy revealed by spectral-domain optical coherence tomography," *American Journal of Ophthalmology*, vol. 156, no. 5, pp. 981.e2–988.e2, 2013.
- [107] J. H. Kim, Y. S. Chang, J. W. Kim, C. G. Kim, and D. W. Lee, "Prechoroidal cleft in type 3 neovascularization: incidence, timing, and its association with visual outcome," *Journal of Ophthalmology*, vol. 2018, Article ID 2578349, 8 pages, 2018.
- [108] S. Khan, M. Engelbert, Y. Imamura, and K. B. Freund, "Polypoidal choroidal vasculopathy: simultaneous indocyanine green angiography and eye-tracked spectral domain optical coherence tomography findings," *Retina*, vol. 32, no. 6, pp. 1057–1068, 2012.
- [109] R. Dolz-Marco, J. P. Glover, O. Gal-Or et al., "Choroidal and sub-retinal pigment epithelium caverns: multimodal imaging and correspondence with friedman lipid globules," *Ophthalmology*, vol. 125, no. 8, pp. 1287–1301, 2018.
- [110] G. Querques, E. Costanzo, A. Miere, V. Capuano, and E. H. Souied, "Choroidal caverns: a novel optical coherence tomography finding in geographic atrophy," *Investigative Ophthalmology & Visual Science*, vol. 57, no. 6, pp. 2578–2582, 2016.
- [111] E. Friedman and T. R. Smith, "Clinical and pathological study of choroidal lipid globules," *Archives of Ophthalmology*, vol. 75, no. 3, pp. 334–336, 1966.
- [112] X. Xu, X. Liu, X. Wang et al., "Retinal pigment epithelium degeneration associated with subretinal drusenoid deposits in age-related macular degeneration," *American Journal of Ophthalmology*, vol. 175, pp. 87–98, 2017.
- [113] P. Fernández-Avellaneda, K. B. Freund, R. K. Wang et al., "Multimodal imaging features and clinical relevance of subretinal lipid globules," *American Journal of Ophthalmology*, vol. 222, pp. 112–125, 2021.
- [114] J. Wang and L. R. Yin, "The application of enhanced depth imaging spectral-domain optical coherence tomography in macular diseases," *Journal of Ophthalmology*, vol. 2020, Article ID 9503795, 7 pages, 2020.
- [115] S. R. Singh, K. K. Vupparaboina, A. Goud, K. K. Dansingani, and J. Chhablani, "Choroidal imaging biomarkers," *Survey of Ophthalmology*, vol. 64, no. 3, pp. 312–333, 2019.
- [116] X. Wang, L. Zeng, M. Chen, and L. Liu, "Choroidal vascular changes in age-related macular degeneration: a protocol for systematic review and meta-analysis," *Medicine*, vol. 99, no. 46, Article ID e23200, 2020.
- [117] T. C. M. Kanadani, C. E. Veloso, and M. B. Nehemy, "Subfoveal choroidal thickness in eyes with neovascular age-related macular degeneration treated with anti-vascular endothelial growth factor agents," *Ophthalmologica*, vol. 240, no. 4, pp. 200–207, 2018.
- [118] H. Koizumi, M. Kano, A. Yamamoto et al., "Subfoveal choroidal thickness during aflibercept therapy for neovascular age-related macular degeneration: twelve-month results," *Ophthalmology*, vol. 123, no. 3, pp. 617–624, 2016.
- [119] C. M. G. Cheung, W. K. Lee, H. Koizumi, K. Dansingani, T. Y. Y. Lai, and K. B. Freund, "Pachychoroid disease," *Eye*, vol. 33, no. 1, pp. 14–33, 2019.
- [120] C. E. Pang and K. B. Freund, "Pachychoroid neovascularopathy," *Retina*, vol. 35, no. 1, pp. 1–9, 2015.
- [121] R. Agrawal, P. Gupta, K.-A. Tan, C. M. G. Cheung, T.-Y. Wong, and C.-Y. Cheng, "Choroidal vascularity index as a measure of vascular status of the choroid: measurements in healthy eyes from a population-based study," *Scientific Reports*, vol. 6, no. 1, Article ID 21090, 2016.
- [122] X. Wei, D. S. W. Ting, W. Y. Ng, N. Khandelwal, R. Agrawal, and C. M. G. Cheung, "Choroidal vascularity index: a novel optical coherence tomography based parameter in patients with exudative age-related macular degeneration," *Retina*, vol. 37, no. 6, pp. 1120–1125, 2017.
- [123] P. Gupta, D. S. W. Ting, S. G. Thakku et al., "Detailed characterization of choroidal morphologic and vascular features in age-related macular degeneration and polypoidal choroidal vasculopathy," *Retina*, vol. 37, no. 12, pp. 2269–2280, 2017.
- [124] E. Midena, M. Varano, E. Pilotto et al., "Real-life patient journey in neovascular age-related macular degeneration: a narrative medicine analysis in the Italian setting," *Eye*, 2021.
- [125] E. Li, S. Donati, K. B. Lindsley, M. G. Krzystolik, and G. Virgili, "Treatment regimens for administration of anti-vascular endothelial growth factor agents for neovascular age-related macular degeneration," *The Cochrane Database of Systematic Reviews*, vol. 5, no. 5, Article ID CD012208, 2020.

Research Article

Characterizing Flow and Structure of Diabetic Retinal Neovascularization after Intravitreal Anti-VEGF Using Optical Coherence Tomography Angiography: A Pilot Study

Christof Haensli ¹, Katrin Fasler ¹, Daniel Barthelmes ^{1,2} and Sandrine A. Zweifel ¹

¹Department of Ophthalmology, University Hospital and University of Zurich, Zurich, Switzerland

²Save Sight Institute, University of Sydney, Sydney, New South Wales, Australia

Correspondence should be addressed to Sandrine A. Zweifel; sandrine.zweifel@usz.ch

Received 9 April 2021; Accepted 2 July 2021; Published 14 July 2021

Academic Editor: Serena Fragiotta

Copyright © 2021 Christof Haensli et al. This is an open access article distributed under the Creative Commons Attribution License, which permits unrestricted use, distribution, and reproduction in any medium, provided the original work is properly cited.

Background/Aims. This study evaluates changes of flow and structure of diabetic retinal neovascularization (NV) treated with intravitreal anti-vascular endothelial growth factor (VEGF) agents using optical coherence tomography angiography (OCTA). With OCTA, retinal blood vessels are visualized at high resolution to separately look at flow and structure information without the need for dye injection. We introduce a new measurement method including and combining information of flow and structure. **Methods.** Retrospective observational case series. Patients with proliferative diabetic retinopathy (PDR) were treated with intravitreal anti-VEGF injections. Retinal NV were repeatedly imaged using swept-source OCTA (Zeiss PlexElite 9000) at baseline, after initial treatment block with 3–4 monthly injections, and during a follow-up period of up to 51 weeks. Change of size and flow density of the structural and angio area of NV was assessed. **Results.** Nine NV in eight eyes of five patients were analyzed with a median follow-up time of 45 weeks. After the initial treatment block, en face structural area regressed, $18.7\% \pm 39.0\%$ (95% CI 44.2–6.8%, $p = 0.26$), and en face angio area regressed, $51.9\% \pm 29.5\%$ (95% CI 32.6 to 71.2%, $p = 0.007$). Flow density within the en face structural area decreased by $33\% \pm 19.2\%$ (95% CI 20.5–45.5%, $p = 0.0077$). Flow density within the en face angio area decreased by mean $17.9\% \pm 25.2\%$ (95% CI 1.4–34.4%, $p = 0.066$). In two fellow eyes, NV recurrence could be observed before the onset of vitreous bleeding in one. **Conclusion.** Our study introduces a new quantitative measurement for NV in PDR, combining structure and flow measurement. The structure area remained after treatment, while its flow density and angio area regressed. We propose this measurement method as a more physiological and possibly more comparable metrics.

1. Introduction

Diabetic retinopathy (DR) is a leading cause of vision loss and blindness worldwide and presumably on the rise with expected demographics [1, 2]. Specifically, proliferative diabetic retinopathy (PDR), characterized by retinal neovascularization (NV), is responsible for severe visual impairment (e.g., due to vitreous hemorrhage or tractional retinal detachment) [3]. The mainstay of treatment has been panretinal photocoagulation (PRP) for almost 50 years [4]. However, PRP is associated with significant side effects, such as (contrast) vision loss, restriction of visual field, and development and worsening of macular edema [5, 6].

Anti-vascular endothelial growth factor (VEGF) is currently emerging as a promising treatment alternative for PDR [7–10]. Two multicenter, prospective clinical trials showed noninferior visual acuity (VA) results of intravitreal anti-VEGF (CLARITY for aflibercept; Protocol S for ranibizumab) compared to PRP [7, 9]. The CLARITY trial even showed improved VA, better treatment satisfaction scores, lower incidence of center-involving macular edema and vitreous hemorrhage, and less visual field loss with aflibercept than PRP [7]. Five-year data of Protocol S recently reported sustained noninferior VA outcomes and lower incidence of macular edema in the ranibizumab group [8]. Both of these studies have made treatment decisions about

anti-VEGF injection based on clinical and photographic assessment of activity of NV [7, 11].

Optical coherence tomography (OCT) has been shown to be superior to the clinical detection of neovascular changes in PDR [12]. Recently, OCT Angiography (OCTA) has been used to further characterize NV with the aid of flow information additive to the structural OCT image [13–17]. Few studies have analyzed changes of NV in PDR after treatment with OCTA to date, and mainly on a short-term basis [17–24]. Significant advantages of OCTA are the practical repeatability due to its speed and noninvasiveness, the combination of flow information (similar to conventional fluorescein angiography (FA)) and structural information (OCT image), and the possibility of quantitative analysis. The aim of this pilot study is to introduce a new method of quantitative analysis of diabetic retinal neovascularizations. We use OCTA to measure, link, and assess structural and flow changes of NV in eyes with PDR undergoing treatment with anti-VEGF.

2. Methods

2.1. Ethics. Institutional review board approval (Ethics Committee of the University of Zurich, BASEC-No. PB_2016-00264) was obtained and all patients gave informed consent to publish their clinical data. The study adhered to the tenets of the Declarations of Helsinki.

2.2. Study Population. This study is a single-center, retrospective observational case series of patients diagnosed with PDR, confirmed on clinical exam and FA with or without previous treatment for DR (i.e., PRP, anti-VEGF, and vitrectomy >3 months from baseline) who were treated with anti-VEGF. Measurements were made on the basis of clinical needs. Data were included from April 2018 until September 2019 from patient records. Exclusion criteria were other causes of proliferative retinopathy (e.g., retinal venous occlusions and ocular ischemia), neovascular glaucoma, media opacities precluding good quality imaging of less than 7/10 in the manufacturer's quality index (e.g., advanced cataracts and dense vitreous hemorrhage) or NV not accessible for quantitative measurements, and patients with combined treatment consisting of PRP and anti-VEGF. Patients with a follow-up of less than 4 months were excluded from the study.

All patients underwent a comprehensive ophthalmic examination at baseline including best-corrected VA measured in Early Treatment Diabetic Retinopathy Study (ETDRS) letters or Snellen decimal, intraocular pressure, slit lamp examination, dilated fundus examination using indirect ophthalmoscopy, widefield FA, spectral-domain OCT (Heidelberg Spectralis, Heidelberg Engineering, Heidelberg, Germany) of the macula, and swept-source OCTA (Zeiss PLEX® Elite 9000, Zeiss Meditec, Dublin, California, USA) scans of all detected neovascularizations for which OCTA achieved sufficient image quality for quantitative analysis. Scanning patterns of 3 × 3 mm, 6 × 6 mm, 12 × 12 mm, or 9 × 15 mm were chosen depending on size, location, and visibility.

2.3. Treatment and Follow-Up. Patients diagnosed with active PDR were informed about treatment options, including PRP or intravitreal anti-VEGF (aflibercept or ranibizumab), and involved in the treatment decision based on their respective needs and preferences. Patients with small NV on FA, which were hard to detect using indirect ophthalmoscopy, received repetitive OCTA imaging, as needed for clinical decision-making. Treatment consisted of an initial treatment block of three to four monthly anti-VEGF injections with ranibizumab or aflibercept. Further follow-up was carried out on the basis of the clinical course of the disease, with intervals of four to ten weeks. Further treatment was indicated as needed in the case of recurrent active proliferative diabetic retinopathy or visual impairment due to diabetic macular edema. The retreatment decision was based on indirect ophthalmoscopy and OCTA imaging as needed.

All NV were recorded at least at baseline and one month after the initial treatment block (posttreatment). For analysis, also the last available follow-up OCTA measurement was included (last follow-up). The in-between measurements were included in the longitudinal graphs.

2.4. Image Processing. Image analysis and quantitative evaluation were performed separately for en face and B-scan images. The manufacturer's OCTA software (Zeiss PLEX® Elite Review-Software, Zeiss Meditec Inc., Dublin CA, USA) provides B-Scan OCTA images consisting of a black and white structural image with flow overlay in red (Figure 1(a)). En face images of the vitreoretinal layer were generated for the flow (angio) and the structural (structure) image (Figure 1(d) for angio and Figure 1(g) for structure). The vitreoretinal interface layer (VRI) starts at the internal limiting membrane (ILM) and includes the vitreous cavity as far as the NV reached. The automated retinal layer segmentation provided by the software was manually checked and adjusted where necessary to smoothly follow the plane of the ILM underneath the protruding NV. En face images of the angio and structure images of the VRI layer were built using maximum intensity projection and exported as tagged image file format (TIFF) for further analysis. B-scan image stack with flow overlay was manually searched for the section with the highest projection of the NV towards the vitreous space. The height of maximum projection from the ILM towards the vitreous cavity of the NV was manually measured for both structure and flow information within the manufacturer's software. The respective image with flow overlay was exported as a TIFF file for further analysis.

2.5. Image Analysis. Image analysis was performed using the open source Fiji software (<https://imagej.net/Fiji> version 2.1.0/1.52) [25]. In the en face images, NV were manually delineated in the angio and the structure image separately, resulting in separate dimensions of the NV in angio (NV-angio) and structure images (NV-structure) (Figure 1(e) for angio and Figure 1(h) for structure). As necessary, the referenced B-scan image stack was used to guide demarcation in the usually low contrast structure slab. The area of

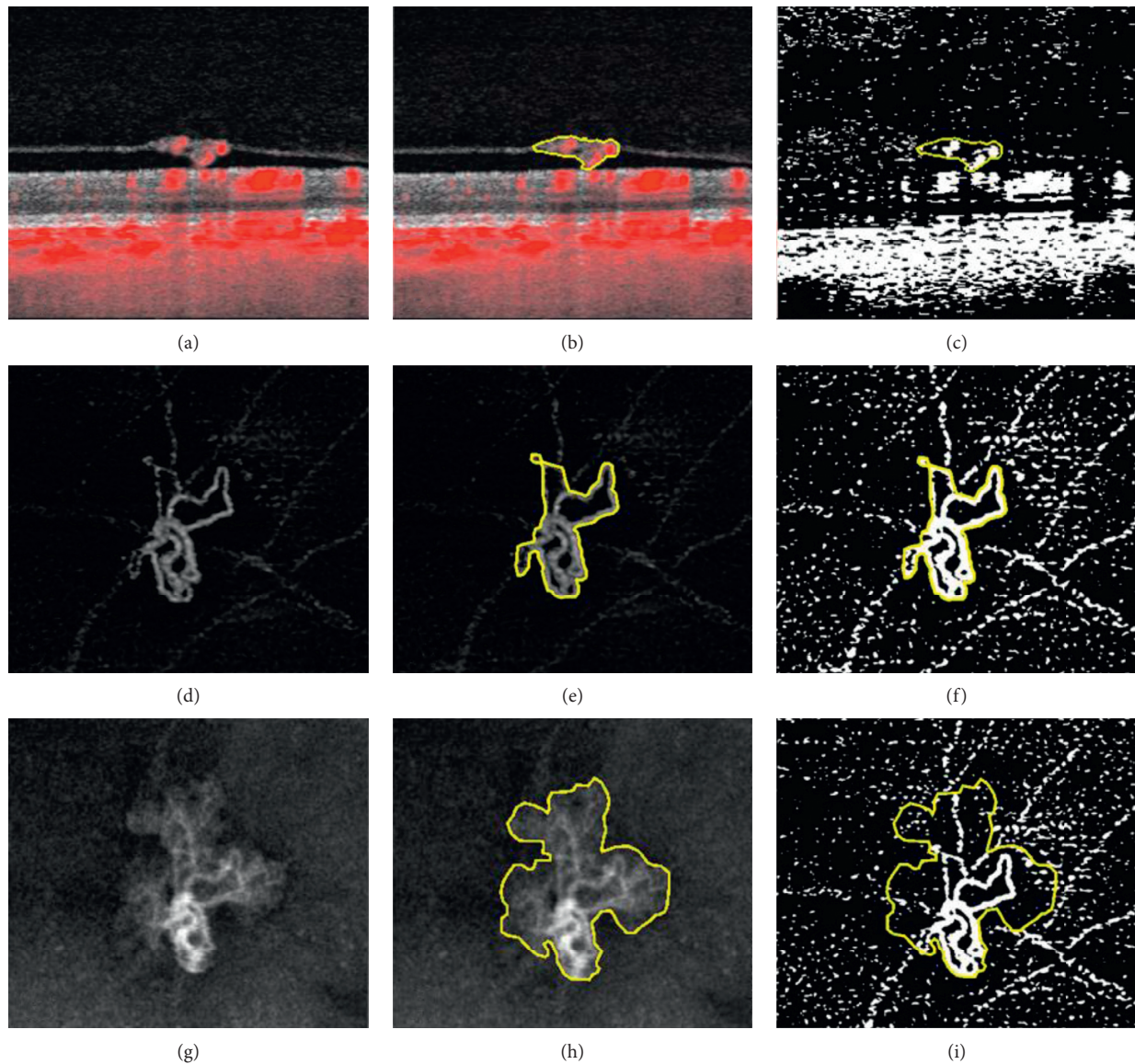


FIGURE 1: Summary of image processing steps. The first column shows the images generated by the optical coherence tomography angiography; a B-scan structure image with flow overlay in red (a), an en face flow (angio) image (d), and an en face structural (structure) image (g). Borders of the neovascularization were manually delineated for each image (second column: (b, e, h)), and the areas were measured. After binarization of the flow information, flow density was measured in percentages of white pixels within the respective area (last column: (c, f, i)).

the NV in the angio and structure images was measured. The angio images were binarized using the Phansalkar auto local threshold method (Figures 1(c), 1(f), and 1(i)) [26]. Flow density (FD) was defined as the percentage of white pixels after binarization. Flow density was measured in the binarized angio images within borders of NV-angio (FD-angio) and NV-structure (FD-structure) separately (Figure 1(f) for FD-angio and Figure 1(i) for FD-structure). Sequential measurements were performed during treatment and every available follow-up over time.

In the selected B-scan, the structural borders of the NV were manually delineated, the borders defined by the ILM and the vitreous space (Figure 1(b)). Subtraction of blue from red color information was performed after color

splitting of the image, revealing the isolated flow information (red in the exported RGB-image file). The result was binarized using the Phansalkar auto local threshold method [26]. This method resulted in isolated binarized flow information in the respective B-scan with flow information in white (Figure 1(c)). Flow density was defined as the percentage of white pixels within the NV area. Area of the NV and FD within the NV area was measured.

2.6. Outcome Measures. Primary outcomes were changes of FD in the en face structure and angio area and changes of the size of NV-angio area and NV-structure area in the en face images at baseline, 5 ± 1 weeks after the initial treatment

block with three to four monthly injections and at the last follow-up. Secondary outcomes were changes of height, area, and FD in the B-scan images. Visual acuity measurements and complications during observation time were recorded.

2.7. Statistical Analysis. Data of en face images for NV sizes in angio and structure imaging (NV-angio and NV-structure) and flow density within both areas (FD-angio and FD-structure) are presented as median with range and presented as box-plot graphs for changes from baseline to posttreatment (one month after initial treatment block) and last follow-up. Longitudinal graphs allow for some comparability of the in-between measurements, with weeks in the x -axes and scales for the y -axes standardized to set baseline size as 1 for areas and percentages for flow density. Data from B-scan imaging are summarized as longitudinal graphs in the supplementary material. Data were analyzed and visualized using Python Version 3.6 with Pandas library Version 1.2 and Microsoft® Excel for Mac, Version 16.47.1. Wilcoxon signed-rank test was used for calculation of p -values of measurements, compared to baseline. Confidence intervals were calculated for mean differences from baseline as 95% CI.

3. Results

3.1. Study Cohort. Eleven NV in nine eyes of six patients were treated as described. One patient was lost to follow-up. Nine NV in eight eyes of five patients were included in this study. Five patients were treatment-naïve PDR with type 2 diabetes; one eye had high-risk diabetic retinopathy with minor vitreous hemorrhage. In three patients, both eyes with one NV each were included. In one patient and two NV of one eye were included. One patient (two eyes with one NV each) had type 1 diabetes and had previous PRP treatment in both eyes, three months before baseline in one eye and ten months before baseline in the other eye. At baseline, no DME was present. The initial treatment block included three injections for eight eyes and four injections for three eyes of two patients. The median of the last OCTA follow-up period was 45 (range 19–51) weeks. Both eyes of one patient received three additional monthly anti-VEGF injections 37 weeks from baseline due to recurrent PDR, as described in the case presentation. One eye of the patient with type 1 diabetes received two anti-VEGF injections 27 and 45 weeks from baseline due to diabetic macular edema, while on OCTA, no NV was detectable.

3.2. NV Changes

3.2.1. En Face NV Area in Structure and Angio Slabs. The neovascularization en face area showed different changes for structure and flow area (see Table 1 and Figure 2(a)). As visible in the longitudinal graph, no general trend of en face NV-structure regression can be observed over all NV (Figure 3(a)), while the en face NV-angio area regressed in all patients during and after initial treatment block (Figure 3(b)). After the initial treatment block, en face

NV-structure regressed posttreatment by median 15% (range –28%–100%) and mean regression $18.7\% \pm 39.0\%$ (95% CI 44.2 to –6.8%, $p = 0.26$). At the last follow-up, en face NV-structure was regressed by median 6% (range –196%–100%) and mean regression $5\% \pm 82.7\%$ (95% CI 49.1 to –29.1%, $p = 0.48$).

En face NV-angio regressed posttreatment by median 48% (range 11–100%) and mean regression $51.9\% \pm 29.5\%$ (95% CI 32.6 to 71.2%, $p = 0.007$). At the last follow-up, en face NV-angio was regressed by median 34% (range –13%–100%) and mean regression $42.1\% \pm 39.1\%$ (95% CI 16.6 to 67.7%, $p = 0.015$).

3.2.2. En Face Flow Density Measurements. Flow density measurements show a regression within the en face structural area of the NV, while flow density within the en face angio area of the NV showed a less distinct regression (see Table 1 and Figure 2(b)). When measured within the structural NV-area (en face FD-structure, Figure 3(c)), from baseline to posttreatment after the initial treatment block, en face FD-structure decreased from median 72% (range 44–82%) to 38% (range 0–73%), mean decrease of $33\% \pm 19.2\%$ (95% CI 20.5–45.5%, $p = 0.0077$). At the last follow-up, en face FD-structure decreased to median 40% (range 0–70%), mean decrease of $34.3\% \pm 19.8\%$ (95% CI 21.4–47.3%, $p = 0.0077$).

When measured within the NV-angio area (en face FD-angio, Figure 3(d)), from baseline to posttreatment after the initial treatment block, en face FD-angio decreased from median 72% (range 48–89%) to median 58% (range 0–84%), mean decrease of $17.9\% \pm 25.2\%$ (95% CI 1.4–34.4%, $p = 0.066$). At the last follow-up, en face FD-angio decreased to median 54% (range 0–75%), mean decrease from baseline $19.7\% \pm 22.0\%$ (95% CI 5.31–34.0%, $p = 0.025$).

At baseline, most NV showed a densely and interlaced flow structure corresponding to a high vessel density. After treatment, regressed NVs resembled one or several residual truncated main arcs of the previous fan-like vascular structure. Such vascular arcs did not show fluorescein leakage as it is known from active NVs (Figure 4).

3.2.3. B-Scan Structural Images with Flow Overlay. Analysis of B-scan images for structure and flow density showed similar but less distinct changes (Supplementary Figures 1(a)–1(c)).

3.2.4. Visual Acuity and Complications. Visual acuity remained stable within 5 ETDRS letters (or one line on a Snellen chart) with the exception of one patient, whose VA increased 8 and 13 letters (right and left eye, respectively) during the follow-up period. In one eye, a vitreous hemorrhage after treatment discontinuation with anti-VEGF occurred without reduction in VA (see case presentation below). One eye showed diabetic macular edema without sign of recurrent NV, for which anti-VEGF treatment was resumed. No endophthalmitis or other severe complications from intravitreal injection occurred.

TABLE 1: Demographics and primary endpoints of changes of diabetic neovascularization measured with optical coherence tomography angiography (OCTA) after intravitreal anti-VEGF.

Patient	Age	Eye	NV#	Previous treatment	Initial treatment	Retreatment/cause	Change (%) of NV-structure size from baseline (=100%)	Change (%) of NV-angio size from baseline (=100)	Flow density within structural area (FD-structure) in %	Flow density within angio area (FD-angio) in %	Last follow-up in weeks from baseline (and from last anti-VEGF)	Comments				
							NV-structure posttreatment last follow-up	NV-angio posttreatment last follow-up	FD-structure posttreatment last follow-up	FD-angio posttreatment last follow-up	FD-angio last follow-up	Last clinical OCTA follow-up imaging				
A	59	Right	1	Treatment-naïve	4 monthly IVT	Yes NV recurrence	-51%	-76%	64%	81%	28%	38%	59%	46 (0)	46 (0)	Recurrence of NV with vitreous bleeding at week 34 was observed. Rapid regression of NV after retreatment.
A	59	Left	2	Treatment-naïve	4 monthly IVT	Yes NV recurrence	-8%	-78%	62%	62%	16%	25%	75%	45 (0)	45 (0)	Retreatment after 37 weeks due to recurrence of NV and vitreous bleeding of fellow eye.
B	30	Right	3	PRP, 3 months before baseline	3 monthly IVT	Yes for DME	-100%	-100%	61%	62%	0%	0%	0%	50 (5)	50 (5)	Complete regression after initial treatment block. At weeks 27 and 44 anti-VEGF was administered for DME.
B	30	Left	4	PRP, 10 months before baseline	3 monthly IVT	No	+12%	-11%	81%	89%	40%	42%	53%	51 (42)	51 (42)	—

TABLE 1: Continued.

Patient	Age	Eye	Previous treatment	NV#	Initial treatment	Retreatment/cause	Change (%) of NV-structure size from baseline (=100%)	Change (%) of NV-angio size from baseline (=100)	Flow density within structural area (FD-structure) in %	Flow density within angio area (FD-angio) in %	Last follow-up in weeks from baseline (and from last anti-VEGF)	Comments	
							NV-structure posttreatment	NV-angio posttreatment	FD-structure posttreatment	FD-angio postbaseline	FD-angio last follow-up	Last clinical follow-up OCTA imaging	
C	48	Right	Treatment-naïve	5	3 monthly IVT	No	+28%	-65%	82%	71%	54%	65 (53) 19 (9)	Consistent regression of % flow in structure and % flow in flow area, inconsistent changes of structure and flow area. Stable and clinically inactive PDRP in clinical follow-up for one year after last treatment
C	48	Left	Treatment-naïve	6	3 monthly IVT	No	-15%	-24%	79%	82%	57%	64 (53) 23 (13)	Regression of % flow in structure and % flow in flow area, and flow area with grossly unchanged structure area. Partial recurrence in OCTA over time without clinical signs of recurrence for one year after the last treatment.

TABLE 1: Continued.

Patient	Age	Eye	NV#	Previous treatment	Initial treatment	Retreatment/cause	Change (%) of NV-structure size from baseline (=100%)	Change (%) of NV-angio size from baseline (=100)	Flow density within structural area (FD-structure) in %	Flow density within angio area (FD-angio) in %	Last follow-up in weeks from baseline (and from last anti-VEGF)	Comments			
							NV-structure posttreatment	NV-angio posttreatment	FD-structure posttreatment	FD-angio postbaseline	FD-angio last follow-up	FD-angio last follow-up	FD-angio last follow-up	Last clinical follow-up	Comments
D	49	Left	7	Treatment-naïve	3 monthly IVT	No	+16%	-32%	30%	48%	63 (45)	45%	44 (26)		Regression of structure and % flow in flow area. Lesser regression of flow. Grossly unchanged structure area. Partial recurrence in OCTA over time without clinical signs of recurrence for 10 months after the last treatment. Previously treated for DME with anti-VEGF.
E	51	Right	8	Treatment-naïve	3 monthly IVT	No	-23%	-33%	73%	79%	48 (38)	54%	48 (38)		Delayed reduction of % flow in structure and flow area. Earlier, but inconsistent regression of structure and flow areas. Clinically stable for 9 months after last treatment.

TABLE 1: Continued.

Patient	Age	Eye	NV#	Previous treatment	Initial treatment	Retreatment/cause	Change (%) of NV-structure size from baseline (=100%)	Change (%) of NV-angio size from baseline (=100)	Flow density within structural area (FD-structure) in %	Flow density within angio area (FD-angio) in %	Flow density within structural area (FD-structure) in %	Flow density within angio area (FD-angio) in %	Last follow-up in weeks from baseline (and from last anti-VEGF)	Comments				
							NV-structure posttreatment last follow-up	NV-angio posttreatment last follow-up	FD-structure posttreatment baseline	FD-structure posttreatment last follow-up	FD-structure posttreatment baseline	FD-angio posttreatment last follow-up	Last clinical follow-up	Last OCTA imaging				
E	51	Right	9	Treatment-naïve	3 monthly IVT	No	-27%	+3%	-48%	-2%	72%	65%	70%	72%	73%	48 (38)	29 (19)	Initial reduction of % flow in structure area and regression of flow area, followed by inconsistent recurrence. Strong fluctuations of structure area and % flow area around the baseline value.

Summary table of all evaluated diabetic retinal neovascularizations (NV), baseline characteristics, and special observations. Measurements at baseline, posttreatment three months after the initial treatment block, and at the final OCTA measurements. Follow-up time for OCTA imaging and clinical follow-up are reported from baseline and from the last anti-VEGF injection. Continuous lines are separating patients, separated lines are separating eyes, and fine lines are separating NV within the same eye. DME = diabetic macular edema; IVT = intravitreal therapy with anti-VEGF (ranibizumab or aflibercept); OCTA = optical coherence tomography angiography; PRP = panretinal laser photocoagulation; RT = retreatment.

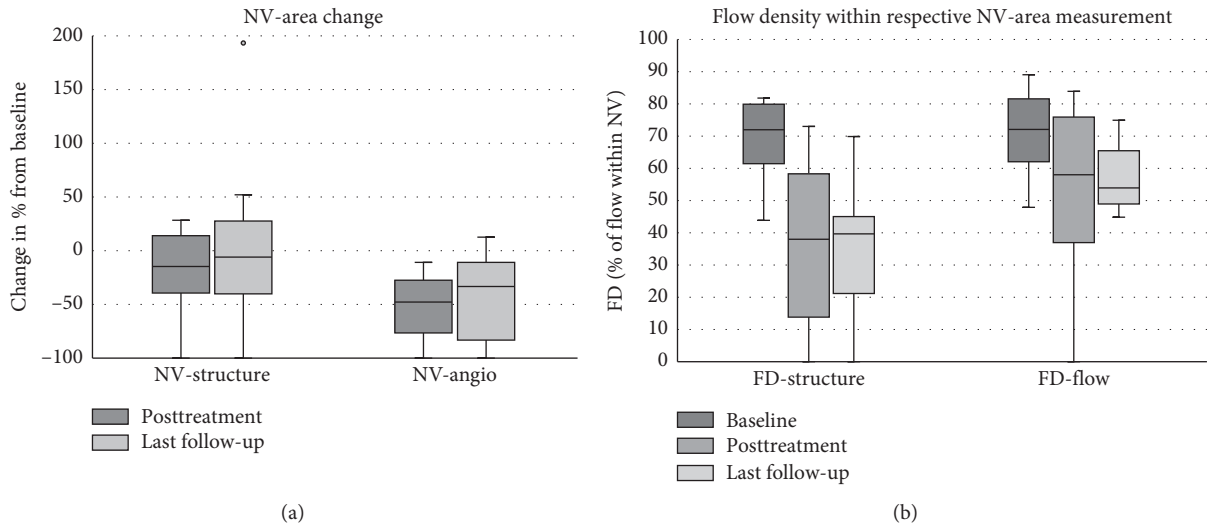


FIGURE 2: (a) Changes of neovascularization- (NV-) size measurements relative to baseline after the initial treatment block of three to four intravitreal anti-VEGF injections, and at the last follow-up. En face structural area (NV-structure) decreased by median 15% (range -28%–100%) and remained decreased by median 6% (-196%–100%). En face flow area (NV-angio) decreased by median 48% (range 10–100%) and remained by median 34% less than baseline (-13%–100%). The graph shows the reduction of NV size is more prominent in the angio than the structural en face OCTA image. (b) En face flow density (FD) measurements within the structural neovascularization (NV-area (FD-structure) and the flow NV-area (FD-angio)) at baseline, after the initial treatment block of three to four intravitreal anti-VEGF injections, and at the last follow-up: FD-structure started at median 64% (range 41–82%), decreased to median 32% (0–73%), and remained at median 32% (0–70%). FD-angio started at median 71% (range 48–89%), decreased to median 51% (0–84%), and remained at median 54% (0–75%). The graph shows that the difference in flow density between baseline, after treatment, and with apparently quiescent diabetic retinal neovascularization is more pronounced within the structural than the angio area of a NV.

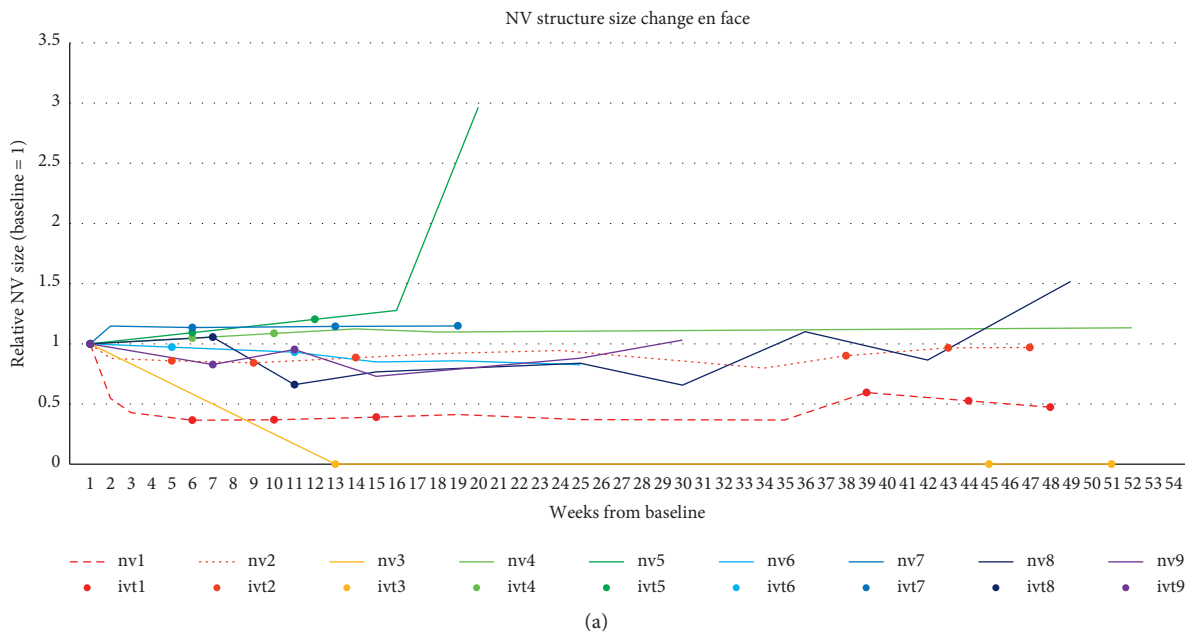
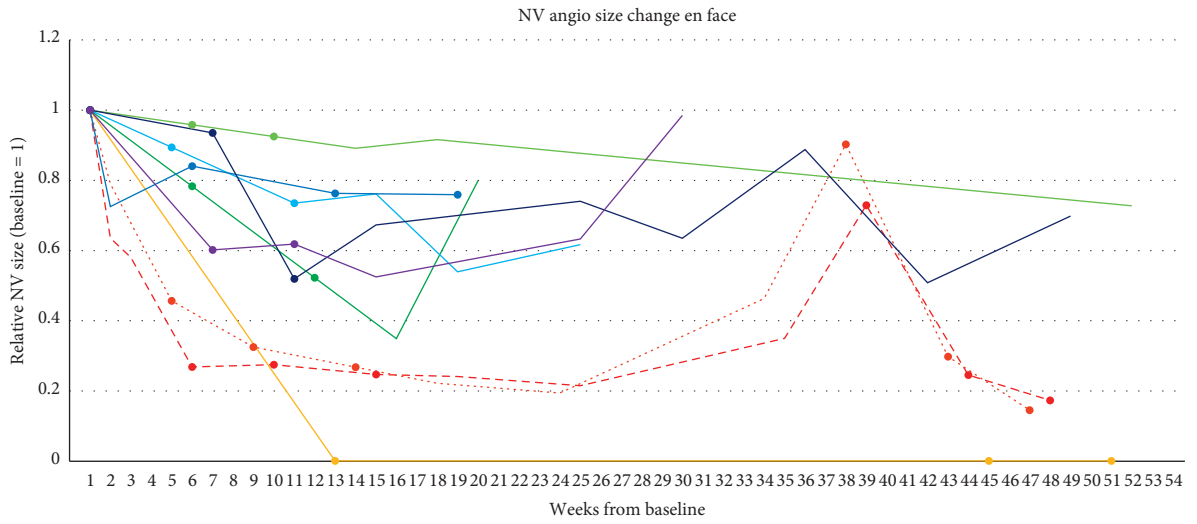
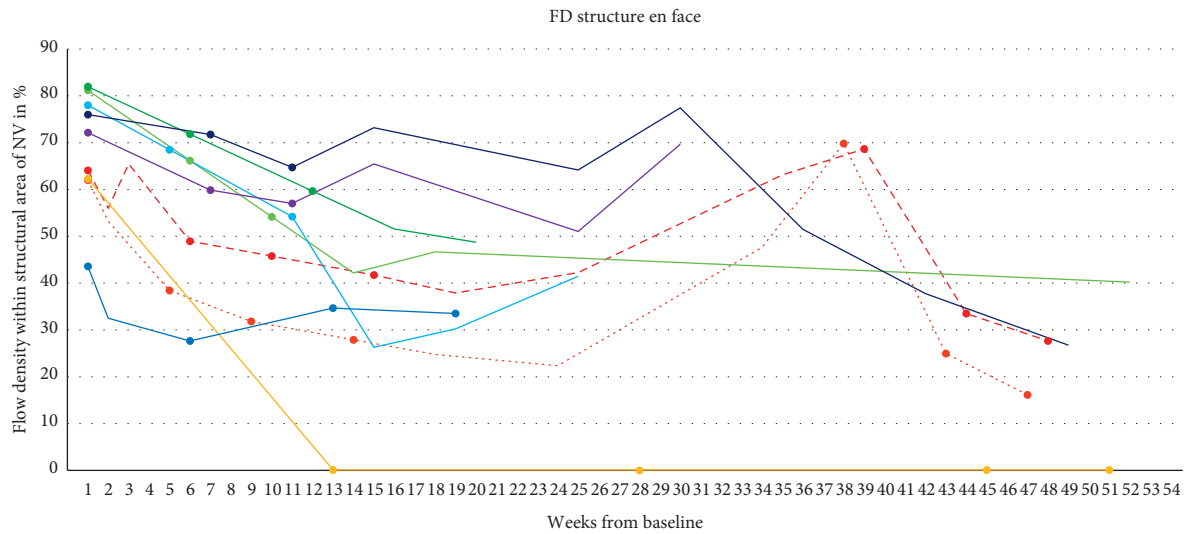


FIGURE 3: Continued.



(b)



(c)

FIGURE 3: Continued.

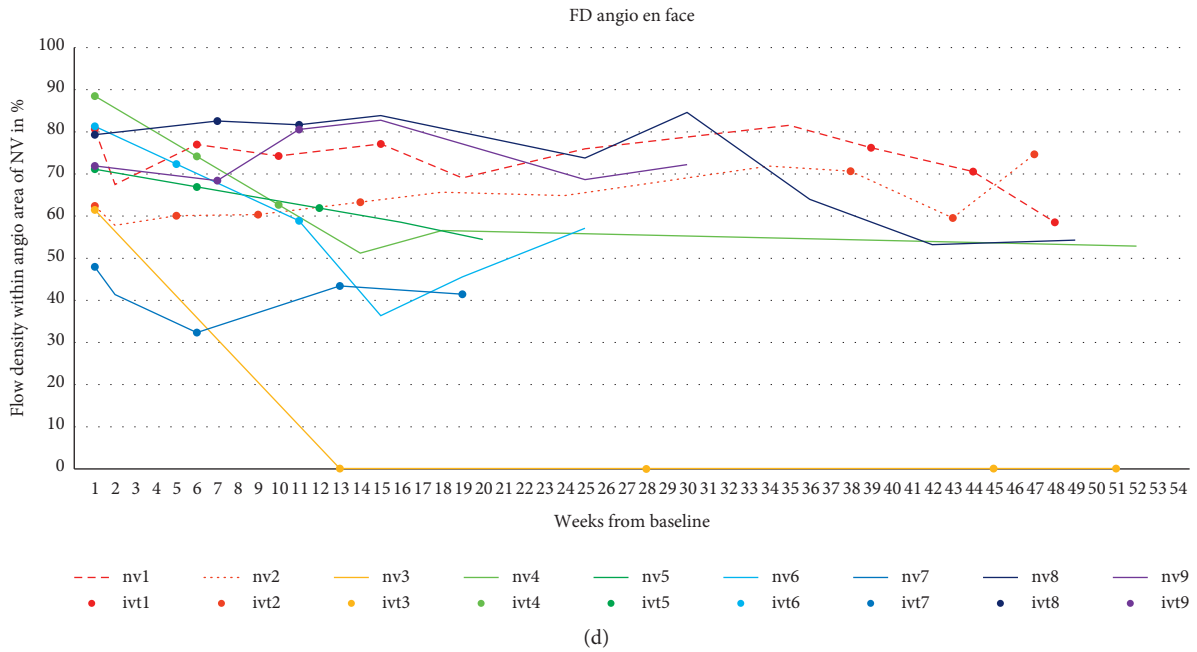


FIGURE 3: (a–d) Visualizing changes of area size and flow density of neovascularization (NV) for the flow and the angio area for every NV separately (data series NV 1–9). Bullet points represent time points of anti-vascular endothelial growth factor (anti-VEGF) injections in the respective eyes (data series IVT 1–9). It is indicated that in en face imaging, the structural framework (NV-structure) is at least partly remaining despite the fact that perfusion area (NV-angio) and flow density within the structural area (FD-structure) are regressing, while flow density within the angio area (FD-angio) is relatively stable. The two NV from the case presentation (NV 1 with vitreous hemorrhage and NV 2) are represented in dotted lines for better recognition. (a) Relative change of NV-structure from baseline (=1). The graph shows that the structural areas of the NV decrease only slightly. (b) Relative change of NV-angio from baseline (=1). The graph shows that in most NV, the angio area en face is decreasing after treatment with anti-VEGF. Two NV are growing back to a significant proportion after a long treatment-free interval. In one of these eyes, a new vitreous hemorrhage occurred before retreatment. (c) Flow density within the structural NV-area (FD-structure) in %. The graph indicates the consistent decrease of flow density within the structural areas of the NVs after treatment, as well as a new increase of the two NVs with recurrent proliferative diabetic retinopathy (PDR) activity. (d) Flow density within the angio NV-area (FD-angio) in %. The graph indicates the lesser decrease of flow density within the structural areas of the NVs after treatment. Also, in the case of the two NVs with recurrent PDR activity, it cannot be determined by the flow density of the NV measured on the OCTA angio image.

3.3. Case Presentation. A 59-year-old treatment-naïve male was diagnosed with bilateral PDR. The small NV was clinically difficult to detect but clearly visible on fluorescein angiography (FA, left eye on Figure 4(a)) and OCTA (Figure 5 column A). He presented with a light vitreous hemorrhage in the right eye caused by a similarly sized NV. In both eyes, one posterior NV could clearly be imaged by 3 × 3 mm OCTA. After informed consent, the patient opted for anti-VEGF treatment with an initial treatment block of four monthly injections in both eyes. The NV regressed in OCTA (Figure 5, row 1) and FA posttreatment showed regression of NV size and leakage in both eyes (Figure 4(b), for the left eye). Upon further observation, slow growth of the NVs could not definitely be detected clinically but was clearly observed in both eyes in OCTA imaging. Hence, retreatment was suggested 20 weeks after the last injection but declined by the patient. A few days later, another light vitreous hemorrhage without reduction of VA occurred in the right eye, and the patient then consented to the resumption of anti-VEGF treatment in both eyes at the next visit, which was 25 weeks after the last injection. A fast regression of the NV was observed, similar to the first treatment response.

In both eyes, size of en face NV-angio area and flow density of en face FD-structure rapidly decreased after the initial treatment block with anti-VEGF. After cessation of treatment, the measurements increased again in both eyes (data series nv1 and nv2 in Figures 2(a)–2(d)). While en face FD-angio showed unchanged flow density in both eyes, en face NV-structure area decreased in one eye and remained unchanged in the eye without vitreous hemorrhage.

4. Discussion

As new diagnostic and therapeutic possibilities emerge for PDR, there is the potential for gaining new insights into the pathophysiology of the development of NVs and their response to treatment. This pilot study shows that the structure and flow of NVs respond differently to treatment and can be quantitatively analyzed, followed by repeated OCTA. Also, we propose several interesting imaging aspects for further exploration.

In our study, retinal NVs were observed on OCTA imaging. Retinal NV have been shown to be reliably detectable on OCTA and characterized by shape and assumed

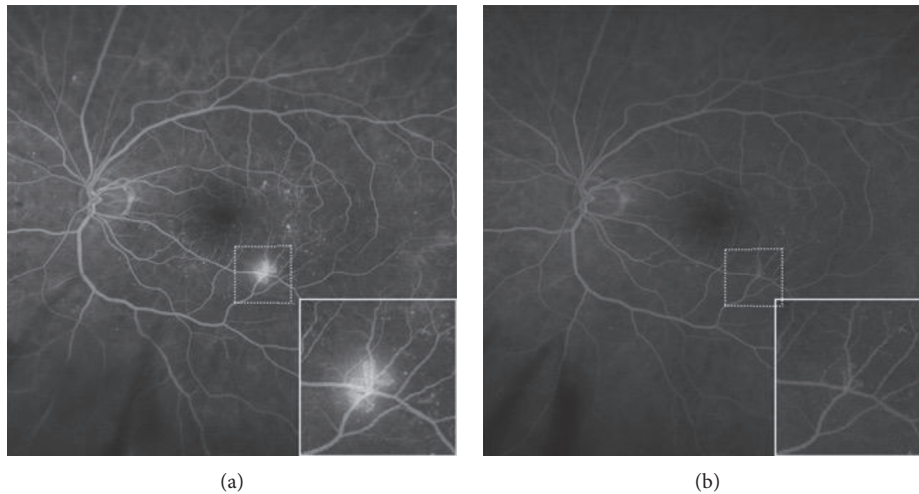


FIGURE 4: Diabetic neovascularization (NV) of the left eye of a 59-year-old patient with newly diagnosed proliferative diabetic retinopathy on both eyes, with the NV magnified equally (a, b). Initial imaging shows a densely interlaced vascular pattern of the NV with leakage (a) and follow-up imaging after four monthly anti-VEGF injections shows a regressed truncated vascular pattern of the NV without leakage (b), equivalent to column D in Figure 5.

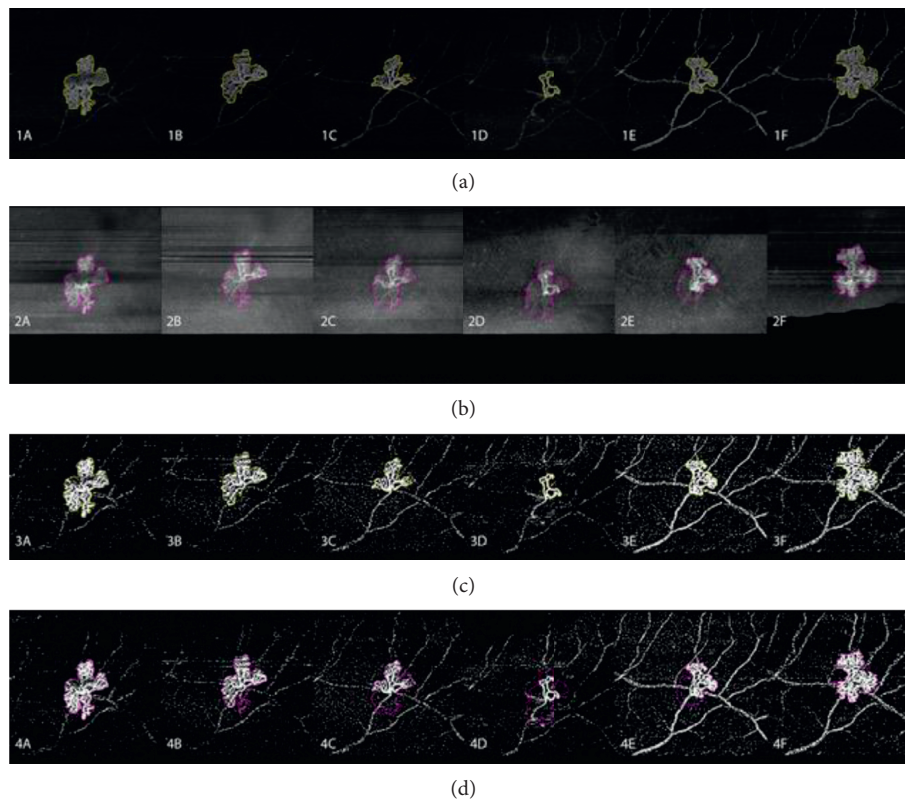


FIGURE 5: Exemplary follow-up measurements of one neovascularization (NV) with initial regression and later recurrence after cessation of anti-VEGF treatment, as described in the case presentation section, equivalent to the NV in Figure 4 and NV2 in the graphs of Figures 3(a)–3(d). (a) The optical coherence tomography angiography (OCTA) en face angiography (OCTA) en face angiography image with the outline of NV-angio. (b) The OCTA en face structural image with the outline of NV-structure. (c) The binarized OCTA en face angiography image with the outline of NV-angio from (a), visualizing flow density (FD) within the angio area (en face FD-angio). While the angiographic size of the NV regresses, the relative flow density remains high. (d) The binarized OCTA en face angiography image with the outline of the NV-structure from (b) (en face FD-structure). While the structural area remains relatively stable, its flow density reduces. Recurrence of the NV occurs within the preexisting structural area of the NV. Column A is at baseline, column B is after one week, and column C is one month after the first anti-VEGF injection. Column D represents 22 weeks from baseline, one month after the fourth injection and at the minimal dimensions of NV. Column E shows early recurrence 32 weeks from baseline, 20 weeks after the last injection. Column F shows subtotal recurrence 37 weeks from baseline and 25 weeks after the last anti-VEGF injection, when recurrent vitreous hemorrhage on the fellow eye had occurred, and before retreatment. After retreatment a similar regression was observed.

origin [13, 17, 27–30]. Russel et al. also found similar progression or regression of NV comparing en face OCTA (12×12 mm patterns) with ultrawidefield fluorescein angiography (FA) in a longitudinal series of patients treated with PRP, whereas vascular changes over time were more detailed on OCTA imaging compared to FA [17]. These studies in principle have highlighted the comparability of OCTA with ultrawidefield FA in diagnosis and follow-up of PDR. On the other hand, Schwartz et al. have found B-Scan OCTA to be the most sensitive tool assessing detection rate in NV reactivation [31]. These results highlight the importance of taking into account both planes-en face and B-Scans when using OCTA for follow-up measurements of NV.

Our study has shown that there is a reduction of flow in NVs under anti-VEGF that is sustained over a variable period of time in individual NVs. This confirms existing evidence. Zhang et al. [23] have quantitatively shown regression of neovascularization of the disc in 15 eyes after intravitreal anti-VEGF injection with conbercept. Hu et al. [22] showed a significant decrease in NV vessel length and vessel density within one week of intravitreal conbercept injection compared to untreated patients in a preoperative setting prior to surgical treatment of diabetic neovascular membranes. Elbendary and Abouelkheir [32] have described short-term regression of blood flow in the structural B-scan OCT with overlaid flow information 3 weeks after anti-VEGF treatment of NV of the disc. Ishibazawa et al. have described a rapid regression of flow density after anti-VEGF injection over the optic disc head with recurrence after eight weeks in neovascularization of the disc [14]. He and Yu have described the regression of NV size after PRP and combined anti-VEGF and PRP with similar results to our study [33]. However, the magnitude and sustainability of this flow reduction and what factors may lead to recurrence are still unknown.

To our knowledge, our study is the first to obtain a quantitative combined measure of NV size and vessel density. Also, we assessed the difference of the measurements for the structural and the angiographic areas in the evaluation of NV change under anti-VEGF treatment. Our data showed a much smaller regression of en face NV-structure than that of en face NV-angio. On the other hand, we have shown a much more pronounced regression of flow density within the en face NV's structure compared to the flow density within the detectable NV in the en face angio image. Furthermore, in two cases, we could show detection of reactivation of NV by flow density within the residual en face structural area of the NV, both quantitatively by the increase of FD-structure and qualitatively by the recurrence of perfused vessels within the residual structure.

One could argue that a quantitative measurement of the angiographic NV-outlines is similar and more feasible in clinics. We think taking the structural dimensions of the NV into account allows for more physiological measurements, including the momentarily nonperfused vessels of NV, which can be reactivated in the future. The delineation of the NV in structural en face images is not always easy but very obvious when you look at the B-scan images. Future image analysis methods using the possibilities of artificial

intelligence (AI) may allow automated three-dimensional segmentation, detection, analysis, and follow-up of NV in OCTA.

This will open up various prospects for further investigation with regard to the characterization of NVs and early detection of PDR reactivation and retinal NV recurrences, using the full potential of OCTA and clever image analysis. Equivalence of OCTA compared to FA in NV detection has been shown, and future OCTA devices may enable treatment guidance of PDR with OCTA, which may become partially automated. Besides facilitating three-dimensional measurements, there are several advantages to including both structural and flow information in NV analysis. Firstly, as our results show, the change of flow density within the NV's structure seems to be more pronounced than the size change of the NV's angio signal. Secondly, as shown in our presented case, recurrences may be detectable before the occurrence of complications. And thirdly, it is possible to visualize and thus monitor the remaining structure of regressed neovascularizations independent of their current perfusion state, something clinically often referred to as nonperfused vessels, ghost vessels, or fibrotic membranes. VEGF level is a known important factor in the pathogenesis of PDR and effect of its treatment [34]. A changing balance towards vitreous VEGF levels after stopping anti-VEGF injections may lead to reperfusion of previously regressed ghost vessels and thus may be the cause for recurrence of flow in active NV within its preexisting structure. Whether these remnants of vascular structures can permanently occlude remains unanswered by our study. However, the observations of several patients without recurrence of NV during long follow-up periods after stopping anti-VEGF suggest this possibility. This could mean that future therapies might also need to target the residual structural scaffold to prevent recurrences.

Our study confirmed previous observations that regressed NVs remain as a truncated vessel loop not leaking on FA [17]. As discussed by Russel et al., it could be that those larger caliber vessels do not respond as well to blocked VEGF as smaller caliber vessels [17]. However, the implication for recurrence or retreatment of those residual changes remains unclear.

Taken together, the structure of retinal NVs can be measured using OCTA, which, together with its flow (angio) information, might lead to further insight into quantitative analysis and estimation of NV activity after treatment and possibly treatment and retreatment decisions. Based on our findings, we suggest that in the evaluation of retinal NVs, flow density should be measured within the detectable structural area and not only using the en face OCTA angio image.

4.1. Limitations. This study has several limitations. Due to its retrospective nature and small sample size, there is some inhomogeneity in initial treatment with three or four anti-VEGF injections and in length of follow-up periods. Measurement pattern sizes were chosen according to clinical needs, which limits the quantitative comparability between

patients. A relevant selection bias is introduced to the data. Patients in the working-age population or depending on their ability to keep their driving licence and with presumably good adherence to treatment and follow-up were rather recommended anti-VEGF, while for patients with poor glycaemic control or presumed difficult treatment adherence, PRP was favored, resulting in preferring younger patients with better-estimated treatment adherence and thus possibly better glycaemic control. Also, the need for OCTA as a decision support tool is greater in the case of smaller NV, with possibly less severe PDR. Second, owing to the current technical limitations for OCTA imaging at the time of the study, only the posterior retina until mid-periphery was accessible for OCTA imaging with sufficient image quality for quantitative analysis. Also, all image processing and binarization will introduce imperative biases due to the chosen algorithms. This is inherent to OCTA as an imaging technique based on complex computations of originally measured signals to calculate flow signal and to calculate en face angiographic images, which are then further modified in the process of image analysis, e.g., by binarization [35, 36]. Since angio images are calculated from sequential structural A-Scans, technically, OCTA does not measure actual flow, in contrast to true Doppler-OCT [37]. Another inherent feature of current OCTA devices is their inability to distinguish flow velocity, which is currently addressed in prototype devices or measuring algorithms using variable maybe better variable interscan time analysis [38, 39]. Such principal limitations need to be taken into account in OCTA research. However, current state-of-the-art swept-source OCTA vascular axial and transversal resolution and directional independence surpasses alternative techniques. Moreover, measurement of single B-scan slices shows high variability due to some minor misalignments in follow-up imaging, limiting the observed effects in the B-scan results. Longitudinal graphs may only indicate similar change patterns as described for en face images, but formal quantitative analysis would not be reliable. Furthermore, we have not investigated the role of the posterior vitreous, which has been shown to be of importance as being a scaffold for NV growth, as this lies outside of the scope of this manuscript [40]. Finally, our patients did not routinely receive FA follow-up measurements in the routine clinical setting, so we cannot compare the intensity of the leakage with the NV pattern in the OCTA.

5. Conclusions

In summary, our study demonstrates a new quantitative measure of diabetic NV using OCTA. We measure NV size and flow density separately for the structure and angio areas of diabetic NV elsewhere. In our case series, we demonstrate different treatment responses after anti-VEGF between structural and angiographic NV for both area and flow density. The structure remained stable with regression of flow density, while NV-angio regressed with more constant flow density. We thus propose that structural information, which is frequently ignored in the case of OCTA interpretation, should be taken into account in the case of retinal

NV, as should be the relation of structure and flow signal. In short, flow density should be measured within the structure of retinal NVs. The rise of AI-based automated image analysis and true three-dimensional structure and flow analysis and faster widefield OCTA will enable better treatment guidance in PDR. Further prospective studies are needed to evaluate clinical benefit for patients, establish reproducible quantitative flow density and retreatment criteria, and compare OCTA to FA as a guiding imaging technique. Our work shows the potential of OCTA in the follow-up of PRD, which is worthy of further investigation.

Abbreviations

DR:	Diabetic retinopathy
PDR:	Proliferative diabetic retinopathy
NV:	Neovascularization
PRP:	Panretinal photocoagulation
VEGF:	Vascular endothelial growth factor
DME:	Diabetic macular edema
OCT:	Optical coherence tomography
OCTA:	Optical coherence tomography angiography
FA:	Fluorescein angiography.

Data Availability

Table 1 shows all primary output measures for the statistical analysis, allowing reproduction of reported statistical analysis and box-plot graphs. The longitudinal graphs represent all measurements. Ground data cannot publicly be released due to local data protection laws, which could possibly allow the deanonymization of single patients.

Disclosure

This work was performed as part of the employment of the authors at the Department of Ophthalmology, University Hospital and University of Zurich, Zurich, Switzerland, without specific support.

Conflicts of Interest

Sandrine A. Zweifel is a consultant for Bayer HealthCare, Novartis and Roche. She receives research support from Bayer HealthCare and Novartis. Daniel Barthelmes is a consultant for Bayer HealthCare, Novartis, and Alcon. He receives lecture fees and grant support from Bayer HealthCare and Novartis. Katrin Fasler has been an external consultant for DeepMind.

Supplementary Materials

Supplementary Figure 1(a): longitudinal plot of the height change from baseline (=1) of the protrusion height of the neovascularization (NV) towards the vitreous cavity, measured from the internal limiting membrane to the highest point of flow signal in the B-scan slice with maximal protrusion of the NV. No consistent regression of height can be observed after anti-VEGF treatment. Supplementary Figure 1(b): longitudinal plot of the structural

neovascularization (NV) area visible on the OCT in the B-scan slice with maximal protrusion of the NV. Some regression of the structural NV size can be observed in the B-scan, but not across all NVs. Supplementary Figure 1(c): longitudinal plot of the flow density within the B-scan OCT/OCTA with structural information and flow overlay. A reduction of flow density is observed in the B-Scans of all neovascularizations. Nevertheless, the flow density seems to be more variable compared to en face imaging. (*Supplementary Materials*)






References

- [1] X. Zhang, J. B. Saaddine, C.-F. Chou et al., "Prevalence of diabetic retinopathy in the United States, 2005–2008," *JAMA*, vol. 304, no. 6, pp. 649–656, 2010.
- [2] R. L. Thomas, F. D. Dunstan, S. D. Luzio et al., "Prevalence of diabetic retinopathy within a national diabetic retinopathy screening service," *British Journal of Ophthalmology*, vol. 99, no. 1, pp. 64–68, 2015.
- [3] Early Treatment Diabetic Retinopathy Study Research Group, "Fundus photographic risk factors for progression of diabetic retinopathy: ETDRS report number 12," *Ophthalmology*, vol. 98, pp. 823–833, 1991.
- [4] "Photocoagulation treatment of proliferative diabetic retinopathy. Clinical application of diabetic retinopathy study (DRS) findings, DRS report number 8. The diabetic retinopathy study research group," *Ophthalmology*, vol. 88, pp. 583–600, 1981.
- [5] H. R. McDonald and H. Schatz, "Visual loss following panretinal photocoagulation for proliferative diabetic retinopathy," *Ophthalmology*, vol. 92, no. 3, pp. 388–393, 1985.
- [6] "Early photocoagulation for diabetic retinopathy. ETDRS report number 9. Early treatment diabetic retinopathy study research group," *Ophthalmology*, vol. 98, pp. 766–785, 1991.
- [7] S. Sivaprasad, A. T. Prevost, J. C. Vasconcelos et al., "Clinical efficacy of intravitreal aflibercept versus panretinal photocoagulation for best corrected visual acuity in patients with proliferative diabetic retinopathy at 52 weeks (CLARITY): a multicentre, single-blinded, randomised, controlled, phase 2b, non-inferiority trial," *The Lancet*, vol. 389, no. 10085, pp. 2193–2203, 2017.
- [8] J. G. Gross, A. R. Glassman, D. Liu et al., "Five-year outcomes of panretinal photocoagulation vs. intravitreal ranibizumab for proliferative diabetic retinopathy: a randomized clinical trial," *JAMA Ophthalmology*, vol. 136, no. 10, pp. 1138–1148, 2018.
- [9] Writing Committee for the Diabetic Retinopathy Clinical Research Network, J. G. Gross, A. R. Glassman et al., "Panretinal photocoagulation vs. intravitreal ranibizumab for proliferative diabetic retinopathy: a randomized clinical trial," *JAMA*, vol. 314, no. 20, pp. 2137–2146, 2015.
- [10] T. W. Krick and N. M. Bressler, "Recent clinically relevant highlights from the diabetic retinopathy clinical research network," *Current Opinion in Ophthalmology*, vol. 29, no. 3, pp. 199–205, 2018.
- [11] J. K. Sun, A. R. Glassman, W. T. Beaulieu et al., "Rationale and application of the protocol S anti-vascular endothelial growth factor algorithm for proliferative diabetic retinopathy," *Ophthalmology*, vol. 126, no. 1, pp. 87–95, 2019.
- [12] M. M. K. Muqit and P. E. Stanga, "Fourier-domain optical coherence tomography evaluation of retinal and optic nerve head neovascularisation in proliferative diabetic retinopathy," *British Journal of Ophthalmology*, vol. 98, no. 1, pp. 65–72, 2014.
- [13] J. Pan, D. Chen, X. Yang et al., "Characteristics of neovascularization in early stages of proliferative diabetic retinopathy by optical coherence tomography angiography," *American Journal of Ophthalmology*, vol. 192, pp. 146–156, 2018.
- [14] A. Ishibazawa, T. Nagaoka, H. Yokota et al., "Characteristics of retinal neovascularization in proliferative diabetic retinopathy imaged by optical coherence tomography angiography," *Investigative Ophthalmology & Visual Science*, vol. 57, no. 14, pp. 6247–6255, 2016.
- [15] K. B. Schaal, M. R. Munk, I. Wyssmueller, L. E. Berger, M. S. Zinkernagel, and S. Wolf, "Vascular abnormalities in diabetic retinopathy assessed with swept-source optical coherence tomography angiography widefield imaging," *Retina*, vol. 39, no. 1, pp. 79–87, 2019.
- [16] J. Huemer, H. Khalid, S. K. Wagner et al., "Phenotyping of retinal neovascularization in ischemic retinal vein occlusion using wide field OCT angiography," *Eye*, 2020.
- [17] J. F. Russell, Y. Shi, J. W. Hinkle et al., "Longitudinal wide-field swept-source OCT angiography of neovascularization in proliferative diabetic retinopathy after panretinal photocoagulation," *Ophthalmology Retina*, vol. 3, no. 4, pp. 350–361, 2019.
- [18] F. I. Shakarchi, A. F. Shakarchi, and S. A. Al-Bayati, "Timing of neovascular regression in eyes with high-risk proliferative diabetic retinopathy without macular edema treated initially with intravitreal bevacizumab," *Clinical Ophthalmology*, vol. 13, pp. 27–31, 2019.
- [19] I. P. Chatziralli, T. N. Sergentanis, and S. Sivaprasad, "Prediction of regression of retinal neovascularisation after panretinal photocoagulation for proliferative diabetic retinopathy," *Graefe's Archive for Clinical and Experimental Ophthalmology*, vol. 254, no. 9, pp. 1715–1721, 2016.
- [20] L. Nicholson, R. Crosby-Nwaobi, J. C. Vasconcelos et al., "Mechanistic evaluation of panretinal photocoagulation versus aflibercept in proliferative diabetic retinopathy: CLARITY substudy," *Investigative Ophthalmology & Visual Science*, vol. 59, no. 10, pp. 4277–4284, 2018.
- [21] D. Shroff, P. Gupta, C. Gupta, and C. Shroff, "Post-laser regression of diabetic neovascularization: an optical coherence tomography angiography study," *Indian Journal of Ophthalmology*, vol. 66, no. 12, pp. 1855–1856, 2018.
- [22] Z. Hu, Y. Su, P. Xie et al., "OCT angiography-based monitoring of neovascular regression on fibrovascular membrane after preoperative intravitreal conbercept injection," *Graefe's Archive for Clinical and Experimental Ophthalmology*, vol. 257, no. 8, pp. 1611–1619, 2019.
- [23] X. Zhang, C. Wu, L.-J. Zhou, and R.-P. Dai, "Observation of optic disc neovascularization using OCT angiography in proliferative diabetic retinopathy after intravitreal conbercept injections," *Scientific Reports*, vol. 8, no. 1, p. 3972, 2018.
- [24] A. S. Vergmann, K. T. Sørensen, T. L. Torp et al., "Optical coherence tomography angiography measured area of retinal neovascularization is predictive of treatment response and progression of disease in patients with proliferative diabetic retinopathy," *International Journal of Retina and Vitreous*, vol. 6, no. 1, p. 49, 2020.
- [25] J. Schindelin, I. Arganda-Carreras, E. Frise et al., "Fiji: an open-source platform for biological-image analysis," *Nature Methods*, vol. 9, no. 7, pp. 676–682, 2012.
- [26] N. Phansalkar, S. More, A. Sabale, and M. Joshi, "Adaptive local thresholding for detection of nuclei in diversity stained

- cytology images,” in *Proceedings of the 2011 International Conference on Communications and Signal Processing*, pp. 218–220, Kerala, India, February 2011.
- [27] O. Sawada, Y. Ichiyama, S. Obata et al., “Comparison between wide-angle OCT angiography and ultra-wide field fluorescein angiography for detecting non-perfusion areas and retinal neovascularization in eyes with diabetic retinopathy,” *Graefe’s Archive for Clinical and Experimental Ophthalmology*, vol. 256, no. 7, pp. 1275–1280, 2018.
- [28] T. E. de Carlo, M. A. Bonini Filho, C. R. Bauman et al., “Evaluation of preretinal neovascularization in proliferative diabetic retinopathy using optical coherence tomography angiography,” *Ophthalmic Surgery, Lasers and Imaging Retina*, vol. 47, no. 2, pp. 115–119, 2016.
- [29] Q. S. You, Y. Guo, J. Wang et al., “Detection of clinically unsuspected retinal neovascularization with wide-field optical coherence tomography angiography,” *Retina*, vol. 40, no. 5, pp. 891–897, 2020.
- [30] J. F. Russell, H. W. Flynn Jr., J. Sridhar et al., “Distribution of diabetic neovascularization on ultra-widefield fluorescein angiography and on simulated widefield OCT angiography,” *American Journal of Ophthalmology*, vol. 207, pp. 110–120, 2019.
- [31] R. Schwartz, H. Khalid, S. Sivaprasad et al., “Objective evaluation of proliferative diabetic retinopathy using OCT,” *Ophthalmology Retina*, vol. 4, no. 2, pp. 164–174, 2020.
- [32] A. M. Elbendary and H. Y. Abouelkheir, “Bimodal imaging of proliferative diabetic retinopathy vascular features using swept source optical coherence tomography angiography,” *International Journal of Ophthalmology*, vol. 11, pp. 1528–1533, 2018.
- [33] F. He and W. Yu, “Longitudinal neovascular changes on optical coherence tomography angiography in proliferative diabetic retinopathy treated with panretinal photocoagulation alone versus with intravitreal conbercept plus panretinal photocoagulation: a pilot study,” *Eye*, vol. 34, no. 8, pp. 1413–1418, 2020.
- [34] A. W. Stitt, T. M. Curtis, M. Chen et al., “The progress in understanding and treatment of diabetic retinopathy,” *Progress in Retinal and Eye Research*, vol. 51, pp. 156–186, 2016.
- [35] J. C. Wang and J. B. Miller, “Optical coherence tomography angiography: review of current technical aspects and applications in chorioretinal disease,” *Seminars in Ophthalmology*, vol. 34, no. 4, pp. 211–217, 2019.
- [36] N. Anegondi, A. Kshirsagar, T. B. Mochi, and A. Sinha Roy, “Quantitative comparison of retinal vascular features in optical coherence tomography angiography images from three different devices,” *Ophthalmic Surgery, Lasers and Imaging Retina*, vol. 49, no. 7, pp. 488–496, 2018.
- [37] J. F. Bille, *High Resolution Imaging in Microscopy and Ophthalmology: New Frontiers in Biomedical Optics*, Springer, Cham, Switzerland, 2019.
- [38] D. Richter, A. M. Fard, J. Straub, W. Wei, Q. Zhang, and R. K. Wang, “Relative retinal flow velocity detection using optical coherence tomography angiography imaging,” *Biomedical Optics Express*, vol. 11, no. 11, pp. 6710–6720, 2020.
- [39] M. Arya, R. Rashad, O. Sorour, E. M. Moul, J. G. Fujimoto, and N. K. Waheed, “Optical coherence tomography angiography (OCTA) flow speed mapping technology for retinal diseases,” *Expert Review of Medical Devices*, vol. 15, no. 12, pp. 875–882, 2018.
- [40] S. Vaz-Pereira, J. J. Silva, K. B. Freund, and M. Engelbert, “Optical coherence tomography angiography features of neovascularization in proliferative diabetic retinopathy,” *Clinical Ophthalmology*, vol. 14, pp. 3351–3362, 2020.

Research Article

Clinical Characteristics of Paracentral Acute Middle Maculopathy in Eyes with Retinal Vascular Occlusion Diseases in Chinese Patients

Zhengwei Zhang ^{1,2,3} Yunjia Jiang ^{1,2,3} Xiaoli Huang ^{2,3} Zhifeng Wu ^{2,3}
and Bilian Ke ^{1,4,5,6,7,8}

¹Department of Ophthalmology, Shanghai General Hospital of Nanjing Medical University, Shanghai, China

²Department of Ophthalmology, The Affiliated Wuxi No. 2 People's Hospital of Nanjing Medical University, Wuxi, Jiangsu Province, China

³Department of Ophthalmology, Wuxi No. 2 People's Hospital, Affiliated Wuxi Clinical College of Nantong University, Wuxi, Jiangsu Province, China

⁴Department of Ophthalmology, Shanghai General Hospital, School of Medicine, Shanghai Jiao Tong University, Shanghai, China

⁵National Clinical Research Center for Eye Diseases, Shanghai, China

⁶Shanghai Key Laboratory of Fundus Disease, Shanghai, China

⁷Shanghai Engineering Center for Visual Science and Photomedicine, Shanghai, China

⁸Shanghai Engineering Center for Precise Diagnosis and Treatment of Eye Diseases, Shanghai, China

Correspondence should be addressed to Bilian Ke; kebilian@126.com

Received 5 April 2021; Revised 6 June 2021; Accepted 12 June 2021; Published 19 June 2021

Academic Editor: Gianluca Scuderi

Copyright © 2021 Zhengwei Zhang et al. This is an open access article distributed under the Creative Commons Attribution License, which permits unrestricted use, distribution, and reproduction in any medium, provided the original work is properly cited.

Aim. To investigate the incidence and clinical characteristics of paracentral acute middle maculopathy (PAMM) and its relationship with prominent middle limiting membrane (p-MLM) sign in eyes with retinal artery occlusion (RAO) or retinal vein occlusion (RVO) in a Chinese clinical setting. **Methods.** In this retrospective observational study from January 2015 to May 2020, multimodal imaging data of 807 eyes including 555 consecutive patients with RVO or 252 consecutive patients with RAO were reviewed. All patients were scanned using the spectrum-domain optical coherence tomography (OCT), and some of them underwent color fundus photography, fundus fluorescence angiography, en face OCT, and OCT angiography. **Results.** PAMM was detected in 49 eyes of 49 RAO patients and 29 eyes of 29 RVO patients. The mean ages at presentation were 64.49 ± 13.90 years and 54.00 ± 18.48 years in RAO and RVO patients ($P = 0.006$), respectively. Eyes with RAO were more prone to develop PAMM (19.44% [49/252] vs. 5.23% [29/555]; $P < 0.001$). Of the 78 eyes with PAMM, 24 eyes (7 eyes with RVO and 17 eyes with RAO) were found with p-MLM sign. An interesting phenomenon that had been overlooked before was that the hyperreflective line of the p-MLM sign was usually continuous, regardless of the type of PAMM lesion. **Conclusions.** This series is the largest to date to describe the clinical characteristics of PAMM and p-MLM sign in Chinese patients. The incidence of PAMM and p-MLM sign in patients with RAO was relatively higher than that in patients with RVO. These signs alone probably represent milder ischemia and prompt us to carry out a comprehensive and meticulous examination to prevent the further development of the disease. In addition, the hyperreflective line of the p-MLM sign was usually continuous, which could support the totally venous nature of the retinal deep capillary plexus to some extent.

1. Background

Paracentral acute middle maculopathy (PAMM), which was first defined by Sarraf et al. in 2013, is characterized by the presence of a hyperreflective band spanning the inner nuclear layer (INL) with subsequent permanent INL thinning [1]. It is being increasingly reported and demonstrated not to be a distinct entity but a common sign of several ocular diseases [2], uneventful ocular surgeries [3, 4], or even systemic diseases [5–7]. Although its pathophysiology is not yet fully understood, impaired perfusion through the retinal capillary system, leading to hypoperfusion or ischemia of the deep vascular complex (DVC), has been proven to play a major role [8]. The DVC comprises two deeper capillary networks, located above and below the INL, that are supplied by vertical anastomoses from the superficial vascular plexus [9]. It is well acknowledged that the mechanism associated with PAMM is primarily due to sublethal ischemic hypoxia of the middle retinal tissue, mainly the layer of INL [2, 10].

Also, in 2013, Chu et al. [11, 12] introduced the “prominent middle limiting membrane (p-MLM) sign,” a hyperreflective line in the inner synaptic portion of the outer plexiform layer (OPL) on spectral-domain optical coherence tomography (SD-OCT) B-scan images, as an indicator of acute ischemic retinal damage in retinal artery occlusion (RAO) and diagnostic tool to distinguish ischemic from the nonischemic retinal vein occlusion (RVO). The pathogenesis of the p-MLM sign is similar to that of PAMM; however, the relationship between them is poorly investigated.

PAMM is associated with RVO [13–16] and RAO [17, 18], including cilioretinal arterial occlusion [19, 20]. In the first and largest study of PAMM involving eyes with nonischemic central RVO (CRVO), approximately 5.17% (25/484) of the American patients with nonischemic CRVO showed PAMM on SD-OCT [13]. However, no large-scale study has reported the prevalence or clinical characteristics of PAMM in Chinese patients with RVO or RAO, although a few case reports and small case series exist [21–23]. Therefore, the purpose of this study was to investigate the incidence and clinical characteristics of PAMM and its relationship with the p-MLM sign in eyes with RVO or RAO in a Chinese clinical setting with the largest sample size to date. In addition, we aimed to infer the nature of the retinal deep capillary plexus through optical coherence tomography (OCT) features of PAMM and the p-MLM sign.

2. Methods

In this retrospective study, consecutive cases with a clinical diagnosis of any type of RAO or RVO (branch or central and ischemic or nonischemic) from January 2015 to May 2020 were included. The clinical diagnosis was based on retinal findings, patient symptoms, and supplemental evidence from fundus fluorescence angiography (FFA) findings. If an eye showed RVO and cilioretinal artery occlusion simultaneously, it was classified as having RVO for the cause analysis. Exclusion criteria were as follows: (1) medium too cloudy to be scanned with SD-OCT; (2) quality of the OCT image too poor to be evaluated; and (3) a history of eye

surgery within one month before the first visit. The Institutional Review Board of the Affiliated Wuxi No.2 People's Hospital of Nanjing Medical University approved the protocol. This study complied with the tenets of the Declaration of Helsinki.

Each patient underwent complete ocular examination, including best-corrected visual acuity (BCVA) assessment, noncontact tonometry, slit-lamp examination, and indirect ophthalmoscopy. Retinal imaging was performed using a high-speed 840 nm-wavelength SD-OCT instrument RTVue XR Avanti (Optovue, Inc., Fremont, California, USA) or Cirrus HD-OCT with eye-tracking ability (Model 4000; Carl Zeiss Meditec, Inc., Dublin, CA). To detect the presence/absence of PAMM lesions and p-MLM sign, each OCT B-scan image was assessed by two researchers (Z.W.Z. and X.L.H.) in a blinded manner. Particularly, band-like hyperreflective lesions of the INL corresponded to PAMM lesions [1], and a hyperreflective line in the inner synaptic portion of the OPL corresponded to the p-MLM sign [11]. Disagreements regarding PAMM lesions and p-MLM sign were resolved by a third senior observer (Z.F.W.).

In some cases, en face OCT and OCT angiography were performed using the RTVue XR Avanti SD-OCT with AngioVue software (Optovue, Inc., Fremont, California, USA), which has a light source of 840 nm wavelength and 45 nm bandwidth with an A-scan rate of 70 kHz. A 3×3 mm scan or, 6×6 mm or cube scan centered on the fovea was acquired by two repeated B-scans at 304 raster positions, with each B-scan comprising 304 A-scans. Two volumetric raster scans with orthogonal fast-scan directions (horizontal and vertical) were acquired for each eye and merged to remove motion artifacts [24]. This has been described in detail in our previous work [25]. PAMM can be divided into three patterns of these areas on en face OCT [26]: arteriolar (band-like areas in the distribution of major arterioles), globular (ovoid focal or multifocal areas), and fern-like patterns (multilobulated central area tracking along veins).

In a few patients, color fundus photographs were acquired with a Topcon TRC-50IX color fundus camera (Topcon Medical Systems, Tokyo, Japan), and FFA was performed with Spectralis HRA (Heidelberg Engineering, Heidelberg, Germany).

Statistical analyses were performed using SPSS software version 21.0 (SPSS, Chicago, IL, USA). A one-sample Kolmogorov-Smirnov test was performed to assess the normality of distribution of continuous variables. Subsequently, a significance test was performed. When data were normally distributed, an independent-samples *t*-test was performed for group comparisons. Categorical data were compared using a Fisher's exact test. All tests were two-tailed, and *P* values <0.05 were considered to be statistically significant.

3. Results

Table 1 shows baseline patient demographics and ocular examination findings of patients with PAMM. Multiple imaging scans were reviewed for a total of 807 consecutive eyes of 807 patients, including 252 eyes with RAO (143 central RAO, 105 branch RAO, and four cilioretinal artery occlusion

only) and 555 eyes with RVO (226 CRVO and 329 branch RVO). Seventy-eight eyes of 78 patients, with a mean age at onset of 60.59 ± 16.45 years (range: 20–84 years), demonstrated hyperreflective plaque-like lesions at the INL on cross-sectional SD-OCT B-scans, and these were regarded as PAMM lesions. Visual acuity ranged from 0 to 2.0 logMAR at the first clinical examination. Regarding preexisting systemic comorbidities, 41 patients had known histories of systemic arterial hypertension, six had open-angle glaucoma, 10 had diabetes mellitus, and the remaining 21 patients denied a history of systemic diseases.

Of these 78 patients with PAMM lesions, 49 eyes of 49 patients (49/252 or 19.44%; mean age: 64.49 ± 13.90 years; age range: 23–84 years) had RAO, and 29 eyes of 29 patients (29/555 or 5.23%; mean age: 54.00 ± 18.48 years; age range: 20–78 years) had RVO. Regarding the type of retinal vascular occlusion, there were 32 eyes with central RAO (32/143 or 22.38%), 17 eyes with branch RAO (17/109 or 16.0%; including two eyes with cilioretinal artery occlusion only), 22 eyes with CRVO (22/226 or 9.73%), and seven eyes with branch RVO (7/329 or 2.13%). Compared with patients with RVO, those with RAO were more prone to develop PAMM (19.44% vs. 5.23%; $P < 0.001$, Fisher's exact test) and older (64.49 ± 13.90 years vs. 54.00 ± 18.48 years; $P = 0.006$; independent-samples *t*-test). The development of PAMM showed a male predilection (55 men, 70.5%; 23 women, 29.5%), but no left or right eye predilection (OD: 44 eyes; OS: 34 eyes).

Of 78 eyes with PAMM, 24 (seven eyes with RVO and 17 eyes with RAO) also showed the p-MLM sign (24/78; 30.77%). All seven eyes with the p-MLM sign associated with RVO revealed skip PAMM lesions (Figure 1). However, in the RAO group, the p-MLM sign was associated with various types of PAMM lesions. Compared with patients without the p-MLM sign, patients with the p-MLM sign were significantly older (66.17 ± 11.26 vs. 58.11 ± 17.82 years; $P = 0.019$; Table 2). However, no significant differences were found in terms of BCVA, sex, or eye distribution between the two groups (Table 2).

En face OCT images were available for 44 of 78 eyes (44/78 or 56.41%). En face OCT segmentation of the INL illustrated well-defined areas of hyperreflectivity corresponding to focal or multifocal PAMM on OCT B-scans. Three distinct patterns of PAMM lesions on en face OCT were observed: arteriolar in 24 eyes (24/44 or 54.54%), globular in seven eyes (7/44 or 15.91%), and fern-like in 13 eyes (13/44 or 29.55%). Table 3 shows the detailed distribution of the three PAMM lesion patterns by etiology. Of 13 eyes with perivenular fern-like PAMM lesions, nine had RVO, whereas only four had RAO. One eye of central RAO with follow-up data displayed fern-like PAMM lesions with skip lesions in the INL at baseline, and subsequent progression of ischemia, diffusely involving the entire middle and inner retinal layers, was observed at the one-week follow-up visit (Figure 2).

4. Discussion

This was the largest study to date to characterize PAMM and first to show its association with the p-MLM sign in a

Chinese clinical setting. As for the incidence of PAMM, we found that it was the most common in eyes with central RAO (32/143 or 22.38%) and the least common in eyes with branch RVO (7/329 or 2.13%). In eyes with RVO, the incidence of PAMM in this study (5.23%; 29/555) was consistent with that of the retrospective study conducted by Rahimy et al. (5.17%; 25/484) [13], although they only enrolled eyes with nonischemic CRVO. We were the first to assess the incidence of PAMM in eyes with RAO, which was as high as 19.44% (49/252). Consistently, in a retrospective, nonconsecutive, observational study, Yu et al. [27] identified PAMM in 22.5% (9/40) of cases with branch or central RAO, which was very close to our results. However, the incidence of PAMM in all cases of RVO and RAO may be much higher than that reported in this study because of the evanescent nature of PAMM lesions, which are covered by hemorrhage, or hyperreflectivity induced by severe ischemia of the whole inner retina. Nonetheless, our results could provide a general understanding of the clinical incidence of PAMM. More recently, Pichi et al. [20] reported that PAMM was present in 100% of the cases of isolated cilioretinal artery obstruction with or without CRVO, which may be because of hypoperfusion of the involved cilioretinal artery (as the author termed "cilioretinal artery insufficiency"), rather than complete occlusion. Together with the previous results, it is noteworthy that artery hypoperfusion or insufficiency resulted in more PAMM lesions compared to RVO.

Using en face OCT, three patterns of PAMM lesions were found, as described previously [26]. In our study, the most common pattern was arteriolar (24/44 or 54.54%), followed by fern-like (13/44 or 29.55%) and globular (7/44 or 15.91%). Therefore, although the fern-like pattern is distinctive, it is relatively common. The fern-like pattern of PAMM lesions correlates more strongly with RVO than RAO [15, 26]. In our study, 13 patients showed the perivenular fern-like PAMM lesion pattern, nine of whom had RVO and the remaining four had RAO (Table 3). Our results are consistent with previous observations that arterial hypoperfusion secondary to outflow obstruction from an RVO obstruction appears to be the most common cause of this presentation [15], and our study verified this phenomenon in a relatively large sample size. However, not all patients in the present study had undergone en face OCT, which may lead to omission of some cases of PAMM with the perivenular fern-like lesion pattern. Nonetheless, this possibility was minimized by identifying the skip pattern of PAMM lesions at the INL on cross-sectional SD-OCT, which is characteristic of perivenular fern-like PAMM lesion pattern [15, 28].

Since the concept of PAMM was widely accepted and applied in published articles, the usage of the p-MLM sign has been decreasing. The p-MLM sign could be present or absent and fails to account for the etiologic mechanism of deep retinal capillary ischemia; thus, it does not provide information about the extent of the ischemic damage [10, 27]. However, the pathogenesis of the p-MLM sign and its relationship with PAMM are still poorly understood. On OCT B-scans, the p-MLM sign was defined as a hyperreflective line, which had higher intensity of reflectivity

TABLE 1: Patient demographics and ocular findings in PAMM and p-MLM sign.

	RVO	RAO	Total
Eyes (right/left)	29 (21/8)	49 (23/26)	78 (44/34)
Age (range), years	54.00 ± 18.48 (20–78)	64.49 ± 13.90 (23–84)	60.59 ± 16.45 (20–84)
Gender (female/male)	7/22	16/33	23/55
BCVA (range), logMAR	0.86 ± 0.52 (0–2.0)	1.04 ± 0.43 (0.3–2.0)	0.97 ± 0.47 (0–2.0)
Combined with p-MLM sign	7	17	24
Systemic/ocular associations			
Hypertension	17	24	41
Diabetes mellitus	3	7	10
Open-angle glaucoma	6	0	6
No positive medical history	3	18	21

PAMM: paracentral acute middle maculopathy; p-MLM: prominent middle limiting membrane; RVO: retinal vein occlusion; RAO: retinal artery occlusion; BCVA: best-corrected visual acuity; logMAR: logarithm of the minimum angle of resolution.

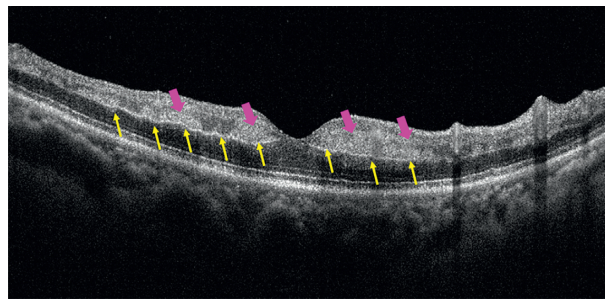


FIGURE 1: OCT displayed combined PAMM and p-MLM in one case with RVO. Pink arrows indicate skip PAMM lesions around the central macula. Yellow arrows indicate a continuous hyperreflective line being referred to as p-MLM sign on both sides of the fovea.

TABLE 2: Clinical characteristics of PAMM eyes with and without p-MLM sign.

	With p-MLM sign	Without p-MLM sign	<i>P</i>
Eyes (right/left)	24 (12/12)	54 (32/22)	0.469 [#]
Gender (female/male)	7/17	16/38	1.000 [#]
Age (range), years	66.17 ± 11.26 (33–79)	58.11 ± 17.82 (20–84)	0.019*
BCVA (range), logMAR	0.98 ± 0.50 (0–2.0)	0.97 ± 0.46 (0.3–2.0)	0.939*

p-MLM: prominent middle limiting membrane; BCVA: best-corrected visual acuity; logMAR: logarithm of the minimum angle of resolution. [#]Fisher's exact test. *Independent sample *t*-test.

TABLE 3: The distribution of three types of PAMM with different etiologies.

	Arteriolar pattern	Globular pattern	Fern-like pattern	Total
BRAO	10	1	2	13
CRAO	12	1	2	15
BRVO	0	1	0	1
CRVO	6 [#]	4	9	19
Total	24	7	13	44

[#]Combined with cilioretinal artery occlusion. BRAO: branch retinal artery occlusion; CRAO: central retinal artery occlusion; BRVO: branch retinal vein occlusion; CRVO: central retinal vein occlusion.

compared with the adjacent normal retinal structures, located in the inner synaptic portion of the OPL. This probably develops due to cytoplasmic swelling of these synaptic portions of the OPL [11]. Similar to PAMM, the p-MLM sign could be found in cases of both RAO [11] and RVO [12, 29]. Moreover, both PAMM lesions and p-MLM sign are almost always identified at paracentral location although they often extend outward from the center [30]. In our study,

compared with patients without the p-MLM sign, those with the p-MLM sign were significantly older but showed no significant differences in BCVA, sex, or eye distribution (Table 2). It seems that both PAMM and p-MLM sign have similar clinical significance.

Recently, Furashova and Matthè [29] reported that the p-MLM sign could be seen on OCT in 94% of ischemic and 66% of nonischemic RVO cases. In the present study,

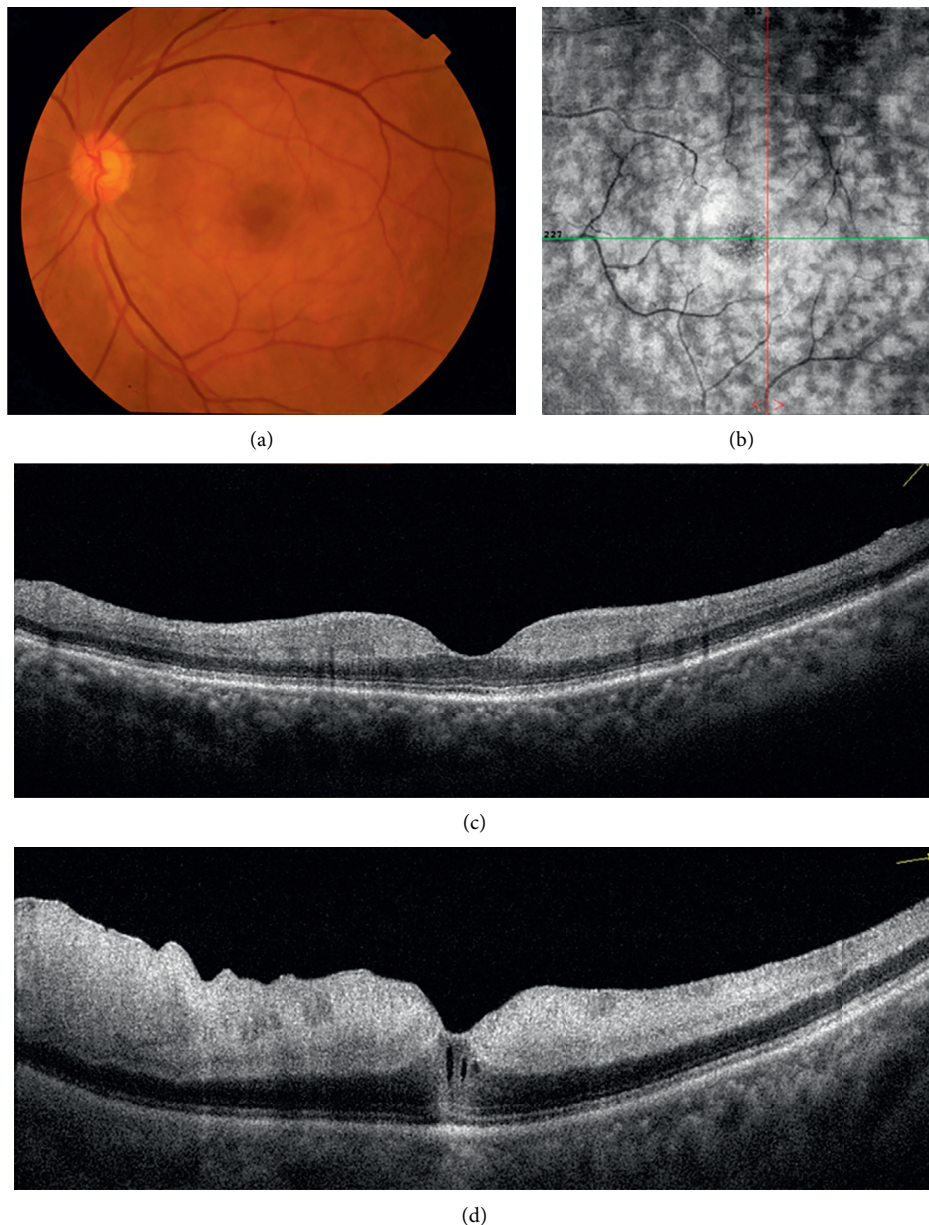


FIGURE 2: Multimodal imaging from a 55-year-old hypertensive man with partial CRAO and fern-like pattern PAMM at baseline and complete CRAO with diffuse middle and inner retinal ischemia. (a) Fundus photography illustrated perifoveal retinal whitening in the central macular region. (b) En face OCT illustrated a perivenular fern-like pattern with periarterial sparing. (c) PAMM lesions (hyper-reflective bands at the level of INL) in a skip pattern revealed on the cross-sectional OCT B-scan. (d) One week later, the patient's vision declined to 2/200, and SD-OCT illustrated diffuse middle and inner retinal ischemia.

however, only 24 (seven with RVO and 17 with RAO) of 78 PAMM cases had the p-MLM sign. Evidently, PAMM cases associated with RAO were more likely to present with the p-MLM sign than were those associated with RVO. This may be because the inner synaptic portion of the OPL is more sensitive to retinal arterial ischemia or hypoperfusion than other retinal tissues. All seven eyes with the p-MLM sign that were associated with RVO had skip PAMM lesions. However, in the RAO group, p-MLM sign could be associated with various types of PAMM lesions. This phenomenon was reported previously [11, 12], but the concept of PAMM had not been proposed at the time.

In addition, the hyperreflective line of the p-MLM sign was usually continuous, regardless of the types of PAMM lesions, even with a skip pattern (Figure 1), which is an interesting phenomenon that has not been paid sufficient attention before. According to the concept of misery perfusion [31, 32], reduced oxygenation would preferentially affect the efferent retinal circulation more than afferent retinal circulation, which may cause an ischemic cascade that starts at the level of the deep capillary plexus (DCP) closer to the perivenular pole and manifests as perivenular fern-like PAMM lesions on en face OCT segmentation or skip PAMM lesions on OCT B-scans [16]. The inner synaptic

portion of the OPL is located at the functional anteroposterior watershed between the DCP and choriocapillaris [33]. Due to the absence of direct blood supply from retinal vessels, oxygen supply of the inner synaptic portion of the OPL mainly originates from oxygen diffusion from the DCP and choriocapillaris. Continuity of the hyperreflective line of the p-MLM sign may be related to vascular components of the DCP. As the hyperreflective line is usually continuous, oxygen saturation in the inner synaptic portion of the OPL may be relatively uniform, which further supports the venous nature of DCP and the serial organization of the three main capillary plexuses in the macula [34]. When milder retinal hypoperfusion occurs, the entire level of the inner synaptic portion of the OPL (near the outer part of the DCP) and INL tissue near the vein develop ischemia and edema, manifesting as a continuous hyperreflective line, p-MLM sign, and skip PAMM lesions. The p-MLM sign may be present in patients with retinal ischemia because of the individual differences in the contribution of choroidal blood supply to the inner synaptic portion of the OPL. Therefore, the role of choroidal blood supply in the pathogenesis of the p-MLM sign should be investigated.

As for the order of occurrence of PAMM and the p-MLM sign, due to rapid progression of RAO, PAMM and p-MLM sign appeared almost simultaneously, or the p-MLM sign was hidden in the hyperreflective inner retina. Relatively, RVO leads to ischemia at a slower rate compared with RAO; therefore, the p-MLM sign may appear first, followed by PAMM. Recently, Browning et al. [35] reported that PAMM could evolve over time into the p-MLM sign. However, the p-MLM sign was evident at the initial visit (Figure 7 in their article) and was rarely found on OCT without other ischemic lesions. This may be because the patient had not undergone the initial examination for a long time, thereby eliciting the impression that the p-MLM sign and PAMM or hyperreflectivity in the inner retina occur simultaneously.

It is a challenge to sufficiently supply the required nutrients to millions of retinal neurons with only a limited blood supply after fulfilling the optical requirement. Evidently, the limited blood supply cannot consistently be received by all retinal neurons. Spatially and temporally heterogeneous capillary perfusion may be the most effective way to deal with this challenge [36]. Such heterogeneous perfusion involves the use of well-controlled intermittent blood redistribution patterns that require strong regulatory capacity and sophisticated structural arrangement of the retinal capillary plexuses. Connections between the retinal capillary plexuses are more complicated than previously thought. However, the results of our study and previous studies demonstrated that the DVC is likely to be subjected to hypoperfusion or ischemia in retinal vascular occlusion presenting with PAMM, the p-MLM sign, or both. These signs alone represent milder ischemia and should prompt clinicians to carry out a comprehensive and meticulous examination to prevent disease progression. If not treated early and effectively, symptoms would further aggravate and even seriously affect the visual prognosis (Figure 2).

This study had several limitations. First, we applied a retrospective study design and did not use a control group. Second, not all patients had undergone FFA; therefore, we could not accurately distinguish between ischemic and nonischemic RVO cases. Finally, follow-up data on ancillary imaging were unavailable for most patients. Nevertheless, this is the largest case series to date describing PAMM and p-MLM sign and the relationship between them in a Chinese clinical setting.

5. Conclusions

We found that PAMM occurred at a rate of 5.23% and 19.44% in eyes with RVO and RAO, respectively, in a Chinese clinical setting. In addition, 24 eyes developed both PAMM and p-MLM sign. These signs alone suggest mild ischemia and should prompt us to carry out a comprehensive and meticulous examination to prevent further disease progression and obtain a good prognosis. In addition, the hyperreflective line of the p-MLM sign was usually continuous, which could support the venous nature of the retinal DCP to some extent.

Data Availability

The datasets used and/or analyzed during the current study are available from the corresponding author upon reasonable request.

Ethical Approval

The procedure of the investigation conformed to the tenets of the Declaration of Helsinki, and the Institutional Review Board of the Affiliated Wuxi No. 2 People's Hospital of Nanjing Medical University approved the retrospective revision of the clinical data.

Conflicts of Interest

The authors declare that they have no conflicts of interest.

Authors' Contributions

Zhengwei Zhang conceived, designed, and supervised the study, as well as drafted the manuscript. Yunjia Jiang and Xiaoli Huang collected and analyzed the data. Zhifeng Wu interpreted the data. Bilian Ke made a critical revision of the article. All authors read and approved the final manuscript.

Acknowledgments

This study was supported by the Fund of Top Talent Support Program for Young and Middle-Aged People of Wuxi Health Committee (Grant no. HB2020030), the Development Fund of Wuxi Science and Technology (Grant no. WX18IIAN019), and the Social Development Project of Jiangsu Provincial Science and Technology Department (Grant no. BE2017627).

References

- [1] D. Sarraf, E. Rahimy, A. A. Fawzi et al., "Paracentral acute middle maculopathy: a new variant of acute macular neuroretinopathy associated with retinal capillary ischemia," *JAMA Ophthalmology*, vol. 131, no. 10, pp. 1275–1287, 2013.
- [2] N. Moura-Coelho, T. Gaspar, J. T. Ferreira, M. Dutra-Medeiros, and J. P. Cunha, "Paracentral acute middle maculopathy—review of the literature," *Graefes Archive for Clinical and Experimental Ophthalmology*, vol. 258, no. 12, pp. 2583–2596, 2020.
- [3] C. Bernal-Morales, D. Velazquez-Villoria, J. M. Cubero-Parra et al., "Paracentral acute middle maculopathy after uneventful ocular surgery with local anaesthetic blocks," *Eye (London)*, 2021.
- [4] H. Nakashima, Y. Iwama, K. Tanioka, and K. Emi, "Paracentral acute middle maculopathy following vitrectomy for proliferative diabetic retinopathy: incidence, risk factors, and clinical characteristics," *Ophthalmology*, vol. 125, no. 12, pp. 1929–1936, 2018.
- [5] B. P. Sander, "Spectral-domain optical coherence tomography in paracentral acute middle maculopathy associated with vasopressor exposure," *Clinical and Experimental Optometry*, vol. 104, no. 4, pp. 544–546, 2021.
- [6] S. K. Padhy, R. P. Dacruz, and A. Kelgaonkar, "Paracentral acute middle maculopathy following SARS-CoV-2 infection: the D-dimer hypothesis," *BMJ Case Reports*, vol. 14, no. 3, Article ID e242043, 2021.
- [7] M. A. Burnasheva, D. S. Maltsev, A. N. Kulikov, K. A. Sherbakova, and A. V. Barsukov, "Association of chronic paracentral acute middle maculopathy lesions with hypertension," *Ophthalmology Retina*, vol. 4, no. 5, pp. 504–509, 2020.
- [8] S. Chu, P. L. Nesper, B. T. Soetikno, S. J. Bakri, and A. A. Fawzi, "Projection-resolved OCT angiography of microvascular changes in paracentral acute middle maculopathy and acute macular neuroretinopathy," *Investigative Ophthalmology & Visual Science*, vol. 59, no. 7, pp. 2913–2922, 2018.
- [9] J. Provis, "Development of the primate retinal vasculature," *Progress in Retinal and Eye Research*, vol. 20, no. 6, pp. 799–821, 2001.
- [10] J. Scharf, K. B. Freund, S. Sadda, and D. Sarraf, "Paracentral acute middle maculopathy and the organization of the retinal capillary plexuses," *Progress in Retinal and Eye Research*, vol. 81, Article ID 100884, 2021.
- [11] Y. K. Chu, Y. T. Hong, S. H. Byeon, and O. W. Kwon, "In vivo detection of acute ischemic damages in retinal arterial occlusion with optical coherence tomography: a "prominent middle limiting membrane sign," *Retina*, vol. 33, no. 10, pp. 2110–2117, 2013.
- [12] J. Ko, O. W. Kwon, and S. H. Byeon, "Optical coherence tomography predicts visual outcome in acute central retinal vein occlusion," *Retina*, vol. 34, no. 6, pp. 1132–1141, 2014.
- [13] E. Rahimy, D. Sarraf, M. L. Dollin, J. D. Pitcher, and A. C. Ho, "Paracentral acute middle maculopathy in nonischemic central retinal vein occlusion," *American Journal of Ophthalmology*, vol. 158, no. 2, pp. 372–380, 2014.
- [14] G. Casalino, M. Williams, C. McAvoy, F. Bandello, and U. Chakravarthy, "Optical coherence tomography angiography in paracentral acute middle maculopathy secondary to central retinal vein occlusion," *Eye*, vol. 30, no. 6, pp. 888–893, 2016.
- [15] K. Ghasemi Falavarjani, N. Phasukkijwatana, K. B. Freund et al., "En face optical coherence tomography analysis to assess the spectrum of perivenular ischemia and paracentral acute middle maculopathy in retinal vein occlusion," *American Journal of Ophthalmology*, vol. 177, pp. 131–138, 2017.
- [16] M. F. Bakhroum, K. B. Freund, R. Dolz-Marco et al., "Paracentral acute middle maculopathy and the ischemic cascade associated with retinal vascular occlusion," *American Journal of Ophthalmology*, vol. 195, pp. 143–153, 2018.
- [17] G. Querques, C. La Spina, E. Miserocchi, M. Gagliardi, F. Corvi, and F. Bandello, "Angiographic evidence of retinal artery transient occlusion in paracentral acute middle maculopathy," *Retina*, vol. 34, no. 10, pp. 2158–2160, 2014.
- [18] J. G. Christenbury, M. A. Klufas, T. C. Sauer, and D. Sarraf, "OCT angiography of paracentral acute middle maculopathy associated with central retinal artery occlusion and deep capillary ischemia," *Ophthalmic Surgery, Lasers and Imaging Retina*, vol. 46, no. 5, pp. 579–581, 2015.
- [19] M. L. G. da Fonseca, A. Souza, M. B. Pereira, R. N. G. Vianna, L. M. Cravo, and E. Demori, "Paracentral acute middle maculopathy associated with hypoperfusion of the cilioretinal artery and impending central retinal vein occlusion," *European Journal of Ophthalmology*, vol. 31, no. 2, pp. NP46–NP48, 2021.
- [20] F. Pichi, S. Fragiotta, K. B. Freund et al., "Cilioretinal artery hypoperfusion and its association with paracentral acute middle maculopathy," *British Journal of Ophthalmology*, vol. 103, no. 8, pp. 1137–1145, 2019.
- [21] M. Li, T. Qian, X. Li et al., "The clinical and multimodal imaging characteristics of paracentral acute middle maculopathy," *Chinese Journal of Ocular Fundus Diseases*, vol. 35, no. 4, pp. 322–326, 2019.
- [22] Z. Wang, X. Chen, H. Liu, and X. Li, "Clinical features of paracentral acute middle maculopathy," *Chinese Journal of Ophthalmology*, vol. 37, no. 1, pp. 16–20, 2019.
- [23] Y. Chen and Y. Hu, "The optical imaging of idiopathic paracentral acute middle maculopathy in a Chinese young man and review of the literature," *Photodiagnosis and Photodynamic Therapy*, vol. 19, pp. 383–387, 2017.
- [24] Y. Jia, O. Tan, J. Tokayer et al., "Split-spectrum amplitude-decorrelation angiography with optical coherence tomography," *Optics Express*, vol. 20, no. 4, pp. 4710–4725, 2012.
- [25] Z. Zhang, X. Huang, X. Meng et al., "In vivo assessment of macula in eyes of healthy children 8 to 16 years old using optical coherence tomography angiography," *Scientific Reports*, vol. 7, no. 1, Article ID 8936, 2017.
- [26] J. Sridhar, A. Shahlaee, E. Rahimy et al., "Optical coherence tomography angiography and en face optical coherence tomography features of paracentral acute middle maculopathy," *American Journal of Ophthalmology*, vol. 160, no. 6, pp. 1259–1268, 2015.
- [27] S. Yu, C. E. Pang, Y. Gong et al., "The spectrum of superficial and deep capillary ischemia in retinal artery occlusion," *American Journal of Ophthalmology*, vol. 159, no. 1, pp. 53–63, 2015.
- [28] S. T. Garrity, V. L. Tseng, and D. Sarraf, "Paracentral acute middle maculopathy in a perivenular fern-like distribution with en face optical coherence tomography," *Retinal Cases & Brief Reports*, vol. 12, no. 1, pp. S25–S28, 2018.
- [29] O. Furashova and E. Matthè, "Hyperreflectivity of inner retinal layers as a quantitative parameter of ischemic damage in acute retinal vein occlusion (RVO): an optical coherence tomography study," *Clinical Ophthalmology*, vol. 14, pp. 2453–2462, 2020.
- [30] K. K. Dansingani, M. Inoue, M. Engelbert, and K. B. Freund, "Optical coherence tomographic angiography shows reduced

- deep capillary flow in paracentral acute middle maculopathy,” *Eye*, vol. 29, no. 12, pp. 1620–1624, 2015.
- [31] D. McLeod and S. Beatty, “Evidence for an enduring ischaemic penumbra following central retinal artery occlusion, with implications for fibrinolytic therapy,” *Progress in Retinal and Eye Research*, vol. 49, pp. 82–119, 2015.
- [32] D. McLeod, “Misery perfusion, diffusive oxygen shunting and interarterial watershed infarction underlie oxygenation-based hypoperfusion maculopathy,” *American Journal of Ophthalmology*, vol. 205, pp. 153–164, 2019.
- [33] N. N. Osborne, R. J. Casson, J. P. M. Wood, G. Chidlow, M. Graham, and J. Melena, “Retinal ischemia: mechanisms of damage and potential therapeutic strategies,” *Progress in Retinal and Eye Research*, vol. 23, no. 1, pp. 91–147, 2004.
- [34] D. An, P. Yu, K. B. Freund, D. Y. Yu, and C. Balaratnasingam, “Three-dimensional characterization of the normal human parafoveal microvasculature using structural criteria and high-resolution confocal microscopy,” *Investigative Ophthalmology & Visual Science*, vol. 61, no. 10, pp. 3–16, 2020.
- [35] D. J. Browning, O. S. Punjabi, and C. Lee, “Assessment of ischemia in acute central retinal vein occlusion from inner retinal reflectivity on spectral domain optical coherence tomography,” *Clinical Ophthalmology (Auckland, N.Z.)*, vol. 11, pp. 71–79, 2017.
- [36] D.-Y. Yu, S. J. Cringle, P. K. Yu et al., “Retinal capillary perfusion: spatial and temporal heterogeneity,” *Progress in Retinal and Eye Research*, vol. 70, pp. 23–54, 2019.

Research Article

Clinical Features, Prognosis, and Long-Term Response to Ranibizumab of Macular CNVs in Pattern Dystrophies Spectrum: A Pilot Study

Lorenzo Casillo , Stefano Tricarico , Laura Contento , and Enzo M. Vingolo 

UOC Ophthalmology, Ospedale A. Fiorini Terracina, Sapienza University of Rome, Terracina 04120, Italy

Correspondence should be addressed to Lorenzo Casillo; lorenzo.casillo@uniroma1.it

Received 27 December 2020; Revised 14 March 2021; Accepted 5 April 2021; Published 17 April 2021

Academic Editor: Yoichi Sakurada

Copyright © 2021 Lorenzo Casillo et al. This is an open access article distributed under the Creative Commons Attribution License, which permits unrestricted use, distribution, and reproduction in any medium, provided the original work is properly cited.

Introduction. To analyze the morphological and functional features of choroidal neovascularizations (CNVs) in eyes affected by pattern dystrophies (PD), evaluating their long-term response to intravitreal ranibizumab, and comparing them with CNVs in age-related macular degeneration (AMD). The main goal is to identify possible disease biomarkers and to evaluate the long-term prognosis of CNVs in PD. **Materials and Methods.** A retrospective study of 42 patients with naïve CNV (26 PD and 16 AMD), for a total of 47 eyes (29 eyes in the PD group and 18 eyes in the AMD group). Each patient received a loading dose of ranibizumab (one monthly for three months) followed by pro re nata (PRN) reinjection protocol for a period of at least three years. Morphological OCT parameters (CRT, central retinal thickness; SRF, subretinal fluid; IRF, intraretinal fluid; SHRM, subretinal hyperreflective material; HRF, hyperreflective foci; HCD, hyperreflective crystalline deposits; cCT, central choroidal thickness; sCT, sublesional choroidal thickness; EZd, ellipsoid zone disruption; and best corrected visual acuity (BCVA in logMAR scale)) were reported at baseline and last follow-up. **Results.** At baseline, no significant differences were found between the two groups, except for choroidal thickness parameters that were significantly greater in the PD group ($p = 0.009$). Longitudinal PD analysis demonstrated reduction in BCVA ($p = 0.009$), decrease in CRT ($p = 0.046$), resolution of SRF in 61.6% of cases ($p = 0.004$) and SHRM in 30% ($p = 0.034$), and choroidal thinning both centrally ($p = 0.004$) and sublesional ($p = 0.011$) compared to baseline. At 3 years, the PD group received significantly more injections than the AMD ($p = 0.011$) and showed significantly thicker choroid ($p = 0.033$) and more frequent HRF ($p = 0.006$). Regarding the PD group, we found a negative correlation between age and choroidal thicknesses at baseline and at 3 years ($p < 0.05$); significant positive correlations were found between baseline BCVA and at 3 years ($p < 0.001$), BCVA at 3 years and IRF ($p = 0.003$) and SHRM at 3 years ($p = 0.003$); CRT baseline and CRT 3 years ($p = 0.017$); HCD at 3 years was associated with greater CRT ($p = 0.04$) and IRF at 3 years ($p = 0.019$). **Conclusions.** Early and long-term morphofunctional features of CNVs in PD and in AMD are overlapping. CNVs in PD have poorer long-term response to ranibizumab and higher choroidal thickness suggesting different pathogenetic and evolutionary mechanisms.

1. Introduction

Pattern dystrophies (PD) are a group of hereditary macular diseases characterized by the accumulation of lipofuscin material at the level of the retinal pigment epithelium (RPE). Based on the different RPE alteration patterns, five different subtypes of PD have been identified [1]: adult-onset foveomacular vitelliform dystrophy (AOFVD), butterfly-shaped dystrophy, reticular Sjogren dystrophy, and

multifocal pattern dystrophy simulating fundus flavimaculatus and fundus pulverulentus.

The evolution of PD has been considered erroneously benign for a long time, probably due to their clinical, phenotypic, and demographic features, determining their frequent misdiagnosis with more frequent and known macular diseases, above all age-related macular degeneration (AMD). Today, we know that 42% of the affected subjects will develop severe and irreversible visual damage due to the

atrophic (26%) or neovascular (18%) complications [2]. However, the etiopathogenetic bases, the morphological features, and the treatment indications and response are controversial.

This retrospective study aims to analyze the morphological and functional characteristics of choroidal neovascularizations (CNVs) in eyes affected by PD, evaluating their long-term response to intravitreal ranibizumab, and comparing them with CNVs in AMD. The mean goal is to identify possible disease biomarkers and to evaluate the long-term prognosis of CNVs in PD compared to conventional AMD.

2. Materials and Methods

We collected data from 42 patients with naïve CNV, of which 26 with PD and 16 with AMD, for a total of 47 eyes including 29 eyes in the PD group and 18 eyes in the conventional AMD group. The PD group included 20 subjects affected by adult-onset foveomacular vitelliform dystrophy (23 eyes), 6 with butterfly-shaped dystrophy (6 eyes), and 2 with reticular dystrophy (2 eyes). Each patient received a loading dose of ranibizumab (one monthly for three months) followed by pro re nata reinjection protocol for a period of at least three years. Patients who had previously received any treatment for CNV were excluded, as well as subjects who switched to any other anti-VEGF drug during the follow-up period. We also excluded patients affected by other macular diseases, recent anterior or posterior segment surgery, cataract surgery during the follow-up period, and positive or negative spherical refractive error >6 diopters. This study adhered to the Tenets of the Declaration of Helsinki and complied with the Health Insurance Portability and Accountability Act of 1996. This study was approved by the institutional review board (IRB) committee.

All patients underwent a complete eye exam, including best corrected visual acuity (BCVA), anterior and posterior segment examination, fundus autofluorescence (FAF), fluorescein (FA), indocyanine green angiography (ICGA), and optical coherence tomography (OCT). All data were evaluated by two independent retina experts, and in doubtful cases, a third senior expert was consulted. The diagnostic criteria for PD included the (a) absence of drusen on funduscopic examination; (b) absence of any focal RPE elevation compatible with drusen on OCT b scans and showing hyperfluorescence on FAF and FA; (c) the presence of RPE alterations of any type from focal hyperreflective thickening, RPE attenuation, to more extensive RPE alterations detectable through clinical examination, FAF, and OCT b scans; and (d) if present, the vitelliform material accrual was visible at OCT b scans as subretinal material at medium to high reflectivity and hyperfluorescent at FAF.

Morphological and functional data were reported at baseline and after a three years follow-up. BCVA was measured using the logMAR scale. Morphological parameters were collected through SD-OCT Heidelberg Spectralis (software version 5.4.7.0; Heidelberg Engineering, Germany). OCT scans were acquired with a vertical and horizontal 100 frames enhanced depth imaging (EDI) single line

centered on the fovea and $20 \times 15^\circ$ (5.8×4.3 mm) rectangular scan raster centered on the fovea consisting of 25 high-resolution lines each comprising an average of 50 acquisitions. The “baseline” scan was used as a reference for all the following images acquired in the “follow-up” mode, in order to ensure reproducibility of the method. At time 0 and at 3 years, we evaluated the following parameters: central retinal thickness (CRT, automatically measured by the software), subretinal fluid (SRF, presence/absence), intraretinal fluid (IRF, including cystic formations, excluding tubulation phenomena, presence/absence), subretinal hyperreflective material (SHRM, defined as the hyperreflective material located between the neuroretina and the anterior lamina of RPE [3], presence/absence), hyperreflective crystalline deposits (HCD, diagnosed in OCT as single or multiple highly reflective lines between the RPE and Bruch’s membrane [4]. On near-infrared reflectance, HCD appeared as intensively reflective plaques [5], presence/absence), hyperreflective foci (HRF, diagnosed in OCT as small and well-circumscribed hyperreflective particles in the outer retinal layers. In fundus color photography, they could appear as hard exudates; no alterations in fluorescein angiography, presence/absence), central choroidal thickness (cCT, manually measured as the distance between the outer edge of the hyperreflective line of Bruch’s membrane and the inner surface of the choriocleral junction at the level of the foveola), sublesional choroidal thickness (slCT, manually measured as the distance between the outer edge of the hyperreflective line of Bruch’s membrane and the inner surface of the choriocleral junction at the level of the center of the neovascular formation), and ellipsoid zone disruption (EZd, diagnosed in OCT as disappearance of ellipsoid zone, presence/absence). Each parameter was evaluated according to the judgment of two independent expert operators.

The data analysis was conducted using both descriptive and inferential statistics. For the descriptive statistics, quantitative and qualitative variables were used and analyzed according to a general linear model. Quantitative data were reported as mean \pm standard deviation, and distribution normality was verified by the Shapiro–Wilk normality test. For the inferential statistic, significant differences between groups or intragroups were tested using the *t* test for unpaired or paired data, respectively.

The chi-square test was used to compare patient categorical variables, while the Wilcoxon test was chosen to evaluate changes in the nominal variables over time. The analysis of the relationships between variables was conducted using Spearman’s tau coefficient. In all cases, *p* values less than 0.05 were considered statistically significant. Each analysis was conducted using the SPSS statistical program (ver. 25; SPSS, Inc., Chicago, IL., USA).

3. Results

3.1. Between-Groups Baseline Analysis before Treatment. Baseline demographic characteristics were assimilable between groups for age (years; PD: 74.62 ± 6.35 ; AMD: 75.22 ± 7.44 ; $p = 0.32$), sex (% female/male; PD: 61.1/38.9; AMD: 62.1/37.9; $p = 0.95$), and months of follow-up (PD:

TABLE 1: PD and AMD parameters at baseline and after 3 years.

	Baseline			3 years		
	PD	AMD	<i>p</i> value	PD	AMD	<i>p</i> value
LogMAR, mean ± SD	0.55 ± 0.15	0.72 ± 0.44	0.13	0.86 ± 0.66	0.85 ± 0.58	0.95
CRT, μm , mean ± SD	413.66 ± 92.54	431.56 ± 142.39	0.13	365.90 ± 135.28	374.61 ± 162.27	0.85
SRF (%)	89.66	83.33	0.53	55.2	38.9	0.28
IRF (%)	31.03	44.44	0.35	37.9	38.9	0.95
SHRM (%)	69.0	66.7	0.87	48.3	61.1	0.39
HRF (%)	96.55	88.89	0.3	82.8	44.4	0.006
HCD (%)	0	0	-	10.3	5.6	0.57
cCT, μm , mean ± SD	214.14 ± 79.13	164.67 ± 45.81	0.009	186.66 ± 78.20	146.06 ± 48.33	0.033
slCT, μm , mean ± SD	211.44 ± 85.27	156.33 ± 53.07	0.009	183.52 ± 89.18	151.33 ± 58.08	0.14
EZd (%)	55.17	66.7	0.43	68.96	83.33	0.27
INJ N, mean ± SD	—	—	—	8.72 ± 1.16	7.28 ± 2.54	0.011

PD, pattern dystrophies; AMD, age-related macular degeneration; LogMAR, visual acuity; CRT, central retinal thickness; SRF, subretinal fluid; IRF, intraretinal fluid; SHRM, subretinal hyperreflective material; HRF, hyperreflective foci; HCD, hyperreflective crystalline deposits; cCT, central choroidal thickness; slCT, sublesional choroidal thickness; EZd, ellipsoid zone disruption; SD, standard deviation; μm , micrometer. The chi-square test is for quantitative data, and the unpaired-*t* test is for qualitative data.

TABLE 2: Longitudinal analysis.

	PD		AMD	
	Variation	<i>P</i> value	Variation	<i>P</i> value
LogMAR, mean ± SD	0.31 ± 0.6	0.009	0.13 ± 0.65	0.4
CRT, μm , mean ± SD	-47.75 ± 123.07	0.046	-56.94 ± 204.28	0.25
SRF (%)	-61.6	0.004	-53.3	0.011
IRF (%)	22.1	0.52	-22.1	0.65
SHRM (%)	-30	0.034	-12.5	0.74
HRF (%)	-14.3	0.1	-50.0	0.011
HCD (%)	10.3	0.08	5.6	0.32
cCT, μm , mean ± SD	-27.48 ± 47.26	0.004	-18.61 ± 27.88	0.012
slCT, μm , mean ± SD	-27.93 ± 55.27	0.011	-5.0 ± 24.39	0.4
EZd (%)	13.79	0.21	16.63	0.08

PD, pattern dystrophies; AMD, age-related macular degeneration; LogMAR, visual acuity; CRT, central retinal thickness; SRF, subretinal fluid; IRF, intraretinal fluid; SHRM, subretinal hyperreflective material; HRF, hyperreflective foci; HCD, hyperreflective crystalline deposits; cCT, central choroidal thickness; slCT, sublesional choroidal thickness; EZd, ellipsoid zone disruption; SD, standard deviation; μm , micrometer. The chi-square test is for quantitative data, and the unpaired-*t* test is for qualitative data.

40.72 ± 3.27; AMD: 40.11 ± 2.72; $p=0.55$). Functional and morphological parameters of both groups were collected at the baseline (Table 1). At baseline, the visual acuity ($p=0.13$) and the CRT ($p=0.13$) were similar between the PD and AMD groups. Furthermore, no significant differences were found between the two groups in terms of the presence of SRF ($X^2=0.39$; $p=0.53$), IRF ($X^2=2.29$; $p=0.13$), SHRM at baseline ($X^2=0.03$; $p=0.87$), and HRF at baseline ($X^2=1.09$; $p=0.30$). At this time, HCD were not detected in any of the groups. The choroidal thickness parameters were

significantly greater in the PD group than in AMD (cCT + 49.47 μm and slCT + 55.12 μm both with $p=0.009$).

3.2. In-Group Longitudinal Long-Term Analysis before-after Treatment. At 3 years of follow-up, all the parameters considered at the baseline were reevaluated to identify any evolutions and correlations (Tables 1 and 2). In particular, the PD group demonstrated significant reduction in BCVA, considered as increasing of logMAR value ($p=0.009$), despite a significant decrease in central retinal thickness (CRT variation $pp=0.046$), with the resolution of SRF in 61.6% of cases ($Z=-2.89$; $p=0.004$) and SHRM in 30% ($Z=-2.12$; $p=0.034$). There were no significant changes in IRF ($Z=-0.63$; $p=0.53$) and HRF ($Z=-1.6$; $p=0.1$). The presence of HCD was detected in 3 cases, but it does not satisfy the significance criteria, despite an encouraging trend ($Z=-1.73$; $p=0.08$). The choroid showed significant thinning both centrally (cCT V: $p=0.004$) and sublesional (slCT V: $p=0.011$) compared to baseline. Furthermore, no significant variation was observed in ellipsoid zone disruption ($p=0.21$).

In the AMD group, the BCVA was substantially stable at 3-year compared to the initial value ($p=0.4$). The CRT also showed no significant changes ($p=0.25$), despite a significant reduction in the presence of SRF ($Z=-2.53$; $p=0.01$) and HRF ($Z=-2.53$; $p=0.011$). The reduction in IRF ($Z=-0.45$; $p=0.65$) and SHRM ($Z=-0.33$; $p=0.74$) was also not significant, as was the appearance of HCD in a single case ($Z=-1.0$; $p=0.32$). Similar to the PD group, a significant decrease in cCT was detected ($p=0.012$), and no significant variation of the ellipsoid zone integrity was detected ($p=0.08$). However, unlike the PD group, the AMD subjects did not show a similar thinning of the slCT ($p=0.4$).

3.3. Between-Groups Long-Term Analysis after Treatment.

The final analysis of the two groups allowed us to compare the long-term response to intravitreal ranibizumab. The first interesting finding is that the PD group received significantly more injections than the AMD ($p = 0.011$). Despite this, the final BCVA between the two groups was similar ($p = 0.95$), as well as the CRT ($p = 0.85$) and the persistence of SRF ($X^2 = 1.18$, $p = 0.28$), IRF ($X^2 = 0.004$, $p = 0.95$), SHRM ($X^2 = 0.74$, $p = 0.39$), and HCD ($X^2 = 0.33$, $p = 0.57$). A highly significant difference was found in the presence of HRF, more frequent in the PD group ($X^2 = 7.50$; $p = 0.006$). Finally, the cCT of the PD group was significantly thicker than the AMD group ($p = 0.033$); therefore, the cCT variance did not differ between groups ($p = 0.21$).

3.4. PD In-Group Quantitative and Qualitative Correlations.

Each quantitative and qualitative parameter was cross-compared to each other, but only the most clinically relevant correlations were reported. Analyzing the PD group, we found a negative correlation between age and cCT at baseline and cCT at 3 years (respectively, $R = -0.46$, $p = 0.012$; $R = -0.58$, $p = 0.001$) and also showed in the sublesional measurements slCT baseline and slCT at 3 years (respectively, $R = -0.41$, $p = 0.027$; $R = -0.51$, $p = 0.004$). Moreover, we found a significant positive correlation between BCVA at baseline and at 3 years ($R = +0.64$; $p < 0.001$) and between BCVA at 3 years (considered as logMAR value) and the presence of IRF ($R = +0.53$, $p = 0.003$) and SHRM at 3 years ($R = +0.54$, $p = 0.003$). Interestingly, we noticed no correlation between BCVA 3 years and SRF 3 years ($R = -0.28$, $p = 0.14$), whereas the CRT baseline and CRT 3 years showed a positive correlation, with $R = +0.44$ and $p = 0.017$. However, except for the correlations between CRT and SHRM at baseline ($R = +0.54$, $p = 0.003$) and SRF 3 years-cCT 3 years ($R = +0.44$, $p = 0.016$), none of the morphological parameters considered showed a predominant role in influencing the CRT in the PD subgroup. The presence of SHRM at baseline correlated not only with the CRT baseline but also with the presence of IRF at 3 years ($R = +0.37$, $p = 0.048$) and SHRM 3 years ($R = +0.50$, $p = 0.005$). Of note, the presence of HCD at 3 years was associated with greater CRT ($R = +0.38$, $p = 0.04$) and IRF at 3 years ($R = +0.44$, $p = 0.019$).

On the AMD group, we observed positive correlations between choroidal thickness parameters longitudinally, cCT baseline-cCT 3 years ($R = +0.83$, $p < 0.001$), slCT baseline-slCT 3 years ($R = +0.91$, $p < 0.001$) but also cCT baseline-slCT baseline ($R = +0.80$, $p < 0.001$), cCT 3 years-slCT 3 years ($R = +0.86$, $p < 0.001$). Contrariwise to the PD group, no correlations were found between choroidal thickness and age: cCT at baseline-age ($R = -0.33$, $p = 0.18$) and cCT 3 years age ($R = -0.27$; $p = 0.27$). The final BCVA (logMAR at 3 years) was associated with the presence of SHRM at 3 years ($R = +0.62$, $p = 0.007$), as seen in the PD subgroup. The CRT baseline increased with the presence of IRF baseline ($R = +0.49$, $p = 0.039$), while after 3 years, it was influenced by the presence of both SRF (CRT 3 years-SRF 3 years: $R = +0.63$, $p = 0.005$) and HRF ($R = +0.56$, $p = 0.016$). In this regard, the increasing SRF at 3 years was strongly accompanied by the presence of HRF ($R = +0.66$, $p = 0.003$).

4. Discussion

The clinical and morphological features of the two groups were similar at baseline exhibiting no differences in visual acuity, central macular thickness, subretinal or intraretinal fluid, subretinal material, and hyperreflective crystalline deposits, with the only exception of choroidal thicknesses. The PD subgroup showed thicker choroidal thicknesses both centrally and underneath the neovascular lesion at baseline and at last follow-up. These findings appear to be comparable with similar but not analogous findings already present in the literature.

In fact, while Palacios et al. in 2016 demonstrated a comparable choroidal thickness between PD patients and healthy population [6], Coscas et al. highlighted how subjects with wet AMD had thinner choroids compared to adult-onset foveomacular vitelliform dystrophy (AOFVD) not yet complicated by CNV, indicating a possible role in the differential diagnosis [7]. Grenga et al. confirmed these findings and observed a progressive increase in the choroidal thickness based on the evolutive stage of the not yet neovascular disease, assuming a possible prognostic and pathogenetic role of the choroid in the AOFVD [8]. In this regard, our data show a moderate agreement between choroidal thickness and subretinal fluid at last follow-up. This correlation was not observed in the AMD group; therefore, this finding may suggest the possible role of choroidal hyperpermeability in sustaining the subretinal fluid often present even without detectable neovascularization in AOFVD [9–12].

It is reasonable to hypothesize that the variation in choroidal thickness based on the evolutionary stage may represent a compensatory mechanism for the elimination of vitelliform/lipofuscin material by the hypertrophic pigment epithelium. Therefore, it would be plausible that the thickening of the outer retinal vessels in the Haller layer could cause secondary damage to the overlying choriocapillaris network, triggering ischemic phenomena responsible for subsequent neovascularization. This may represent an alternative pathogenic mechanism in contraposition to the AMD, where the progressive choroidal thinning is mainly related to aging [13]. Our data confirm the progressive choroidal thinning over time in the AMD group, as previously reported in the literature [14, 15]. In AMD eyes, the choroid and the choriocapillaris present progressive thinning inducing ischemic alterations of the microcirculation, similar to other vascular systemic diseases (e.g., atherosclerosis and cerebrovascular insufficiency). In the PD eyes, despite a progressive choroidal thinning similar to the AMD group, likely due to aging and/or bevacizumab treatment, the choroid remained thicker through the 3 years of follow-up. This finding further corroborates the different role of the choroid in driving the development of macular complications in such cases.

The baseline visual acuity was similar in both groups; however, while the PD group had very homogeneous values among the enrolled subjects (logMAR baseline: mean = 0.55; SD = 0.15), the AMD group showed markedly greater variability (mean = 0.72; SD = 0.44). The

visual acuity after 3 years showed clearly more similar values compared to the initial data: logMARPD (mean = 0.86; SD = 0.66); logMARAMD (mean = 0.85; SD = 0.58). In fact, the longitudinal evaluation of the PD group demonstrated a significant loss of vision over the 3 years, while the functional progression in the AMD group was not significant.

Based on the arguments, our data suggest that CNVs in AMD and PD may have different evolution trends, as already partially demonstrated in the literature [16]. Another interesting finding is that both groups, AMD and PD, showed worse visual acuity at 3 years when subretinal hyperreflective material and, but only in the PD group, intraretinal fluid were present. A comparison with other intravitreal medications would be required, in order to evaluate differences in terms of functional and morphological responses.

With regard to the therapeutic response of the PD group, it is also interesting to observe that the average lowering of visual acuity is unexpectedly associated to a significant improvement in morphological parameters, such as central macular thickness, presence of fluid and subretinal hyperreflective material, and ellipsoid zone integrity but with persistence of hyperreflective intraretinal foci. The AMD group, on the other hand, shows greater volatility in the variation of the central thickness, despite the resolution of subretinal fluid in more than 50% of the subjects, associated to a reduction of hyperreflective foci. In this regard, it is interesting to observe that in the AMD group, the permanence of subretinal fluid and hyperreflective foci are associated with each other and with a higher central retinal thickness.

It is important to underline that a good short-term morphofunctional response of CNVs in PD is commonly reported in literature [17–19]. Many long-term follow-up studies, on the other hand, confirm a morphological improvement, nevertheless emerging divergences in terms of functional recovery [16, 20]. This apparent difference between functional and morphological features could depend on several factors, for example, the trend of these lesions to early damage the photoreceptors that were already suffering due to the presence of accumulation of vitelliform material and/or dysfunction of the EPR; an alternative explanation is the greater tendency to fibrosis than conventional CNVs. This point would deserve further investigation with other observational studies with adequate follow-up time.

Another noteworthy aspect is the presence of hyperreflective crystalline deposits. These cholesterol-based crystalline formations [5] were not observed in any patient at baseline, but appeared only in the long term, in double (albeit not significant) percentages in the PD group compared to AMD. Furthermore, in the PD group, HCD was associated with the permanence of intraretinal fluid and the final central macular thickness, confirming and integrating their already known nature of the negative prognostic factor, demonstrated to date in relation to the dry forms of AMD [4, 21]. Furthermore, their presence could represent a further point in support of the greater tendency to atrophic evolution of the disease; this evidence was also observed in the course of avascular lesions, such as drusenoid detachments of the retinal pigment epithelium. This could open a new scenario for the treatment of CNV associated with PD,

which should not be “overtreated” to avoid a further atrophic effect. In fact, we reported a higher number of injections at 3 years in the PD group. One of the possible reasons for over-treatment lies in the hypothesis that a part of subretinal fluid could be due to RPE pump failure instead of CNV activity.

Data collected allow us to state that both at baseline and at 3 years follow-up, morphological and functional parameters between the two groups are similar, with the exception of a greater central choroidal thickness and a greater percentage of hyperreflective foci in the PD group; however, the real difference between the two groups lies in the type of progression and response to therapy.

The limit of our study is the retrospective nature and the small sample size, negatively influenced by the stringent inclusion criteria regarding the use of monotherapy and the availability of complete multimodal imaging. Furthermore, the choice of ranibizumab as the only drug and the administration with the PRN protocol are limiting choices, but necessary to guarantee homogeneity of the data collected, which come, in part, from databases created when more modern drugs and protocols, such as aflibercept and “Treat and extend,” had not yet entered common clinical practice.

5. Conclusions

The differential diagnosis between neovascular age-related macular degeneration and CNV on pattern dystrophies is still challenging even for the most experienced retinologists. Our study highlights the clinical and morphological overlap of the two forms both in the onset and in the long-term, confirming the necessity of complete multimodal imaging in order not to incur erroneous diagnoses. Furthermore, we report a poor therapeutic response at 3 years of the forms associated with pattern dystrophies compared to those in AMD which, instead, show a tendency to stabilization. Finally, the higher choroidal thickness could open new perspectives in understanding the pathogenetic and evolutionary mechanisms underlying the development of neovascularizations in the eyes affected by pattern dystrophies.

The main limitation of our study is represented by low and poorly balanced numerosity of the two groups. This is due to our strict inclusion criteria, including age, complete multimodal imaging, PRN monotherapy administration, and no surgery in the follow-up period.

Further studies are needed to deepen these topics.

Data Availability

The data used to support the findings of this study are available from the corresponding author upon request.

Conflicts of Interest

The authors declare that they have no conflicts of interest.

References

- [1] J. D. Gass, *Stereoscopic Atlas of Macular Diseases: Diagnosis and Treatment*, C. V. Mosby, St Louis, USA, 4th edition, 1997.

- [2] P. J. Francis, D. W. Schultz, A. M. Gregory et al., "Genetic and phenotypic heterogeneity in pattern dystrophy," *British Journal of Ophthalmology*, vol. 89, no. 9, pp. 1115–1119, 2005.
- [3] P. K. Roberts, S. Zotter, A. Montuoro et al., "Identification and quantification of the angiofibrotic switch in neovascular AMD," *Investigative Ophthalmology & Visual Science*, vol. 60, no. 1, p. 304, 2019.
- [4] C. E. Hitzenger, J. D. Messinger, E. C. Zanzottera, K. B. Freund, and C. A. Curcio, "The onion sign in neovascular age-related macular degeneration represents cholesterol crystals," *Ophthalmology*, vol. 122, no. 11, pp. 2316–2326, 2015.
- [5] S. Fragiotta, P. Fernández-Avellaneda, M. P. Breazzano, L. A. Yannuzzi, C. A. Curcio, and K. B. Freund, "Linear and planar reflection artifacts on swept-source and spectral-domain optical coherence tomography due to hyperreflective crystalline deposits," *Graefes' Archive for Clinical and Experimental Ophthalmology*, vol. 258, no. 3, pp. 491–501, 2019.
- [6] R. M. Palacios, T. S. Mendes, R. Y. Sano, D. C. Wu, T. Aihara, and R. P. de Almeida Manzano, "Choroidal thickness using EDI-OCT in adult-onset vitelliform macular dystrophy," *International Journal of Retina and Vitreous*, vol. 2, no. 1, p. 5, 2016.
- [7] F. Coscas, N. Puche, G. Coscas et al., "Comparison of macular choroidal thickness in adult onset foveomacular vitelliform dystrophy and age-related macular degeneration," *Investigative Ophthalmology & Visual Science*, vol. 55, no. 1, pp. 64–69, 2014.
- [8] P. L. Grenga, S. Fragiotta, A. Cutini, A. Meduri, and E. M. Vingolo, "Enhanced depth imaging optical coherence tomography in adult-onset foveomacular vitelliform dystrophy," *European Journal of Ophthalmology*, vol. 26, no. 2, pp. 145–151, 2016.
- [9] H. Koizumi, T. Yamagishi, T. Yamazaki, R. Kawasaki, and S. Kinoshita, "Subfoveal choroidal thickness in typical age-related macular degeneration and polypoidal choroidal vasculopathy," *Graefes' Archive for Clinical and Experimental Ophthalmology*, vol. 249, no. 8, pp. 1123–1128, 2011.
- [10] S.-W. Kim, J. Oh, S.-S. Kwon, J. Yoo, and K. Huh, "Comparison of choroidal thickness among patients with healthy eyes, early age-related maculopathy, neovascular age-related macular degeneration, central serous chorioretinopathy, and polypoidal choroidal vasculopathy," *Retina*, vol. 31, no. 9, pp. 1904–1911, 2011.
- [11] Y. Imamura, T. Fujiwara, R. Margolis, and R. F. Spaide, "Enhanced depth imaging optical coherence tomography of the choroid in central serous chorioretinopathy," *Retina*, vol. 29, no. 10, pp. 1469–1473, 2009.
- [12] I. Maruko, T. Iida, Y. Sugano, A. Ojima, and T. Sekiryu, "Subfoveal choroidal thickness in fellow eyes of patients with central serous chorioretinopathy," *Retina*, vol. 31, no. 8, pp. 1603–1608, 2011.
- [13] G. Yiu, S. J. Chiu, P. A. Petrou et al., "Relationship of central choroidal thickness with age-related macular degeneration status," *American Journal of Ophthalmology*, vol. 159, no. 4, pp. 617–626, 2015.
- [14] H. Zhou, Y. Dai, Y. Shi et al., "Age-related changes in choroidal thickness and the volume of vessels and stroma using swept-source OCT and fully automated algorithms," *Ophthalmology Retina*, vol. 4, no. 2, pp. 204–215, 2020.
- [15] I. Tuncer, E. Karahan, M. O. Zengin, E. Atalay, and N. Polat, "Choroidal thickness in relation to sex, age, refractive error, and axial length in healthy Turkish subjects," *International Ophthalmology*, vol. 35, no. 3, pp. 403–410, 2015.
- [16] L. Tiosano, T. Jaouni, E. Averbukh, M. Grunin, E. Banin, and I. Chowers, "Bevacizumab treatment for choroidal neovascularization associated with adult-onset foveomacular vitelliform dystrophy," *European Journal of Ophthalmology*, vol. 24, no. 6, pp. 890–896, 2014.
- [17] G. Cennamo, I. Cesarano, E. C. Vecchio, M. Reibaldi, and G. de Crecchio, "Functional and anatomic changes in bilateral choroidal neovascularization associated with vitelliform macular dystrophy after intravitreal bevacizumab," *Journal of Ocular Pharmacology and Therapeutics*, vol. 28, no. 6, pp. 643–646, 2012.
- [18] G. Mimoun, V. Caillaux, G. Querques, P.-R. Rothschild, N. Puche, and E. H. Souied, "Ranibizumab for choroidal neovascularization associated with adult-onset foveomacular vitelliform dystrophy," *Retina*, vol. 33, no. 3, pp. 513–521, 2013.
- [19] G. Querques, L. Querques, N. Leveziel, F. Bandello, and E. H. Souied, "Intravitreal ranibizumab for type 3 choroidal neovascularization complicating adult onset foveomacular vitelliform dystrophy," *Journal Français d'Ophthalmologie*, vol. 36, no. 1, pp. e1–e4, 2013.
- [20] M. B. Parodi, P. Iacono, M. Cascavilla, I. Zucchiatti, D. S. Kontadakis, and F. Bandello, "Intravitreal bevacizumab for subfoveal choroidal neovascularization associated with pattern dystrophy," *Investigative Ophthalmology & Visual Science*, vol. 51, no. 9, pp. 4358–4361, 2010.
- [21] S. Fragiotta, P. Fernández-Avellaneda, M. P. Breazzano et al., "The fate and prognostic implications of hyperreflective crystalline deposits in nonneovascular age-related macular degeneration," *Investigative Ophthalmology & Visual Science*, vol. 60, no. 8, pp. 3100–3109, 2019.

Research Article

Optical Coherence Tomography Predictors of Favorable Functional Response in Naïve Diabetic Macular Edema Eyes Treated with Dexamethasone Implants as a First-Line Agent

Alessandro Meduri , Giovanni William Oliverio , Luigi Trombetta ,
Marta Giordano , Leandro Inferrera , and Costantino John Trombetta 

Department of Biomedical Sciences, Ophthalmology Clinic, University of Messina, Messina, Italy

Correspondence should be addressed to Giovanni William Oliverio; gioliverio@unime.it

Received 31 December 2020; Revised 17 January 2021; Accepted 17 March 2021; Published 24 March 2021

Academic Editor: Akio Oishi

Copyright © 2021 Alessandro Meduri et al. This is an open access article distributed under the Creative Commons Attribution License, which permits unrestricted use, distribution, and reproduction in any medium, provided the original work is properly cited.

Purpose. To evaluate efficacy and safety of intravitreal dexamethasone 0.7 mg implant in treatment-naïve DME patients and to assess the utility of OCT structural biomarkers as predictors of functional response after treatment. **Methods.** Thirty-nine eyes of 39 diabetic patients with center involving DME were enrolled. Best-corrected visual acuity (BCVA) and SS-OCT (DRI SS-OCT Triton, Topcon, Japan) to evaluate central retinal thickness (CRT), serous retinal detachment (SRD), intraretinal cysts (IRC), number of hyper-reflective spots (HRS), integrity of the ellipsoid zone (EZ), disorganization of the inner retinal layers (DRIL), vitreomacular adhesion (VMA), vitreomacular traction (VMT), and posterior vitreous detachment (PVD) were evaluated at baseline and at 3, 6, and 12 months after treatment. Multiple logistic analysis was performed to evaluate the possible OCT biomarker as predictive factors for final visual acuity improvement at the end of treatment. **Results.** At 12 months after treatment, the mean BCVA improved from 51.6 ± 17.5 to 56.9 ± 17.3 ETDRS letters ($p = 0.03$). Furthermore, there were statistically significant changes in CRT, IRC, HRS, and SRD. Nineteen patients presented a >10-letters improvement in BCVA; the presence of SRD at baseline was a predictor of good functional treatment response at 12 months (OR 2.1; 95% C.I. 1.2–4.9; $p = 0.001$) as well as the presence of EZ integrity preoperatively (OR 1.3; 95% C.I. 0.5–2.4; $p = 0.001$) and the absence of vitreoretinal interface alteration (OR 1.1; 95% C.I. 0.3–2.3; $p = 0.02$). No significant changes in the IOP and lens status were observed throughout the follow-up period. **Conclusion.** This study empathized the importance of structural biomarkers as predictors of favorable response and confirmed the efficacy and safety of intravitreal dexamethasone implant in treatment-naïve DME patients showing a better functional response in the presence of SRD integrity of EZ and absence of vitreoretinal alterations.

1. Introduction

Diabetic macular edema (DME) represents one of the major causes of visual impairment in diabetic patients due to the abnormal collection of intra- and/or subretinal fluid in the macular area caused by the alteration of the blood-retinal barrier [1]. DME is classified according to its etiology as vasogenic or nonvasogenic as recent studies highlighted the central role of inflammation in the pathogenic mechanisms [2–4].

The advances in optical coherence tomography (OCT) technology have contributed to improving our understanding

of the pathophysiology and classification of diabetic macular edema and have enabled us to recognize structural biomarkers for a morphologic categorization of the disease that can influence treatment outcome [2, 5–9].

DME presents with different patterns on OCT including sponge-like swelling cystoid macular edema and serous retinal detachment (SRD) [10]. Additionally, subfoveal thickness (CST), the presence of hyper-reflective spots (HRS), the presence of SRD the size of intraretinal cysts (IRC), the occurrence of disorganization of the inner retinal layers (DRIL), the state of the ellipsoid zone (EZ), the external limiting membrane (ELM), and choroidal thickness

(CT) have been used to categorize and grade DME [8]. Furthermore, the effectiveness of dexamethasone intravitreal implant 0.7 mg in the treatment of DME has been demonstrated in several studies; however, there is a lack in literature regarding the prognostic factors after treatment in particular in treatment-naïve DME patients [11, 12].

The aim of this study is to evaluate the efficacy and safety of intravitreal dexamethasone implant in treatment-naïve DME patients and to assess the utility of OCT structural biomarkers as predictors of functional response after treatment.

2. Methods

In this study, data from 39 eyes of 39 diabetic patients with DME were retrospectively analyzed. Patients aged >18 years and treatment-naïve DME with a central macular thickness (CMT) $\geq 300 \mu\text{m}$ who received an intravitreal implant of dexamethasone 0.7 mg (Ozurdex® Allergan, Inc. Irvine California USA) were enrolled.

Patients with a history of vitreoretinal surgery cataracts other macular diseases glaucoma and iris rubeosis were excluded.

Informed consent was obtained from all patients after the explanation of nature and the possible consequences of the study. This study was approved by the Institutional Review Board of the University of Messina, and it was conducted in accordance with the tenets of the Declaration of Helsinki.

Anamnestic data were reported for each patient including type and duration of diabetes and value of the recent glycated hemoglobin (HbA1c). A complete ophthalmologic assessment was carried out comprising best-corrected visual acuity (BCVA) using the Early Treatment Diabetic Retinopathy Study (ETDRS) chart microscopic evaluation of the anterior segment applanation tonometry and swept-source OCT (DRI SS-OCT Triton, Topcon, Japan).

These data were taken at each visit prior to the intravitreal dexamethasone implant and after 3, 6, and 12 months from the treatment.

2.1. Optical Coherence Tomography Analysis. SS-OCT images were obtained using a 9-mm radial OCT scan centered on the fovea. Automatic analysis using the OCT software IMAGEnet 6 (version 1.17.9720; Topcon Medical Systems Inc., Oakland, NJ, USA) was performed to evaluate the structural retinal biomarkers such as the presence of SRD, intraretinal cysts (IRC), continuity of the ellipsoid zone (DRIL), vitreomacular adhesion (VMA) or traction (VMT), and posterior vitreous detachment (PVD).

A count of the total HRS was performed and calculated in the area of 3 mm centered on the fovea (Figure 1).

The height of serous retinal detachment (SRD) was manually calculated using the built-in caliper tool of the instrument as the space between the outer retinal and the RPE surfaces at the fovea (Figure 1).

The height of IRC was measured summing all individual cyst heights within 3 mm of the fovea to give a total height value (Figure 1).

Choroidal thickness (CT) was manually analyzed on the foveal center and on temporal and nasal site tracing two vertical lines at 1.5 mm temporally from the fovea and 1.5 mm nasally from the fovea (Figure 1).

2.2. Statistical Analysis. The fitting of the data to a normal distribution was tested by the Kolmogorov–Smirnov test. In order to evaluate the existence of statistically significant differences in different times of observation, we applied the Wilcoxon test signed-rank test and Student's *t*-test for paired data as appropriate (for numerical variables) and the McNemar test (for dichotomous data). Logistic regression analysis was performed to evaluate the possible OCT biomarker (CRT, IRC, CT, SRD, HRS, EZ, and vitreomacular alterations) as predictive factors for final visual acuity improvement at the end of treatment.

A *p* value smaller than 0.05 was considered to be statistically significant. Statistical analyses were performed using the SPSS 26.0 for the macOS package.

3. Results

3.1. Study Population. Thirty-nine patients (19 males 20 females) with DME were enrolled in this study. The mean age of patients was 66.7 ± 7.3 years, the mean duration of diabetes was 13.5 ± 7.3 years, and the mean recent HbA1c was $7.9 \pm 3.2\%$ (Table 1). Twenty-one patients (53.8%) presented a cystoid macular edema, and 18 patients (46.2%) presented a subfoveal neuroretinal detachment.

3.2. Functional and Morphological Outcome. Baseline and posttreatment data are reported in Table 2. At 3 months, the mean BCVA improved from 51.6 ± 17.1 to 58.9 ± 16.5 ETDRS letters ($p = 0.01$) and to 57.6 ± 17.3 and to 56.9 ± 17.5 at 6 and 12 months, respectively ($p = 0.03$). Furthermore, there were statistically significant changes in CRT, IRC dimension, HRS number, and SRD height after treatment throughout the follow-up (Table 2). No significant changes in CT were observed after treatment. At the end of follow-up, 15 patients presented a complete resolution of the SRD.

Nineteen patients (48.7%) presented a >10-letters improvement in BCVA at the end of follow-up.

At 6 months, a second dexamethasone implant was necessary in 5 patients (12.8%).

No significant increments of the mean IOP were observed. Overall, the follow-up period and no changes in the lens status were recognized after treatment.

3.3. Optical Coherence Tomography Predictors for Treatment Response. The presence of SRD at baseline was a predictor of good functional treatment response at 12 months (OR 2.1; 95% C. I. 1.2–4.9; $p < 0.001$). Additionally, the presence of EZ integrity preoperatively was a predictor of good functional treatment response at 12 months (OR 1.3; 95% C. I. 0.5–2.4; $p = 0.001$). Eyes without vitreoretinal interface alteration at baseline presented a better functional outcome at

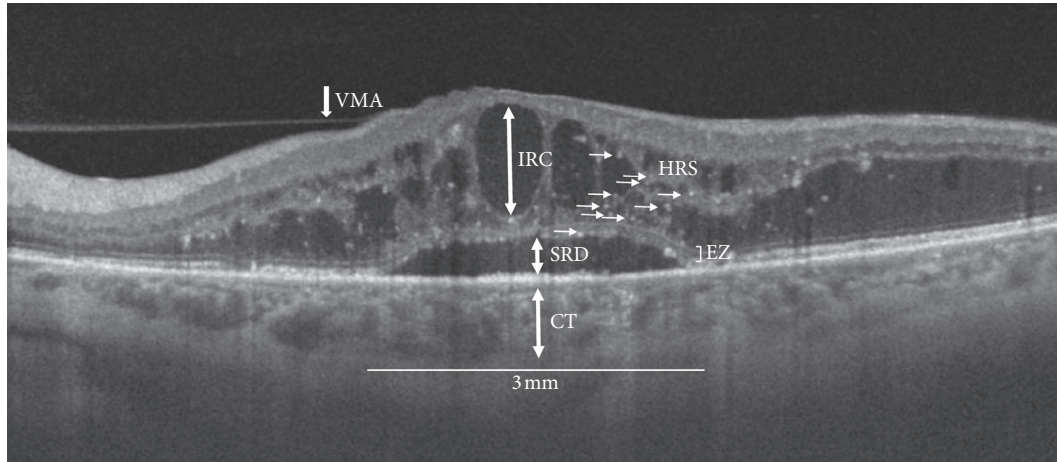


FIGURE 1: Swept-source optical coherence tomography radial scan (9 mm) of a patient with diabetic macular edema and subfoveal neuroretinal detachment showing structural biomarkers evaluated within a 3 mm area centered on the fovea: CT: choroidal thickness; SRD: serous retinal detachment; EZ: ellipsoid zone integrity; IRC: intraretinal cysts; HRS: hyper-reflective spots; VMA: vitreomacula adhesion.

TABLE 1: Clinical characteristics of the study population.

Variables	
Age (years)	65.2 ± 11.3
Gender (male/female)	19/20
Duration of diabetes (years)	13.5 ± 7.3
HbA1c (%)	7.9 ± 3.2
Lens status	
Phakic (n)	12
Pseudophakic (n)	27

HbA1c: glycated hemoglobin.

12 months after treatment (OR 1.1; 95% C. I. 0.3–2.3; $p = 0.02$). There was no significant correlation between DRIL presence number of HRS IRC dimension CT and a >10-letters improvement in BCVA.

4. Discussion

Recent studies have demonstrated the primary role of inflammatory and vascular factors in the pathogenesis and development of DME; however, these mechanisms are complex and still not completely clarified [2–4]. The neurovascular unit consists of Müller cells, astrocytes, ganglion cells, and amacrine cells in a dynamic interaction with retinal vascular endothelial cells and pericyte-releasing factors that induce the formation of tight junctions in retinal vessels [13–15]. Abnormalities in Müller cells probably affect this barrier property in the retinal vessels in diabetic patients [13, 14]. Indeed, blood-retinal barrier disruption is associated with an increase of vascular endothelial growth factor (VEGF), intercellular adhesion molecule-1 (ICAM-1), interleukin-6 (IL-6), and monocyte chemoattractant protein-1 (MCP-1) among others [14, 16]. Furthermore, in the recent years, numerous advances have been made in the treatment of diabetic retinopathy and DME [14–17]. Anti-VEGF is considered first-line treatment; however, corticosteroids represent a fundamental alternative for treating these patients [10, 18]. The efficacy of corticosteroids in DME may be

attributable to the strong anti-inflammatory and antiedema properties of these molecules as previous studies demonstrated the reduced expression of VEGF and other inflammatory mediator-diminished leukostasis and vascular leakage finally improving the barrier function of endothelial cell tight junction [19]. Corticosteroids are mainly used as a second choice due to the possible adverse events occurrence such as increase of IOP and cataract progression [10, 18]. Additionally, corticosteroids are useful for the treatment of refractory forms of DME to anti-VEGF [10, 18].

Nevertheless, the intravitreal implant of dexamethasone could represent a first-line therapy in particular conditions such as patients with a recent history of major cardiovascular events and contraindications to anti-VEGF therapy patients with vitrectomized eye, pregnancy, pseudophakic patients, and uncompliant patients, unable or unwilling to return for regular examinations [10, 18].

Although numerous studies confirmed the efficacy and safety of intravitreal implant of dexamethasone, there is a lack in literature about the outcome and the predictive factors in treatment-naïve patients with DME [18]. The introduction of OCT improved the structural evaluation of the retinal layers introducing several morphological biomarkers that could help to assess and predict the functional outcome and to choose the best treatment for the patient [5, 10].

Several studies demonstrated that macular thickness may serve as a measurement variable in relationship with treatment outcome in DME [5, 10]. Furthermore, recent studies have demonstrated that the presence of SRD and HRS are correlated with high inflammatory component [5–7].

Vujosevic et al. showed that DME patients with SRD and a high number of HRS presented a better response to intravitreal dexamethasone rather than anti-VEGF [6].

In this study, we have evaluated the long-term result of intravitreal implant of dexamethasone in a group of treatment-naïve DME patients. According to previous studies, we have demonstrated the effectiveness of this treatment as a

TABLE 2: Functional and morphological biomarkers before and after treatment.

Variables	Baseline	3 months	<i>p</i> value		<i>p</i> value		<i>p</i> value	
			Baseline vs. 3 Mo	6 months	Baseline vs. 6 Mo	12 months	Baseline vs. 12 Mo	
BCVA ETDRS letters	51.6 ± 17.1	58.9 ± 16.5	0.01	57.6 ± 17.3	0.03	56.9 ± 17.5	0.03	
CMT (μm)	434.4 ± 155.6	284.7 ± 108.7	<0.001	284.7 ± 108.7	0.001	336.8 ± 151.1	0.001	
SRD presence, <i>n</i> (%)	18 (46.2)	2 (5.1)	<0.001	3 (7.7)	<0.001	3 (7.7)	<0.001	
Height (μm)	32.6 ± 52.7	6.5 ± 22.8	<0.001	13.5 ± 32.1	0.001	14.1 ± 28.1	0.001	
HRS (<i>n</i>)	25.5 ± 13.8	16.2 ± 15.2	0.02	18.7 ± 12.6	0.03	25.7 ± 12.6	0.03	
Cysts size (μm)	2216.1 ± 1230.9	631.1 ± 763.1	0.001	1384.4 ± 952.9	0.001	1384.4 ± 952.9	0.01	
CT								
Subfoveal (μm)	178.6 ± 65.9	178.6 ± 65.9	0.32	178.6 ± 65.9	0.41	178.6 ± 65.9	0.19	
Nasal (μm)	155.8 ± 31.8	155.8 ± 31.8	0.44	155.8 ± 31.8	0.15	155.8 ± 31.8	0.28	
Temporal (μm)	163.4 ± 39.7	163.4 ± 39.7	0.32	163.4 ± 39.7	0.31	163.4 ± 39.7	0.33	
DRIL presence, <i>n</i> (%)	8 (20.5)	7 (17.9)	0.77	7 (17.9)	0.77	7 (17.9)	0.77	
EZ integrity, <i>n</i> (%)	23 (58.9)	22 (56.4)	0.82	22 (56.4)	0.82	22 (56.4)	0.82	
Vitreomacular interface								
	7 (17.9)	7 (17.9)	—	8 (20.5)	0.77	8 (20.5)	0.77	
PVD, <i>n</i> (%)	11 (28.2)	11 (28.2)	—	11 (28.2)	—	11 (28.2)	—	
VMA, <i>n</i> (%)	4 (10.3)	3 (7.7)	0.69	3 (7.7)	.69	3 (7.7)	.69	
VMT, <i>n</i> (%)								

BCVA: best-corrected visual acuity; ETDRS: Early Treatment Diabetic Retinopathy study; CMT: central macular thickness; SRD: serous retinal detachment; HRS: hyper-reflective spots; CT: choroidal thickness; DRIL: disorganization of the inner retinal layers; EZ: ellipsoid zone; PVD: posterior vitreous detachment; VMA: vitreomacular adhesion; VMT: vitreomacular traction. Values in bold indicate *p* value < .05.

first-line showing a long-term morphological and functional improvement in DME patients. Zur et al. identified the presence of SRD, EZ continuity, absent HRS, and an attached vitreoretinal interface as biomarkers that predict a better visual acuity improvement after dexamethasone implants in eyes with DME [5].

In our study, at 6 and 12 months, the BCVA and the CMT improved significantly after treatment. Additionally, in the subgroup analysis, patients with preoperative SRD presented a better functional improvement at 6 and 12 months, and the presence of the EZ integrity was associated with a better visual outcome at the end of the follow-up.

However, there was no correlation between DRIL presence, number of HRS, IRC, CT, and visual acuity improvement at 6 and 12 months. Rosenblatt et al. in a multicentric study reported an improvement of >10-letters in BCVA in 46.1% in a treatment-naïve group; this result was in accordance with our findings [12].

The main limitations of this study are the small sample size and the retrospective design.

In conclusion, this study confirmed the efficacy and safety of intravitreal dexamethasone implant in the treatment of naïve DME patients and demonstrated a better functional response in patients with the presence of SRD and EZ integrity and absence of vitreomacular alterations; however, further studies are necessary to assess the usefulness of OCT structural biomarker as predictors of functional response in DME patients. Additionally, our findings emphasized the importance of an accurate evaluation of structural biomarkers to choose the best treatment for the patient.

Data Availability

The data used to support the findings of this study are available from the corresponding author upon request.

Conflicts of Interest

The authors declare that there are no conflicts of interest regarding the publication of this article.

References

- [1] J. W. Y. Yau, S. L. Rogers, R. Kawasaki et al., "Global prevalence and major risk factors of diabetic retinopathy," *Diabetes Care*, vol. 35, no. 3, pp. 556–564, 2012.
- [2] D. J. Browning, A. R. Glassman, L. P. Aiello et al., "Optical coherence tomography measurements and analysis methods in optical coherence tomography studies of diabetic macular edema," *Ophthalmology*, vol. 115, no. 8, pp. 1366–1371, 2008.
- [3] P. Romero-Aroca, M. Baget-Bernaldiz, A. Pareja-Rios, M. Lopez-Galvez, R. Navarro-Gil, and R. Verges, "Diabetic macular edema pathophysiology: vasogenic versus inflammatory," *Journal of Diabetes Research*, vol. 2016, Article ID 2156273, 17 pages, 2016.
- [4] Y. R. Chung, Y. H. Kim, S. J. Ha et al., "Role of inflammation in classification of diabetic macular edema by optical coherence tomography," *Journal of Diabetes Research*, vol. 2019, Article ID 8164250, 8 pages, 2019.
- [5] D. Zur, M. Iglicki, C. Busch et al., "OCT biomarkers as functional outcome predictors in diabetic macular edema treated with dexamethasone implant," *Ophthalmology*, vol. 125, no. 2, pp. 267–275, 2018.
- [6] S. Vujosevic, C. Toma, E. Villani et al., "Diabetic macular edema with neuroretinal detachment: OCT and OCT-angiography

- biomarkers of treatment response to anti-VEGF and steroids,” *Acta Diabetologica*, vol. 57, no. 3, pp. 287–296, 2020.
- [7] I. Ceravolo, G. W. Oliverio, A. Alibrandi et al., “The application of structural retinal biomarkers to evaluate the effect of intravitreal ranibizumab and dexamethasone intravitreal implant on treatment of diabetic macular edema,” *Diagnostics*, vol. 10, no. 6, p. 413, 2020.
- [8] G. Panozzo, M. V. Cicinelli, A. J. Augustin et al., “An optical coherence tomography-based grading of diabetic maculopathy proposed by an international expert panel: the European School for Advanced Studies in Ophthalmology classification,” *European Journal of Ophthalmology*, vol. 30, no. 1, pp. 8–18, 2020.
- [9] G. W. Oliverio, I. Ceravolo, A. Bhatti, and C. J. Trombetta, “Foveal avascular zone analysis by optical coherence tomography angiography in patients with type 1 and 2 diabetes and without clinical signs of diabetic retinopathy,” *International Ophthalmology*, vol. 41, no. 2, p. 649, 2020 Nov 6.
- [10] U. Schmidt-Erfurth, J. Garcia-Arumi, F. Bandello et al., “Guidelines for the management of diabetic macular edema by the European society of retina specialists (EURETINA),” *Ophthalmologica*, vol. 237, no. 4, pp. 185–222, 2017.
- [11] H. Kaldırım, S. Yazgan, K. Atalay, C. Gurez, and F. Savur, “Intravitreal dexamethasone implantation in patients with different morphological diabetic macular edema having insufficient response to ranibizumab,” *Retina*, vol. 38, no. 5, pp. 986–992, 2018.
- [12] A. Rosenblatt, P. Udaondo, J. Cunha-Vaz et al., “A collaborative retrospective study on the efficacy and safety of intravitreal dexamethasone implant (ozurdex) in patients with diabetic macular edema,” *Ophthalmology*, vol. 127, no. 3, pp. 377–393, 2020.
- [13] Y. Usui, “Elucidation of pathophysiology and novel treatment for diabetic macular edema derived from the concept of neurovascular unit,” *JMA Journal*, vol. 3, no. 3, pp. 201–207, 2020.
- [14] J. Grauslund and S. L. Blindbaek, “Diabetic macular oedema: what to fear? How to treat?” *Acta Ophthalmologica*, vol. 95, no. 2, pp. 117–118, 2017.
- [15] B. Galletti, F. Freni, A. Meduri et al., “Rhino-orbito-cerebral mucormycosis in diabetic disease mucormycosis in diabetic disease,” *Journal of Craniofacial Surgery*, vol. 31, no. 4, pp. e321–e324, 2020.
- [16] N. Dong, B. Xu, L. Chu, and X. Tang, “Study of 27 aqueous humor cytokines in type 2 diabetic patients with or without macular edema,” *PLoS One*, vol. 10, Article ID e012532, 2015.
- [17] S. Z. Scalinci, S. Z. Scalinci, L. Scorolli et al., “Potential role of intravitreal human placental stem cell implants in inhibiting progression of diabetic retinopathy in type 2 diabetes: neuroprotective growth factors in the vitreous,” *Clinical Ophthalmology*, vol. 5, pp. 691–696, 2011.
- [18] A. García Layana, A. Adán, F. J. Ascaso et al., “Use of intravitreal dexamethasone implants in the treatment of diabetic macular edema: expert recommendations using a Delphi approach,” *European Journal of Ophthalmology*, vol. 30, no. 5, pp. 1042–1052, 2020.
- [19] M. Figueras-Roca, A. Sala-Puigdollers, S. Alforja et al., “Aqueous humour cytokine changes with intravitreal dexamethasone implant injection for diabetic macular edema,” *Ocular Immunology and Inflammation*, vol. 27, no. 8, pp. 1203–1210, 2019.

Research Article

Retinal Structural and Microvascular Alterations in Different Acute Ischemic Stroke Subtypes

Ying Zhang,¹ Ce Shi,¹ Yihong Chen,¹ Weicheng Wang,¹ Shenghai Huang,¹ Zhao Han,² Xianda Lin,² Fan Lu ¹ and Meixiao Shen ¹

¹School of Ophthalmology and Optometry, Wenzhou Medical College, Wenzhou, Zhejiang, China

²The Second Affiliated Hospital & Yuying Children's Hospital of Wenzhou Medical University, 109 Xueyuan Road, Wenzhou, Zhejiang, China

Correspondence should be addressed to Fan Lu; lufan@mail.eye.ac.cn and Meixiao Shen; smx77@sohu.com

Received 9 September 2020; Revised 6 November 2020; Accepted 16 November 2020; Published 9 December 2020

Academic Editor: Gianluca Scuderi

Copyright © 2020 Ying Zhang et al. This is an open access article distributed under the Creative Commons Attribution License, which permits unrestricted use, distribution, and reproduction in any medium, provided the original work is properly cited.

Introduction. Retinal structural and microvascular damages reflect damage to cerebral microvasculature and neurons. We aimed to investigate neovascular unit abnormalities among patients with large-artery atherosclerosis (LAA) or small-vessel occlusion (SAA) and control subjects. **Methods.** Twenty-eight LAA patients, forty-one SAA patients, and sixty-five age- and gender-matched controls were recruited. Based on optical coherence tomography angiography (OCTA), retinal capillary vessel density was assessed in the general and local sectors, and the thickness of individual retinal layer was extracted from retinal structural images. The differences between structural and microvascular were analyzed. **Results.** The superior peripapillary retinal nerve fiber layer (pRNFL) thickness was significantly different among the three groups, and the LAA group had the thinnest thickness. Compared to the control group, the deep retinal capillary vessel density in other two stroke subgroups were significantly reduced in all regions except in the inferior region ($P < 0.05$), and the fractal dimension in C2 and C4 regions of deep retina was significantly lower in the LAA group ($P < 0.05$). **Discussion.** Compared with superficial microvascular network, deep microvascular network is more sensitive to ischemic stroke. In addition, we have demonstrated quadrant-specific pRNFL abnormalities in LAA and SAA patients. Superior quadrant pRNFL thickness differences between stroke subgroups may suggest that changes in retinal nerve fiber layer are more sensitive to subtype identification than changes in retinal microvascular structure. All in all, the alteration in retinal structural and microvascular may further elucidate the role of the neovascular unit in ischemic stroke, suggesting that the combination of these two indicators could be used for subtype identification to guide prognosis and establish a risk prediction model.

1. Introduction

Stroke is the most common cause of serious disability in adults, and China bears the biggest burden globally [1]. As therapeutic options are limited, effective preventive strategies for early diagnosis are needed. The underlying sub-clinical pathologic process occurs much earlier before the onset of clinical stroke while current neuroimaging technologies may not be capable of directly observing subtle subclinical changes in stroke due to the resolution. Besides, current predictions of stroke are difficult to quantify. Therefore, there is an urgent need for additional surrogate

techniques to detect the subtle changes in vivo. In addition to the importance of finding indicators to establish a model for stroke risk prediction and prognosis assessment, the identification of subtypes of ischemic stroke is vital for guiding clinical treatment and management. However, the current international classification Treatment of Acute Stroke Trial (TOAST) [2] requires a lot of auxiliary examinations which are expensive and time-consuming. The above shortcomings and possible examination contraindications make it challenging for patients to complete the examination in time when they are admitted to the hospital, affecting the early guiding role in clinical treatment. Therefore, finding an

early, especially sensitive and effective, method is of great importance in disease prediction, treatment, and prognosis assessment. Because the retinal and cerebral vessels share similar anatomic, embryological, and physiological characteristics, the retina provides a unique “window” to assess the cerebral microvascular and neurons in vivo noninvasively.

Previous studies based on fundus photography have revealed an independent correlation between retinal vascular parameters and stroke [3–6]. Additionally, several studies also detected vascular changes vary according to stroke subtypes, suggesting the specific cerebral microvasculopathy of subtyping of stroke [7, 8]. Inconsistently, another study showed that vascular changes were similar between stroke subtypes [9]. The reason for the discordant results may be that the fundus photography is only a plane picture, which only reflects the large blood vessels of the retina without microvascular and quantitative retinal structural parameters. With the advancement of the technique, the optical coherence tomography angiography (OCTA) can reflect finer retinal capillary plexuses and choriocapillaris changes by generating three-dimensional images based on the comparisons of the motion of circulating blood cells. Consequently, we can observe retinal microvascular changes of stroke patients.

The concept of the neurovascular unit (NVU) was proposed in 2003 [10], which is composed of endothelial cells, neurons, astrocytes, and pericytes. The NVU provides new insights for the pathogenesis and diagnostic and treatment strategies of stroke [11, 12]. Spectral-domain optical coherence tomography (SD-OCT) with high-resolution retinal imaging can provide cross-sectional images of biologic structures and quantify the thickness of each retinal layer. One previous study observed that the transneuronal retrograde degeneration (TRD) of retinal ganglion cells (RGCs) assessed by SD-OCT is associated with cerebral infarction [13]. Most of the studies containing previous stroke patients with an increased risk of confounding factors concentrated on the association between large retinal vessels or neural structures changes and stroke separately [3, 13]. So far, there have been no in vivo studies on simultaneous microvascular and neural structures in stroke subjects.

In this study, we aimed to find the retinal microvascular and microstructural changes in the subtypes of initial acute stroke patients.

2. Methods

2.1. Study Population. In this study, a total of 85 patients with initial ischemic stroke within 14 days of an acute period were prospectively recruited from the neurology unit at the Second Affiliated Hospital & Yuying Children’s Hospital of Wenzhou Medical University from Jan 2017 to December 2018. One neurologist (Zhao Han) assessed the stroke severity with the National Institutes of Health Stroke Scale (NIHSS) [14] and classified large-artery atherosclerosis (LAA) and small-artery occlusion lacunar (SAA) according to a modified TOAST classification [2]. Besides, 65 age- and gender-matched controls with no self-reported history of

stroke or transient ischemic attack or ophthalmic disease were enrolled consecutively from the relatives of patients or working staff at the Eye Hospital or the Second Affiliated Hospital & Yuying Children’s Hospital of Wenzhou Medical University between Jan 2017 to Aug 2019. Considering the effect of stroke site, parameters of ipsilateral eyes were selected for analysis. Additionally, random eyes were selected in nonunilateral stroke and control subjects. Written informed consent was obtained from patients or their next of kin, and the project was approved by the ethics committee of the Eye Hospital of Wenzhou Medical of Wenzhou Medical University.

2.2. Assessment of Cardiovascular Risk Factors. Patients finished detailed questionnaires for information on history of hypertension, diabetes mellitus, hypercholesterolemia, ischemic heart disease, cigarette smoking status, and medication use. All patients underwent usual examinations of stroke, including brain imaging, fasting blood samples for glycosylated hemoglobinA1C (HbA1C), total cholesterol (TC), total triglycerides (TG), homocysteine (HCY), creatinine (Cr), high-density lipoprotein (HDL-C), low-density lipoprotein (LDL-C), and body mass index (BMI). Besides, as a part of clinical care for stroke, blood pressure was measured three times after participants had been seated for at least 10 minutes at the same sitting. The mean blood pressure of three times was taken as the final result. The mean arterial pressure (MAP) is equal to one-third of systolic blood pressure (SBP) plus two-thirds of diastolic blood pressure (DBP).

Hypertension was diagnosed as SBP ≥ 140 mm Hg or DBP ≥ 90 mm Hg at examination or a self-reported history of physician-diagnosed hypertension or the use of antihypertensive medication. Diabetes mellitus was defined as fasting blood glucose ≥ 7.0 mmol/L and/or random blood glucose ≥ 11.1 mmol/L, hemoglobin A1C $\geq 7\%$, self-reported history of physician-diagnosed diabetes mellitus, or the use of antihyperglycemic medication. Hypercholesterolemia was defined as fasting total cholesterol ≥ 5.2 mmol/L, self-reported history of physician-diagnosed hypercholesterolemia, or the use of antilipemic medication. Current smokers were defined as people who smoke currently or quit smoking less than one year before the examination.

2.3. Assessment of Ophthalmic Parameters and Microstructure of the Retina. All the subjects had detailed ophthalmologic examinations performed by two ophthalmologists (Ying Zhang and Ce Shi), including slit-lamp biomicroscopy, refraction diopter, best-corrected visual acuity (BCVA), and noncontact intraocular pressure (IOP). All patients were imaged by an OCT system (Optovue RTVue-XR Avanti; Optovue, Inc., Fremont, CA, USA) to obtain the OCTA images, with detailed steps described as follows: refraction data were converted to spherical equivalents (SEs) and calculated as the spherical dioptric power plus one-half of the cylindrical dioptric power. The exclusion criteria were presented as follows: patients with contraindications to magnetic resonance, hemorrhagic stroke, recurrent stroke,

those who were unable to complete the eye examinations, and those with spherical equivalent (SE) under $\pm 5.00 D$, IOP >21 mm Hg or previous ophthalmologic diseases (such as cataract, glaucoma, high myopia, and retinal diseases). Other exclusion criteria were systemic diseases that could affect the ocular structures, such as uncontrolled hypertension/diabetes and neurological diseases such as Parkinson's disease and multiple sclerosis.

2.4. MRI Analysis. All patients underwent the 3.0-T MRI (Signa HDxt GE Healthcare), which included T1-weighted and T2-weighted imaging, diffusion weighted imaging (DWI), and fluid attenuated inversion recovery (FLAIR). The slice thickness was 5 mm with an interslice gap of 1 mm. The high signal on DWI sequence of MRI indicates the presence of acute cerebral infarction. In addition, the size and the location of the lesion are conducive to the classification of stroke. In the control group, MRI was also used for the reason of homogeneous management. For ethical reasons, not all controls were willing to undergo the tests for fasting blood tests and magnetic resonance imaging. Therefore, the two indicators are not shown in the Table 1.

2.5. OCT and OCTA Acquisitions. All subjects remained seated under the same conditions, and examinations were performed by an expert examiner. The OCTA system, which employs the split-spectrum amplitude-decorrelation angiography (SSADA) algorithm, operated at a rate of 70000 A-scans per second, with the scan area of $3 \times 3 \text{ mm}^2$, and the results were obtained by orthogonal registration and merging of two consecutive B-scans. The size of the exported OCT images was 304×304 pixels. OCTA combines orthogonal fast-scan directions to correct motion artifacts based on the DualTrac Motion Correction technology [15]. A good set of scans with a signal strength index (SSI) over 40 was selected for further analysis.

2.5.1. Retinal Layer Thickness Analysis on Spectral-Domain Optical Coherence Tomography. Retinal thickness was imaged by the RTVue XR Avanti SD-OCT system (Optovue, Inc, Fremont, California, USA). Besides, the average, superior (S), temporal (T), inferior (I), and nasal (N) quadrants of peripapillary retinal nerve fiber layer (pRNFL) thickness were obtained. The ganglion cell complex (GCC) provides inner retinal thickness values from the internal limiting membrane (ILM) to the inner molecular layer (IPL), shown as average, superior, and inferior regions (Figure 1(f)).

2.5.2. Capillary Vessel Density and Fractal Dimension Analysis on Optical Coherence Tomography Angiography. Retinal microvasculature was evaluated by the RTVue XR with AngioVue (software version 2017.1.0.155; Optovue, Inc, Fremont, CA, USA). Patients underwent different types of scanning: $3 \times 3 \text{ mm}^2$ angioretina around the fovea, $4.5 \times 4.5 \text{ mm}^2$ angioretina scans around the optic nerve head

(ONH), 3D retina scans, retinal map scans, and radial lines scans.

Vessel density (VD) is defined as the percentage of area occupied by OCTA detected vasculature. The software sets the superficial capillary plexuses (SCP) from $3 \mu\text{m}$ below the ILM to $15 \mu\text{m}$ below the IPL. The deep capillary plexuses (DCP) were set from 15 to $70 \mu\text{m}$ below the IPL (Figures 1(b) and 1(c)). In addition, the parafovea vessel density, defined as the area of annular circle with a diameter of 3 mm excluding the fovea zone (diameter = 1 mm), was divided automatically into whole and superior (S), temporal (T), inferior (I), and nasal (N) quadrants. Similarly, the 5 sectors of radial peripapillary capillary (RPC) vessel density were analyzed. The boundary of RPC ranges from ILM to the nerve fiber layer.

To quantify the complexity of the branching pattern and density of the retinal capillary network in OCTA images, the automated fractal analysis system was employed to correct the image magnification based on the axial length [16, 17]. Briefly, the OCTA images in PNG format were imported to the custom automated algorithm software published previously [18]. Then, the grayscale of the two-dimensional OCTA images was first extended by bicubic interpolation to 1024×1024 pixels so as to improve the image details. The binary images of vessels were created by the algorithm. Subsequently, one binary image containing only large arteries and the other binary image containing both large and small vessels were subtracted to obtain the final binary image. Based on the final image of white-pixelated vasculature, a skeletonized image was created by detecting the central axis of each capillary. After the image processing, both the superficial and deep retinal capillary complexities were calculated based on the skeletonized images [19, 20]. The quantitative measured parameter of complexity, D_{box} values, was obtained with the fractal analysis software (Benoit, Trusoft Benoit Fractal Analysis Toolbox; Trusoft International, Inc., St. Petersburg, FL). Both the general and local fractal dimensions were used to describe the complexity of capillary network. At first, after excluding the fovea avascular zone (FAZ) within the diameter of 0.6 mm, the fractal dimension (FD) was automatically calculated for the total annular zone (TAZ) within the 2.5 diameter and for the 4 parafoveal quadrant sectors (superior (S), temporal (T), inferior (I), and nasal (N)) and 6 concentric isometric annular rings (Figures 1(d) and 1(e)). The methods above were implemented using MATLAB v 7.10 (Mathworks, Inc., Natick, Massachusetts, USA).

2.6. Statistical Analysis. All statistical analyses were conducted using SPSS software (version 24.0; SPSS, Inc., Chicago, IL, USA). The data were expressed as the mean \pm standard deviation (SD). One-way analysis of variance (ANOVA) was used to test the differences among patients with large-artery stroke and lacunar stroke and control subjects, and Bonferroni correction was used for pairwise comparisons. The differences in gender and medical history were determined by the χ^2 test.

TABLE 1: Demographic characteristics of study subjects.

	LAA	SAA	Control	P*	P1	P2	P3
Eyes,	28	41	65	—	—	—	—
Age, y, mean ± SD	60.07 ± 10.10	58.83 ± 7.72	59.00 ± 7.20	0.797	0.529	0.557	0.915
Sex, female(%)	8 (28.6)	11 (26.8)	27 (41.5)	0.231	0.874	0.236	0.124
BMI	24.90 ± 2.97	24.53 ± 2.87	25.08 ± 2.38	0.596	0.580	0.776	0.310
SE, diopter	0.43 ± 1.33	0.38 ± 1.18	0.24 ± 1.06	0.741	0.860	0.497	0.567
BCVA, LogMAR	0.02 ± 0.12	0.01 ± 0.10	-0.03 ± 0.08	0.024	0.619	0.018	0.037
AL, mm	23.30 ± 0.95	23.37 ± 0.89	23.14 ± 0.91	0.550	0.777	0.528	0.294
IOP, mm Hg	12.05 ± 2.56	12.68 ± 3.19	12.15 ± 2.53	0.559	0.363	0.877	0.341
SBP, mm Hg	151.61 ± 21.85	155.22 ± 17.15	134.37 ± 14.79	<0.001	0.393	<0.001	<0.001
DBP, mm Hg	87.64 ± 13.28	90.61 ± 12.92	85.80 ± 11.89	0.160	0.335	0.516	0.056
MAP, mm Hg	108.96 ± 14.05	112.15 ± 12.53	101.99 ± 11.50	<0.001	0.296	0.014	<0.001
Hypertension, n(%)	21 (75.0)	35 (85.4)	23 (35.4)	<0.001	0.280	<0.001	<0.001
Hyperlipidemia, n(%)	9 (32.1)	5 (12.2)	17 (26.2)	0.112	0.043	0.555	0.084
Current smoker, n(%)	16 (57.1)	21 (51.2)	24 (36.9)	0.135	0.628	0.071	0.147
Diabetes, n(%)	7 (25.0)	5 (12.2)	3 (4.6)	0.016	0.205	0.007	0.256
Previous ischemic heart disease, n(%)	2 (7.1)	3 (7.3)	2 (3.1)	0.527	>0.999	0.581	0.373
HbA1c, (%)	5.95 (5.53–6.28)	5.80 (5.55–6.20)	—	0.433	—	—	—
TG, mmol/L	1.99 (1.30–2.97)	1.58 (1.18–1.87)	—	0.051	—	—	—
TC, mmol/L	4.81 ± 0.96	4.48 ± 0.76	—	0.117	—	—	—
HDL-C, mmol/L	2.78 (0.80–1.13)	0.95 (0.81–1.13)	—	0.898	—	—	—
LDL-C, mmol/L	2.73 ± 0.68	2.57 ± 0.76	—	0.353	—	—	—
HCY, μmol/L	10.60 (8.75–15.20)	10.20 (8.98–13.90)	—	0.684	—	—	—
Cr, μmol/L	65.65 (57.90–77.83)	68.50 (58.50–81.73)	—	0.501	—	—	—
NIHSS score, mean ± SD (range)	2 (1–3)	1 (1–2)	—	0.097	—	—	—

LAA, large-artery atherosclerosis; SAA, small-vessel occlusion; BMI, body mass index; SE, spherical equivalent; BCVA, best-corrected visual acuity; AL, axial length; IOP, noncontact intraocular pressure; SBP, systolic blood pressure; DBP, diastolic blood pressure; MAP, mean arterial pressure; HbA1c, hemoglobin; TG, total triglycerides; TC, total cholesterol; HDL-C, high-density lipoprotein; LDL-C, low-density lipoprotein; HCY, homocysteine; Cr, creatinine; NIHSS, NIH Stroke Scale; M, male; F, female; * P value among the three groups; $P1$ and P values between LAA and SAA; $P2$ and P values between LAA and control; and $P2$ value between SAA and control.

3. Results

A total of 85 patients were included in the present study. Among them, 16 patients were excluded due to poor image quality of OCTA scans. The remaining 28 patients with LAA, 41 patients with SAA, and 65 age- and gender-matched control subjects were further analyzed. The demographic and clinical characteristics are summarized in Table 1. Normally, distributed data are represented by mean plus or minus standard deviation, while nonnormally distributed data are represented by median and interquartile spacing. Differences in age, sex, BMI, SE, IOP, and DBP, together with the prevalence of hyperlipidemia, currently smoking, and previous ischemic heart disease were not significant among the three groups. Patients with SAA were more likely to have hypertension than the other two groups ($P < 0.001$). Besides, the values of SBP and MAP were significantly higher than those of the other two groups ($P < 0.001$). LAA patients were more likely to undergo diabetes ($P = 0.007$) than the controls. However, there was no statistical difference in demographic data between the two stroke subgroups. Not all subjects completed all tests. The number of eyes that completed each examination is shown in Table 2.

3.1. Intergroup Differences among the Three Groups

3.1.1. Retinal Microstructural Thicknesses. In terms of the quadrants, the superior pRNFL thickness was significantly thinner in the eyes of patients than that in the eyes of the

control group ($P = 0.01$, Table 3, Figure 2(a)). In the eyes of LAA, the pRNFL thickness was significantly thinner in the superior quadrant compared to the eyes of SAA ($P = 0.034$) and control ($P = 0.003$). No significant superior pRNFL thinning was observed in SAA compared to control ($P = 0.438$). Additionally, the thicknesses of GCC were not significantly different among the three groups (all $P > 0.05$, Table 3, Figure 2(b)).

3.1.2. Vessel Density around ONH and Macula. The vessel density around the macula in the deep retinal capillary layer was significantly reduced in patients with LAA or SAA within all regions, except for the inferior region ($P < 0.05$, Table 4, Figure 3(b)). The significant differences mostly existed between the stroke group and control group ($P < 0.05$), and no significant difference was found in the two stroke subgroups, although the LAA group tended to have a lower vessel density. In addition to ONH capillary density, no significant difference was found in the superficial layer of all regions ($P > 0.05$, Table 4, Figure 3(a)).

3.1.3. Fractal Dimension around Macula. Differences in the fractal dimension were only statistically significant in C2 and C4 regions of the deep retina ($P < 0.05$, Table 5, Figure 4(b)) between patients with LAA and the controls. Compared with the control group, the fractal dimension of most regions in

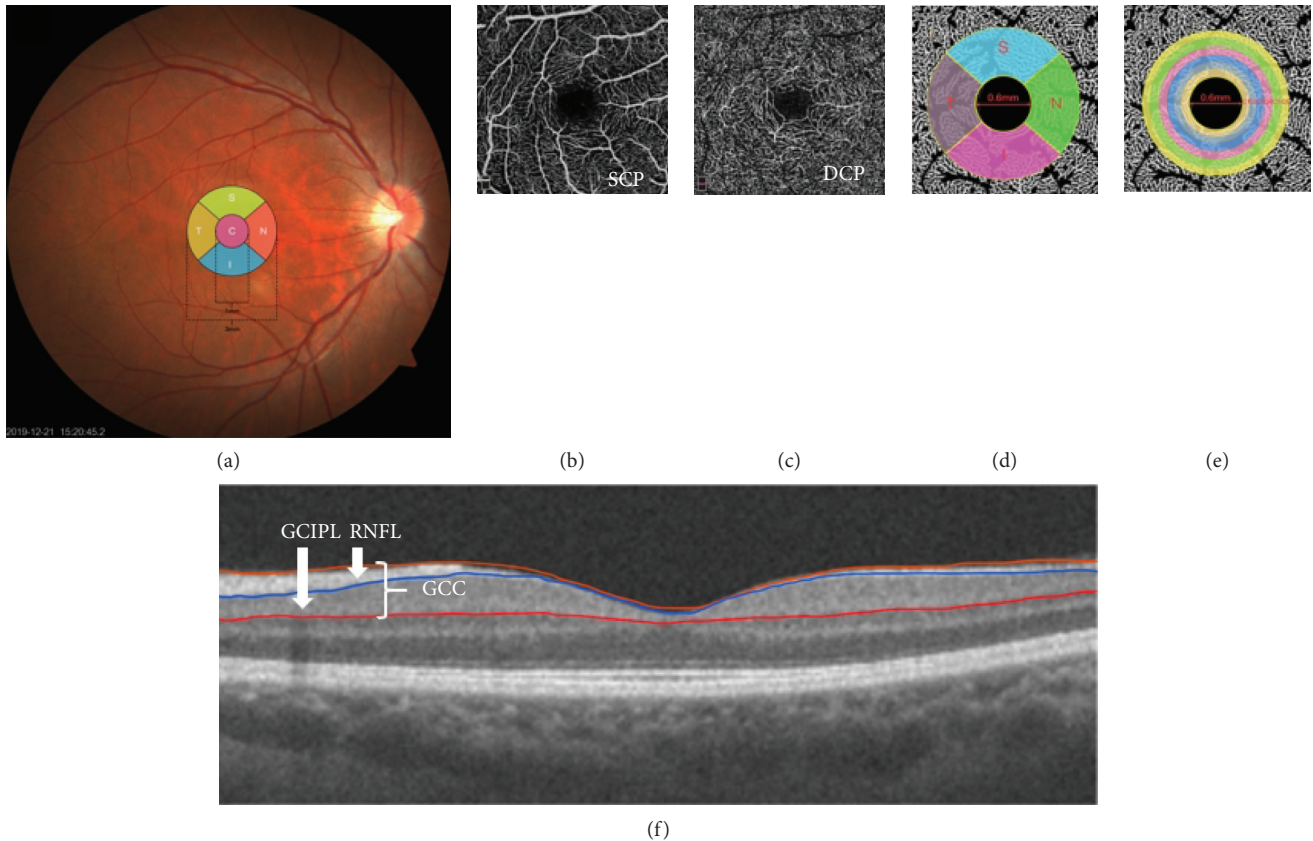


FIGURE 1: Retinal structure and the corresponding microvascular density and fractal dimension in superficial and deep layers imaged by OCT/OCTA. (a) Five regions within a 3 mm area around the fovea: (C) central region; (S) superior; (T) temporal; (I) inferior; (N) nasal. (b, c) OCTA images of superficial capillary plexuses (SCP) and deep capillary plexuses (DCP) in 3 × 3 mm area around fovea. (d, e) Fractal dimension analysis in four quadrants and six annular zones excluding the avascular zone (diameter = 0.6 mm): C1 (diameter = 0.92 mm), C2 (diameter = 1.23 mm), C3 (diameter = 1.55 mm), C4 (diameter = 1.87 mm), C5 (diameter = 2.18 mm), and C6 (diameter = 2.50 mm). (f) Retinal nerve fiber layer (RNFL) and ganglion cell complex (GCC) thickness around the fovea. GCIPL = ganglion cell-inner plexiform layer.

TABLE 2: The numbers of eyes examined in all three subgroups.

	Age	BMI	MAP	SE	BCVA	IOP	AL	RPC	pRNFL	GCC	Superficial VD	Deep VD	FAZ	Superficial FD	Deep FD
LAA	28	26	28	25	27	27	20	17	17	26	27	28	28	28	28
SAA	41	39	41	40	40	40	28	27	27	34	39	40	39	41	41
Control	65	64	65	64	65	65	47	63	63	64	64	65	65	65	65

LAA, large-artery atherosclerosis; SAA, small-vessel occlusion; BMI, body mass index; MAP, mean arterial pressure; SE, spherical equivalent; BCVA, best corrected visual acuity; IOP, intraocular pressure; AL, axial length; RPC, radial peripapillary capillary; pRNFL, peripapillary retinal nerve fiber layer; GCC, ganglion cell complex; VD, vessel density; FAZ, fovea avascular zone; FD, fractal dimension.

the stroke group showed a downward trend, although there was no statistical difference in most regions ($P > 0.05$, Table 5, Figures 4(a) and 4(b)).

4. Discussion

Assuming that the retinal vasculature mirrors the cerebral vasculature, OCTA enables noninvasive imaging of retinal capillaries in multiple layers invisible on fundus images. Based on fundus photography, retinal abnormalities, including arteriovenous nicking and generalized and localized arteriolar thinning, a lower arteriolar/venular diameter ratio and geometric parameters have been demonstrated to be

significantly related to the incidence of stroke [5, 9, 21, 22]. The previous studies using fundus photos could not qualitatively detect the subtle changes at the capillary level while OCTA provides the opportunity to investigate the retinal capillary microcirculation at the micrometer resolution [23].

In terms of vessel density around the macula, our findings demonstrate that the changes of vessel density are more obvious in the deep layers than the superficial layer between stroke patients and control subjects. Our results point to a preferential involvement of the deep layer in patients with stroke which may be attributed to the fact that the deep network consists of a dense and complex system of smaller vessels [24]. It can be speculated that deep retinal

TABLE 3: Retinal thickness (μm) from commercial instruments in patients with LAA, SAA, and controls.

Layers	Regions	LAA	SAA	Control	P^*	P_1	P_2	P_3
pRNFL	Total	109.35 \pm 10.06	111.85 \pm 12.54	114.19 \pm 10.86	0.254	0.472	0.117	0.366
	S	124.65 \pm 21.47	137.41 \pm 21.07	140.84 \pm 17.68	0.010	0.034	0.003	0.438
	N	96.65 \pm 14.85	96.93 \pm 14.68	100.27 \pm 14.01	0.472	0.950	0.356	0.312
	I	143.25 \pm 25.41	141.56 \pm 18.58	144.40 \pm 19.75	0.832	0.793	0.841	0.546
	T	78.47 \pm 10.54	77.52 \pm 11.78	75.35 \pm 10.21	0.468	0.774	0.289	0.382
GCC	Average	98.23 \pm 7.53	96.50 \pm 6.18	98.55 \pm 6.66	0.348	0.325	0.840	0.154
	Superior	96.77 \pm 9.84	97.03 \pm 5.58	98.92 \pm 6.50	0.292	0.888	0.195	0.212
	Inferior	99.81 \pm 7.24	96.09 \pm 7.41	98.20 \pm 7.67	0.158	0.060	0.360	0.187

LAA, large-artery atherosclerosis; SAA, small-vessel occlusion; pRNFL, peripapillary retinal nerve fiber layer; GCC, ganglion cell complex. S = superior; N = nasal; I = inferior; T = temporal; * P value among the three groups; P_1 and P values between LAA and SAA; P_2 and P values between LAA and control; P_3 value between SAA and control.

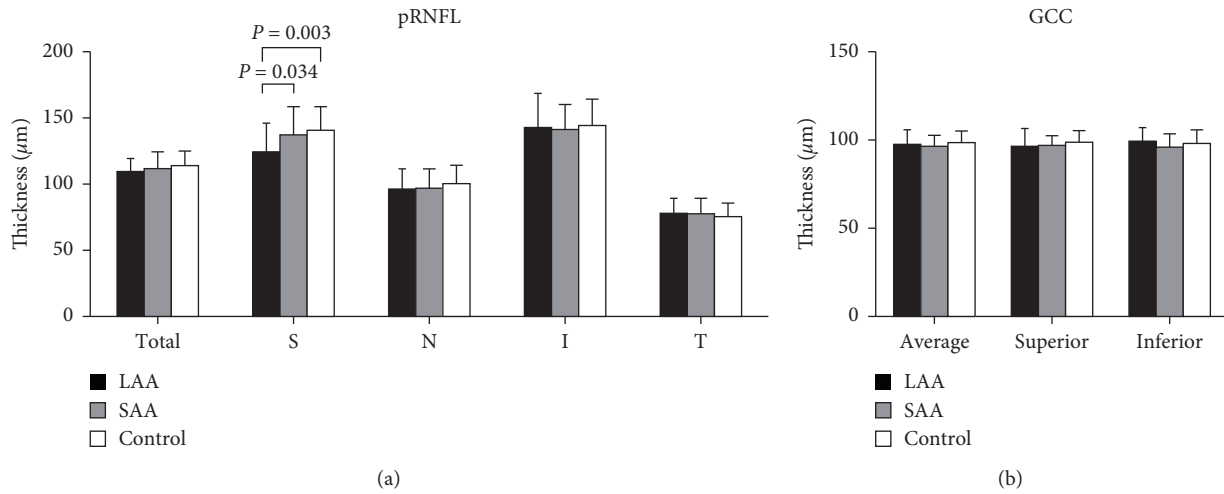


FIGURE 2: (a) Peripapillary retinal nerve fiber layer (pRNFL) thickness in eyes of patients with large-artery atherosclerosis (LAA), small-vessel occlusion (SAA), and controls. S = superior; N = nasal; I = inferior; T = temporal. (b) Ganglion cell complex (GCC) thickness in three groups.

TABLE 4: Comparison of microvascular density in patients with LAA, SAA, and controls between the superficial and deep retinal capillary plexus.

Layers	Regions	LAA	SAA	Control	P^*	P_1	P_2	P_3
RPC	Whole	49.51 \pm 2.54	49.47 \pm 3.14	49.98 \pm 2.28	0.621	0.964	0.504	0.393
	S	52.94 \pm 5.87	53.22 \pm 4.48	53.02 \pm 3.86	0.973	0.836	0.950	0.838
	N	49.00 \pm 5.35	50.63 \pm 5.83	51.79 \pm 5.24	0.155	0.333	0.062	0.352
	I	55.56 \pm 3.65	53.11 \pm 4.37	53.76 \pm 4.21	0.174	0.066	0.127	0.500
	T	53.00 \pm 5.23	51.07 \pm 6.07	52.95 \pm 5.29	0.308	0.260	0.974	0.141
SCP	Whole	45.59 \pm 4.26	46.72 \pm 3.13	45.65 \pm 2.82	0.209	0.478	0.998	0.196
	T	47.72 \pm 4.06	48.50 \pm 3.01	47.15 \pm 3.37	0.157	0.365	0.471	0.055
	S	49.23 \pm 4.82	50.64 \pm 3.63	49.56 \pm 3.67	0.277	0.154	0.717	0.178
	N	47.18 \pm 4.76	49.15 \pm 3.48	47.91 \pm 3.10	0.107	0.169	0.743	0.169
	I	49.62 \pm 4.60	50.30 \pm 3.74	49.58 \pm 3.59	0.631	0.481	0.967	0.360
DCP	Whole	47.49 \pm 3.12	48.11 \pm 3.70	49.46 \pm 3.14	0.017	0.448	0.009	0.044
	T	50.30 \pm 3.17	50.58 \pm 3.55	52.04 \pm 3.05	0.020	0.730	0.018	0.025
	S	49.62 \pm 4.23	50.20 \pm 4.24	51.77 \pm 3.67	0.029	0.556	0.018	0.050
	N	50.26 \pm 3.46	50.67 \pm 4.37	52.19 \pm 3.17	0.027	0.645	0.020	0.039
	I	49.58 \pm 3.65	49.31 \pm 4.46	51.09 \pm 3.67	0.051	0.783	0.090	0.026

LAA, large-artery atherosclerosis; SAA, small-vessel occlusion; RPC, radial peripapillary capillary; SCP, superficial capillary plexuses; DCP, deep capillary plexuses; S = superior; N = nasal; I = inferior; T = temporal; * P value among the three groups; P_1 and P values between LAA and SAA; P_2 and P values between LAA and control; P_3 value between SAA and control.

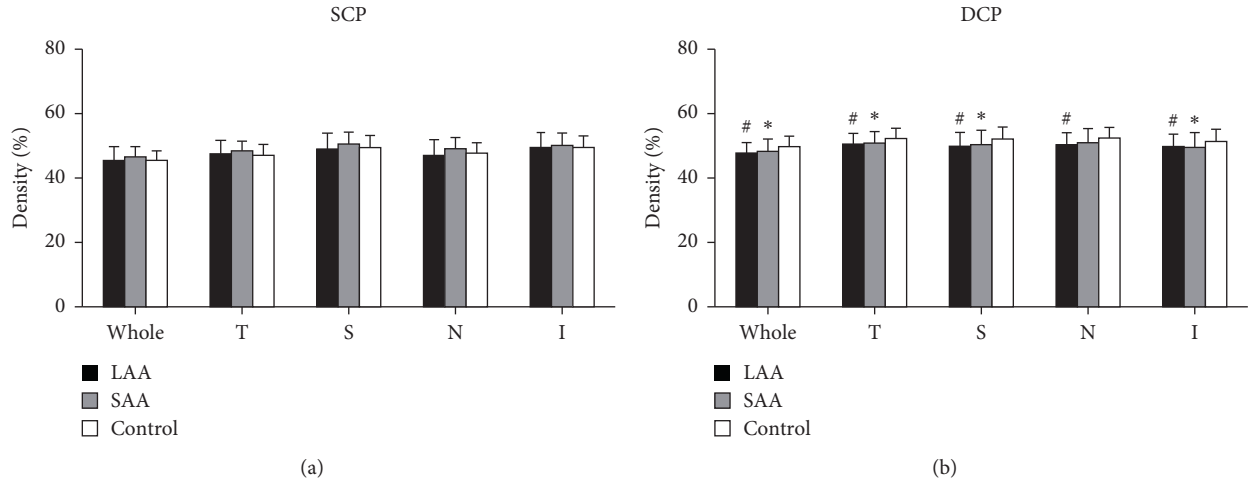


FIGURE 3: Comparisons of the microvascular density on OCTA images in whole and four quadrant sectors of the superficial capillary plexuses (SCP) (a) and deep capillary plexuses (DCP) (b). * $P < 0.05$, the density in the SAA group was lower than that in the control group; # $P < 0.05$, the density in the LAA group was lower than that in the control group.

TABLE 5: D_{box} in the superficial and deep retinal capillary layers.

Layers	Regions	LAA	SAA	Control	P^*	P_1	P_2	P_3
SCP	TAZ	1.754 ± 0.020	1.756 ± 0.025	1.759 ± 0.024	0.530	0.758	0.305	0.432
	C1	1.218 ± 0.285	1.295 ± 0.238	1.210 ± 0.268	0.240	0.230	0.891	0.104
	C2	1.409 ± 0.040	1.416 ± 0.041	1.425 ± 0.041	0.224	0.490	0.098	0.301
	C3	1.415 ± 0.036	1.411 ± 0.037	1.419 ± 0.039	0.520	0.645	0.615	0.257
	C4	1.426 ± 0.029	1.430 ± 0.025	1.432 ± 0.035	0.748	0.606	0.447	0.820
	C5	1.424 ± 0.022	1.428 ± 0.020	1.425 ± 0.028	0.748	0.486	0.829	0.541
	C6	1.423 ± 0.022	1.426 ± 0.024	1.426 ± 0.028	0.857	0.633	0.601	0.996
	S	1.679 ± 0.036	1.683 ± 0.030	1.689 ± 0.028	0.316	0.559	0.149	0.356
	T	1.683 ± 0.036	1.686 ± 0.030	1.689 ± 0.035	0.745	0.681	0.448	0.722
	I	1.681 ± 0.032	1.688 ± 0.034	1.684 ± 0.030	0.607	0.325	0.609	0.527
N	1.682 ± 0.029	1.679 ± 0.033	1.686 ± 0.038	0.670	0.739	0.675	0.376	
DCP	TAZ	1.805 ± 0.023	1.810 ± 0.025	1.816 ± 0.016	0.065	0.753	0.088	0.352
	C1	1.388 ± 0.110	1.362 ± 0.244	1.401 ± 0.098	0.466	0.500	0.721	0.218
	C2	1.479 ± 0.021	1.487 ± 0.023	1.493 ± 0.023	0.019	0.118	0.005	0.204
	C3	1.484 ± 0.033	1.484 ± 0.031	1.489 ± 0.023	0.667	0.956	0.471	0.453
	C4	1.482 ± 0.026	1.490 ± 0.024	1.496 ± 0.019	0.015	0.158	0.005	0.131
	C5	1.473 ± 0.026	1.476 ± 0.035	1.483 ± 0.021	0.172	0.681	0.096	0.166
	C6	1.463 ± 0.036	1.471 ± 0.030	1.479 ± 0.022	0.067	0.622	0.097	0.321
	S	1.736 ± 0.037	1.739 ± 0.026	1.747 ± 0.021	0.126	0.708	0.077	0.121
	T	1.733 ± 0.030	1.746 ± 0.030	1.746 ± 0.018	0.062	0.037	0.029	0.923
	I	1.737 ± 0.023	1.735 ± 0.035	1.743 ± 0.023	0.244	0.779	0.277	0.116
N	1.734 ± 0.025	1.741 ± 0.024	1.746 ± 0.023	0.098	0.271	0.034	0.285	

LAA, large-artery atherosclerosis; SAA, small-vessel occlusion; SCP, superficial capillary plexuses; DCP, deep capillary plexuses; TAZ, total annular zone; * P value among the three groups; P_1 and P values between LAA and SAA; P_2 and P values between LAA and control; P_3 value between SAA and control.

capillaries are more susceptible to ischemic and hypoxia. As per our expectation, patients with SAA displayed much smaller changes than patients with LAA. However, there exists no significant difference between the LAA and SAA. The finding suggested that the retinal vasculopathy may result from downstream effects of large-artery pathology in the cerebral circulation. In addition, we found that fractal dimension was not helpful in identifying stroke subtypes and was significantly lower in the LAA group than in controls only in individual regions of the deep retina. Our results were in consistence with those of others [9], which found that decreased FD was correlated with stroke, suggesting a

loss of complexity. However, previous results of fractal dimension based on the fundus photograph remain controversial. Some considered lacunar stroke subtype was associated with decreased retinal FD [8] while others demonstrated that the lacunar stroke was positively associated with higher FD [7]. We found no significant difference between stroke subgroups, which may indicate that the FD is not applicable to differentiate the disease subgroups who have already had stroke.

Regarding peripapillary vessel density, there was no significance in RPC among the groups. The finding could be related to the anatomical differences between the different

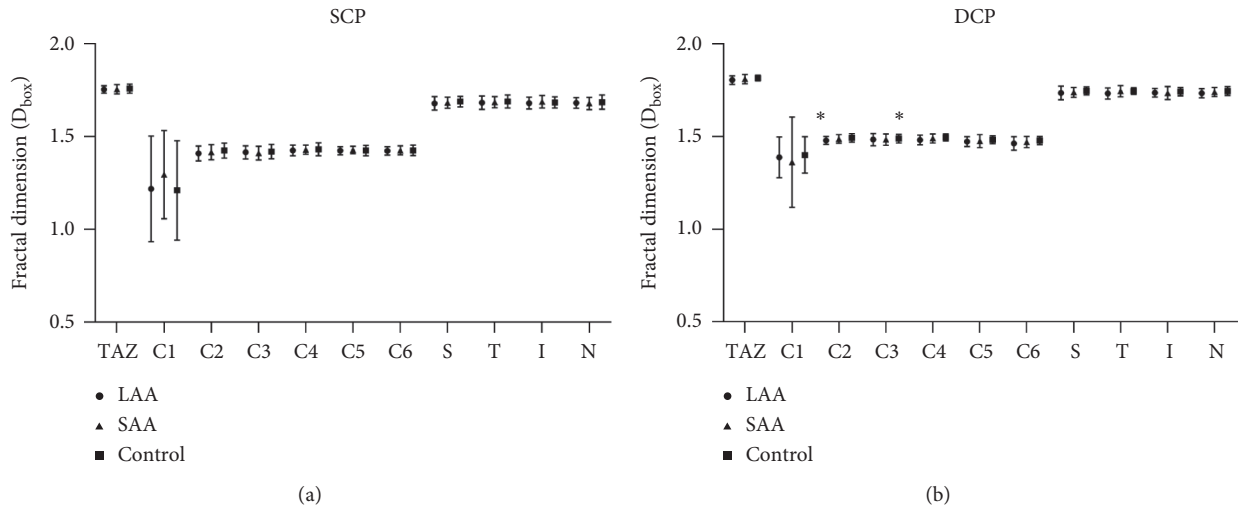


FIGURE 4: Comparisons of the microvascular D_{box} among patients with large-artery atherosclerosis (LAA), small-vessel occlusion (SAA), and controls. Comparisons in (a) superficial capillary plexuses (SCP) and (b) deep capillary plexuses (DCP). A significant reduction was seen in the deep layer of C2 and C4 region in LAA patients when compared to controls. * $P < 0.05$.

areas. The parafoveal superficial capillary plexus originates largely from the retinal circulation, whereas the RPC receives additional blood supply from the choroid [25]. Larger vascular channels around the optic disc may have masked subtle changes in the capillary network. Additionally, RPC contains multiple layers of capillaries that overlap on en-face OCTA images, lacking the ability to detect tiny vascular losses.

In addition to retinal capillary changes, our study observed that the pRNFL thickness was statistically reduced in the superior quadrant of stroke patients, and there was a statistical difference between the stroke subgroups which may indicate different patterns of nerve damage in the two stroke subtypes. Additionally, some research recently also observed that both acute and previous stroke were significantly associated with retinal nerve fiber layer defects (RNFLDs) [13]. These findings were also in accordance those of with others [26], which reported the associations between severity and laterality of RNFLD and laterality of hemispheric damage as well as arterial territory of infarct. They found RNFLDs were significant in the temporal sector of the ipsilateral side and in the nasal sector of the contralateral side of the stroke. Furthermore, they also confirmed that the degree of the transneuronal retrograde degeneration (TRD) was time-dependent. However, we find that the significant RNFLDs only exist in the superior sector in our study although the ipsilateral sides were included.

As is known to all, over 30 morphological types of RGCs compose the structure of the retina. The midget RGCs (80%), with wide retinal dendritic fields located in the peripheral retina, mainly project to the magnocellular layers of the lateral geniculate body. The parasol RGCs (5–15%) predominantly present in the papillomacular bundle (macula) and project to suprachiasmatic nucleus of the hypothalamus. Axons from midget RGCs enter the superior, inferior, and nasal sectors of the optic nerve, and parasol RGCs gather their axons and enter the temporal sector of the optic nerve

[27, 28]. The different degenerative patterns of the ganglion cells and nerve fibers have been demonstrated in several neurodegenerative diseases [29, 30]. Recent studies have described that the parasol RGCs are more involved in the pathogenesis of Alzheimer's disease [31–33]. However, as for the Parkinson syndrome and mitochondrial optic neuropathy, the midget RGCs are mainly involved [30, 34, 35]. Both the above and our study suggest that mean thickness measurement may not reflect the disease well and reduce the diagnostic efficacy of the ocular biomarker. We speculate that detailed analysis of the focal nerve structure alteration may be developed as an ocular imaging biomarker for monitoring disease progression and evaluating prognosis of these diseases.

Nevertheless, as this is the first study on ischemic stroke subtypes based on OCTA, further large samples are required to confirm the universality in the disease. The discrepancies existing between different studies could be ascribed to differences in course and severity of disease as well as various OCT devices and study designs.

Besides, a previous animal study also revealed that the TRD of retinal ganglion cells occurred after shrinkage of the optic tract, and degeneration of the RGC was progressing slowly in the next few years [36]. Thus, our negative results in GCC thickness might be related to the fact that patients were tested within two weeks after stroke.

To conclude, our study provides a side view that the neurovascular unit is affected in ischemic stroke and severely in LAA patients. The components of neurovascular units are interrelated in the microenvironment. Studies have shown that the signal transmission between neurons, astrocytes, and microvascular endothelial cells regulates the brain microenvironment [37] [29]. Briefly, NVU as a structural and functional whole, the relationship between members changes in the state of illness. The mechanism of cerebral ischemia is complex and involves multiple cascading reactions. Therefore, monitoring the NVU as a whole and

improving its function help maintain brain cell function and make stroke treatment more ideal. The retina provides a visualization of the neurovascular units simultaneously to reflect the changes of the brain, which has important implications for disease surveillance.

In addition, we also acknowledge the limits in this study. The cross-sectional study with a small sample limits our ability to identify the different pathogenesis of the capillaries and microstructures of the stroke. The outer structure of the retina which is mainly supplied by the choroid has not been analyzed. Due to the practical difficulty of recruiting and examining the patients, milder patients may be recruited, which may be more likely with milder vascular lesions to differentiate the two subtypes. Despite the weakness, there are several strengths in our study. We recruited different ischemic stroke subtypes with strict inclusion and exclusion criteria. Otherwise, to minimize the confounding of stroke, the patients with a history of previous stroke were excluded. We completed the detailed ophthalmic and clinical examinations within two weeks after the onset of the stroke and maintained the blinding of retinal and brain images to each other. Finally, this is the first attempt to simultaneously observe retinal microvascular and neurological changes in different stroke subtypes *in vivo*.

Moreover, further longitudinal studies with a larger sample size are required to show differences in the characteristics of retinal microstructure and capillaries. It remains to be seen whether the retinal signs are indicative of cerebrovascular risk beyond the conventional risk indicators and whether the retinal imaging technique will be a surrogate or accessory examination system in clinical settings and ultimately become a part of the routine stroke risk or evaluation of treatment assessment.

Data Availability

All data generated or analyzed during this study are included within published article.

Ethical Approval

This study was conducted in accordance with the Declaration of Helsinki and approved by the Ethics Committee Board of the Wenzhou Medical University (2019-027-K-26).

Consent

All subjects, recruited voluntarily, were informed about the purposes, methods, and potential risks of the study. A signed consent form was obtained from each patient.

Conflicts of Interest

The authors declare that they have no conflicts of interest.

Authors' Contributions

Ying Zhang, Fan Lu, and Meixiao Shen designed the study. Ying Zhang, Fan Lu, and Ce Shi conducted the study. Ying Zhang, Xianda Lin, Weicheng Wang, and Shenghai Huang

collected the data. Shenghai Huang wrote the image processing algorithm for data analysis. Ying Zhang and Ce Shi analyzed and interpreted the data. Fan Lu and Meixiao Shen were the main contributors to manuscript discussion. Meixiao Shen, Weicheng Wang, and Zhao Han revised the manuscript. All authors read and approved the final manuscript.

Acknowledgments

This study was supported by the research grants from the National Key Project of Research and Development Program of Zhejiang Province (Grant no. 2019C03045), Wenzhou Municipal Science and Technology Bureau (Grant no. 2018ZY016), and Zhejiang Provincial Natural Science Foundation of China (Grant no. LQ17H180004).

References

- [1] W. Wang, B. Jiang, H. Sun et al., "Prevalence, incidence, and mortality of stroke in China," *Circulation*, vol. 135, no. 8, pp. 759–771, 2017.
- [2] H. P. Adams Jr., B. H. Bendixen, L. J. Kappelle et al., "Classification of subtype of acute ischemic stroke. Definitions for use in a multicenter clinical trial. TOAST. Trial of Org 10172 in acute stroke treatment," *Stroke*, vol. 24, no. 1, pp. 35–41, 1993.
- [3] T. Y. Wong, R. Klein, A. R. Sharrett et al., "Cerebral white matter lesions, retinopathy, and incident clinical stroke," *JAMA*, vol. 288, no. 1, pp. 67–74, 2002.
- [4] T. Y. Wong, R. Klein, D. J. Couper et al., "Retinal microvascular abnormalities and incident stroke: the atherosclerosis risk in communities study," *The Lancet*, vol. 358, no. 9288, pp. 1134–1140, 2001.
- [5] R. I. Lindley, J. J. Wang, M.-C. Wong et al., "Retinal microvasculature in acute lacunar stroke: a cross-sectional study," *The Lancet Neurology*, vol. 8, no. 7, pp. 628–634, 2009.
- [6] C. Y.-l. Cheung, W. T. Tay, M. K. Ikram et al., "Retinal microvascular changes and risk of stroke," *Stroke*, vol. 44, no. 9, pp. 2402–2408, 2013.
- [7] N. Cheung, G. Liew, R. I. Lindley et al., "Retinal fractals and acute lacunar stroke," *Annals of Neurology*, vol. 68, no. 1, pp. 107–111, 2010.
- [8] F. N. Doubal, T. J. MacGillivray, N. Patton, B. Dhillon, M. S. Dennis, and J. M. Wardlaw, "Fractal analysis of retinal vessels suggests that a distinct vasculopathy causes lacunar stroke," *Neurology*, vol. 74, no. 14, pp. 1102–1107, 2010.
- [9] Y.-T. Ong, D. A. De Silva, C. Y. Cheung et al., "Microvascular structure and network in the retina of patients with ischemic stroke," *Stroke*, vol. 44, no. 8, pp. 2121–2127, 2013.
- [10] E. H. Lo, J. P. Broderick, and M. A. Moskowitz, "tPA and proteolysis in the neurovascular unit," *Stroke*, vol. 35, no. 2, pp. 354–356, 2004.
- [11] Y. Lu, C. Li, Q. Chen et al., "Microthrombus-targeting micelles for neurovascular remodeling and enhanced microcirculatory perfusion in acute ischemic stroke," *Advanced Materials*, vol. 31, no. 21, Article ID e1808361, 2019.
- [12] H. Girouard and C. Iadecola, "Neurovascular coupling in the normal brain and in hypertension, stroke, and Alzheimer disease," *Journal of Applied Physiology*, vol. 100, no. 1, pp. 328–335, 2006.

- [13] D. Wang, Y. Li, C. Wang et al., "Localized retinal nerve fiber layer defects and stroke," *Stroke*, vol. 45, no. 6, pp. 1651–1656, 2014.
- [14] T. Brott, H. P. Adams Jr., C. P. Olinger et al., "Measurements of acute cerebral infarction: a clinical examination scale," *Stroke*, vol. 20, no. 7, pp. 864–870, 1989.
- [15] A. Camino, M. Zhang, S. S. Gao et al., "Evaluation of artifact reduction in optical coherence tomography angiography with real-time tracking and motion correction technology," *Biomedical Optics Express*, vol. 7, no. 10, pp. 3905–3915, 2016.
- [16] A. G. Bennett, A. R. Rudnicka, and D. F. Edgar, "Improvements on Littmann's method of determining the size of retinal features by fundus photography," *Graefes's Archive for Clinical and Experimental Ophthalmology*, vol. 232, no. 6, pp. 361–367, 1994.
- [17] S. Nowroozizadeh, N. Cirineo, N. Amini et al., "Influence of correction of ocular magnification on spectral-domain OCT retinal nerve fiber layer measurement variability and performance," *Investigative Ophthalmology & Visual Science*, vol. 55, no. 6, pp. 3439–3446, 2014.
- [18] Q. Chen, Q. Ma, C. Wu et al., "Macular vascular fractal dimension in the deep capillary layer as an early indicator of microvascular loss for retinopathy in type 2 diabetic patients," *Investigative Ophthalmology & Visual Science*, vol. 58, no. 9, pp. 3785–3794, 2017.
- [19] Q. Chen, F. Tan, Y. Wu et al., "Characteristics of retinal structural and microvascular alterations in early type 2 diabetic patients," *Investigative Ophthalmology & Visual Science*, vol. 59, no. 5, pp. 2110–2118, 2018.
- [20] D. Cheng, M. Shen, X. Zhuang et al., "Inner retinal microvasculature damage correlates with outer retinal disruption during remission in behçet's posterior uveitis by optical coherence tomography angiography," *Investigative Ophthalmology & Visual Science*, vol. 59, no. 3, pp. 1295–1304, 2018.
- [21] R. Kawasaki, M. Z. Che Azemin, D. K. Kumar et al., "Fractal dimension of the retinal vasculature and risk of stroke: a nested case-control study," *Neurology*, vol. 76, no. 20, pp. 1766–1767, 2011.
- [22] D. A. De Silva, J. J. F. Manzano, E. Y. Liu et al., "Retinal microvascular changes and subsequent vascular events after ischemic stroke," *Neurology*, vol. 77, no. 9, pp. 896–903, 2011.
- [23] A. H. Kashani, C.-L. Chen, J. K. Gahm et al., "Optical coherence tomography angiography: a comprehensive review of current methods and clinical applications," *Progress in Retinal and Eye Research*, vol. 60, pp. 66–100, 2017.
- [24] M. C. Savastano, B. Lumbroso, and M. Rispoli, "In vivo characterization of retinal vascularization morphology using optical coherence tomography angiography," *Retina*, vol. 35, no. 11, pp. 2196–2203, 2015.
- [25] J. P. Campbell, M. Zhang, T. S. Hwang et al., "Detailed vascular anatomy of the human retina by projection-resolved optical coherence tomography angiography," *Scientific Reports*, vol. 7, Article ID 42201, 2017.
- [26] H.-Y. L. Park, Y. G. Park, A.-H. Cho, and C. K. Park, "Transneuronal retrograde degeneration of the retinal ganglion cells in patients with cerebral infarction," *Ophthalmology*, vol. 120, no. 6, pp. 1292–1299, 2013.
- [27] J. R. Sanes and R. H. Masland, "The types of retinal ganglion cells: current status and implications for neuronal classification," *Annual Review of Neuroscience*, vol. 38, no. 1, pp. 221–246, 2015.
- [28] B. Mead and S. Tomarev, "Evaluating retinal ganglion cell loss and dysfunction," *Experimental Eye Research*, vol. 151, pp. 96–106, 2016.
- [29] C. La Morgia, L. Di Vito, V. Carelli, and M. Carbonelli, "Patterns of retinal ganglion cell damage in neurodegenerative disorders: parvocellular vs magnocellular degeneration in optical coherence tomography studies," *Frontiers in Neurology*, vol. 8, p. 710, 2017.
- [30] C. La Morgia, F. N. Ross-Cisneros, A. A. Sadun, and V. Carelli, "Retinal ganglion cells and circadian rhythms in alzheimer's disease, Parkinson's disease, and beyond," *Frontiers in Neurology*, vol. 8, p. 162, 2017.
- [31] J. C. Blanks, D. R. Hinton, A. A. Sadun, and C. A. Miller, "Retinal ganglion cell degeneration in Alzheimer's disease," *Brain Research*, vol. 501, no. 2, pp. 364–372, 1989.
- [32] J. C. Blanks, Y. Torigoe, D. R. Hinton, and R. H. I. Blanks, "Retinal pathology in Alzheimer's disease. I. Ganglion cell loss in foveal/parafoveal retina," *Neurobiology of Aging*, vol. 17, no. 3, pp. 377–384, 1996.
- [33] C. La Morgia, F. N. Ross-Cisneros, Y. Koronyo et al., "Melanopsin retinal ganglion cell loss in Alzheimer disease," *Annals of Neurology*, vol. 79, no. 1, pp. 90–109, 2016.
- [34] C. E. Mendoza-Santiesteban, J.-A. Palma, J. Martinez, L. Norcliffe-Kaufmann, T. R. Hedges, and H. Kaufmann, "Progressive retinal structure abnormalities in multiple system atrophy," *Movement Disorders*, vol. 30, no. 14, pp. 1944–1953, 2015.
- [35] P. Yu-Wai-Man, P. G. Griffiths, and P. F. Chinnery, "Mitochondrial optic neuropathies-disease mechanisms and therapeutic strategies," *Progress in Retinal and Eye Research*, vol. 30, no. 2, pp. 81–114, 2011.
- [36] A. Cowey, I. Alexander, and P. Stoerig, "Transneuronal retrograde degeneration of retinal ganglion cells and optic tract in hemianopic monkeys and humans," *Brain A Journal of Neurology*, vol. 134, no. 7, pp. 2149–2157, 2011.
- [37] M. Zonta, A. Sebelin, S. Gobbo, T. Fellin, T. Pozzan, and G. Carmignoto, "Glutamate-mediated cytosolic calcium oscillations regulate a pulsatile prostaglandin release from cultured rat astrocytes," *The Journal of Physiology*, vol. 553, no. 2, pp. 407–414, 2003.